Synthesis of novel organic semiconductors for optoelectronic devices

Thesis submitted in fulfilment of the requirements
for the degree of
Doctorate of Philosophy

School of Chemistry
College of Science and Engineering
University of Glasgow

April 2016

Michele Cariello

Abstract

This thesis describes the synthesis and characterisation of novel conjugated organic materials with optoelectronic application. The first chapter provides an introduction about organic semiconductors and in particular about their working principle from a physical and chemical point of view. An overview of the most common types of solar cells is provided, including examples of some of the best performing materials.

The second chapter describes the synthesis of a new library of flavin derivatives as potential active materials for optoelectronic applications. Flavins are natural redox-active molecules, which show potential application in optoelectronics, thanks to their stability and versatility. FPF-Flavins, for instance, could be used either as acceptor units in *push-pull* polyconjugated systems or as acceptor unit in dyes for DSSCs. In the same chapter a first attempt of synthesising *bis*-flavins to be used as N-type semiconductors in BHJ devices is described.

The third chapter describes the successful synthesis and characterization of a series of conjugated organic molecules based on the benzothiadiazole moiety. Among these, three molecules containing ferrocene as donor unit were tested as sensitizers for DSSCs, reporting a PCE of 0.3% as the best result. Further studies indicated a significant problem of charge recombination which limits the performance. A near-infrared absorbing *push-pull* polymer, based on BbT as acceptor unit, was also synthesised and tested in BHJ devices as P-type semiconductor in blend with $PC_{71}BM$, showing a V_{OC} of 0.71 V.

Finally, the last chapter describes the synthesis of several tetrathiafulvalene derivatives in order to explore this moiety as donor unit in dyes for DSSCs and as HTM for perovskite-based solar cells. In particular, two very simple dyes were synthesised and implemented in DSSCs reporting a PCE 0.2% and 0.4%, respectively. The low efficiency was associated to the tendency to aggregate at the solid state, with the absorption shifting from the visible to the infrared range. A conjugated molecule, containing a DPP core, was also synthesised and tested as HTM for perovskite solar cells. The best reported PCE of 7.7% was obtained without any additives. A case study about dehalogenation and “halogen dance” in TTF iodide is also presented.

Table of Contents

Acknowledgements

It is hard to acknowledge all the people that contributed, in different ways, to help me enjoying this 4-year long trip. Thanks to these people I have been able to grow up from a human point of view, other than intellectual. Firstly, I would like to express my sincere gratitude to my supervisor Prof. Graeme Cooke for the continuous support during my PhD study, for his patience, motivation, and immense knowledge. His guidance helped me all the time by giving me precious advises. I could not have imagined having a better boss and mentor for my PhD study. The enthusiasm and commitment that I kept during my work are justified by his skilful direction.

My sincere thanks also go to Dr. Alan Wiles and Dr. Brian Fitzpatrick, who were always keen on helping me to overcome the issues I have encountered. Without their valuable support it would have not been possible to conduct this research. I thank my fellow labmates for the stimulating discussions at lunchtime, for the nights spent together behind endless columns and for all the fun we have had in the last four years. In particular Dr. Luis Serrano, who was there when I started and Nabeel, Saif, Nor, Sondos, Cosma, Stefan, John and Liam.

I would like to thank all the people who contributed in some way to the work described in this thesis, with an emphasis in our main collaborators: Prof. Ifor Samuel at the University of St. Andrews, Prof. Jongin Hong at the Chung-Ang University and Prof. Peter Holliman at Bangor University. My genuine thankfulness goes to Prof. Anders Hagfeldt and his group at EPFL for hosting me for one month and for teaching me everything I know about device fabrication. While there, I have had the possibility to meet very lovely and brilliant people, particularly Marina, Yasemin, Juanpa and Mahboubeh, who shared with me their knowledge and their table at the pub.

Last but not least, I would like to thank my family. Stefania, my wife, for her infinite love and patience: I can't imagine my life without her presence, her friendship and true love. My parents with whom I spent the first 26 years of my life and whose support has been fundamental, allowing me to become the person I am. My younger brother, in whom I can see myself ten years ago, and Kimi, who still keeps waiting for my return to Italy.

Finally, I would like to thank all the people who won't stop at the Acknowledgements page but will read this work till the end: thanks both!

Sincerely,

Michele

Author's Declaration

This thesis represents the original work carried out by Michele Cariello, unless otherwise stated in the text.

The research described herein was carried out at the University of Glasgow, in the Department of Chemistry, under the supervision of Prof. Graeme Cooke, during the period of October 2012 – March 2016.

Pictures and schemes containing a reference number in the caption were reprinted/adapted with permission from the related publisher, according to the copyright regulations.

List of tables

List of figures and schemes

Figures

Figure 57 – UV-Vis absorption spectra of compounds **38** and **57**, in solution (C = 10^{-5} M, in DCM). The concentration of the polymer was calculated by assuming the repeating unit as the analyte.

Figure 58 – Emission spectrum of compound **57** in solution (C = 10^{-5} M, in DCM), with λ_{exc} = 390 nm.

Figure 59 – CV plot of polymer **57**, in solution (C = 10^{-3} M, in DCM), performed using a Pt disk working electrode, a Pt wire counter electrode and a Ag wire reference electrode. $TBAPF_6$ (0.1 M) was used as supporting electrolyte and the redox potential of the Fc/Fc^+ couple as internal standard.

Figure 60 – SWV plot of polymer **57**, in solution (C = 10^{-3} M, in DCM), performed using a Pt disk working electrode, a Pt wire counter electrode and a Ag wire reference electrode. $TBAPF_6$ (0.1 M) was used as supporting electrolyte and the redox potential of the Fc/Fc^+ couple as external standard.

Figure 61 – UV-Vis absorption spectra of compounds **38** and **39**, in solution (C = 10^{-5} M, in DCM).

Figure 62 – CV plots of compounds **38** and **39** in solution (C = 10^{-3} M, in DCM), performed using a Pt disk working electrode, a Pt wire counter electrode and a Ag wire reference electrode. $TBAPF_6$ (0.1 M) was used as supporting electrolyte and the redox potential of the Fc/Fc^+ couple as internal standard.

Figure 63 – SWV plots of compounds **38** and **39** in solution (C = 10^{-3} M, in DCM), performed using a Pt disk working electrode, a Pt wire counter electrode and a Ag wire reference electrode. $TBAPF_6$ (0.1 M) was used as supporting electrolyte and the redox potential of the Fc/Fc^+ couple as internal standard.

Figure 64 – Chemical structure of compound **83**.

Figure 65 – Chemical structure of compound **87**.

Figure 66 – Chemical structure of compound **88**.

Figure 67 – UV-Vis absorption spectra of compounds **38** and **88** in solution (C = 10^{-5} M, in DCM).

Figure 68 – CV plot of compound **88** in solution (C = 10^{-3} M, in DCM), performed using a Pt disk working electrode, a Pt wire counter electrode and a Ag wire reference electrode. $TBAPF_6$ (0.1 M) was used as supporting electrolyte and the redox potential of the Fc/Fc^+ couple as external standard.

Figure 69 – SWV plot of compound **88** in solution (C = 10^{-3} M, in DCM), performed using a Pt disk working electrode, a Pt wire counter electrode and a Ag

wire reference electrode. $TBAPF_6$ (0.1 M) was used as supporting electrolyte and the redox potential of the Fc/Fc^+ couple as external standard.

Figure 70 – Chemical structure of compounds **38**, **39** and **57**.

Figure 71 – Chemical structure of compounds **40**, **41** and **42**.

Figure 72 – Chemical structure of thiadiazole isomers.

Figure 73 – Chemical structure of compounds **88** and **89**.

Figure 74 – Chemical structure of compounds **90** – **96**.

Figure 75 – Chemical structure of polymers **2** and **97**.

Figure 76 – Chemical structure of compounds **98** – **100**.

Figure 77 – Chemical structure of dyes **101** – **103**.

Figure 78 – Chemical structures of compounds **104** – **110**.

Figure 79 – (a) Chemical structure of Vinylferrocene and p-*N*,*N'*-dimethylamino stirene; (b) electrochemical transformation of Fc to Fc^+.

Figure 80 – Chemical structure of dye **111**.

Figure 81 – Chemical structure of dye 123.

Figure 82 – Chemical structures of polymers **137**, with its quinoidal form **137'**, and **138**.

Figure 83 – Ground state optimized geometry of the dyes, and electron density distribution representations: (a) **104**, (b) **105**, (c) **106**. Calculations were run using B3LYP functional and 6-311+G(d,p) basis set for H, C, N, O, S and LanL2DZ functional for Fe, under vacuum.[218]

Figure 84 – UV-Vis absorption spectra of dyes **104 – 106** in solution ($C = 10^{-5}$ M, in DMF).[218]

Figure 85 – CV (left) and SWV (right) plots of dyes **104 – 106** in solution ($C = 10^{-3}$ M, in DMF), performed using a Pt disk working electrode, a Pt wire counter electrode and a Ag wire reference electrode. $TBAPF_6$ (0.1 M) was used as supporting electrolyte and the redox potential of the Fc/Fc^+ couple as external standard.

Figure 86 – Energy level diagram showing I_P and E_A of each dye, and their position relative to the TiO_2 conduction band and I^-/I_3^- redox potential.

Figure 87 – EIS plots of the DSSC devices using dye **106** as sensitiser.[218]

Figure 88 – (a) Optimised geometry and (b) energy level distribution for compound **107**. The calculations was run using B3LYP functional and 6-311+G(d) basis set for H, C, N, O, S and Lanl2DZ functional for Fe.

Figure 89 – Absorption spectrum of compound **107** ($C = 10^{-5}$ M, in DCM).

Figure 90 – CV plot of compound **107** in solution (C = 10^{-3} M, in DCM), performed using a Pt disk working electrode, a Pt wire counter electrode and a Ag wire reference electrode. $TBAPF_6$ (0.1 M) was used as supporting electrolyte and the redox potential of the Fc/Fc^+ couple as external standard.

Figure 91 – SWV plot of compound **107** in solution (C = 10^{-3} M, in DCM), performed using a Pt disk working electrode, a Pt wire counter electrode and a Ag wire reference electrode. $TBAPF_6$ (0.1 M) was used as supporting electrolyte and the redox potential of the Fc/Fc^+ couple as external standard.

Figure 92 – (a) Optimised geometry and (b) frontier molecular orbital distributions for dyes **108** and **109**. Calculations were run using B3LYP functional and 6-311+G(d) basis set.

Figure 93 – Absorption spectra of dyes **108** and **109** (C = 10^{-5} M, in DMF).

Figure 94 – CV (left) and SWV (right) plots of dyes **108** and **109** in solution (C = 10^{-3} M, in DMF), performed using a Pt disk working electrode, a Pt wire counter electrode and a Ag wire reference electrode. $TBAPF_6$ (0.1 M) was used as supporting electrolyte and the redox potential of the Fc/Fc^+ couple as external standard.

Figure 95 – Energy level diagram showing I_P and E_A values of each dye, and their position relative to the TiO_2 conduction band and I^-/I_3^- redox potential.

Figure 96 – IV-plots of DSSCs fabricated using dyes **108** (left) and **109** (right) as sensitisers.

Figure 97 – GPC plots for the two isolated fractions of polymer **110**.

Figure 98 – (a) Optimised geometry and (b) energy level distribution for polymer **110** (two repeating units). Calculations were run using B3LYP functional and 6-311+G(d) basis set.

Figure 99 – UV-Vis absorption spectrum of polymer **110** in solution (C = 10^{-5} M, in DCM).

Figure 100 – Absorption and emission spectra of compound F8BT. The emission was recorded by exciting the sample at the maximum of absorption.[230]

Figure 101 – Emission spectrum of polymer **110** in solution (C = 10^{-5} M, in DCM), using λ_{exc} = 650 nm.

Figure 102 – CV plot of polymer **110** in solution (C = 10^{-3} M, in DCM), performed using a Pt disk working electrode, a Pt wire counter electrode and a Ag wire reference electrode. $TBAPF_6$ (0.1 M) was used as supporting electrolyte and the redox potential of the Fc/Fc^+ couple as external standard.

Schemes

Definitions and abbreviations

f_{peak}: Peak frequency

τ_e: Electron lifetime

A: Acceptor

AcOH: Acetic acid

BbT: Benzo[1,2-c:4,5-c']*bis*[1,2,5]thiadiazole

BDT: Benzo[1,2-b:4,5-b']-dithiophene

BHJ: Bulk heterojunction

BMT: 1,2-Bis(5-methyl-1,3,4-thiathiazole-2-yl)sulphide

Boc: tert-Butyloxycarbonyl

BT: Benzo[*c*][1,2,5]thiadiazole

CB: Conduction band

CPDT: Cyclopenta[2,1-b:3,4-b']dithiophene

CT: Charge transport

CV: Cyclic voltammetry

D: Donor

DAT: Diaminotriazine

DCM: Dichloromethane

DFT: Density functional theory

DIPA: Diisopropylamine

DMAP: 4-Dimethylaminopyridine

DMF: Dimethylformamide

DMSO: Dimethyl sulfoxide

DPP: Pyrrolo[3,4-c]-pyrrole-1,4-dione

DSSC: Dye-sensitised solar cell

DT: Dithiophene

DTBT: 4,7-Dithieno-2,1,3-benzothiadiazole

E_b: Exciton binding energy

EDTA: Ethylenediaminetetraacetic acid

E_A: Electron affinity

E_AS: Electrophilic aromatic substitution

E_F: Fermi energy level

E_G: Energy gap

$E_{G,fund}$: Fundamental bandgap

$E_{G,opt}$: optical bandgap

EIS: Electrochemical impedance spectroscopy

E_{OX}: Oxidation potential

EPFL: École Polytechnique Fédérale de Lausanne

EPR: Electronic paramagnetic resonance

EQE: External quantum efficiency

E_{RED}: Reduction potential

ETA: Extremely thin absorber

ETM: Electron transporting material

E_V: Vacuum energy level

FAD: Flavin adenine dinucleotide

FC: Fully-conjugated

Fc: Ferrocene

Fc^+: Ferrocenium

FF: Fill factor

Fl: Flavin

FMN: Flavin adenine mononucleotide

FPF: Furan-Phenyl-Furan

FTO: Fluorine-doped tin oxide

GPC: Gel permeation chromatography

HD: Halogen dance

HOMO: Highest occupied molecular orbital

HTM: Hole transporting material

ICT: Intramolecular charge transfer

I_{light}: Light intensity

I_P: Ionization potential

ISC: Intersystem crossing

ITO: Indium-doped tin oxide

J_{SC}: Short circuit current

K_a: Association constant

LDA: Lithium diisopropylamide

Li-TFSI: Lithium *bis*-trifluoromethanesulfonimide

LUMO: Lowest unoccupied molecular orbital

MA: Methylammonium

McMT: 2-Mercapto-5-methyl-1,3,4-thiadiazole

MIM: Metal–insulator–metal

M_n: Number average molar mass

mp: Melting point

M_w: Mass average molar mass

NBS: N-Bromosuccinimide

NIR: Near-infrared

NMP: N-Methyl-2-pyrrolidone

OFET: Organic field-effect transistor

OLED: Organic light emitting diode

OPV: Organic photovoltaics

P3HT: Poly(3-hexylthiophene)

PTB7-Th: Poly[4,8-bis(5-(2-ethylhexyl)thiophen-2-yl)benzo[1,2-b:4,5-b′]dithiophene-alt-3-fluorothieno[3,4-b]thiophene-2-carboxylate]

$PC_{71}BM$: [6,6]-Phenyl-C_{71}-butyric acid methyl ester

PCBM: [6,6]-Phenyl-C_{61}-butyric acid methyl ester

PCE: Power conversion efficiency

PDI: Perylene diimide

PDI: Polydispersity index

PE: Petroleum ether

PEDOT: Poly(3,4-ethylenedioxythiophene)

P_{IN}: Input power

POLED: Plastic organic light emitting diode

P_{OUT}: Output power

PSS: Polystirene sulfonate

PSSC: Perovskite-sensitised solar cell

PVD: Physical vapour deposition

SCE: Standard calomel electrode

SMOC: Single material organic solar cell

S_N2: Bimolecular nucleophilic substitution

S_NAr: Aromatic nucleophilic substitution

spiro-MeOTAD: 2,2′,7,7′-Tetrakis-(*N*,*N*-di-p-methoxy phenyl-amine)-9,9’spirobifluorene ssDSSC: Solid-state dye-sensitised solar cell

SSSC: Semiconductor-sensitized solar cell

SubPC: Subphthalocyanine

SWV: Square wave voltammetry

QDSSC: Quantum dot sensitised solar cell

$TBAPF_6$: Tetrabutylammonium hexafluorophosphate

TBP: Tri-*tert*-butylpyridine

TCNQ: Tetracyanoquinodimethane

TEMPO: (2,2,6,6-Tetramethylpiperidin-1-yl)oxyl

THF: Tetrahydrofuran

TLC: Thin layer chromatography

TPA: Triphenyl amine

TPD: Thieno[3,4-c]pyrrole-4,6-dione

TPT: Thiophene-Phenyl-Thiophene

TTF: Tetrathiafulvalene

UV: Ultraviolet

VB: Valence band

Vis: Visible

V_{OC}: Open circuit voltage

Chapter 1: Introduction

1.1 Organic Electronics

For over forty years inorganic semiconductors (mostly silicon, germanium and gallium arsenide) have been at the core of electronic devices and leading the way in the era of electronics. Nevertheless, during the last twenty five years, the field of organic electronics, which can be commonly defined as the branch of electronics based on semiconductors made of organic molecules, has emerged as an area of research which has attracted much attention.

The reasons for this interest are identified in the following three important aspects:[1]

1. Technology – Organic semiconductors can be manufactured at low temperatures, unlike modern silicon technologies that require high temperatures (above 1000 °C), which cause problems of mechanical stress due to the different thermal expansion coefficients of the materials constituting the single multilayer device.
2. Versatility - Organic molecules can be easily chemically modified. Furthermore, they are suitable to be deposited on substrates of any material, shape and size, at relatively low costs (even on flexible substrates such as polymeric sheets).
3. Costs - The vacuum deposition techniques, traditionally used for inorganic semiconductors, can be replaced with other deposition techniques, like spin coating or ink-jet printing. This makes organic semiconductors a valuable low-cost technology.

According to the trends, organic electronics is going to revolutionise the market in the following fields:

- power supply: photovoltaic panels, batteries, fuel cells;
- lighting: light devices which absorb less energy than actual bulbs and that can be applied as wallpapers;
- displays for electronic devices (even flexible);
- other components: from sensors, to printed lasers, up to the light detectors.

1.2 Historical background

Although organic chemistry has been at the forefront of many research areas for over

a hundred years, interest in polymers and small molecules with intrinsic conducting or semiconducting properties is very recent.[2] The work done in 1977 by Chiang and co-workers about the high conductivity of doped polyacetylene,[3] has opened an entire horizon for physicists, chemists and the whole scientific community. Following studies demonstrated that the electronics behind polymers – and in general all the organic materials showing conductive properties – are mainly linked to the presence of π-orbitals, which allow to form a "network" of *π-conjugated* molecules, able to increase the interactions among molecules and modify the opto-electronic properties, resulting from these interactions. In 1981, Bell Research Center manufactured the first organic-inorganic heterojunction,[4] in order to understand the working principle of organic semiconductors. The fabrication of a device entirely made with organic materials remained a difficulty to overcome, mainly due to the instability in atmospheric conditions.

During the following twenty years very unexpected and surprising results were achieved, regarding the characterization and synthesis of metallic and semiconducting polymers. During the early 1980s, thanks to the introduction of emerging techniques based on ultra-high vacuum, the fabrication of thick, thin and ultra-thin films of high quality was made possible. Also, in the second half of the decade the introduction of solution self-assembly lead to the manufacture of the first organic devices.

In 1986, Kodak Laboratories created the first organic heterojunction cell with an efficiency of about 1%,[5] thanks to the new deposition techniques, as well as the development of new organometallic synthetic protocols. At that time, laboratory cells of crystalline silicon had a record efficiency of as much as 20 percent after 30 years of development. In 1987, Koezuka and co-workers reported the first organic field-effect transistor able to behave as a current amplifier.[6] In the same period, a first prototype of OLED was made by Kodak.[7] Only three years later, Friend and co-workers introduced polymeric films as organic emitters (POLED).[8] This great work shifted the attention of the scientific community towards organic electronics, leading the Chemistry Nobel Committee to award the 2000 prize to Shirakawa, Heeger and MacDiarmid for their studies on electronic properties of polyacetylene.[9]

1.3 Polyconjugated systems

Organic semiconductors are a class of organic molecules, also called polyconjugated systems, formed by a long sequence of sp^2 hybridised carbon atoms (as well as heteroatoms) with the formation of an extended π system, due to the overlay of p_z orbitals within the molecule (Fig. 1).

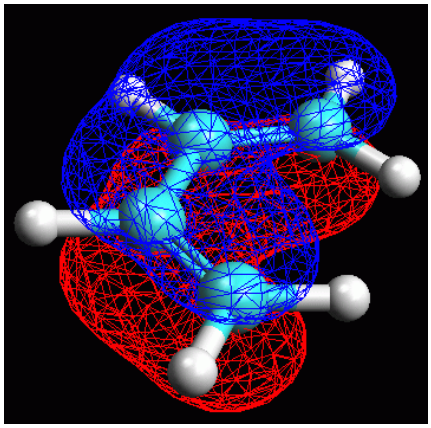

Figure 1 – Graphical representation of p_z orbital overlay in 1,3-butadiene.[10]

So, while the σ orbitals confer planarity, the π orbitals determine the delocalization of the electrons along the molecule. This particular conformation has high impact on physical and chemical properties. For instance, the energy gap between *lowest unoccupied molecular orbital* (LUMO) and *highest occupied molecular orbital* (HOMO), in the polyconjugated systems is usually between 1 and 3.5 eV, while for non-conjugated polymers (like polyethylene), it rises to 8 eV and over. The low gap gives to these molecules the same peculiar properties of semiconductors, both from the optical and electronical point of view. In most of them, in fact, optical transitions in the visible range can be recorded, both in absorption and emission.

In order to apply the band theory, we should refer to infinitely long molecules; in fact, according to the Bloch theorem, an array of ordered atoms leads to the overlay, and degeneration (according to the Pauli exclusion principle), of discrete energy levels which will form continuum energy bands, if the number of atoms of the lattice tends to infinity.[11] Nevertheless, it has been observed that, even for limited conjugation lengths, this theory allows a reasonably accurate description of the physical properties.[12] Thus, we use the same nomenclature employed for inorganic semiconductors for polyconjugated systems, identifying HOMO and LUMO with

valence band (VB) and *conduction band* (CB), respectively, and the *energy gap* (E_G) between them with the forbidden band.

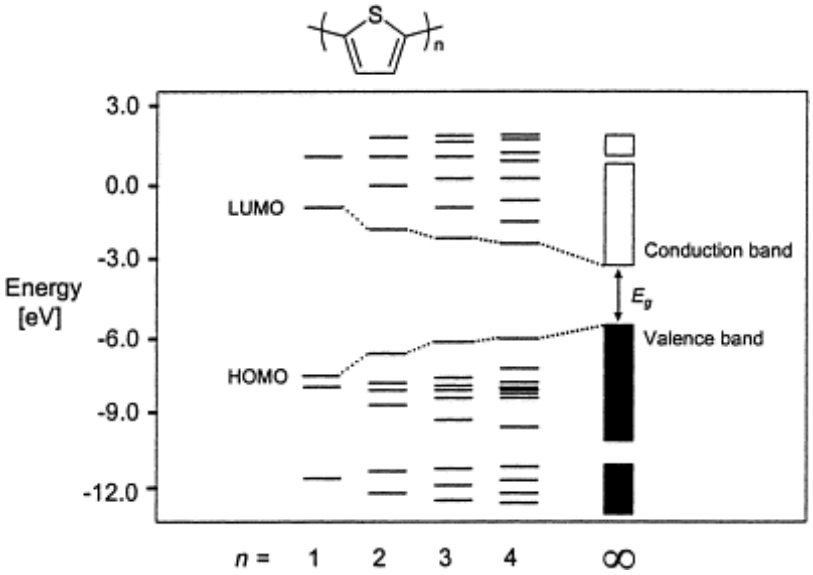

Figure 2 – Electronic levels distribution as a function of the number of conjugated double bonds in polythiophene.[12]

1.3.1 Factors affecting the energy gap

As suggested in Fig. 2, the E_G decreases as a negative function of the extent of conjugation, represented by the number, n, of double bonds of the molecule. However, this trend is not linear, but it tends asymptotically to a set value, given by several energy contributions. This concept was introduced by Roncali[13] in the following equation:

$$E_G = E_{\delta r} + E_{res} + E_{sub} + E_{\theta} + E_{int}$$

These contributions are due to:

- The conjugation length ($E_{\delta r}$), as already mentioned.
- The resonance energy (E_{res}) of the aromatic rings in the molecule, if present.
- The electronic effect of substituents (E_{sub}); generally electron-rich groups stabilise the onset of the oxidation state, thus increasing the magnitude of the HOMO, while electron-withdrawing groups decrease the magnitude of both HOMO and LUMO.[14]
- The planarity of the molecule (E_{θ}); if θ is the dihedral angle between two consecutive conjugated units, the likelihood for the p orbitals to overlap decreases as a function of $\cos\theta$.

- The possible interchain interactions (E_{int}); this effect is often responsible for the variation of E_G of the polymer, in solution and in the solid state, since in the latter case the intermolecular interactions become stronger.

1.3.2 Hopping charge transport

Organic semiconductors show some important differences, when compared with their inorganic counterparts. For instance, the definition of charge transport relies on the band model and cannot be applied for most of the operative conditions (except at low temperatures). For polyconjugated molecules there is a distinction between *electronic gap* and *optical gap*. The former is the energetic distance between HOMO and LUMO, as previously described, while the latter represents the minimum energy to give to the system in order to have the formation of an electron-hole pair, also known as *exciton*.

The exciton can be described as a molecular excited state, represented by an electron-hole system (connected together by a Coulombic electrostatic interaction), which can diffuse through the system, along the molecule or to the surrounding molecules, via a *hopping* charge transport mechanism.[15] The most common type of exciton in organic semiconductors is the *Frenkel exciton*,[16] (Fig. 3a) in which electron and hole are strongly bonded with a binding energy (E_b) of about 0.5-1 eV. This system is generally localised on a single molecule and has a range of the order of 1 nm. In high ordered molecular crystals, or in very aligned polymers, we are likely to observe *charge-transport excitons* (Fig. 3b).[17] In this case, electron and hole are localised on adjacent molecules. Because of the longer distance, their E_b is weaker than that of Frenkel exciton (between 10 and 100 meV).

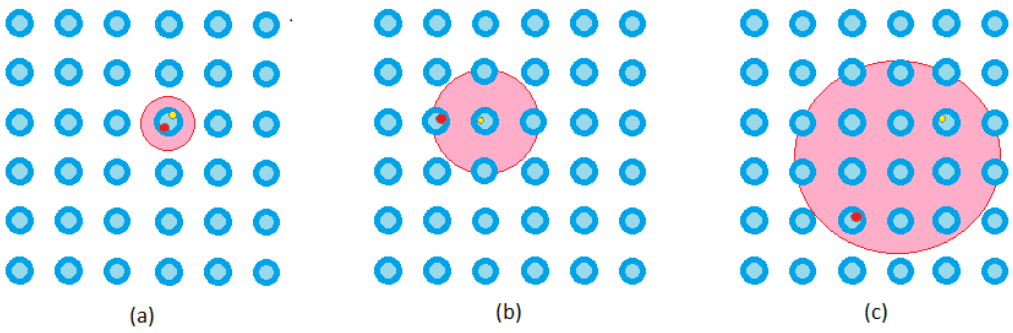

Figure 3 – Graphical representation of the excitons (red and yellow particles) in the crystalline lattice, according to the Frenkel (a), charge-transfer (b) and Wannier-Mott (c) models.

A third type (Fig. 3c) is the *Wannier-Mott exciton* (very common for inorganic semiconductors),[18] in which electron and hole are strongly delocalised within the lattice, with E_b of less than 10 meV.

The exciton localization (and thus E_b) depends on several factors, such as electrical shielding of the material, polarizability of its molecules and their proximity to each other. In order to have current flowing, the excitons must dissociate before they could recombine, and to do that it is necessary to provide them enough energy to break their electrostatic bonds. For an organic photodiode, for instance, the photo-generated excitons are broken by the internal electric field due to the difference of the working functions of the two electrodes.

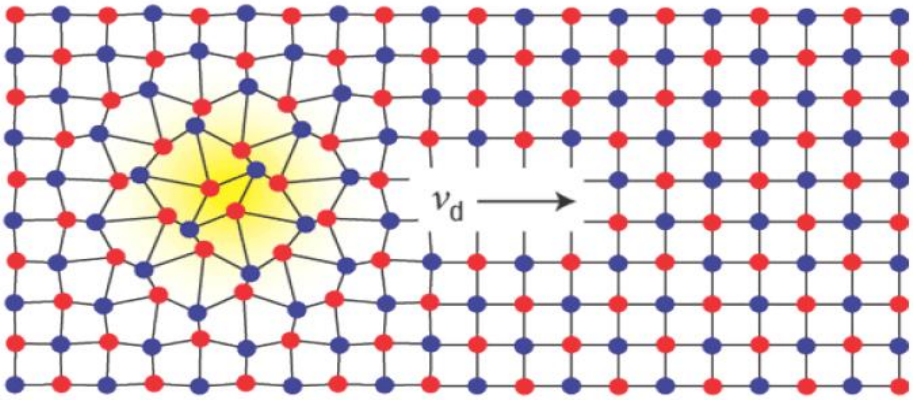

Figure 4 – Graphical representation of a polaron (in yellow), drifting after the application of an external electric field.[19]

The exciton dissociation leads to the formation of two *polarons*, quasiparticles denoting the system of the charge and the lattice distortion induced by the charge. More simply, a polaron is defined as a charge carrier, localised inside the bandgap, which induces an atom displacement in the region of the molecule where the charge is (Fig. 4). This displacement is denoted by the permutation of C–C and C=C alternation. Chemically speaking, a polaron is a radical ion with spin ½, associated to a distortion of the molecule. Because of its nature of charge carrier, the polaron moves through the lattice, with a drift speed, if a potential is applied.[20]

1.4 Technological applications

1.4.1 Organic photovoltaics

Although photovoltaics (PV) is so far the most expansive among alternative renewable energy technologies, there is a continued high interest in this field, due to

the potentially inexhaustible energy provided by sun. Classical PV technology is based on inorganic semiconductors, such as Si for commercially available modules and GaAs for niche applications. Even though these materials offer high efficiencies and durability, they represent the cost-driving factor for the production of PV cells, due to the expensive investment into costly semiconductor processing technologies. On the other hand, the emerging organic semiconductor technology represents a potential cost effective alternative to inorganic semiconductors, because of the ease of manufacture, which does not make use of high temperature furnaces and ultra-high vacuum equipment. For instance, solution processable organic semiconductors would make possible the fabrication of large area PV modules by printing and coating techniques from reel to reel. Furthermore, the design of organic semiconductors can be chemically tailored in order to meet the physical requirements for the various printing techniques.[1]

Altogether, organic photovoltaics (OPV) have many attractive features, such as versatility, flexibility and costs, as previously mentioned. These features are beneficial for commercialisation, however, like its classical counterpart, OPV has to fulfil the basic requirements for renewable energy production. In the energy market the competitive position of every solar technology is mainly determined by efficiency, lifetime and cost (per W_p). The potential of organic photovoltaics has to be judged by these key figures as well. It is quite believable that if organic photovoltaics are able to realise a certain technological profile, then there will be substantial freedom for commercialisation.[1]

As the exciton binding energy (E_b) in organic semiconductors is generally large compared to silicon (see Par. 1.3.2), devices fabricated from single organic semiconductors achieve very low power conversion efficiencies (PCE), due to charge-recombination. In this type of devices, the driving force for the charge splitting and transport (given by the difference in work functions of the two electrodes) is not large enough, resulting in low *external quantum efficiencies* (EQE). The EQE denotes the fraction of photoexcitations that survive both charge separation and transport processes and high EQEs represent a requirement for high PCEs. For inorganic photovoltaic devices EQEs approaching 100% are often achieved. OPV devices made of a single semiconductor layer typically reach EQEs below 1%.

A significant step forward was made by several research groups in 1995.[19, 21, 22] By blending two materials with relative preferences for positive (p-type or donor) and

negative (n-type or acceptor) charges, they observed that the EQE could be enhanced by several orders of magnitude. Those excitons photogenerated at the interface between the two materials are split by a force created by the difference in electron affinities between the two semiconductors. Hence, the device will be more efficient if the interface between the two materials is extended throughout the device, maximising the likelihood of photogenerated excitons to split before recombining either radiatively or non-radiatively. Typically the two materials are blended on a nanostructured scale of about 10 nm and the resulting device is known as *bulk-heterojunction* (BHJ) composites.[23] Using the BHJ concept the EQE has been increased up to 80%.[24] This impressively high value has been obtained for blends of conjugated polymers with fullerenes.

Unfortunately, despite the progresses reported so far, overall PCEs under the normalized solar conditions are still low. For laboratory cells, the highest reported efficiencies exceed 10%,[25-27] while modules touch PCEs of 7–8.5%.[27] There are several issues that can explain the reason of such low PCEs, despite the high EQE. In the first instance, most of organic semiconductors employed for light harvesting applications have their maximum absorption in the visible range, while the solar radiation has the maximum intensity at around 700 nm. Furthermore, the excitation of organic compounds promotes the population of anti-bonding orbitals, increasing the likelihood of decomposition. Finally, in order to have an efficient charge separation and transport, the BHJ device should be optimised from the point of view of the chemical composition of the active layer and of its architecture. It is important, for example, that the energy bands of the two organic semiconductors cascade in order to guarantee charge generation after photoexcitation (Fig. 5c). At the same time, a continuous path for the charge transport to the electrodes must be provided (Fig. 5b). Furthermore, the extension of the interface between the two materials should be maximized in order to increase the number of charge separation processes. This implies that the blend of the two compounds should form a highly complex morphology, with interconnected domains in the nanometer scale to prevent trapping and more ordered regions in the 100 nm scale to guarantee efficient transport channels (Fig. 5a).

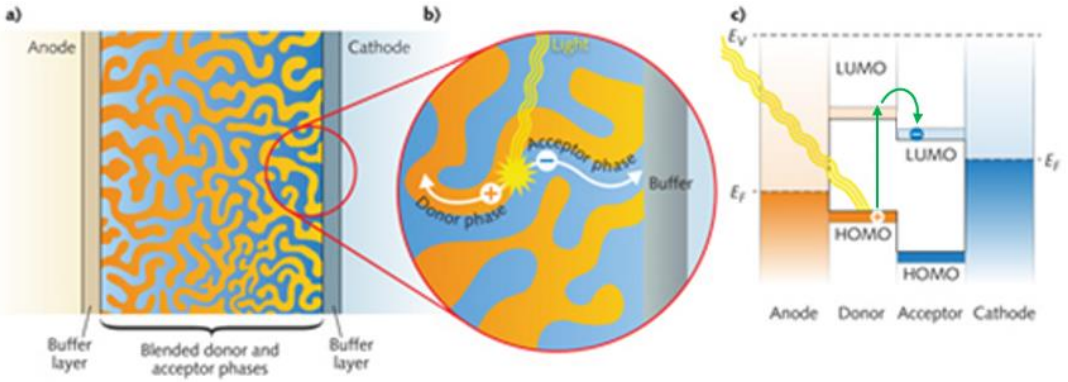

Figure 5 – (a) Cross-section of an ideal bulk-heterojunction cell; (b) light absorption generates electrons and holes that traveling through the donor and acceptor phases; (c) an ideal energy level diagram, E_V represents the vacuum level and E_F represents the Fermi level.[28]

The typical cross-section of BHJ solar cells is depicted in Fig. 6. Indium doped tin oxide (ITO) glasses are typically used as semi-transparent substrates with a transmissivity of about 90% in the visible range and a sheet resistance of about 20 Ω/square.[28]

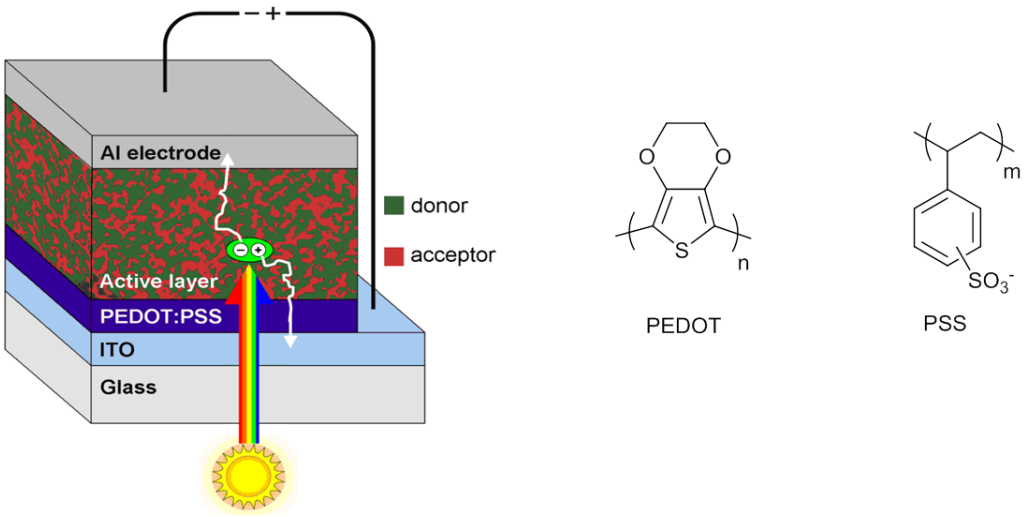

Figure 6 – Typical architecture of a BHJ device (left).[29] Chemical structure of PEDOT and PSS (right).

Poly(ethylene dioxythiophene) doped with polystyrene sulphonic acid (PEDOT:PSS, Fig. 6) is spin-coated on top of the ITO from a water solution, giving a conductive ($\sigma \approx 10^{-3}$ S/cm) layer which prevents short circuits and allows a better extractions of holes from the active layer.[30] The photoactive layer consisting of polymer/fullerene composites is coated on top of the PEDOT to a thickness of about 100 nm from solution. The cathode (typically Al, because of its relative stability in air compared with other low work function metals) is thermally deposited through a shadow mask. The geometrical overlap between positive and negative electrode defines the active area. Compared to conventional inorganic cells, organic solar cells are affected by a

much lower carrier mobility. However, this disadvantage is partly balanced by the strong optical absorption coefficient (> 10^5 cm^{-1}), which allows for a very thin active layers (< 100 nm).[31] Photon absorption can be increased by increasing the thickness of the active layer, but this decreases the fill factor due to a larger serial resistance.

1.4.1.1 Efficiency

Efficiency is the essential parameter for BHJs and, in general, for all kinds of solar cells with respect to energy production and cost. The PCE of a solar cell is calculated by the following formula:

$$PCE = \frac{P_{OUT}}{P_{IN}} = \frac{V_{OC} \cdot J_{SC} \cdot FF}{I_{light}}$$

where V_{OC} is the open circuit voltage, measured in V, J_{SC} the short circuit current density, in A/m^2 , FF the fill factor and I_{light} the incident solar radiation, in W/m^2.[32]

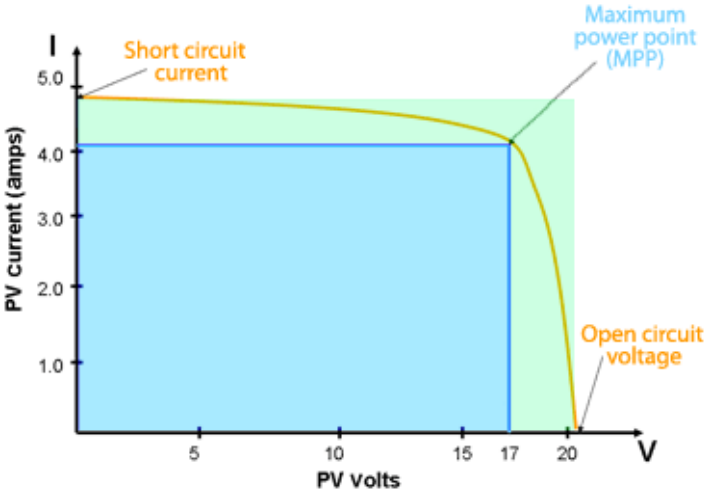

Figure 7 – Typical Voltage-Current diagram of a PV cell.[33]

In order to understand the strategies to optimize the efficiency of BHJ solar cells, a brief discussion about the physical parameters previously reported is necessary.

Open circuit voltage (V_{OC}): It is the maximum voltage provided by a solar cell, which occurs when there is no current flowing in the circuit. There has long been a controversy about the origin of the V_{OC} in conjugated polymer–fullerene solar cells. Following the classical thin-film solar-cell concept, the metal–insulator–metal (MIM) model was applied to BHJ devices. In the MIM model, V_{OC} is simply equal to the work-function difference of the two metal electrodes. The model had to be modified after the observation of the strong influence of the reduction potential of the

fullerene on the open-circuit voltage by introducing the concept of Fermi-level pinning.[34] It has also been shown that the V_{OC} of polymer–fullerene solar cells is affected by the morphology of the active layer[35] and that it can be influenced by the electrochemical potential of the cathode.[36] However, even an extended MIM model was found to be insufficient for a complete explanation of the V_{OC} of BHJ solar cells. Gadisa *et al.*[37] studied the correlation of electrochemical properties of six similar polythiophene derivatives and the open-circuit voltage of polymer-fullerene solar cells using [6,6]-phenyl-C_{61}-butyric acid methyl ester (PCBM) as an acceptor and the same polythiophenes derivatives as donors (Fig. 8). The authors attributed the variation of the photovoltage to variation of the oxidation potential of the conjugated polymer.

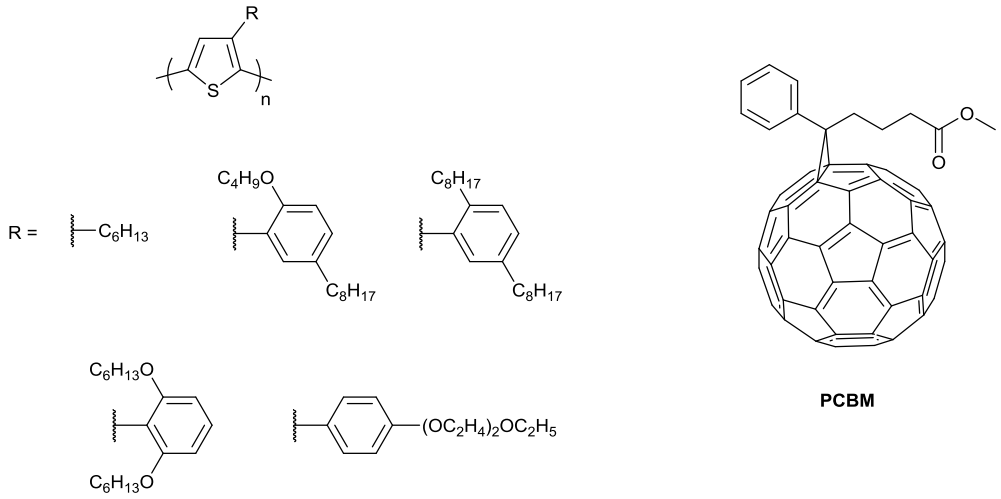

Figure 8 – Chemical structure of PCBM and the conjugated polythiophenes studied by Gadisa *et al.*

Finally, Scharber *et al.*[38] demonstrated the existence of a linear relationship between V_{OC} and the difference between the energy levels of the two materials of the active layer, as follows:

$$V_{OC} = (1/e)(|E^{D}_{HOMO}| - |E^{A}_{LUMO}|) - 0.3V$$

This equation is used to estimate the maximum efficiency of BHJ solar cells.

Short-Circuit Current (J_{SC}): It is the current that flows through the cell when the load resistance is zero. It is strongly affected by the light intensity, I, and by the carrier mobility. A relationship between these three parameters has been found[24, 39] to be:

$$J_{SC} \propto I^{\alpha}$$

with $0.75 < \alpha < 1$, depending on the carrier mobility. For high values of mobility, J_{SC} becomes proportional to I. An improvement of the mobility can be obtained by following two directions: first, the molecules must be as planar as possible, in order to facilitate the charge transport between them; second, in order to facilitate the charge transport between two consecutive molecules (*hopping*), the polymer matrix should have a high grade of crystallinity. In this context, it is important to point out the role of the alkyl chains, attached to the molecule: in fact, if on the one hand, they enhance the solubility of the polymer, giving it a higher molecular weight and a higher degree of crystallinity, on the other hand they can cause the distortion of the molecule and a longer distance of packing.

Fill Factor (FF): Referring to Fig. 7, the FF is defined by the ratio between the area of the sky blue rectangle and that of the green one. Like J_{SC}, it is strongly linked to the mobility of charge carriers. The FF also depends on the internal resistance of the cell. Generally, a high internal resistance, due to a poor adhesion between the film and the metal contacts,[40, 41] reduces the FF value.

1.4.1.2 Push-pull systems

In early studies, regioregular homopolymers, such as poly-3-hexylthiophene (P3HT),[42, 43] were usually applied as donor materials in BHJ solar cells. However, the solar cell devices using these polymers generally delivered limited PCEs, which retarded the practical application of these materials in BHJs. The relatively low PCEs of solar cells based on these polymers have been attributed to their narrow absorption spectra and non-ideal frontier molecular orbitals, which limited both J_{SC} and V_{OC} in the resulting BHJ devices. Therefore, the development of new photovoltaic materials with smaller optical E_G, and suitable HOMO and LUMO energy levels, is crucial to further improve the PCEs of BHJ solar cells.

Donor–Acceptor (D–A) alternating conjugated molecules (also known as *push-pull* systems), were thus extensively developed and have dominated the library of donor materials for solar cells because of their intrinsic optical and electronic properties (including light-absorption ability and energy levels), which can be tuned readily by controlling the intramolecular charge transfer (ICT) from donor to acceptor.

The working principle of band gap and energy level manipulation in *push–pull* conjugated systems can be easily understood from the molecular orbital theory. As

depicted in Fig. 9, the HOMO level of the donor will interact with that of the adjacent acceptor to generate two new occupied molecular orbitals after covalent bond connection of two different moieties; one of them is higher and the other one is lower than the two initial HOMOs before molecular orbital hybridization. Likewise, two new unoccupied molecular orbitals would also be generated after hybridization, where one is lower and the other is higher than the two initial LUMOs.

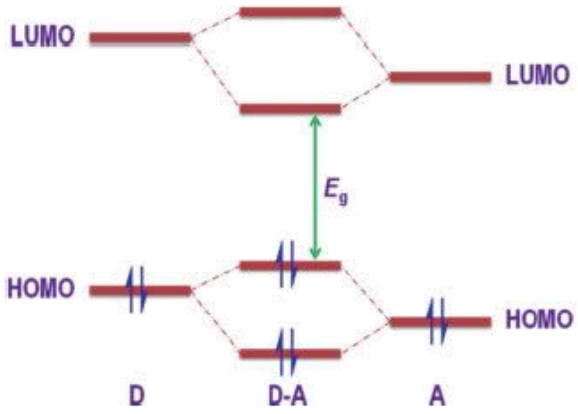

Figure 9 – Molecular orbital interactions of donor and acceptor units, resulting in a narrowing of the band gap in push–pull conjugated copolymers.

Hence, the overall effect of this redistribution of frontier molecular orbitals is the formation of a higher-positioned HOMO and a lower-positioned LUMO in the whole conjugated main chain, and this accordingly leads to the narrowing of the band gap.

Clearly, the rational choice of building blocks, including both donor and acceptor units, is critical in order to meet the requirements for BHJ solar cells applications. Therefore, various aromatic heterocycles were used as building blocks to develop highly efficient donor systems for BHJ solar cells, based on the *push–pull* design. Several reviews have already comprehensively summarized the major classes of push–pull conjugated polymers and oligomers employed as donors in organic solar cells according to the classification of subunits.[44-46] Generally, alkylated fluorenes and carbazoles, benzo[1,2-b:4,5-b']-dithiophene (BDT), cyclopenta[2,1-b:3,4-b']dithiophene (CPDT), etc. are used as donor units, while benzo[*c*][1,2,5]thiadiazole (BT), quinoxaline, thieno[3,4-c]pyrrole-4,6-dione (TPD), pyrrolo[3,4-c]-pyrrole-1,4-dione (DPP), etc. are used as acceptor units for constructing push–pull photovoltaic materials (Fig. 10).

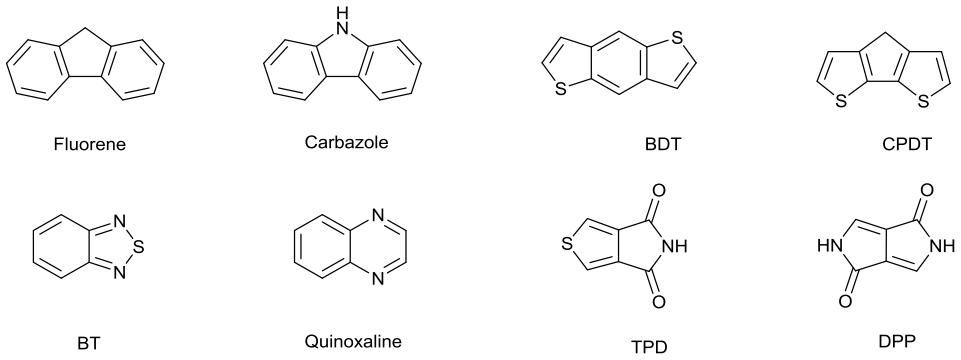

Figure 10 – Chemical structures of some common donor and acceptor units.

OPV devices based on polymer push-pull systems have been dominant and a PCE exceeding 10%[47] has been achieved for a single layer device, using PTB7-Th (Fig. 11) as donor. Nevertheless, small molecules are year by year getting closer in terms of performance, with the record so far reported of 8.1%[48] for a device using compound **1** as donor. The reasons why research is focusing on small molecules is mainly attributable to the easy and reproducible synthesis and purification. Polymers, in fact, are hard to purify and suffer from intrinsic batch to batch variation issues, due to their different polydispersity index.[49]

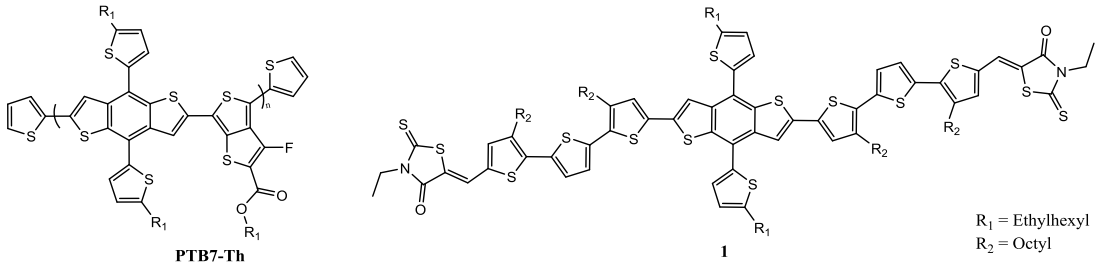

Figure 11 – Chemical structure of compounds PTB7-Th and **1**.

In contrast, small molecules have uniform and defined molecular structure and can be easily purified. The major drawback of small molecules is the poor capability to blend PCBM, which is the standard acceptor for OPVs (see Par. 1.4.1.3), owing to their rigid structure and commonly bad film-forming properties.

1.4.1.2.1 Fine tailoring of push-pull systems

Although the nature of the conjugated backbone dominates the intrinsic electronic properties of the resulting molecule, the fine tuning of the structure is also critical for obtaining high-performing donor molecules.

Functional groups

It has been demonstrated that the incorporation of electron-withdrawing fluorine atoms onto the backbone of conjugated copolymers can effectively lower the energy of the HOMO levels of the resulting molecule and accordingly lead to an enhanced V_{OC} in solar cells.[50, 51] Furthermore, conjugated polymers containing fluorine would have a smaller surface energy, which provides the possibility of getting optimal blend film morphology by selecting proper processing solvents or additives.[52] For example, polymer **2** (Fig. 12) exhibits a close E_G but clearly decreased both HOMO and LUMO levels relative to its non-fluorinated analogue. Leading to a device with a PCE of 7.2% (vs. 5.0% of its counterpart).[53]

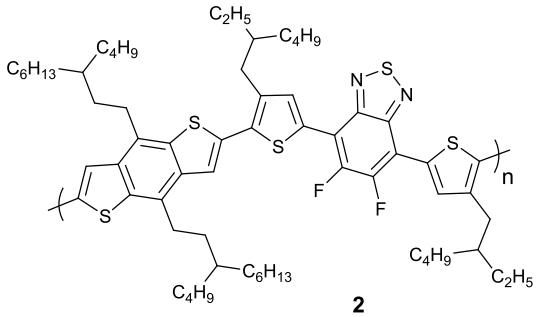

2

Figure 12 - Chemical structure of compound **2**.

Coplanarity

In principle, improving the coplanarity of the molecules and thereby enhancing the intermolecular π-π stacking to form an efficient hopping channel for charge carriers is an effective approach to improve the charge transporting properties of the resulting molecules and thus to improve the overall photovoltaic properties.[54] For example, the hole mobility of the *push–pull* copolymer **3** (Fig. 13) is only 4.21×10^{-6} cm^2 V^{-1} s^{-1}, due to the two pendant substituted thiophenes on BDP retarding the efficient π-π interaction between the polymer chains.

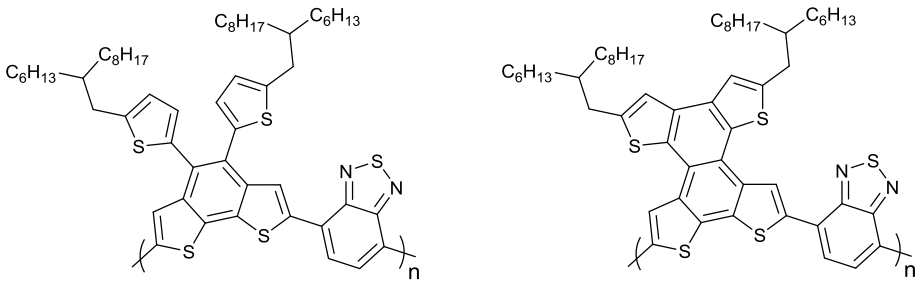

3 **4**

Figure 13 – Chemical structure of compounds **3** and **4**.

After converting the two freely rotating pendant thiophenes into an enlarged planar polycyclic aromatic unit, polymer **4** exhibited a substantially enhanced hole mobility of $1.3x10^{-5}$ cm^2 V^{-1} s^{-1}. The resulting device delivered a PCE of 2.6% (against 0.6% for its counterpart).[55, 56]

Molecular weight

The molecular weight of polymers plays an important role on many aspects, including the processability, thermal transition temperatures, optical properties, charge transporting capabilities, self-organization abilities, etc. This in turn determines the overall device performances. Studies involving a copolymer of fluorene and DTBT[57] demonstrated that the photovoltaic characteristics (PCE, J_{SC} and FF) improved with increasing M_n of the polymer when the M_n is lower than 10 kg/mol. Nevertheless, the photovoltaic characteristics become less sensitive to small changes in the degree of polymerization when the M_n is larger than 10 kg/mol. Further studies on polymer **6**[58, 59] (Fig. 14) revealed that increasing the molecular weight from 9 kg/mol to 38 kg/mol both the photoresponsivity and the charge transporting properties significantly improved. The higher molecular weight polymer exhibited a substantially red-shifted absorption spectrum, and 700 times higher hole mobility. The significant improvement in the charge transporting ability of the higher molecular weight polymer was revealed to be due to the improved polymer chain orientation in solid state.

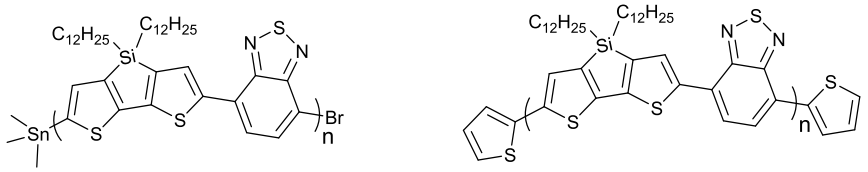

5 **6**

Figure 14 – Chemical structure of compounds **5** and **6**.

End-capping and impurities

It is well known that small concentrations of structural defects in active materials can significantly influence the overall device performance.[52, 60] Generally, the *push–pull* conjugated copolymers synthesised by Pd-catalyzed carbon-carbon coupling reactions possess reactive end-groups, which are potential structural defects. Therefore, understanding the influence of the reactive end-groups on the electronic properties is critical for further design and preparation of new materials. Studies involving the conjugated copolymer **5** (Fig. 14), as obtained immediately after

polymerization and after treatment with chain-end capping thiophene reagents (**6**, Fig. 14), revealed that the end-capped polymer showed improved performances, making the devices less sensitive to the active layer thickness. More importantly, end-capping has an important influence on increasing the thermal stability of the devices. These results clearly indicate that the end-capping of photovoltaic active polymers is indispensable, although there is negligible influence on the optical and morphological features of the BHJ blends.[61] In addition, the impurities can undoubtedly influence the final photovoltaic properties of conjugated polymers.[62, 63] It has been revealed that the decrease of the residual palladium content can significantly enhance the hole mobility of the *push-pull* copolymer, and also lead to enhancements in all photovoltaic parameters (including J_{SC}, V_{OC} and FF) and the overall PCEs in resulting solar cell devices.[64]

Side chains

In the literature there are plenty of examples indicating that the solubilizing alkyl side chains are by no means a negligible factor and also play an important role in many aspects (such as solubility and processability, band gap and energy level, charge transporting ability and self-organization capability, etc.).[65] Generally, long and branched alkyl side chains were the first choice to provide sufficient solubility and to obtain high molecular weights for the resulting polymers.

However, the long and branched alkyl groups may affect the properties of the active molecule in many aspects, such as the intermolecular packing, the interaction with fullerene acceptors and so on. Therefore, a careful selection of the alkyl side chains, including shape, length and position on the conjugated backbone is critical for obtaining high performances materials.

By studying the influence on the photovoltaic properties of different alkyl side chains, in copolymers with identical conjugated backbone, it has been revealed that long and branched side chains would weaken the intermolecular interactions, resulting in an enhanced V_{OC}. On the other hand, short and straight side chains would facilitate the intermolecular interactions, which is beneficial for the J_{SC} but detrimental to V_{OC}. Moreover, it was observed that short and branched side chains (such as 2-ethylhexyl) can lead to a desirable balance between V_{OC} and J_{SC}.[66]

Besides the length and shape, the positions of the alkyl side chains on the conjugated backbone is another important factor that should be carefully considered. Wang *et al.* compared a series of polymers (**7**, Fig. 15) differing on the position of the alkyl side

chains. They found that polymers with alkylated thiophenes in position 3 (R_1) or 3' (R_2) exhibited better performances than those with alkyl chains in position 4' (R_3) in the thiophene rings, likely because of the larger steric hindrance effect, which led to a smaller molecular weight and blue-shifted absorption.[65]

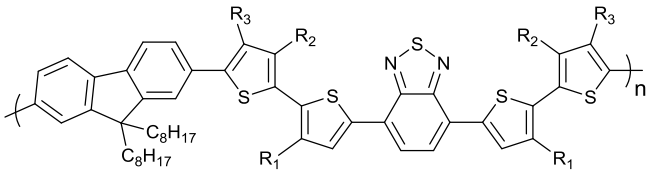

7

Figure 15 – Chemical structure of compound **7**.

More detailed work[67] led to the formulation of a general rule: the introduction of alkyl side chains on positions adjacent to six-membered rings would generate large steric hindrance and lead to poorer photovoltaic performances, while the introduction of alkyl side chains on positions adjacent to five-membered rings would minimize the negative effects.

1.4.1.3 Organic non-fullerene acceptor systems

For many years, N-type organic semiconductors incorporating fullerenes, such as PCBM, have been the most employed for OPVs, largely due to their (i) ability to form favourable nanoscale morphological network with donor polymers; (ii) strong tendency to accept electrons from donor semiconducting polymers; and (iii) high electron mobilities even in composite form.[68]

The development of new, high-performances acceptors for OPVs may add some versatility to the selection of donor/acceptor pair to maximize, for example, absorption across the solar spectrum, or allow the use of polymers with energy levels not suited to fullerene derivatives. Along with the obvious requirements of good photostability and ability to be reversibly reduced, the acceptor must have a high LUMO energy when compared to the donor HOMO to yield a large voltage (see Par. 1.4.1.1, V_{OC} equation), yet the acceptor LUMO must also be sufficiently below the donor LUMO to allow efficient electron transfer. In the case of polymers with very narrow bandgaps, this tuning of the acceptor LUMO can be a delicate task. The acceptor should of course be soluble to allow blending with the donor polymer, but it must also be tuned to phase separate from the donor. To achieve this, there must be some functionality that prevents intimate intercalation of the acceptor into the

lamellar donor polymers. The acceptor must also be tuned to control crystallization: it cannot form domains that are too large, but it should also self-aggregate to an extent that allows facile charge transport.[69]

With these design criteria in mind, a variety of approaches to small-molecule acceptors have been presented in the literature, based on an array of chromophore types. For instance, in 2015, Wang *et al.*[70] reported a PCE of 5.4% for a BHJ device obtained by blending PTB7-Th with a perylene diimide (PDI) derivative (**8**, Fig. 16). In the same year, Cooke *et al.*[71] reported the synthesis of a subphthalocyanine (SubPC) derivative (**9**, Fig. 16) achieving a PCE of 3.5% when blended with PTB7-Th.

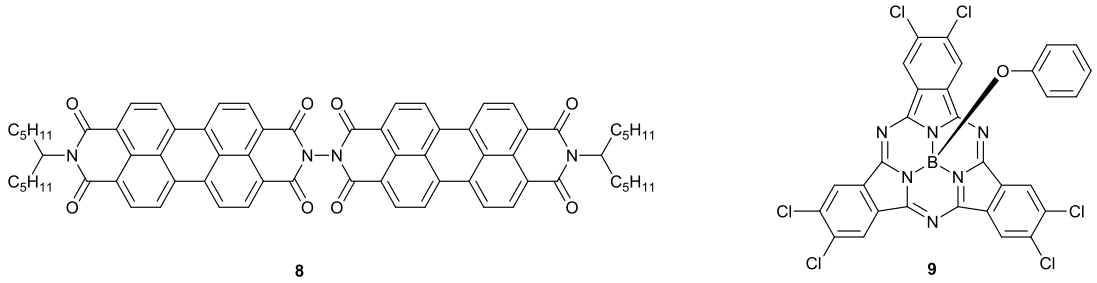

Figure 16 – Chemical structure of compounds **8** and **9**.

Also the slight modification of push-pull systems already employed as donor units has been proved to be effective. For example, McCulloch *et al.*[72] reported the synthesis of a symmetric small molecule (**10**, Fig. 17) containing a fluorene-BT based push-pull system achieving a PCE of 4.1% if blended with P3HT.

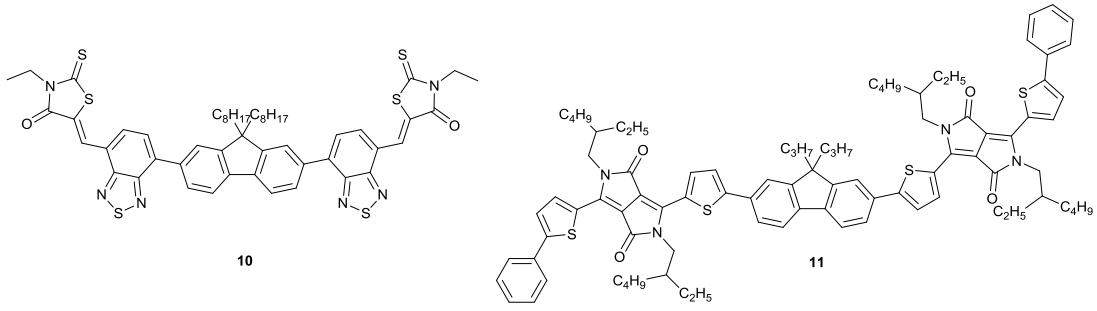

Figure 17 – Chemical structure of compounds **10** and **11**.

Likewise, Chen *et al.*[73] demonstrated that the same DPP-based push-pull system (**11**, Fig. 17) could be used as a donor unit, if blended with PCBM, as well as an acceptor unit, if blended with P3HT, with the BHJ devices achieving a PCE that exceeded 3.0% in both cases.

Clearly, the performances achieved by devices containing non-fullerene acceptor units are still far away from those containing fullerene derivatives. The reason for

such a gap of performances has to be found in the lower currents, due to lower electron mobility, and in a non-perfect blending with the donors, leading to poor FF.

1.4.2 Dye-sensitised solar cells

A completely new concept of solar cell has been developed by M. Graetzel and B. O'Regan in 1991.[74] The so called *Dye Sensitised Solar Cells (DSSCs)*, in fact, are based on a principle reminiscent of photosynthesis, since they are the only PV devices that separate light absorption and charge transportation during the photoelectric conversion. In DSSCs light is absorbed by a monolayer of a dye located at the junction between an *electron*- and a *hole-transporting materials* (ETM and HTM, respectively), where the first is a wide band gap semiconductor material, typically TiO_2 (anatase), while the latter is a redox shuttle, usually a solution of I^-/I_3^- (Fig. 18).

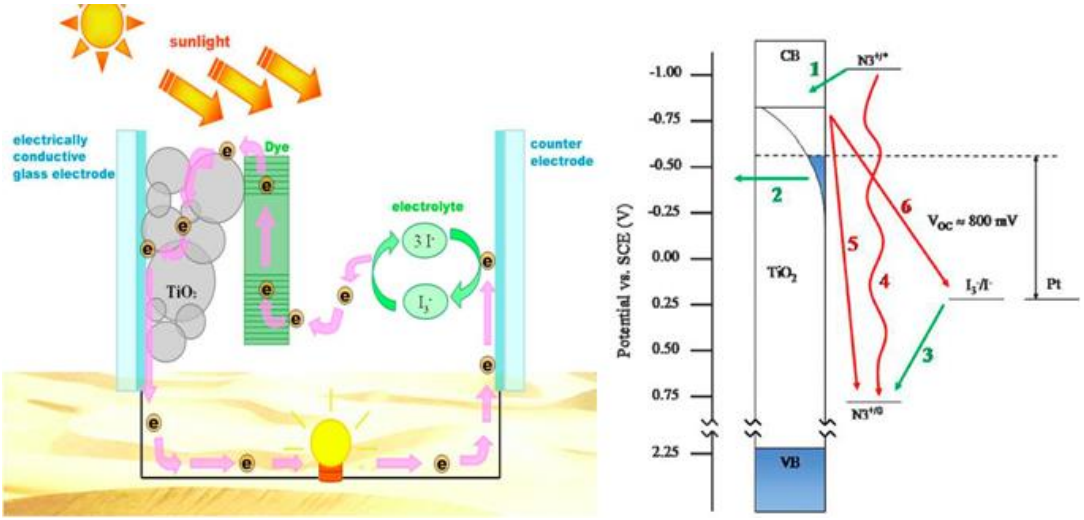

Figure 18 – On the left, typical architecture of a BHJ solar cell.[75] On the right, energy diagram of a prototype device; the green arrows represent the desired processes: electron injection (1), charge collecting (2) and dye regeneration (3), while the red arrows represent the undesired processes: radiative and non-radiative decay (4), recombination (5), electron interception by the electrolytic mediator (6).

The ETM is coated on a transparent photoanode, usually made of *fluorine doped tin oxide* (FTO), while the counter-electrode is generally Pt. On light-irradiation, the dye injects an electron and a hole into the ETM and HTM materials, respectively, generating free charge carriers, which then travel through the nanostructures to be collected as current, flowing through the external circuit.[76]

The PCE of DSSCs depends on optimization and compatibility of each of its components. The basic requirement to satisfy concerns the energy levels of the dye: in particular, it is fundamental that the LUMO level of the dye physically lies close

to the anchoring groups, and energetically above the conduction band of the TiO_2 layer, while the HOMO level must be below the redox potential of the electrolyte couple and physically far away from the TiO_2 layer. In order to increase the PCE, it is also important that the dye has a wide absorption in the visible and near infrared region (J_{SC} optimization), and that the dye is uniformly distributed on the TiO_2 surface and contains a hydrophobic periphery (in order to avoid the contact between the TiO_2 surface and the electrolyte, thus maximizing the V_{OC}).

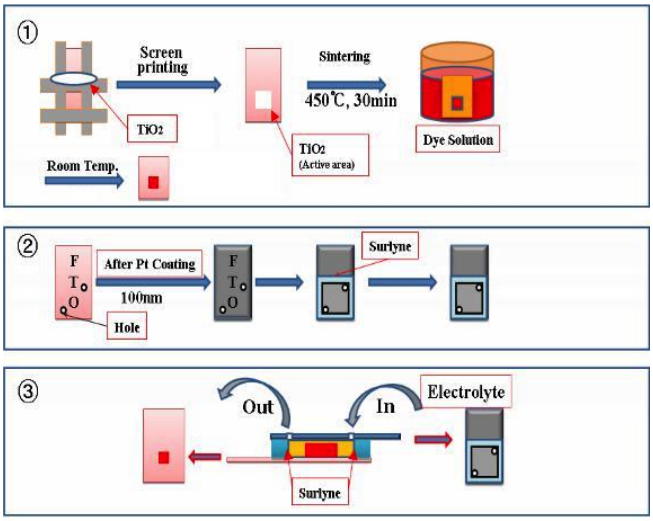

Figure 19 – Fabrication process of DSSCs.[77]

DSSC technology is a viable alternative to conventional silicon based PV, owing to its low cost, ease of fabrication, short energy payback time, flexibility and high efficiency under low and diffuse light. The "trivial" fabrication, in particular, is one of the key factors, as summarised in Fig. 19: a layer of TiO_2 is screen printed onto a FTO substrate. After a short annealing process, the substrate is dipped in a solution containing the dye. The counter-electrode, previously drilled, is prepared via *drop cast*, using a solution of Pt, then the two glasses are joint together, by using a special thermoset (*Surlyn*®) and the electrolyte is injected through one of the drills. Finally the holes are sealed with a sticky tape. Unlike what happens for most of the organic and inorganic semiconductor devices, the fabrication of DSSCs does not need to take place in modified environments, such as clean rooms or glove boxes, and the deposition techniques do not require vacuum.

In the last two decades, great efforts have been made to optimize all the components of the device, reaching PCE values of up to 13%.[78]

1.4.2.1 Metal-free dyes for DSSCs

The first DSSCs were fabricated using Ru-based dyes, such as N719 (Fig. 20). However, although performing very well in the devices, they are often criticized for the use of a platinum group metal, tricky purification and synthesis steps, and for their low molar extinction coefficients. For these reasons, the last decade has witnessed a tremendous progress in the use of organic metal-free dyes,[79] such as C219 (Fig. 20) for DSSCs, which do not contain platinum group metals and exhibit high flexibility of the molecular design along with high molar extinction coefficients. The typical design of metal-free dyes consists of a donor and an acceptor unit linked together via a conjugated *π-bridge*. The acceptor unit is usually functionalized in order to anchor the ETM surface.

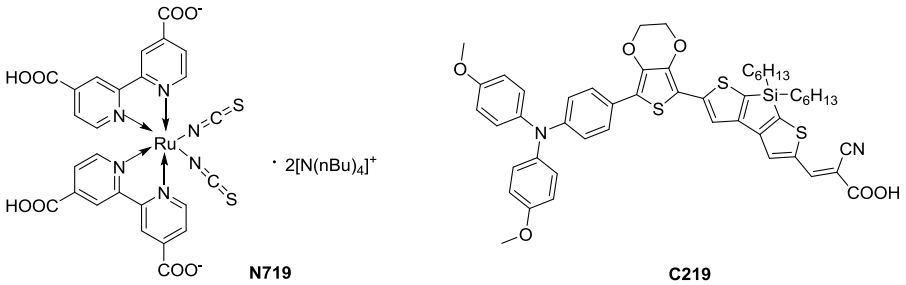

Figure 20 – Chemical structure of two common sensitisers.

The D-π-A configuration facilitates photo-induced charge separation, since the HOMO level is mainly localized on the donor unit, while the LUMO is mainly localized on the acceptor part of the molecule. This spatial orientation not only favors the electron injection but also slows down the recombination between electrons in the conduction band of the semiconductor and oxidized molecules. Additionally D–π–A dyes offer wide possibilities for rational designing and structural modification and this is vital towards achieving efficient light harvesting. Research on the optimization of D–π–A dyes has mainly been focused on:

a. tuning the absorption of the dye to achieve a better match with the solar spectrum and a broader absorption in the near infrared region;
b. minimizing the energy level mismatch between the LUMO level of the dye and the TiO_2 conduction band, as well as the one between the HOMO level of the dye and electrolyte redox potential to avoid potential losses;
c. lowering the charge recombination rate at the TiO_2/electrolyte interface;
d. suppressing dye aggregation;

e. increasing the stability of the dyes under solar harvesting radiation.

Indeed, molecular engineering is the best way to improve the performances of sensitizers and numerous studies have established that chemical modification of the different units which form a D–π–A dye can lead to the achievement of those objectives highlighted above.

Tuning of the donor unit

The choice of a suitable donor group and the optimisation of its structure not only affect the absorption properties of the dye, but can also dictate the charge recombination rate in the device, adjust the energy levels of the sensitizer, avoid dye aggregation and enable stability of the sensitizer.[79] In fact, minor changes in the structure of the donors can lead to notable enhancement in the performance of the dye, and its thermal and photochemical stability. Several organic compounds (Fig. 21) such as fluorene, coumarin, indoline, carbazole, perylene, triphenylamine (TPA), etc. have been employed as donors in D–π–A dyes.

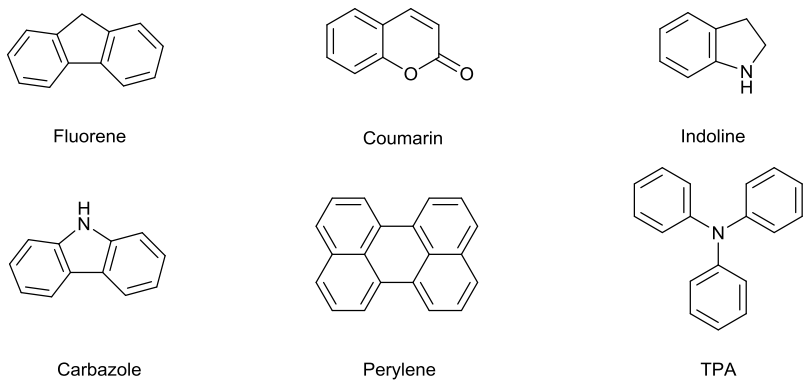

Figure 21 – Chemical structures of some common donor units in metal-free dyes.

TPA, which shows a strong electron-donating ability and hole-transport properties, has been the most widely employed. The most efficient metal-free organic dye so far reported is the phenyldihexyloxy-substituted TPA dye Y123 (Fig. 22) synthesized by Nazeeruddin *et al.*,[80] which exhibits a PCE of 10.3% in combination with a cobalt redox shuttle. TPA has been shown to be one of the most efficient donor moieties: it exhibits high electron-donating ability, mentioned above, and the bulky phenyldihexyloxy groups slow down interface charge recombination.

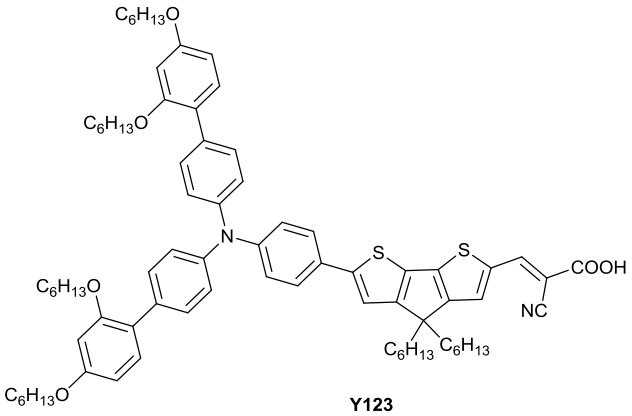

Figure 22 – Chemical structure of dye Y123.

Several strategies have been adopted to enhance the performance of TPA dyes. In order to increase the donor strength Do *et al.*[81] incorporated a planarized donor unit that extended the spectral response of the sensitizer. This effect, together with the increase of lifetime and inhibition of dye aggregation provided by bulky units incorporated into the planar TPA unit, led to a PCE of 8.7% for **12** (Fig. 23). The use of branched TPA sensitizers such as **13** (Fig. 23) with two arylamine moieties at the donor part[82] has also been explored. Branched organic dyes PCE are still below those of TPA dyes or substituted TPA dyes, in all likelihood due to decreased surface coverage. However, the positive influence of these donor groups is the blocking effect, which reduces recombination and consequently improves the V_{OC}.

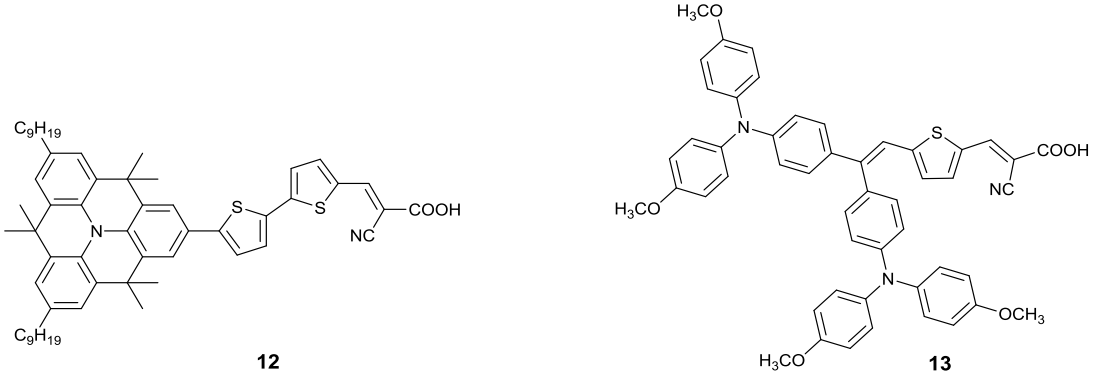

Figure 23 – Chemical structure of dyes **12** and **13**.

A very interesting approach has been the introduction of multiple electron-donating substituents at the arylamine core to form a D–D–π–A structure.[83] It was demonstrated by several groups that these starburst donor groups could lead to a bathochromic shift of the absorption spectra, enhanced absorptivity and better photochemical and thermal-stability over the simple D–π–A configuration, and will help suppress recombination due to extended delocalization of the radical cation. A

PCE of 6.0% was reported by Tian *et al.*[84] with **14** (Fig. 24), which incorporates additional carbazole moieties onto the outside of the donor group to facilitate charge separation and thereby decrease recombination between the conduction band electrons and the oxidized sensitizer. The same group[85] observed a bathochromic shift of the absorption spectra when replacing a triphenylamine unit by indoline in the donor moiety, which is an indication of the more powerful electron donating capability of the latter. The PCE of the resulting device, which incorporates dye **15** (Fig. 24), was 7.4%.

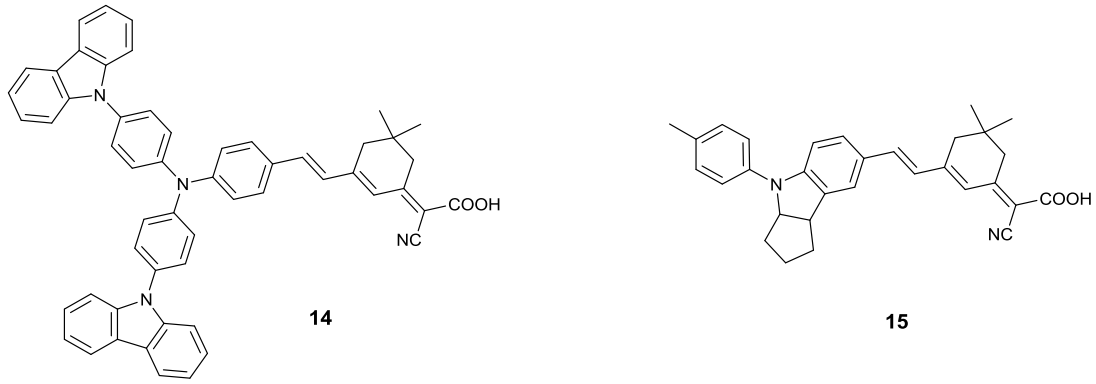

Figure 24 – Chemical structure of compounds **14** and **15**.

Indoline dyes are one of the most efficient types of organic dyes due to their high absorption coefficient to result in high photocurrents. For example, Uchida *et al.*[86] reported an indoline dye (**16**, Fig. 25) with an absorption coefficient (68700 $M^{-1}cm^{-1}$ at 541 nm) five times higher than that of the conventional benchmark N719 dye, and with a 6.1% PCE for the resulting device. With the introduction of a second rhodamine network to the dye framework[87] (**17**, Fig. 25), which contributes to red shift the absorbance, the group succeeded in increasing the PCE to 9.5%.

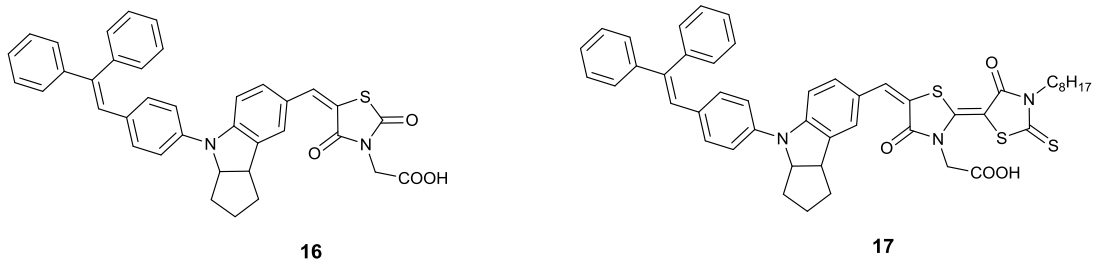

Figure 25 – Chemical structure of compounds **16** and **17**.

As mentioned above, carbazole has also been employed as an electron donor in D–π–A dyes. With the aim of structural optimization of carbazole dyes, several attempts have been made. Hara *et al.*[88] showed that the incorporation of hexyloxyphenyl

substituents to the carbazole unit increased the electron lifetime and led to better V_{OC}. A PCE of 8.1% was obtained with the use of **18** (Fig. 26).

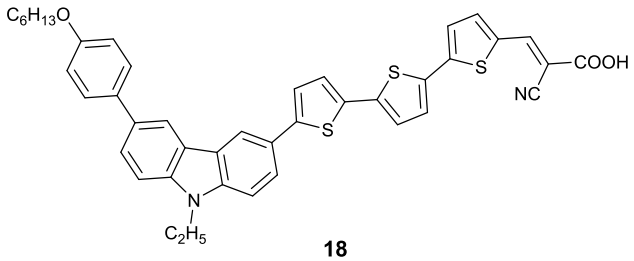

18

Figure 26 – Chemical structure of compound **18**.

Tuning of the π-bridge

The work of Yanagida and Hara[89] based on phenyl dyes, demonstrated that the absorption spectra and redox potential of the sensitizers could be controlled by expansion of the π-conjugation length by introducing double or triple bonds. Since then, a huge number of modifications of the π-conjugation has been carried out and it has been observed that the spacer plays a key role in the final performance of the dye. Both electron-rich (benzene, thiophene, fluorene, furan, pyrrole, etc.) and electron-deficient units (BT, 2,20-bithiazole, quinoxaline, benzotriazole, DPP, pyrimidine, pyridine, 2-thiazole, etc.) have been incorporated to the π-bridge. The linker must effectively relay electron density from the donor to the acceptor, facilitating charge separation upon excitation. With the introduction of various linkers between the acceptor and the donor, the HOMO and LUMO levels of the sensitizer can be tuned, extending the major absorption peak of the sensitizer and maximizing sunlight absorption.[90] Moreover, other effects which determine the performance of the dye (such as suppression of dye aggregation on the semiconductor, redox potential optimization of the sensitizer, or lowering the recombination rate) can also be achieved by fine tuning of the conjugated bridge. Usually, the extension of the bridge significantly contributes to a red shift in the absorption spectra of the dyes. The best moieties for the π-conjugated bridge very frequently contain thiophene units, which exhibit excellent charge-transport properties. Hagfeldt *et al.*[91] observed that the incorporation of thiophene to extend the number of π-conjugations in a TPA dye prompted an enhanced spectral response. With reference to the 6.9% efficiency of **19** (Fig. 27),[92] with a single thiophene in the π-bridge, successive improvements of the performances have been achieved, by replacing the thiophene with one thienothiophene (**20**, Fig. 27),[93] or two (**21**, Fig.

27),[94] delivering 7.5% and 8.0% efficiency respectively. It was also observed that, beside the bathochromic shift, the molar extinction coefficient increases with the extension of the π-conjugation (i.e. **21** > **20** > **19**). Wang *et al.*[95] incorporated 4,4-dihexyl-4H-cyclopenta[2,1-b:3,4-b0]dithiophene (CPDT) unit as π-segment in the TPA dye **22** (Fig. 27) achieving a twice higher molar absorption coefficient (62700 $M^{-1}cm^{-1}$ at 555 nm) in comparison to the analogue with a dithiophene (DT) unit as linker, with PCE of 8.9% and 7.1%, respectively.

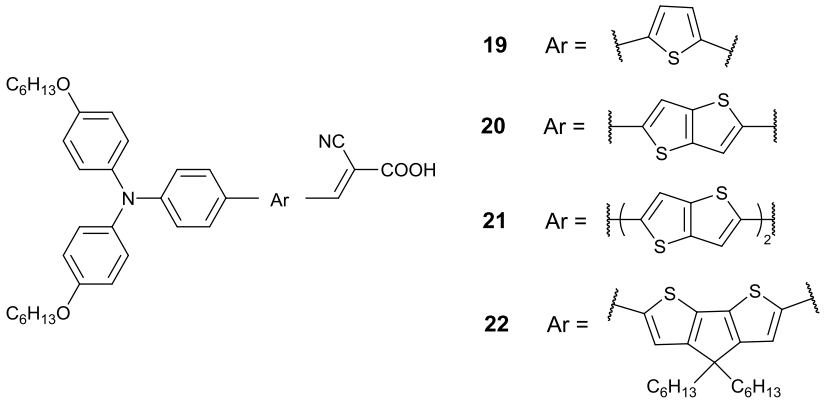

Figure 27 – Chemical structure of dyes **19** to **22**.

Other electron-rich units different from thiophene, i.e. benzene, fluorene, furan and pyrrole have been also employed in order to improve the performance of D–π–A dyes. It was found that linkers such as furan or fluorene gave better PCE than for thiophene, under the same conditions. However, PCE obtained with these spacers are still below the record PCE achieved with thiophene derivatives, which gave the way for further optimization and benefiting from their potential.

Several studies on the design and optimization of metal-free organic dyes have been focused on the introduction of bulky groups such as alkyl chains or aromatic rings on the spacer segment with the aim of inhibiting dye aggregation as well as increasing the electron lifetime. Nakamura *et al.*[96] reported a PCE of 7.1% with the arylamine **23** (Fig. 28) based on a bulky linked moiety made of a carbon-bridge phenylenevinylene with octyl side chains. As a consequence of suppression, charge recombination voltages close to 0.8 V with an iodide/triiodide redox shuttle were obtained for this dye. Hara *et al.*[97] synthesised several carbazole sensitizers with a π-conjugation based on thiophene. They observed that the presence of n-hexyl chains linked to the thiophene units lead to an increase of the lifetime of **24** (Fig. 28) with respect to **25** (Fig. 28). Due to this longer electron lifetime, the former exhibited a V_{OC} significantly higher (0.75 V) than the latter (0.67 V). The authors claimed that

these hexyl chains also contribute to the stability of the dye, thus increasing the tolerance to the presence of water in the electrolyte and therefore avoiding possible water induced desorption of the dye.

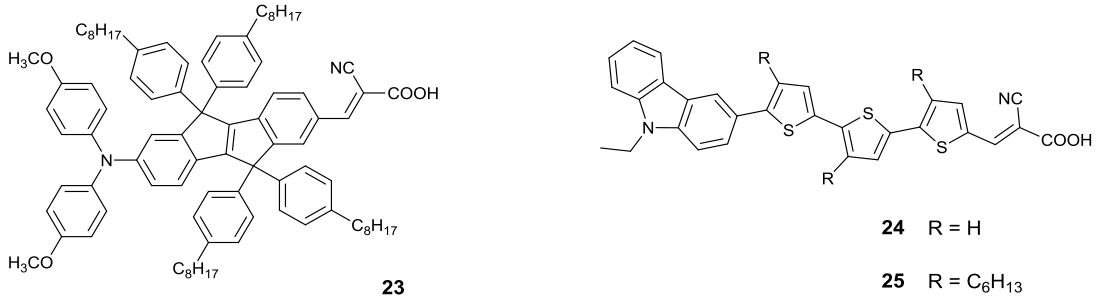

Figure 28 – Chemical structure of dyes **23** to **25**.

The incorporation of low-band gap chromophore units, such as benzothiadiazole, phtalimide, quinoxaline and DPP in the bridging framework has appeared as a very interesting strategy for molecular engineering. A structure of the type D–A–π–A is formed, where the additional unit is expected to act as an electron trap to separate charge and to facilitate migration to the final acceptor.[98] This incorporation provides better long term stability under light soaking of the sensitizer and often leads to panchromatic absorption. Zu *et al.*[99] obtained a PCE of 9.0% for indoline **26** (Fig. 29) which incorporates a benzothiadiazole unit in the π-bridge. More importantly, this dye has demonstrated stability for 500 hours in combination with an ionic liquid based redox shuttle. Qu *et al.*[100] reported the synthesis of the DPP-based dye **27** (Fig. 29), which could deliver a relatively low PCE of 3.4%, attributed by the authors to high dye aggregation and electron recombination. Adding 1.5 mM of chenodeoxycholic acid (CDCA) partly resolved the aggregation issue and raised the PCE to 4.1%

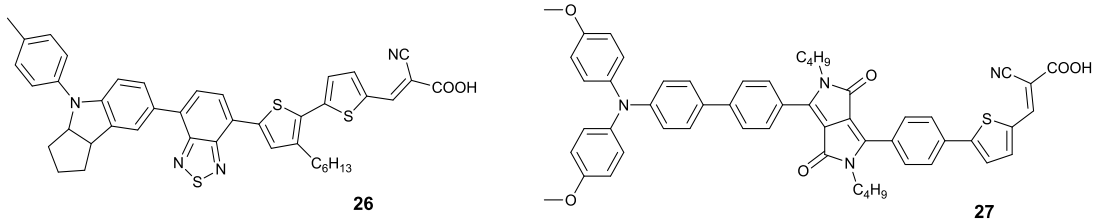

Figure 29 – Chemical structure of dyes **26** and **27**.

Looking for a better exploitation of the absorption towards the near-infrared (NIR) light, some groups focused their research on the incorporation of small push-pull structures in the conjugated bridge of the dyes. For instance, Zhang *et al.*[78] reported the synthesis of two dyes (**28** and **29**, Fig. 30) incorporating a

cyclopentadithiophene–BT unit, delivering PCEs of 8.9% and 10.0% respectively.

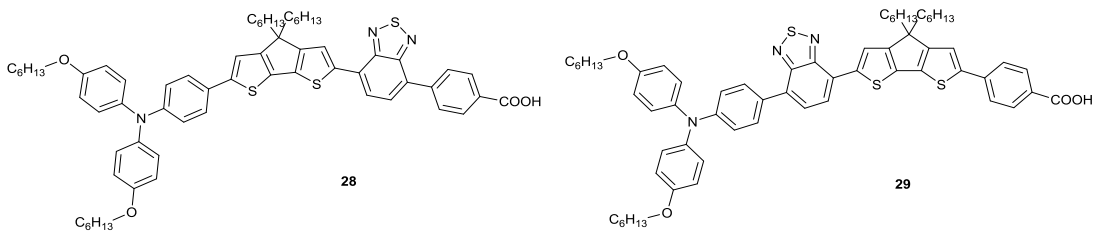

Figure 30 – Chemical structures of dyes **28** and **29**.

1.4.3 Perovskite Solar Cells

Despite the efforts made in the last decade, organic dyes for DSSCs have inevitably been limited by their low light-harvesting ability and poor lifetime stability. Another issue with DSSCs is the liquid electrolyte, which, although on one hand provides advantages from an economic and manufacturing point of view, on the other hand poses a toxicity hazard and makes the cells susceptible to leaks. Particularly the liquid HTM represents the major drawback for the industrialization, for this reason, solid-state DSSCs (ssDSSCs) have also been investigated, where the liquid electrolyte was replaced by solid HTMs, such as 2,2′,7,7′-tetrakis-(*N*,*N*-di-p-methoxy phenyl-amine)-9,9'spirobifluorene (spiro-MeOTAD, Fig. 31) and P3HT.[101, 102]

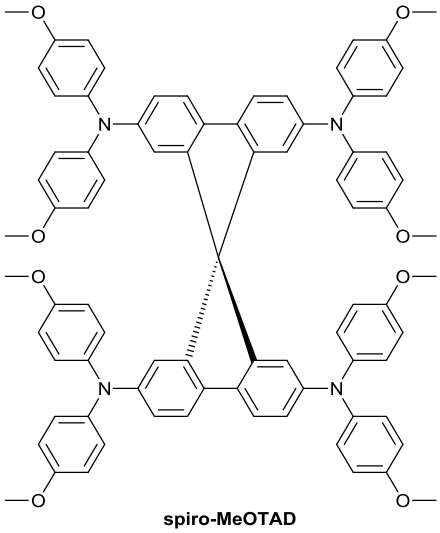

Figure 31 – Chemical structure of spiro-MeOTAD.

However, ssDSSCs suffer from faster electron recombination dynamics between electrons in the TiO_2 and holes in the solid HTM,[103] which results in the low efficiency of ssDSSCs. A solution for this problem would be an increase of the thickness of the sensitizer layer (which would consequentially increase the rate of

electron-hole recombination within the dye), or the replacement of the organic dye with a sensitizer with a much higher molar extinction coefficient. Inorganic absorber materials were investigated leading to several families of semiconductor-sensitized solar cells (SSSCs), such as extremely thin absorber (ETA) solar cells,[104] quantum-dot-sensitised solar cells (QDSSCs),[105] and the more recent and promising perovskite solar cells (PSSCs).

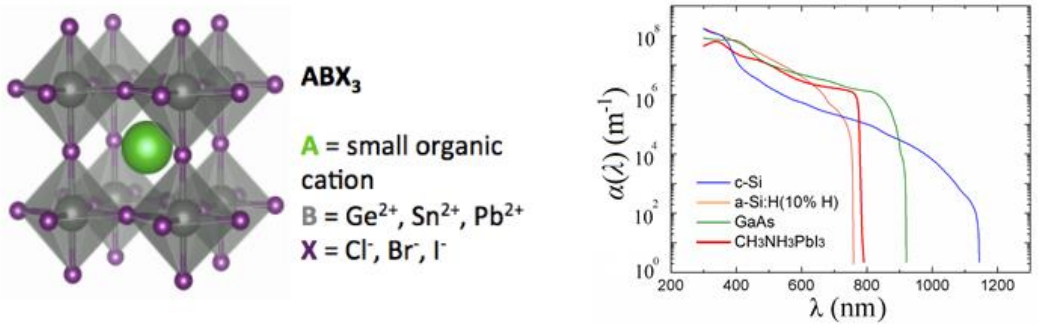

Figure 32 – On the left: crystallographic distribution of perovskite. On the right: molar extinction coefficient of perovskite, compared with other common adsorbers for PV.[106]

Perovskite is a mineral, discovered by the Russian Lev Perovski at the end of the 19th century, and gives its name to a wider class of minerals with the same ABX_3 mineral structure (Fig. 32), where X can be oxygen, carbon, nitrogen or a halogen, A cation is occupied in a cubooctahedral site and B cation is occupied in an octahedral site. For the organic–inorganic halide perovskites of present interest, the larger cation A is organic, generally methylammonium (MA). The halogen is commonly iodine, although bromine, chlorine and mixtures of the three are also used, and the B cation is lead, although less efficient lead-free cells are currently under development.[107] In 2006, Miyasaka *et al.*[108] first reported $MAPbBr_3$ cells with an efficiency of 2.2%. In 2009, by replacing bromine with iodine, the same group managed to increase the efficiency to 3.8%.[109] For their devices they used an organic electrolyte containing lithium halide and the corresponding halogen formed the HTM. By applying TiO_2 surface treatment prior to deposition, Park *et al.*[110] realised an efficiency of 6.5% in 2011, but the perovskite layer dissolved in the electrolyte, resulting in a rapid degradation of performance. The final input to the development of perovskite solar cells came one year later from Grätzel *et al.*[111] who introduced spiro-MeOTAD as HTM. When dissolved in an organic solvent, spiro-MeOTAD penetrates nanoporous TiO_2, leaving only solute molecules after solvent evaporation. Spiro-MeOTAD not only improved the stability, as expected, it also boosted the reported efficiency to

9.7%. Since then, almost every month improvements in the performances were reported, till December 2015, when Dyesol LTD announced the new record of 21.0%, achieved by Grätzel and collaborators.[112]

What gives perovskite high efficiency is its extraordinary wide absorption, covering all the UV and Vis spectrum, up to 800 nm, with a molar extinction coefficient between 10^5 and 10^6 cm^{-1} (Fig. 32). Furthermore, perovskite, as common inorganic absorbers, has high intrinsic carrier diffusion length of ~1 μm, effective mobilities of roughly 10 $cm^2 \cdot V^{-1} \cdot s^{-1}$, [113] exciton E_b of 2 meV,[114] and increased thermodynamic and optical stability. The major drawbacks to sort out, in order to make the commercialisation of PSSCs feasible, are related to the low stability of perovskite to moisture, which adds an extra manufacture cost, and some issues related to HTM. From the point of view of the manufacture, PSSCs are not as easy to make as DSSCs, as a moisture-free environment must be ensured. Fig. 33 shows one of the most common techniques employed.

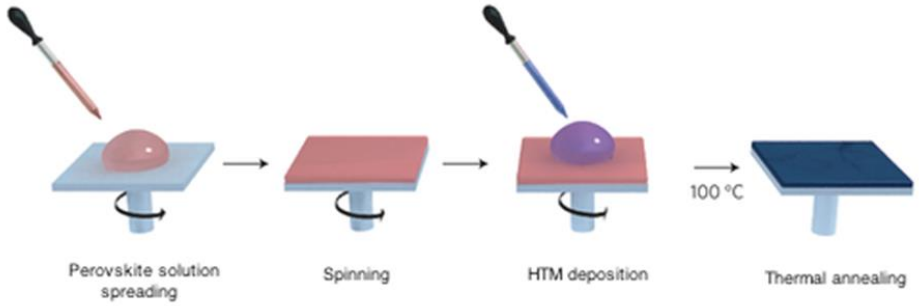

Figure 33 – Fabrication process of a PSSC.[115]

A solution containing the perovskite material, in DMF, is *spin coated* on a FTO layer, previously coated with a mesoporous TiO_2 layer. Afterwards, the HTM solution is *spin coated* on the perovskite layer and thermally annealed. Alternatively, the perovskite is made *in situ*, by sequentially spin coating two equimolar solutions of PbX_2 and MAX. Finally, a gold back contact is deposited *via physical vapour deposition* (PVD).

1.4.3.1 Organic HTMs

Although it has been demonstrated that spiro-MeOTAD is the most effective small molecule for PSSCs, the spiro-bifluorene core is relatively expensive due to its tedious synthesis (and purification) and low hole mobility (10^{-4} $cm^2 \cdot V^{-1} \cdot s^{-1}$), which results in high interfacial recombination losses.[116] The solution for such a mobility

issue was found by adding some dopants, usually tri-*tert*-butylpyridine (TBP), lithium *bis*-trifluoromethanesulfonimide (Li-TFSI) and other cobalt complexes. On the other hand, this doping is very sensitive to the experimental conditions, and the performance can significantly drop by a small variation of the amount of doping agents. Another issue that the dopants are likely to contribute to is the poor stability of PSSCs.[117] Thus, many research groups have focused on replacing spiro-MeOTAD with alternative low-cost and high efficiency HTMs. The basic requirement for an organic material to be a potential HTM for PSSCs is related to the position of the energy levels. In order to facilitate hole transfer processes from the perovskite layer, it is essential in fact that the HOMO level of the HTM is slightly superior to that of the perovskite, providing the suitable driving force for charge transfer, as shown in Fig. 34. Furthermore, its LUMO level should be significantly higher than that of the perovskite absorber, in order to block electron transfer to the back contact.

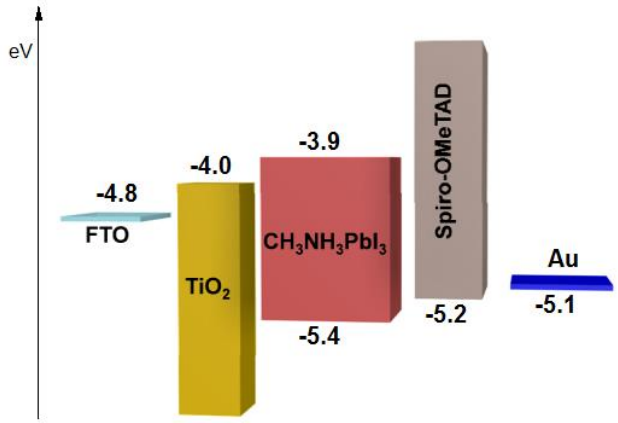

Figure 34 – Energy diagram of a PSSC with Spiro-MeOTAD as HTM.

Another key factor to have good performances is the affinity of the HTM for the perovskite surface. This implies the ability to form uniform and homogeneous films, via *spin coating*, using solvents that do not dissolve the perovskite layer. It is also desirable that the HTM is hydrophobic and moisture stable, in order to protect the perovskite layer, and that its optical transmission is maximum at the maximum of perovskite absorption (between 400 and 750 nm), so that most of the incident photons can be absorbed in the photo-active absorber. In 2013, Seok *et al.*[118] reported three novel HTMs having pyrene (**30**, **31**, and **32**, Fig. 35) as core and changing just in the number of peripheral *N*,*N*-di-methoxyphenyl amines. They found out that the electron donating effect of the methoxy groups enhanced the electron density, which modifies HOMO and LUMO energy levels.

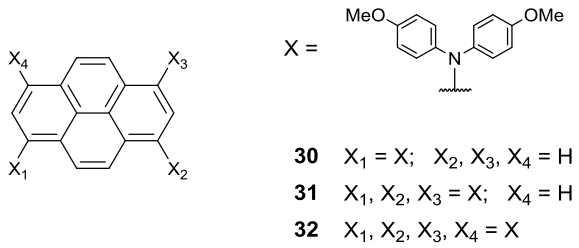

Figure 35 – Chemical structure of compounds **30** to **32**.

In particular, the HOMO levels were found to be –5.41 eV, –5.25 eV and –5.11 eV, respectively. As a consequence, devices fabricated with HTM **31** and **32** delivered a PCE of 12.3% and 12.4% respectively (against 12.7% obtained for Spiro-MeOTAD, under similar fabrication conditions), while, due to insufficient driving force for hole injection, **30** exhibited a lower PCE (3.3%). The performances of these HTMs are limited by the absorption maxima, centered at 420 nm, 470 nm and 490 nm, respectively.

Li *et al.*[119] reported two TPA-based HTMs (**33** and **34**, Fig. 36) with a butadiene π-conjugated system; these two HTMs have suitable HOMO levels in comparison to $CH_3NH_3PbI_3$ and hole mobilities about one order of magnitude higher than that of spiro-MeOTAD, but the absorption maxima are centered at 451 and 471 nm respectively. As a consequence, they showed comparable PCE (11.3%, 11.6%, respectively) with the one obtained with spiro-MeOTAD, under same conditions (12.1%).

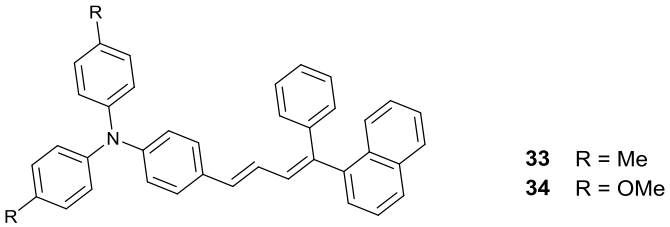

Figure 36 – Chemical structure of compounds **33** and **34**.

Lee *et al.*[120] reported the synthesis of a carbazole-based HTMs (**35**, Fig. 37) with electronic and optical properties comparable with the ones of spiro-MeOTAD. The devices made with **35** as HTM showed a PCE of 14.8%, slightly lower than the one of spiro-MeOTAD (15.2% under the same fabrication conditions). A similar approach was used by Getautis *et al.*,[121] who synthesised a very simple carbazole based molecule (**36**, Fig. 37), which could deliver a PCE of 16.9%, with FK209 (a Co(III) complex) as only dopant.

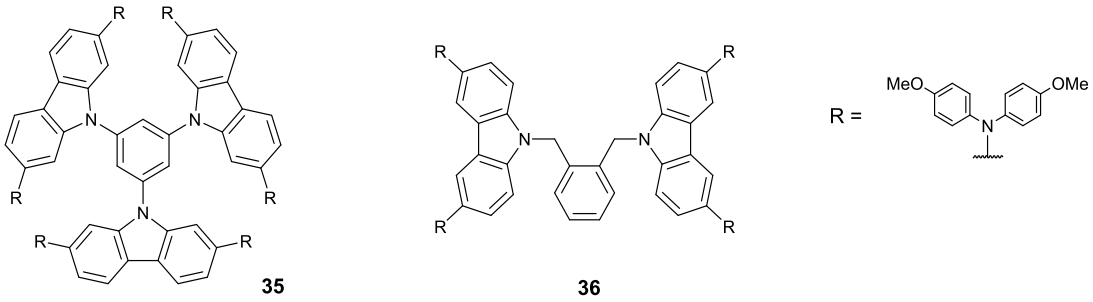

Figure 37 – Chemical structure of compounds **35** and **36**.

Chapter 2: Synthesis of Flavin derivatives

2.1 Introduction

In 1879, riboflavin was first described by Blyth[122] as a bright yellow pigment, isolated from cow milk and named lactochrome. The interest started to grow when, during the late 1920's and early 1930's, the same molecule was obtained from a variety of natural products and it was realised that riboflavin constitutes the vitamin B_2.[123] It was finally synthesised, in 1934, by Kuhn *et al.* who confirmed the molecular structure (Fig. 38).[124] Flavins owe their name to the intense yellow colour (lat.: *flavus* – yellow) that some of them have and which is given by the isoalloxazine unit.

Flavins are natural redox-active molecules that serve as enzyme cofactors, performing redox reactions and working as electron shuttles in the metabolic cycle.[125-127] Riboflavin, for instance, acts as a photoreceptor pigment[128] and, at the same time, takes part in other natural processes, like DNA repair by photolyase[129], bacterial luciferase[130] and the photoresponse of fungal sporangiophores.[125, 131]

Two forms of riboflavin which can commonly be found in nature are flavin adenine dinucleotide (FAD) and flavin adenine mononucleotide (FMN, riboflavin-5'-phosphate, Fig. 38). Enzymes containing FMN and/or FAD catalyse many of the one- and two-electron oxidation/reduction reactions critical to the four major energy metabolism systems (photosynthesis, aerobic respiration, denitrification, and sulfur respiration).[132] Today hundreds of flavoprotein enzymes containing predominantly non-covalently bound FAD or FMN are known.[133]

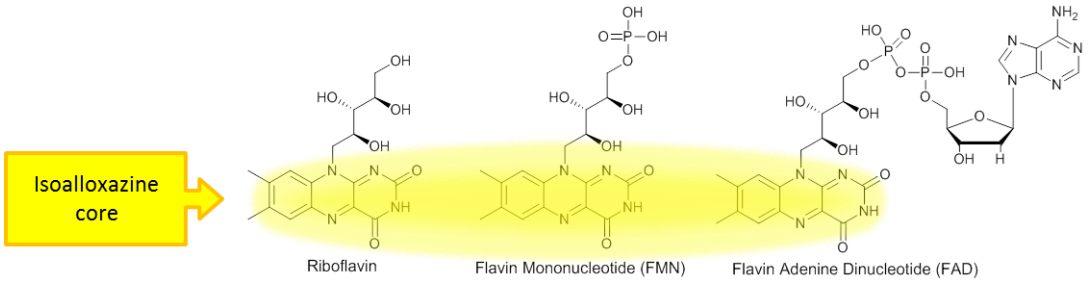

Figure 38 – Structure of three of the most common natural flavins: riboflavin, flavin mononucleotide and flavin adenine dinucleotide.

Riboflavin and its natural derivatives are yellow compounds and hence they can absorb visible light with a maximum absorption in the blue range.[134] The great

strength of flavins is their chemical stability in a wide range of potentials. In fact, they can exist in three redox states: oxidized, one-electron reduced (as semiquinone) or two-fold reduced by two electrons, and each of these redox states has three different protonation states in aqueous or protic medium (Fig. 39).[131]

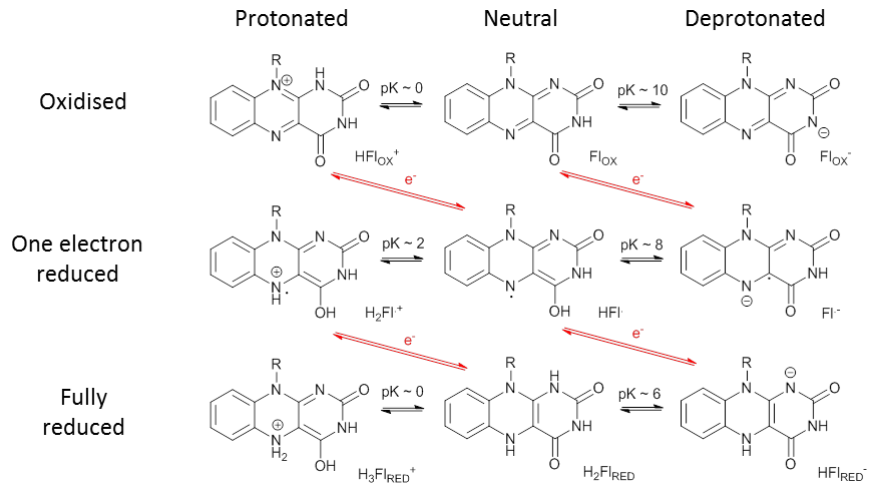

Figure 39 – Different redox and protonation states of flavins (10-substituted isoalloxazines).

As depicted in Fig. 39, the redox chemistry occurs at the central diazabutadiene of the central isoalloxazine head group. Flavins can be tuned by functionalizing the N(3) and N(10) position and likewise by changing the functionality on the phenyl ring (positions C(6) – C(9)). This would lead to a dramatic change in the redox properties, as well as their absorption and chemical reactivity. These properties are also strongly correlated with the non-covalent interactions, such as hydrogen bonds, and the nature of the surrounding media (see Par. 2.2).[135] Riboflavin, for example, undergoes a two-electron reduction process in water and protic solvents at about –0.51 V (*vs.* Fc/Fc^+),[136] while two different one-electron reductions at –1.18 V and –1.87 V (*vs.* Fc/Fc^+) are observed in aprotic solvents.[137]

2.2 Properties and applications of flavins

Flavins have an array of attributes that explain their widespread occurrence in nature. This includes photostability, reversible electrochemistry and the tunability of their optical, electronic and redox properties. Alongside their importance in the biological world these properties are also key features for organic photocatalysis as well as organic electronics and optoelectronic devices.

One of the first applications of flavins was in photocatalysis. The first steps towards this application were made in the 1930s by several groups. In 1939, Lipmann discussed the use of flavins in biochemistry as autoxidisable compounds for the catalysis of pyruvic acid oxidation *via* thiamine (vitamin B_1) oxidation.[138] This certainly inspired its use as catalyst in chemical reactions. In 1948, Krasnovsky[139] explored the use of riboflavin as a photocatalyst for the oxidation of ascorbic acid. In these early years of flavin catalysis the side product of flavin reoxidation was thought to be water, instead of hydrogen peroxide.

The photocatalytic cycle agreed to date starts with the irradiation of the oxidized form of flavin (Fl_{OX}) with blue light, exciting it into the singlet state. Then intersystem crossing (ISC) to the triplet state ($^3[Fl_{OX}]^*$) occurs rapidly (Fig. 40b) in a few nanoseconds (13.5 ns for riboflavin[140]). $^3[Fl_{OX}]^*$ is the active species and key intermediate in catalysis.[141] It can then be reduced by an appropriate substrate to the radical anion ($Fl^{\cdot -}$) which is subsequently protonated (pK_a value of 8.3)[142] and further reduced to the flavohydroquinone anion (HFl_{RED}^-). The different redox states are easily distinguished by UV/Vis spectroscopy. In principle the flavin redox cycle can be used for reductions as well as for oxidations (Fig. 40a). For the reduction of substrates a sacrificial electron donor (e.g. typically triethylamine, EDTA or triethanol amine)[143] is needed while for oxidations, oxygen from the air is sufficient to reoxidize the flavin.[131]

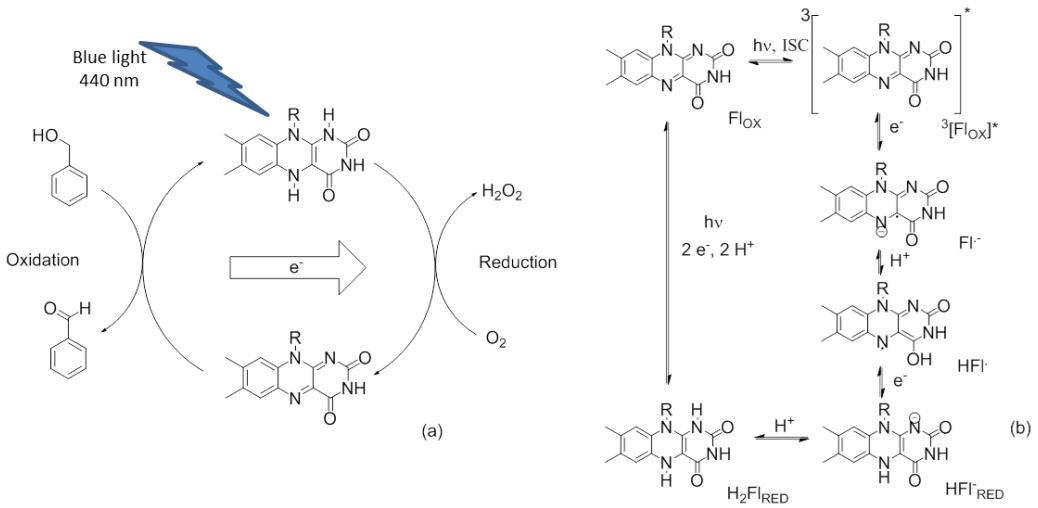

Figure 40 – Catalytic cycle of flavin redox reactions in the example of benzyl alcohol oxidation; air is used for the dark reoxidation of the catalyst.

Over the last two decades, the interest in flavins as possible compounds for organic electronic devices has grown. In the late 1990s, in order to gain a deeper understanding of the π-stacking in flavoenzymes, Rotello *et al.*[144] performed a

variety of investigations, which included hydrogen bonding versus π-stacking, donor atom-π interaction, redox stabilization versus π-stacking and intramolecular hydrogen bonding and π-stacking interactions, by using a xanthene-based model system. In the hydrogen bonding versus π-stacking investigations the xanthene based model systems contained a diaminotriazine (DAT) moiety, which, through hydrogen bonding would orient the flavin over an aromatic surface, which constitutes the aromatic side chain of the flavoenzyme (Fig. 41).

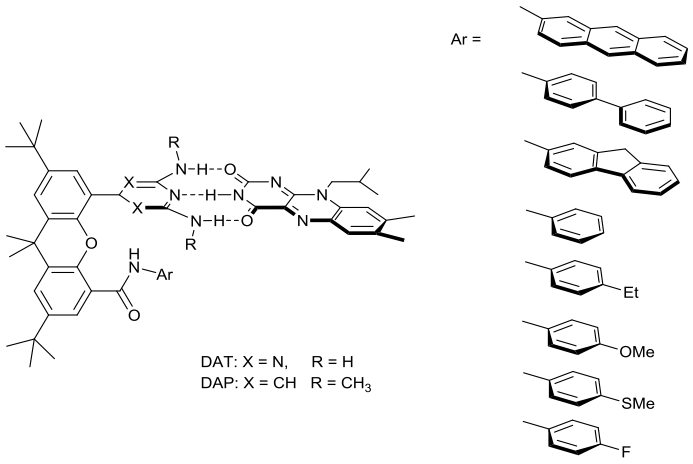

Figure 41 – Schematic representation of flavin binding to xanthene receptors.

The modular receptor design allowed the aromatic surface to be parametrically varied while H-bonding interactions were kept constant, thereby allowing systematic probing of the effect of different aromatic moieties on flavin redox properties. Stacking interactions between the different aromatic side chains and the flavin were measured by NMR titration, demonstrating that there is a strong correlation between the binding energy, and association constant (K_a), and the π-overlap between the two moieties. The same experiment was repeated by attaching different donor groups to the aromatic side chains, resulting in a significant increase of the K_a. They also showed that incorporating a diaminopyridine (DAP) moiety into the model system, in place of DAT, resulted in an increase of K_a by two thirds with respect to the same DAT systems (Fig. 41). In their conclusion, they hypothesised that flavins could be used in organic electronic and opto-electronic devices. Indeed, because of their electron deficiency along with the photostability and ease of tunability, flavins could be ideal candidates for organic devices, such as OLEDs, OFETs and OPVs.

One other property of interest is the capability of flavins to self-assemble selectively into defined structures through non-covalent interactions. In 2008, Cooke, Rotello and co-workers[145] reported the synthesis of two flavin derivatives (ABFL and

MABFL, Fig. 42) differing only in the substitution on N3, and capable to self-assemble into two completely different shapes. Unlike ABFL which formed nanowires, MABFL was unable of self-assembling through H-bonds, resulting in the formation of hexagonal platelets. In both cases, the driving force for the formation of the nanostructures was found to be the large dipole moment of the two molecules, induced by the *push-pull* structure. The authors also observed that the morphology of the nanostructures can be modulated by modulating the ratio of ABFL to MABFL.

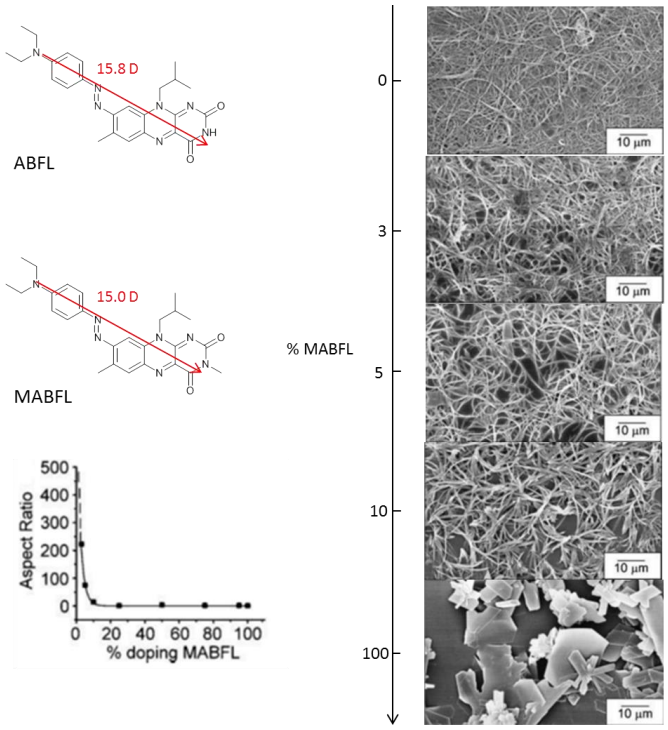

Figure 42 – Chemical structure of ABFL and MABFL (top left); scanning electron microscope images of the transformation from nanowires to hexagonal platelets with increased MABFL doping concentration (right).[145]

Another important aspect that must be taken into account is the ability of the material to transfer electrons (electron mobility). In 2012, Rotello, Cooke and co-workers[125] studied a D-A system composed of a flavin and an oligothiophene covalently linked together by an inert hydrocarbon triazole linker molecule. Their investigation showed very efficient charge and energy transfer processes between the two moieties, when harvested by light. However, the estimated time delay of 3 ps between energy and electron transfer induced the authors to propose an alternative mechanism according to which the formation of an intermediate state is suggested. This corresponds to the system after the energy transfer, which precedes the formation of the final charge-separated state by hole migration from the acceptor to the donor (Fig. 43). They could then conclude that flavins could be a promising class of acceptor compounds for solar energy conversion and storage.

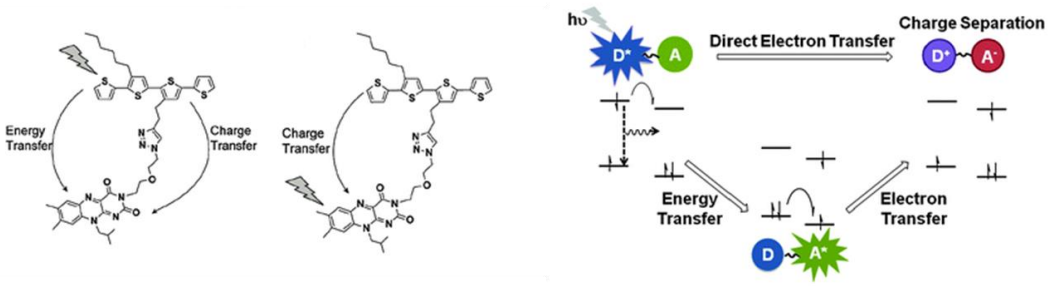

Figure 43 – Representation of energy and charge transfer processes when the oligothiophene or the flavin is excited (left) and schematic representation of energy and charge transfer processes that can take place in the D–A dyads upon excitation of the oligothiophene chromophore.[125]

2.3 Aims

This chapter reports the synthesis of several flavin derivatives (Fig. 44), designed for exploring their use in a wide range of applications in PV devices. The high versatility of flavins, due to the possibility to functionalise the central core in different ways, makes them suitable moieties for *push-pull* systems in BHJ devices, as well as for N-type semiconductors, due to their high electron affinity. Moreover, the imide group could be exploited as recognition group or as anchor group on TiO_2.

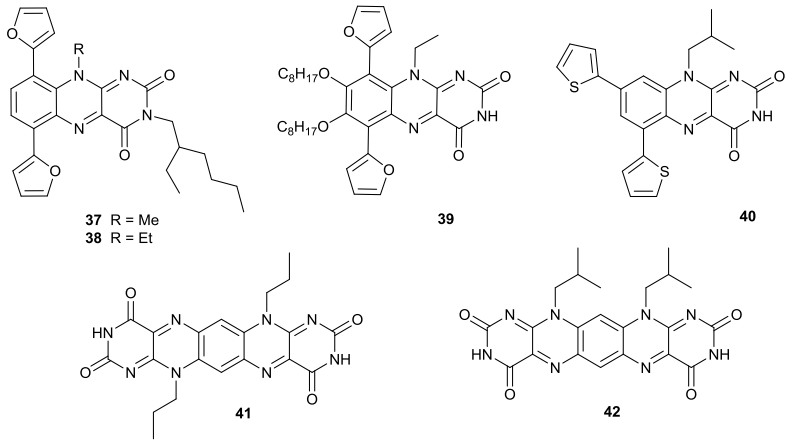

Figure 44 – Chemical structure of the target compounds **37** – **40**.

Furan-phenyl-furan-based Flavins (FPF-Flavins) **37** and **38**, for example, could constitute two building blocks for the synthesis of push-pull polyconjugated systems to be used as donor units in BHJ solar cells. Furans were indicated as an alternative to thiophenes, previously explored by other members of the research group (**44**,[146] and unpublished **43**, Fig. 45). This choice was supported for the following reasons: furan is a biodegradable monomer that can be obtained from biomass, making it a green conjugated building block;[147] the challenging synthesis of furan-based

monomers as well as the suspicion of polyfuran instability[148] have likely contributed to the limited examination of this aromatic unit.

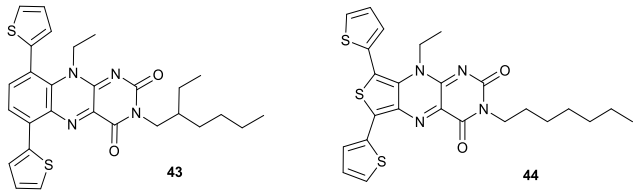

Figure 45 – Chemical structure of compounds **43** and **44**.

Recent reports on oligofurans have illustrated that these materials are relatively stable,[149] and they exhibit increased solubility, higher fluorescence, and a lower propensity to twist as compared to oligothiophenes.[150] Oligofurans are highly planar even with substituents in a head-to-head orientation (3,3′ substitution on adjacent rings).[151] The lower aromaticity of furan enhances quinoidal character in the polymer, resulting in shorter inter-ring bonds.[152] Moreover, the steric strain between adjacent furan rings is lower due to the smaller oxygen atom as compared to sulfur. The latter feature resulted to be particularly attractive. Indeed, one of the issues affecting the thiophene-based analogue **43** (Fig. 45) is its lack of planarity at the solid state: in particular, the thiophene in position C(9) resulted to be orthogonal to the isoalloxazine core, and thus not conjugated with it. At the beginning, this was supposed to be due to the steric hindrance between the thiophene and the ethyl chain in position N(10).

A DFT simulation was run in order to compare the electronic behaviour of FPF-Flavin with Thiophene-Phenyl-Thiophene-based Flavin (TPT-Flavin). For both molecules, the HOMO/LUMO distribution (Fig. 46b) is relatively similar. The HOMO is localised on the TPT and FPF backbone, respectively, while the LUMO is spread over the flavin moiety, but only on the most "in-plane" heterocycle, at C(6). Fig. 46a shows the optimised geometry for the two molecules in the gas phase: according to this model, in TPT-Flavin the dihedral angle between the benzene ring and the thiophene in position C(9) is 66.32º, while the thiophene in position C(6) is twisted of 7.25º. In FPF-Flavin both of the furans are out of plane, but the dihedral angles are 35.27º for position C(9) and 33.13º for the other. This could imply a better conjugation among the aromatic rings.

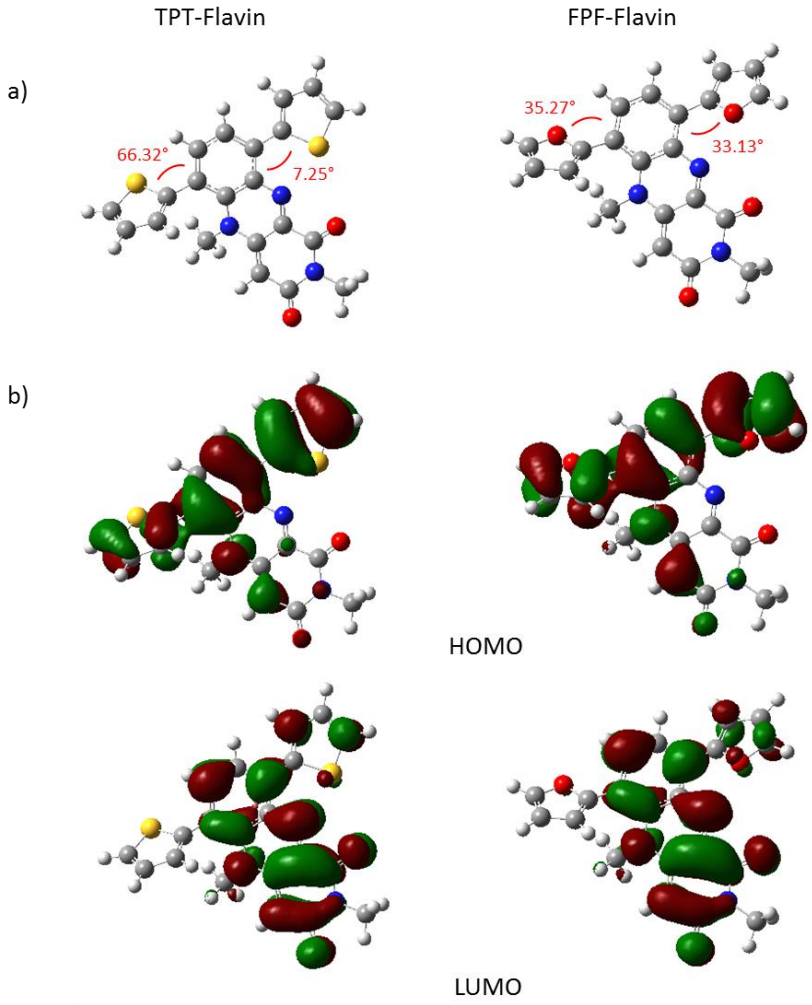

Figure 46 – (a) Optimised geometry and (b) frontier molecular orbital distributions for TPT-Flavin and FPF-Flavin. Calculations were run using B3LYP functional and 6-311+G(d) basis set.

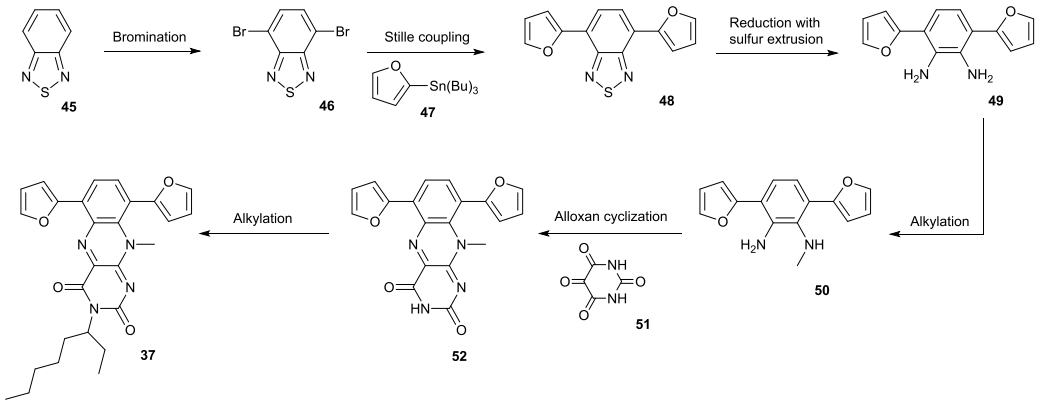

Scheme 1 – Proposed strategy towards the synthesis of compound **37**.

The first FPF-Flavin target was designed with a methyl side chain in position N(10), in order to lower the steric effects as much as possible. The proposed synthetic pathway would start with the synthesis of 4,7-di(furan-2-yl)benzo[*c*][1,2,5] thiadiazole **48** by bromination of benzo[*c*][1,2,5]thiadiazole **44**, followed by Stille

coupling between compound **46** and the 2-(tributylstannyl)furan **47** (Scheme 1). Compound **48** would then be reduced to form the aromatic diamine **49**, followed by monoalkylation of one of the two primary amines and the alloxan-based cyclization to provide flavin **52**. Finally alkylation of N(3) would provide the final compound **37**. However, the first attempts of making compound **37** were unsuccessful, due to the very low solubility of **52**. For this reason the structure of the final compound was slightly modified, by replacing the methyl side chain in position N(10) with an ethyl group (Scheme 2), to obtain compound **54**, which would be further alkylated in position N(10) to afford the final compound **38**.

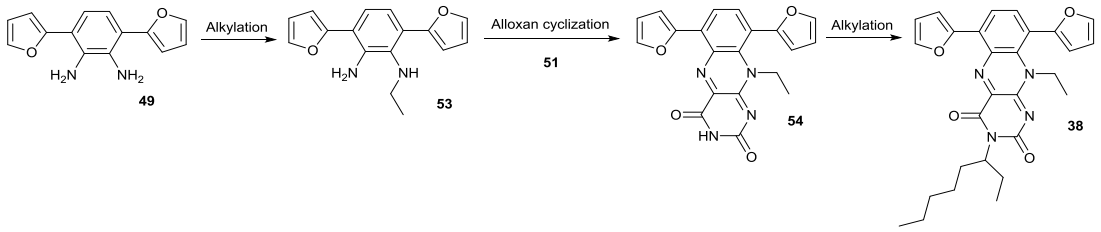

Scheme 2 – Proposed strategy towards the synthesis of compound **38**.

In order to test the effectiveness of flavin **38** as acceptor moiety for push-pull systems in BHJ devices, a polymerization reaction with fluorene, as prototype mild donor moiety, was tried. According to the strategy depicted in Scheme 3, flavin **38** would first undergo bromination on the furan C(5) positions to afford **55**, which would be coupled with the 9,9-dioctylfluorene-2,7-diboronic acid *bis*(1,3-propanediol) ester **56**, *via* Suzuki reaction. The final polymer **57**, would be end-capped with phenyl units before being purified.

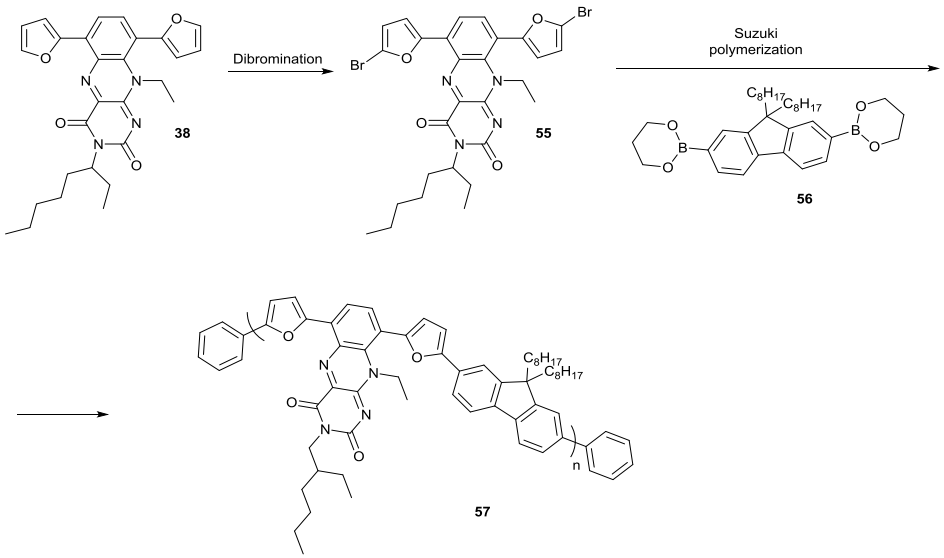

Scheme 3 – Proposed strategy towards the synthesis of compound **57**.

One of the main issues associated with flavins is their solubility: as previously explained, a possible way to overcome this problem is to alkylate position N(3). However this would sacrifice the possibility to exploit the imide unit as non-covalent binding group, for molecular recognition. Thus, the alkylation of positions C(7) and C(8) of flavin **54**, to obtain compound **39**, was thought to be a good compromise to work around the issue. A non-functionalised imide could potentially allow attaching the molecule to TiO_2 particles, in order to use flavins as potential acceptor units for sensitisers in DSSCs.[153] Remarkably, the DFT calculated geometry (Fig. 47a) shows similar planarity for the two analogues **38** and **39** as well as the distribution of HOMO and LUMO levels (Fig. 47b).

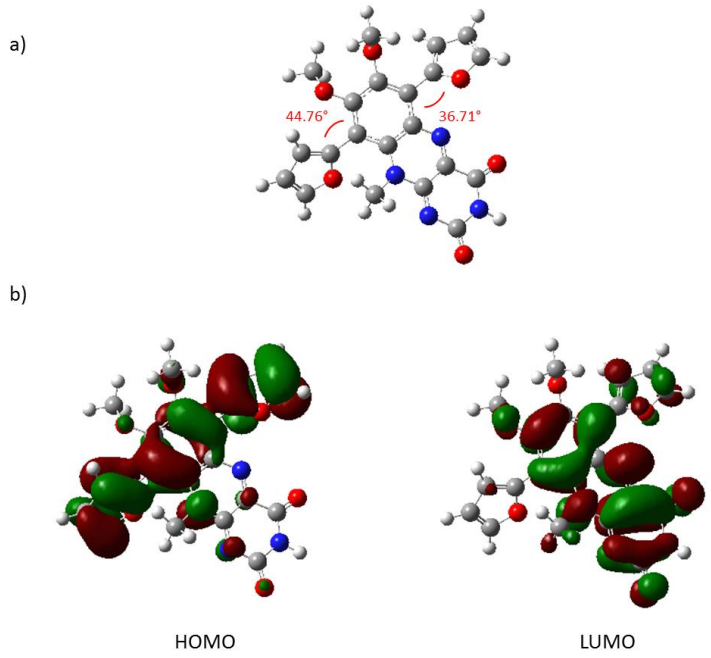

Figure 47 – (a) Optimised geometry and (b) frontier molecular orbital distributions for Flavin **39**. Calculations were run using B3LYP functional and 6-311+G(d) basis set.

The proposed route for the synthesis of compound **39** is depicted in Scheme 4. It would start from pyrocatechol **58**, which would be etherified with bromooctane, *via* Williamson reaction, further nitration would afford **60**. This would be reduced to afford the corresponding diamine **61**, which would undergo the thiadiazole cyclization to give the dialkoxy substituted BT **62**. After dibromination and Stille coupling with **47**, compound **64** would be obtained. This would be reduced to obtain the corresponding aromatic diamine **65**, which would be monoalkylated to afford **66**, starting material for the alloxan cyclization to furnish compound **39**.

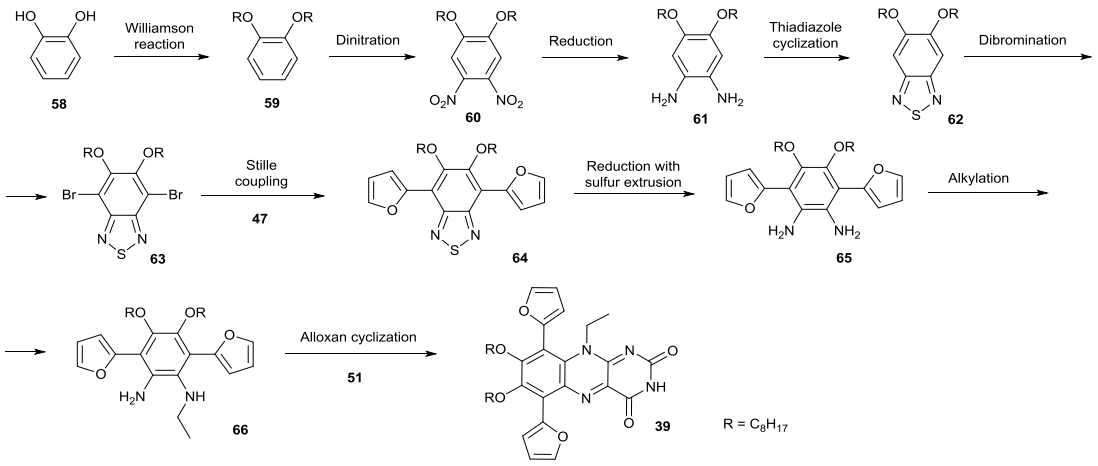

Scheme 4 – Proposed strategy towards the synthesis of compound **40**.

A further investigation upon the effective conjugation of the aromatic units appended to the flavin revealed that the substituents attached in position C(6) and C(8) are canonically conjugated with the core, while for those groups appended in positions C(7) and C(9) the charge transport is interrupted at the level of the sp_3 nitrogen (Scheme 5).

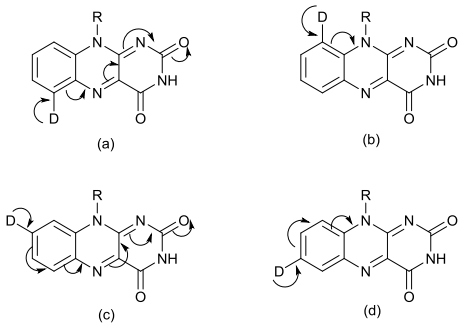

Scheme 5 – Electron pathways for flavins functionalised in different positions (D is a generic donor unit).

In theory this means that by adding an aromatic substitution in position C(8) instead of C(9), the resulting system would be more planar. DFT geometry optimized calculations, for both fully-conjugated (FC) FPF and TPT (Fig. 48a), confirm these expectations. In order for this theory to be proved, a fully conjugated TPT-Flavin was designed and a synthetic strategy was proposed (Scheme 6). In this case, thiophene was chosen as substituent because, according to the calculation, TPT-Flavin resulted to be more planar than FPF-Flavin. The synthesis would start from 2,4-dibromo-6-nitroaniline **67**, which would be coupled with the 2-(tributylstannyl)thiophene **68**, *via* Stille coupling, obtaining compound **69**. This would undergo a Boc protection of the amine group to afford **70** and then a reduction of the nitro group, under mild conditions, to give **71**. This would undergo acylation (compound **72**), followed by the reduction of the acyl group and the Boc cleavage, to afford **73**. Finally, alloxan condensation would provide the desired product **40**.

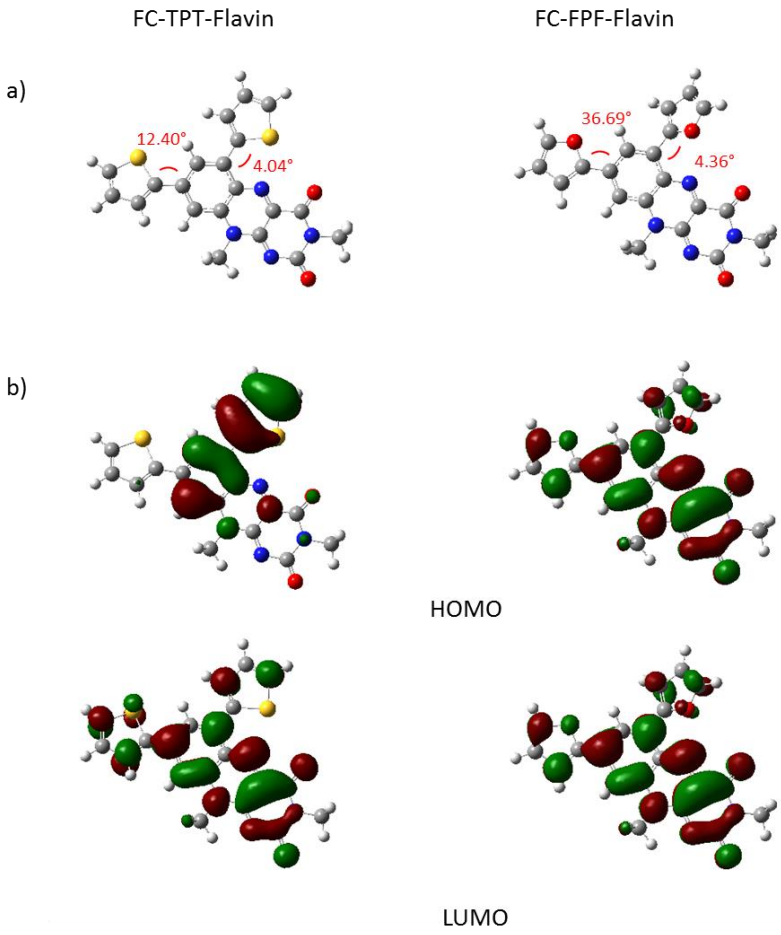

Figure 48 – (a) Optimised geometry and (b) frontier molecular orbital distributions for TPT and FPF FC-Flavins. Calculations were run using B3LYP functional and 6-311+G(d) basis set.

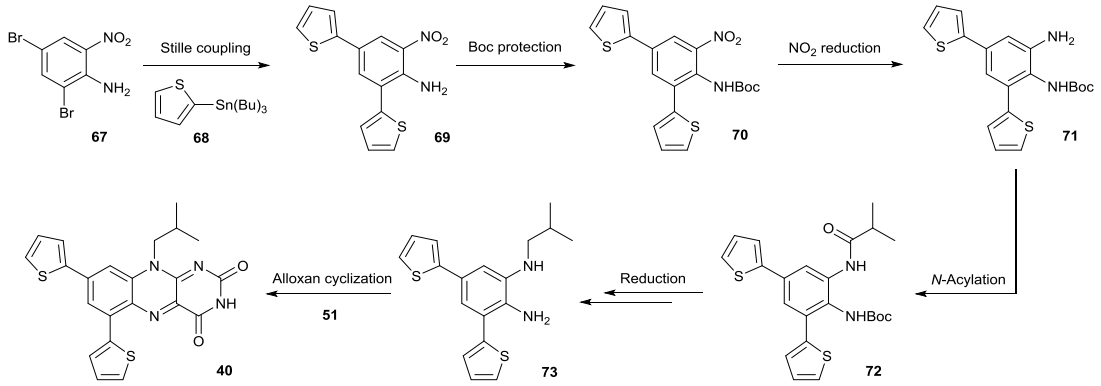

Scheme 6 – Proposed strategy towards the synthesis of compound **39**.

Unfortunately, after the successful synthesis of compound **72** and the reduction with Boc cleavage, the alloxan cyclization did not work, althought many reaction conditions were tried. Therefore, this route was abandoned.

Another possible application for flavins, due to the desirable electrochemical properties, could be their employment as non-fullerene acceptor units for BHJ solar cells. In fact, as mentioned above, it is essential for an acceptor unit to be reversibly

reducible; a requirement that flavins fulfil. *bis*-Flavins **41** and **42** were designed in order to exploit these properties that make flavins so peculiar and at the same time to increase the number of electrons that the molecule can accept by reduction, from two to four. Moreover, such molecules are expected to have more negative HOMO/LUMO levels, approaching to those of PCBM. On this regard, it is very important to design the molecule making sure that the energy levels lay in the right interval of energies. The best way to do this is by using simulation software. However, although by using the proper basis sets they tend to be extremely accurate in predicting the HOMO levels, this accuracy does not often reflect on the prediction of the LUMO levels. Nevertheless, a good way to improve the accuracy could be to compare the predicted HOMO/LUMO of known compounds, with similar structure, with the values of ionization potential (I_P) and electron affinity (E_A) estimated by electrochemistry. This would make it possible to determine the range of confidence associated to the error on energy levels introduced by the software, and take it into account for further calculations. Table 1 reports HOMO/LUMO levels calculated for compounds **38** and **39** and the I_P and E_A values estimated by electrochemistry. In addition, the table reports the same values for flavins **43** and **44** (Fig. 45), which were previously synthesised by other members of the Cooke group.

	HOMO[a] (eV)	I_P[b] (eV)	LUMO[a] (eV)	E_A[b] (eV)
38	–5.96	–5.83	–3.00	–3.73
39	–6.09	–5.89	–3.12	–3.66
43	–5.97	–6.06	–3.13	–3.65
44	–5.95	–5.77	–3.50	–3.73

Table 1 – HOMO/LUMO levels and I_P/E_A data relative to isoalloxazine-based compounds **38**, **39**, **43** and **67**. [a] Data obtained by calculation, using B3LYP functional and 6-311+G(d) basis set. [b] Data estimated by square wave voltammetry of the compounds in solution (C = 10^{-3} M), performed using a Pt disk working electrode, a Pt wire counter electrode and a Ag wire reference electrode. $TBAPF_6$ (0.1 M) was used as supporting electrolyte and the redox potential of the Fc/Fc^+ couple as standard.

By applying the t-Student distribution theory, which works well for such small variable populations, the errors ΔHOMO and ΔLUMO, estimated within a 95% confidence range, are:

$$\Delta HOMO = HOMO - I_P = (-0.10 \pm 0.12)\ eV$$
$$\Delta LUMO = LUMO - E_A = (0.50 \pm 0.18)\ eV$$

Taking this into account, the two *bis*-flavins **41** and **42** were simulated by DFT

calculations and the resulting values of HOMO and LUMO were compared with those of PCBM[154] (Fig. 49).

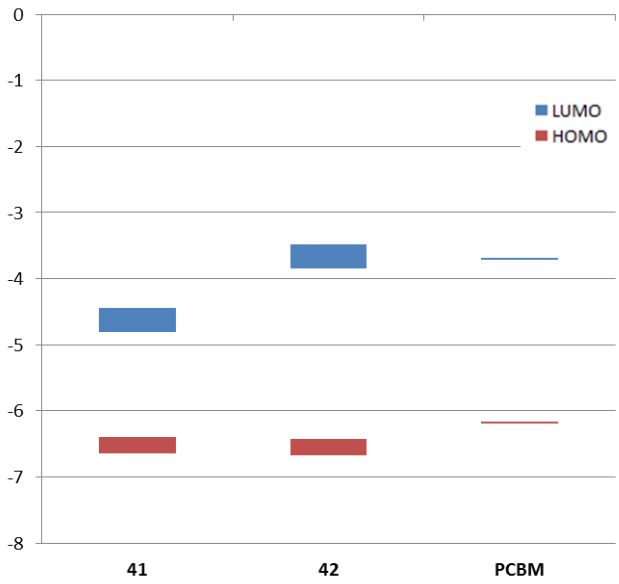

Figure 49 – Comparison between the HOMO/LUMO values of PCBM and the ones of compounds **41** and **42**, obtained by correcting the results of the DFT calculation (B3LYP functional and 6-311+G(d) basis set).

As depicted in Fig. 49, compound **42** would be closer to PCBM, in terms of electronic properties: this means that it would guarantee a high V_{OC} (see Par. 1.4.1.1) but, with a band gap of almost 2.9 eV, it would not absorb light in the visible range. On the other hand, compound **41** would have an ideal band gap of about 1.9 eV, but the low positioned LUMO level is expected to affect the V_{OC} of the device. Nevertheless, in both cases the HOMO levels would be almost 0.40 eV lower than that of PCBM, and this would allow the use of donor units with lower HOMO levels (thus chemically more stable), which would lead to devices with higher V_{OC}.

Scheme 7 shows the proposed route for the synthesis of compound **41**. It would start from commercially available benzene-1,4-diamine **74** which would undergo acylation with acetic anhydride to afford compound **75**. Compound **76**, obtained after reduction of **75** would then be coupled with two equivalents of 6-chlorouracil **77** to afford compound **78**, which after a multi-step reaction, consisting in the nitration and flavin condensation, would give compound **41**.

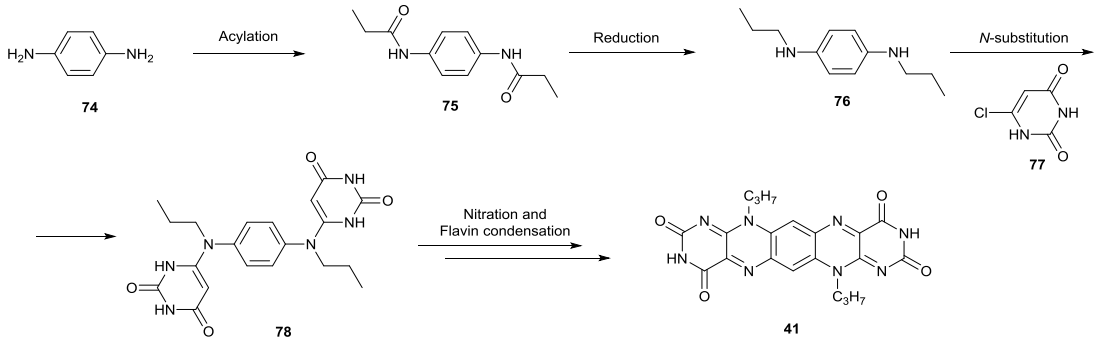

Scheme 7 – Proposed strategy towards the synthesis of compound **41**.

The synthesis of compound **42** (Scheme 8), instead, would consist of a nucleophilic aromatic disubsitution of commercially available 1,5-difluoro-2,4-dinitrobenzene **79** with isopropylamine, to afford compound **80**, which would be further reduced, affording **81**. This would finally undergo the final cyclization with two equivalents of alloxan.

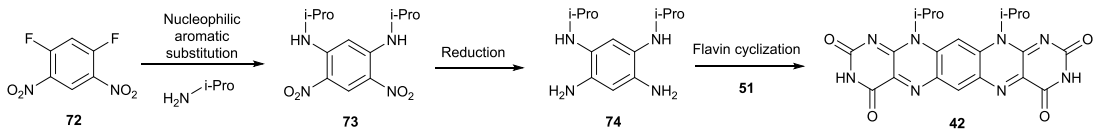

Scheme 8 – Proposed strategy towards the synthesis of compound **42**.

2.4 Results and discussion

2.4.1 FPF-Flavins

- Synthesis of compound **46**

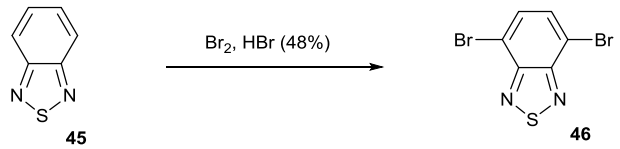

Compound **46** was synthesised following a slight modification of an existing procedure.[155] This step involved the bromination of benzo[*c*][1,2,5]thiadiazole with bromine and hydrobromic acid at 130 ºC for 6 hours. The reaction was quenched with sodium thiosulphate and the precipitate washed with water and recrystallized from acetonitrile to afford **46** in 78% yield.

- Synthesis of compound **48**

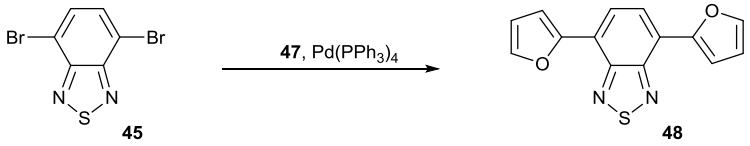

This step was achieved using Stille coupling. This reaction involves the formation of a C–C single bond between two *sp*$_2$ hybridised C (an aromatic organo-tin compound and an aromatic halide) in the presence of a Pd catalyst. It was developed in 1977-1978 by Toshihiko Migita[156] and John K. Stille[157] and is one of the most widely used reactions in organic chemistry. The catalytic cycle is thought to proceed according to Scheme 9.

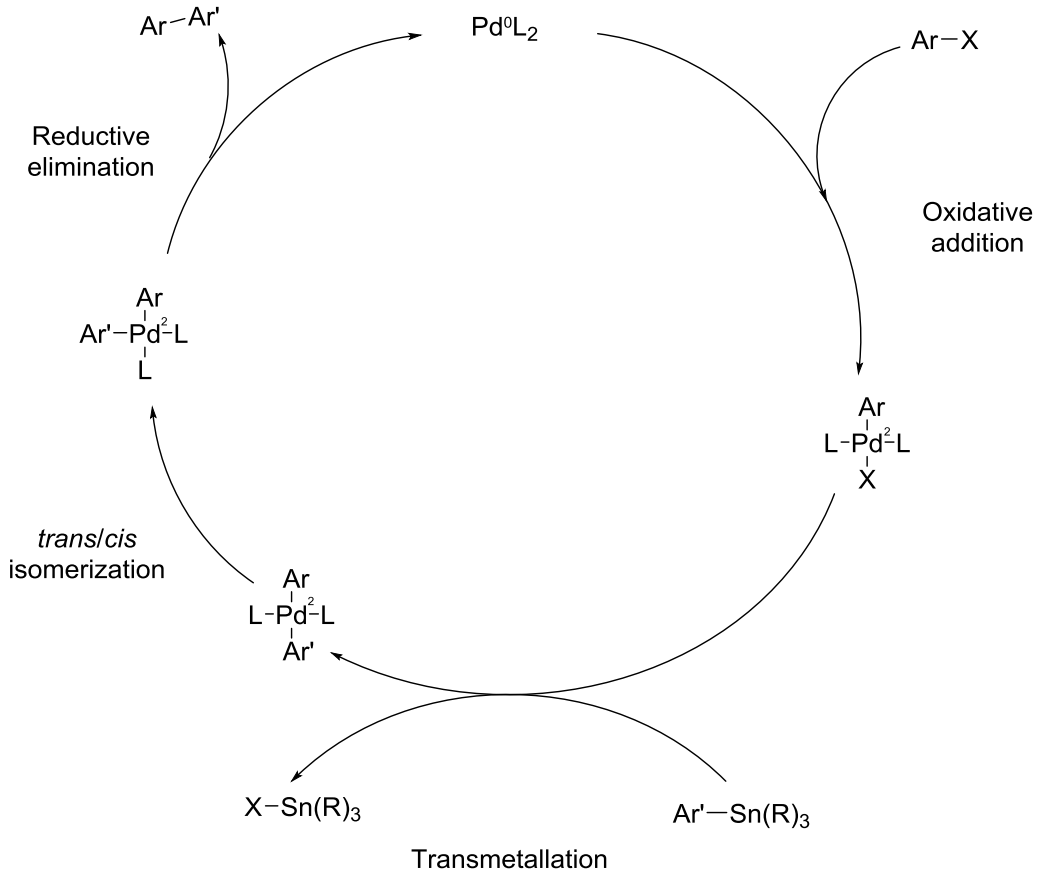

Scheme 9 – Catalytic cycle of the Stille cross-coupling. L denotes a phosphine ligand, Ar and Ar' are generic aromatic groups and R is an alkyl group.

The palladium catalyst undergoes *cis*- oxidative addition with the aryl halide to form the palladium (II) complex, which further undergoes transmetallation with the organo-tin species. Finally, after *trans*/*cis* isomerisation the palladium complex undergoes reductive elimination, in which the desired product is obtained, and the palladium (II) is reduced to palladium (0) to start the cycle again.

For this reaction, a slight modification of an already existing protocol[158] was followed. $Pd^{(0)}$ was used to catalyse the reaction wich was carried out in dry THF for 24 hours. In order to get rid of the toxic stannanes, the mixture was quenched with a solution of potassium fluoride. After purification, compound **48** was isolated in 93% yield.

- Synthesis of compound **49**

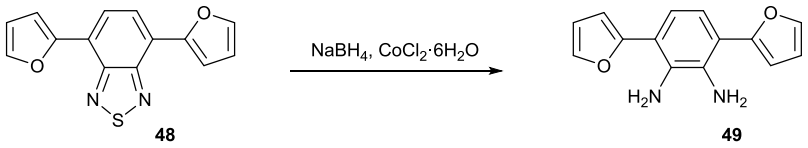

The first step involved the reduction, with sulfur extrusion, of the thiadiazole ring, according to the procedure developed by Neto and co-workers.[159] According to this methodology a catalytical amount of insoluble Co_2B, obtained by reaction of $NaBH_4$ with $CoCl_2$, would act as preferential binding site for imine nitrogens and sulfurs, weakening their bonds, for the following reductive sulfur extrusion (Scheme 10). Compound **49** is unstable in air, and thus after the work up, it was used for the next reaction without purification.

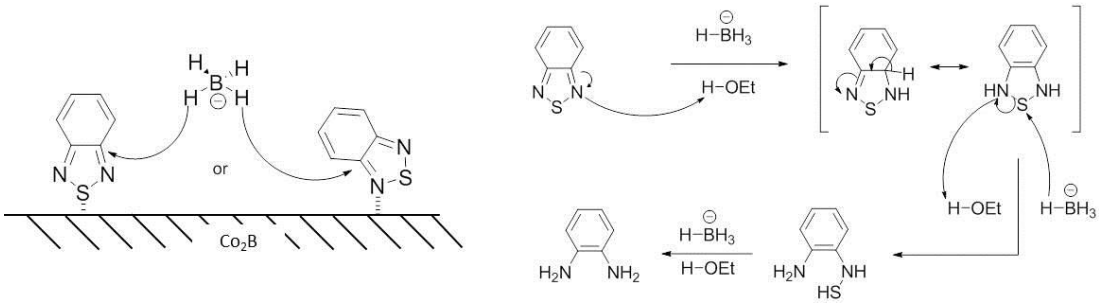

Scheme 10 – On the left, proposed first step of reductive sulfur extrusion reaction of BT compounds with $Co_2B/NaBH_4$.[159] On the right, proposed mechanism of the sulfur extrusion reaction.

- Synthesis of compounds **50** and **53**

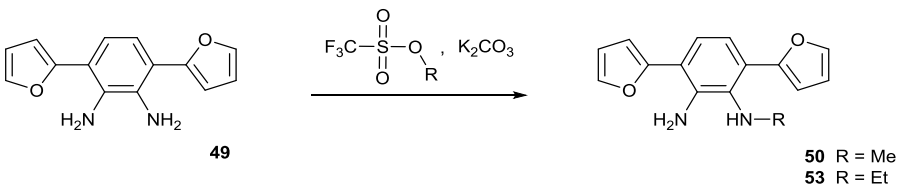

This reaction represents the most critical step for the synthesis of FPF-flavins, as it is

difficult to obtain the mono *N*-alkylated product in high yields. In fact, due to the high reactivity of secondary amines towards S_N2 reactions, the direct alkylation of primary amines usually leads to over alkylated products. In this case the presence of two primary amines makes things even more complicated. In order to reduce the rate of the reaction the temperature was kept at 0 °C, for 6 hours, and a high dilution (7 mM) was used. First attempts of synthesising **50** were made by using methyl halides, either bromide and iodide. Since the final compound is air-sensitive, a qualitative TLC test, followed by a comparison of the yields obtained for the next reaction, provided the evidence that methyl triflate was a better reagent for this reaction.

- Synthesis of compounds **52** and **54**

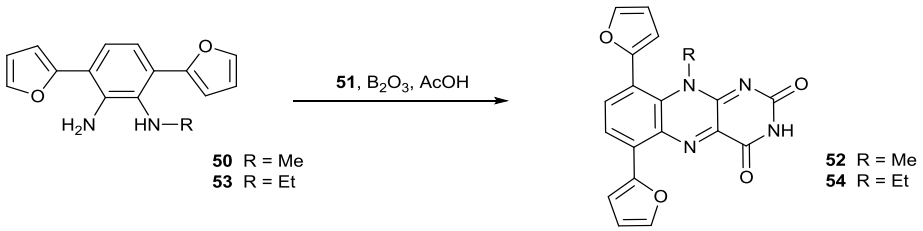

Compounds **52** and **54** were synthesised according to the "alloxan route".[160] This method has been the most widely employed protocol for the synthesis of the isoalloxazines. However, it is characterised by highly variable yields, depending strongly and unpredictably on the number, nature and position of the substituents on the aromatic diamine. Indeed, in 1986 Averill and co-workers[161] showed strong evidence that the reaction is not as straightforward as previously thought. The general procedure, and especially the role of the boric anhydride, is not clear. The proposed mechanism suggests a dual role for B_2O_3: in the first instance, it captures the molecule of water contained in the monohydrate form of alloxan (the most stable and commercially available), making it more reactive towards nucleophilic addition. The so formed boric acid is involved in the activation of alloxan, by reacting with one of the carbonyl oxygens. This promotes the first intermolecular condensation and then the second intramolecular condensation occurs to give the isoalloxazine (Scheme 11).

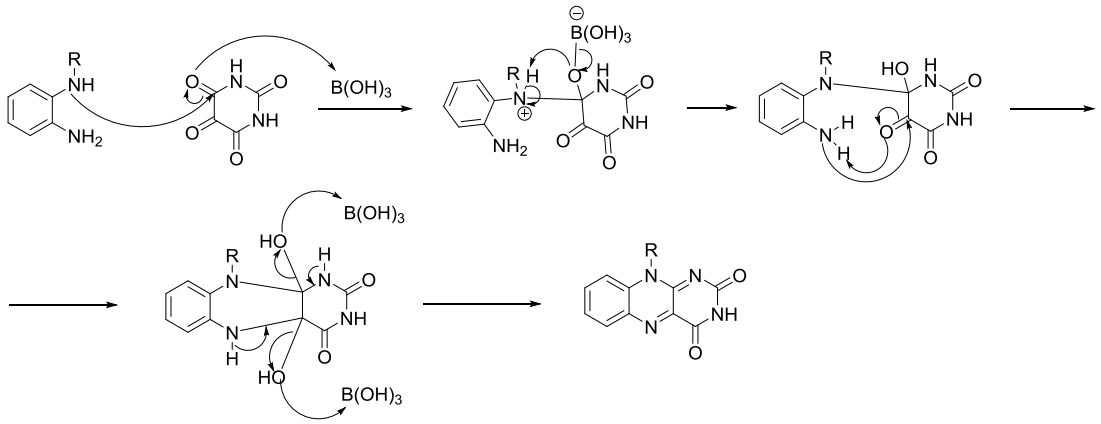

Scheme 11 – Proposed reaction mechanism for the alloxan cyclization.

Computational studies conducted by Gaba and co-workers[162] demonstrated that the protonation of alloxan is preferred on the C(4)/C(6) carbonyl oxygen (tautomer I in Fig. 50). This is in accordance with the proposed reaction mechanism of alloxan cyclization, in which the most reactive secondary amine of the aromatic diamine reacts with the protonated carbon of alloxan (Scheme 11).

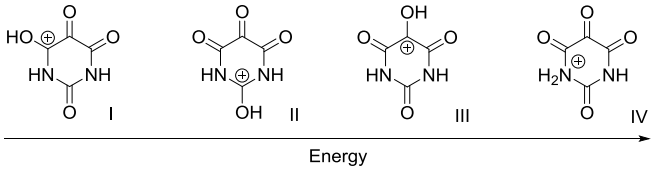

Figure 50 – Possible protonated cations of alloxan.

This final step afforded compound **52** in 45% yield and compound **54** in 33% yield, both over 3 steps, proving the relative success of the alkylation reaction. A crucial observation for the next synthetic step, is the difference in solubility of the two flavins: compound **54** showed a relatively good solubility (roughly 5 mg/mL) especially in very polar solvents, such as DMF and DMSO, while the solubility of compound **52** in the same solvents was poorer. In fact, it started crystallizing from DMF at 80 °C.

- <u>Synthesis of compounds **37** and **38**</u>

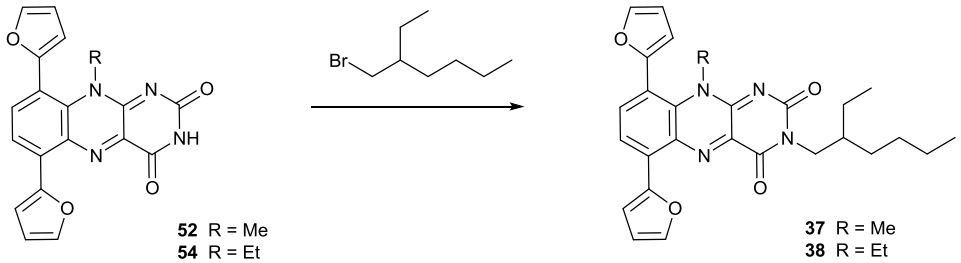

First attempts to perform the *N*-alkylation on **52** with 2-ethylhexyl bromide were unsuccessful. In fact, due to the low solubility of the starting material, it was impossible to carry out the reaction at low temperatures. The reaction was tried in DMF, at 120 °C, in presence of potassium carbonate, but this led to the decomposition of the starting material. The same reaction with compound **54** gave different results: the better solubility allowed to screen the progress of the reaction over a range of temperatures, in order to find the best conditions (Table 2).

T	**38**	**82**	**54** (recovered)
20 °C	5%	/	87%
50 °C	54%	25%	12%
80 °C	8%	57%	6%
120 °C	/	/	/

Table 2 – Reaction temperatures, and relative yields, for the alkylation of compound **52**.

Table 2 also shows the yields of the side-product **82** (Fig. 51), the formation of which has been already reported by other members of the Cooke group for the alkylation of the TPT analogues (Dr. Helen Smith, PhD Thesis).

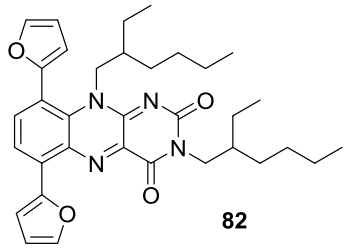

Figure 51 – Chemical structure of compound **82**.

One of the possible explanations for this reaction is the first formation of the quaternary ammonium salt in position N(10), followed by the degradation of the compound with formation of the alkylated (ethyl and/or diethyl) carbonate. Further studies will be done to elucidate the reaction mechanism involved in the synthesis of **82**. As depicted in Table 2, the best yield for compound **38** was achieved at 50 °C. The addition of 18-crown-6, as K^+ scavenger, resulted in an improvement of the yields.

- <u>Analysis and characterisation of compound **38**</u>

Crystals of flavin **38** were grown from toluene and analysed by X-ray diffractometry. The crystal structure (Fig. 52) was found to be very similar to that of the thiophene-based analogue **43**, and in disagreement with the results predicted by DFT

calculations (Fig. 46). Thus, it is likely that both compounds will show similar physical properties.

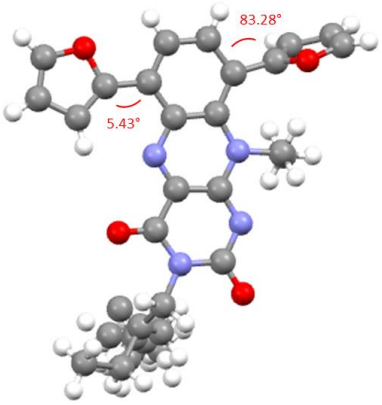

Figure 52 - Crystal structure of flavin **38**.

The UV-Vis absorption spectrum of compound **38** in DCM was recorded and compared with that of parent flavin **43** (Fig. 53), recorded with the same concentration and in the same solvent. Both the compounds have exactly the same spectra, with a strong absorption band between 250 and 350 nm, due to the π-π* and n-π* transitions in thiophene and furan, a moderately strong band in the range from 400 to 500 nm, which is the typical fingerprint pattern of the isoalloxazine chromophore, and a weak tail, up to 600 nm, likely due to the intramolecular charge transfer (ICT) between the donor and the acceptor. Compound **38** shows a small bathochromic shift of roughly 5 nm of the most energetic band, with a higher shift (around 15 nm) for the second band. This could be explained by the relatively stronger inductive effect provided by furans. However, the tail at lower energy is not shifted at all, and this could be expected, considering the relatively similar torsion angles between the hetero-aromatic rings and the isoalloxazine unit, which would lead to relatively similar conjugation strengths. The estimated λ_{ONSET} for both of the compounds is 623 nm, which results in a corresponding optical band gap ($E_{G,opt}$) of 1.99 eV, by applying the Einstein-Planck equation:

$$E_{G,opt} = \frac{hc}{\lambda_{ONSET}}$$

where h = 4.136 · 10^{-15} eV·s is the Planck's constant and c = 3 · 10^{17} nm·s^{-1} is the speed of light.

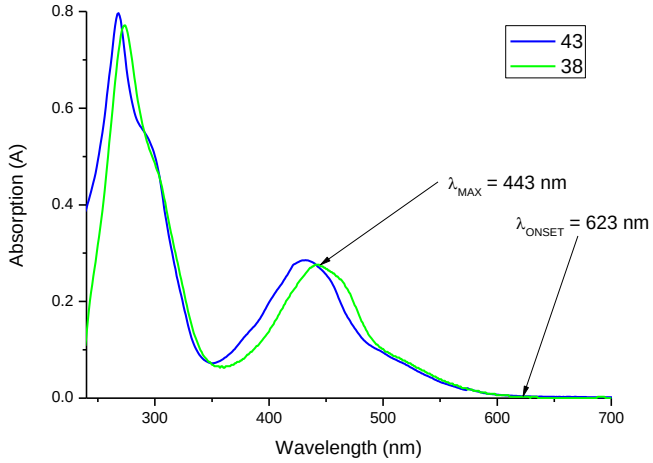

Figure 53 – UV-Vis absorption spectra of compounds **38** and **43**, in solution (C = 10^{-5} M, in DCM).

The cyclic voltammetry (CV) spectra of the two compounds (Fig. 54) show the typical reversible reduction peak of flavins and a non-reversible oxidation peak. A better quantification of the potentials is provided by the square wave voltammetry (SWV), which confirms the differences between the two flavins (Fig. 55). Table 3 summarises the electronic properties of the two compounds; I_P, E_A and $E_{G,fund}$ where calculated by using the following equations:[163, 164]

$$I_P(eV) = -(E_{OX} + 4.80)$$
$$E_A(eV) = -(E_{RED} + 4.80)$$
$$E_{G,fund} = E_A - I_P$$

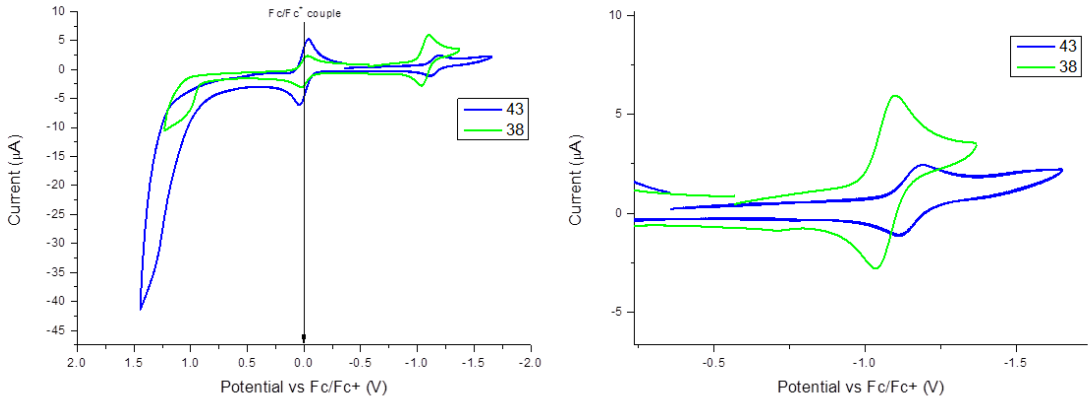

Figure 54 – CV plots of compounds **38** and **43** in solution (C = 10^{-3} M, in DCM), performed using a Pt disk working electrode, a Pt wire counter electrode and a Ag wire reference electrode. $TBAPF_6$ (0.1 M) was used as supporting electrolyte and the redox potential of the Fc/Fc^+ couple as internal standard.

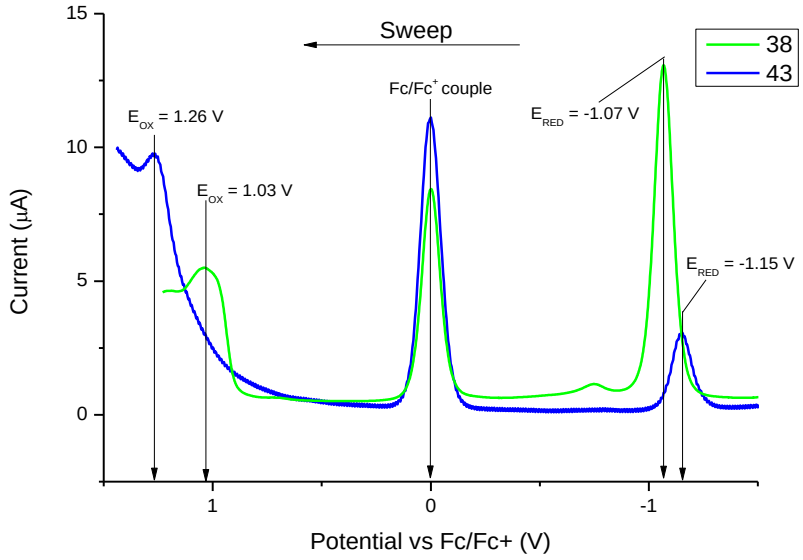

Figure 55 – SWV plots of compounds **38** and **43** in solution (C = 10^{-3} M, in DCM), performed using a Pt disk working electrode, a Pt wire counter electrode and a Ag wire reference electrode. $TBAPF_6$ (0.1 M) was used as supporting electrolyte and the redox potential of the Fc/Fc^+ couple as internal standard.

Compound	I_P (eV)	E_A (eV)	$E_{G,fund}$ (eV)	$E_{G,opt}$ (eV)
38	–5.83	–3.73	2.10	1.99
43	–6.06	–3.65	2.41	1.99

Table 3 – Electronic properties of compounds **38** and **43**.

The difference between the fundamental and the optical band gaps is the expression of the exciton E_b (see Par. 1.3.2), suggesting that the excitons formed upon excitation of compound **38** are weaker than those of compound **43**, making the charge separation easier.

- <u>Synthesis of compounds **55**</u>

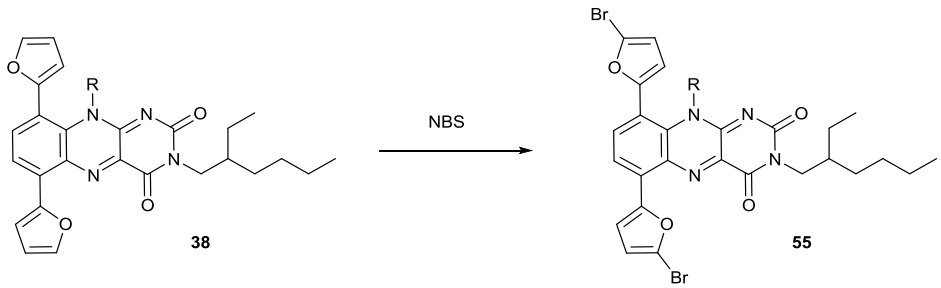

This reaction, which involved a dibromination at the C(5) positions of furans, was performed using NBS in dry DCM, in the dark, affording compound **55** in 83% yield. For bromination of electron-rich aromatic rings, NBS is often preferred to Br_2

because of its capability to selectively brominate the most activated positions, *via* Electrophilic Aromatic Substitution (E_AS). Maintaining a dark environment is essential in order to avoid the competing and unwanted radical reaction. For the same reason NBS was added portion-wise over 30 minutes and at 0 ºC.

- Synthesis of polymer **57**

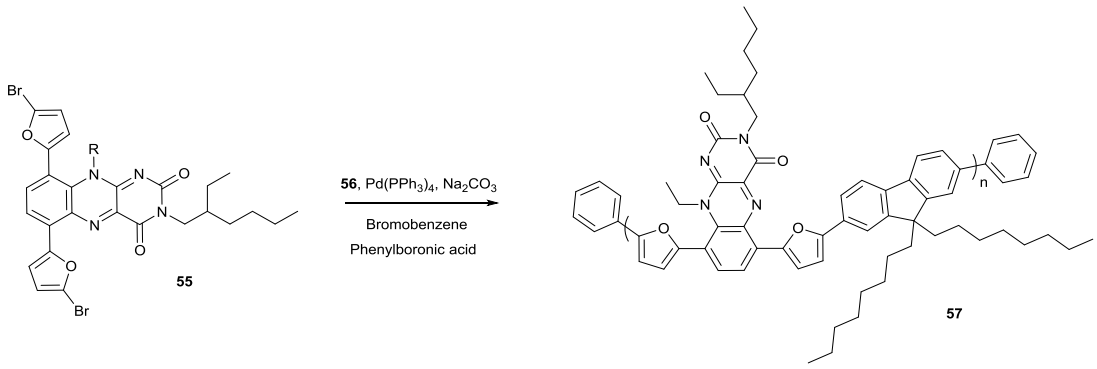

This step requires the use of the Suzuki coupling. This reaction involves the formation of a C-C single bond between a boronic acid (or ester) and a halide in the presence of a palladium catalyst and a suitable base. It was developed in 1979 by Akira Suzuki[165] and allowed him to share the Nobel Prize in Chemistry, with Stille and Negishi, in 2010. The catalytic cycle (Scheme 12) is very similar to that of the Stille coupling, with a base-activated organo-borane taking place of the organo-tin in the transmetallation step. The palladium catalyst undergoes oxidative addition with the aryl halide to form the palladium (II) complex, which further undergoes transmetallation with the activated organoborane species. This is the result of the reaction of the boronic acid (or ester) with the base. Finally, after *trans*/*cis* isomerisation the palladium complex undergoes reductive elimination, in which the desired product is obtained, and the palladium (II) is reduced to palladium (0) to start the cycle again. The advantages of the Suzuki reaction are the extremely mild conditions, with no need of dry solvents, and the limited toxicity and better stability of organoboranes.

The polymerization was carried out in toluene, for 4 days, under N_2, and the end-capping agents were added afterwards, with a gap of 4 hours from each other. After the work-up, the mixture was purified *via* Soxhlet extraction, affording polymer **57** in 58% yield (calculated assuming the repeating unit as product).

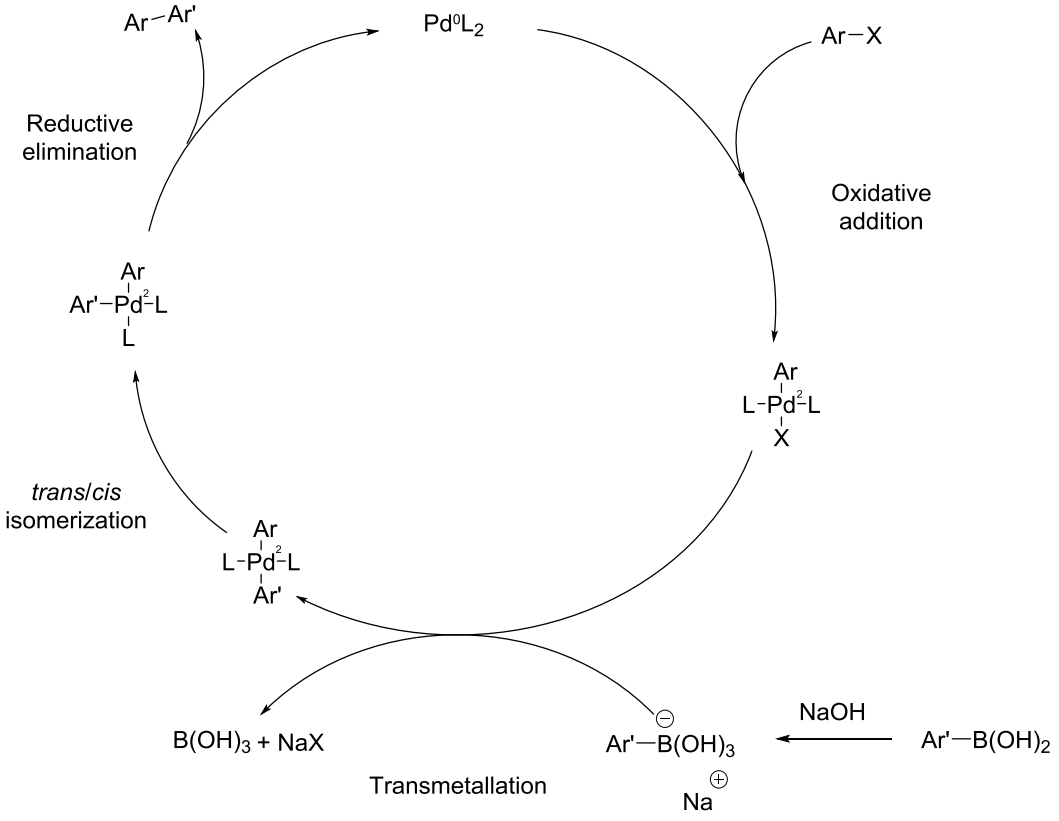

Scheme 12 – Catalytic cycle of the Suzuki cross-coupling. L denotes a phosphine ligand, Ar and Ar' are generic aromatic groups.

- Analysis and characterisation of compound **57**

After the purification steps, polymer **57** was first characterised by gel permeation chromatography (GPC), in order to analyse the molecular weight distribution (Fig. 56). The chromatogram showed a non-homogeneous distribution of the molecular weight over two peaks: a larger bell-shaped curve and a more irregular small peak at lower molecular weights. Taking into account only the biggest peak, it was possible to calculate the significant parameters of the polymer, which are summarised in Table 4.

	M_n (g/mol)	M_w (g/mol)	PDI
57	9074	13522	1.49

Table 4 – Significant parameters of polymer **57**.

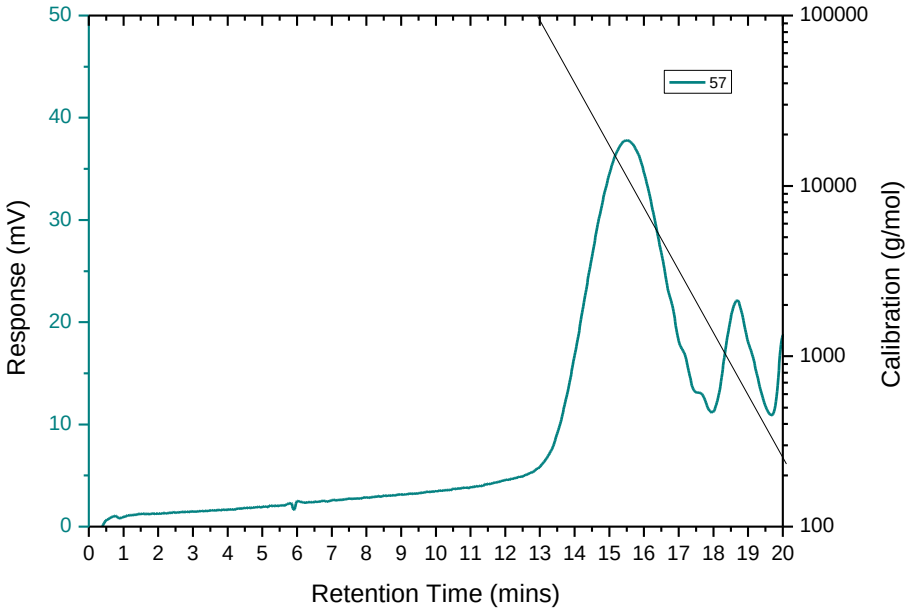

Figure 56 – GPC plot for polymer **57**.

Table 4 suggests that the average number of repeating units in each molecule is between 10 and 15; the polydispersity index (PDI), defined as the ratio between weight average molecular weight (M_w) and number average molecular weight (M_n) gives an idea about how narrow the distribution is.

Fig. 57 shows the UV-Vis absorption spectrum of polymer **57** compared to that of the monomer **38** in solution of DCM. It is evident that the longer conjugation, together with the addition of a stronger donor than the simple furan, resulted in the overall red-shift of the spectrum, which covers all the visible light range, up to 773 nm, corresponding to an optical bandgap of 1.60 eV. The most intense band covers the range between 300 nm and 500 nm, and contains the typical bands associated to the absorption of isoalloxazines (between 400 and 500 nm) and of fluorene[166] (between 300 nm and 450 nm). The band at highest energies (between 250 nm and 300 nm) due to the absorption of furans, as the same band is present in the absorption spectrum of **38**. The band at lowest energies is likely due to the ICT between donor and acceptor units; its relatively high intensity suggests that there is a good conjugation.

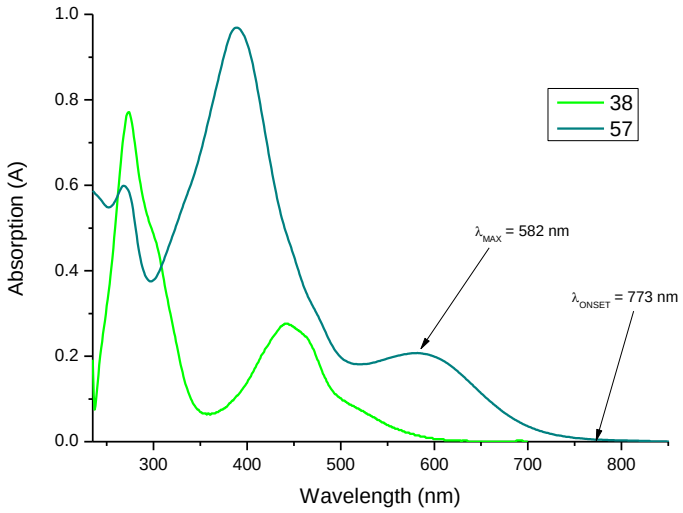

Figure 57 – UV-Vis absorption spectra of compounds **38** and **57**, in solution (C = 10^{-5} M, in DCM). The concentration of the polymer was calculated by assuming the repeating unit as the analyte.

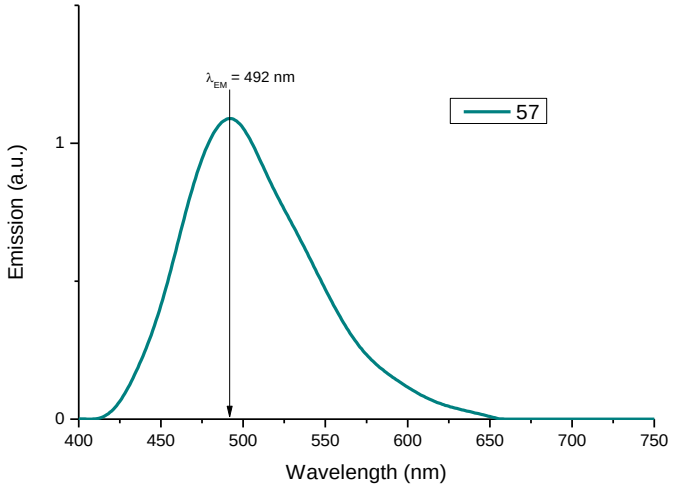

Figure 58 – Emission spectrum of compound **57** in solution (C = 10^{-5} M, in DCM), with λ_{exc} = 390 nm.

Unlike the other flavins synthesised, polymer **57** showed a weak fluorescence (Fig. 58), when exciting at the maximum of the most intense absorption band, with a Stokes shift of exactly 100 nm. Further studies concerning whether or not an acceptor unit (such as PCBM), in solution with **57**, could quench the fluorescence will be undertaken. This would reveal the presence of a good intermolecular charge transfer and, as consequence, it would mean that the polymer could be a good donor material for BHJ devices.

The cyclic voltammetry plot of polymer **57** (Fig. 59) shows the characteristic reversible reduction wave associated to the isoalloxazine and a non-reversible

oxidation part. A better resolution for the definition of the oxidation and reduction peaks is provided by square wave voltammetry (Fig. 60), which allows to estimate I_P, E_A and $E_{G,fund}$. All of them, together with the other properties of polymer **57**, are listed in Table 5.

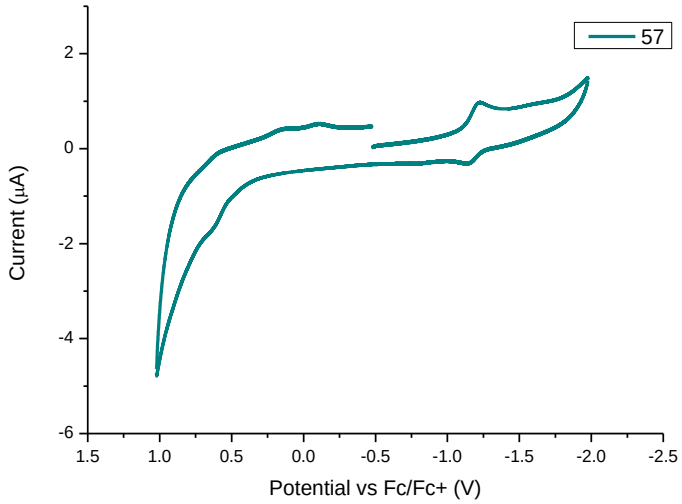

Figure 59 – CV plot of polymer **57**, in solution (C = 10^{-3} M, in DCM), performed using a Pt disk working electrode, a Pt wire counter electrode and a Ag wire reference electrode. $TBAPF_6$ (0.1 M) was used as supporting electrolyte and the redox potential of the Fc/Fc^+ couple as internal standard.

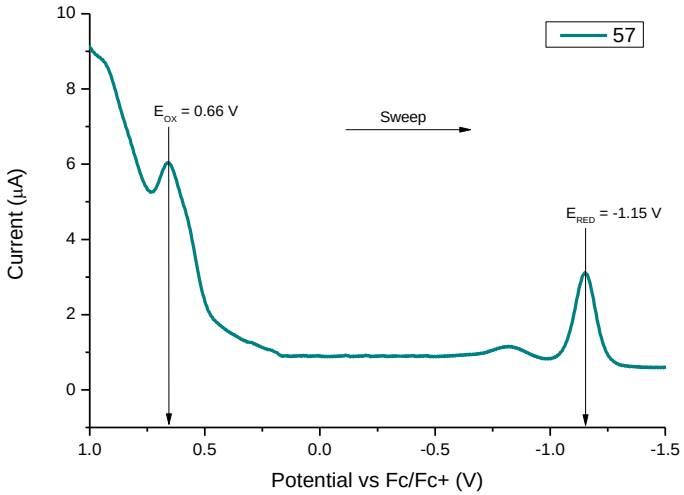

Figure 60 – SWV plot of polymer **57**, in solution (C = 10^{-3} M, in DCM), performed using a Pt disk working electrode, a Pt wire counter electrode and a Ag wire reference electrode. $TBAPF_6$ (0.1 M) was used as supporting electrolyte and the redox potential of the Fc/Fc^+ couple as external standard.

$E_{G,opt}$	$\lambda_{MAX,Abs}$	I_P	E_A	$E_{G,fund}$
1.60 eV	582 nm	–5.46 eV	–3.65 eV	1.81 eV

Table 5 – Summary of the properties of polymer **57**.

Once again, the difference between the two gaps is very small, suggesting that, once formed, the exciton is very easy to dissociate, thus giving an indication about the effectiveness that this system could act as donor material in BHJ devices.

- Synthesis of compound **59**

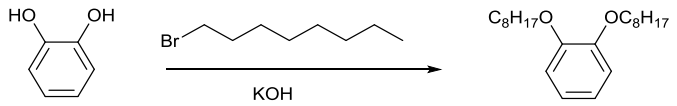

58 **59**

Compound **59** was synthesised following a slight modification of a previously reported protocol.[167] The reaction involved the use of the Williamson reaction: it was developed by Alexander Williamson[168] in 1850 and involves the formation of an ether by reaction of an alcohol with an alkyl halide *via* the S_N2 mechanism. Compound **54** was afforded in quantitative yield after distillation, in order to get rid of the excess halide.

- Synthesis of compound **60**

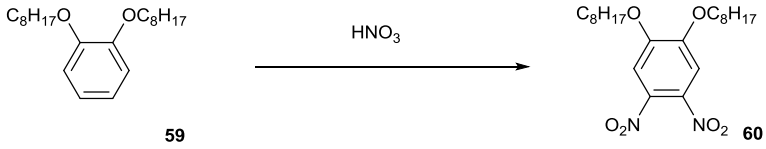

59 **60**

The procedure followed for this reaction is the same as reported in literature.[167] Its conditions are milder than those used for standard benzene nitration, due to the "electron-richness" of the starting material **59**. In fact, instead of a mixture of concentrated sulfuric and nitric acids, in this case a mixture of acetic acid and nitric acid are used. The electrophile NO_2^+ is generated by the reaction of two molecules of nitric acid, mediated by acetic acid, as suggested in Scheme 13.

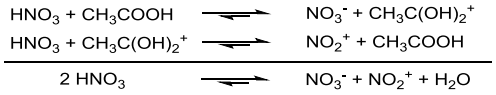

Scheme 13 – Proposed mechanism for the formation of NO_2^+.

Compound **60** was isolated in an excellent yield, after a very easy purification by recrystallization.

- Synthesis of compound **61**

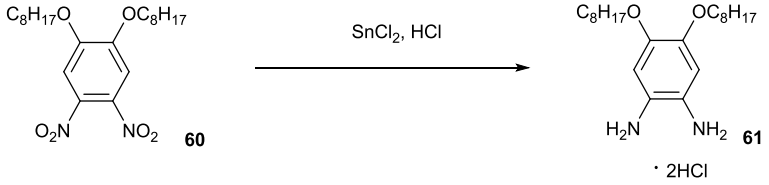

Compound **61** was synthesised according a slightly modified version of the procedure described in literature.[167] This strategy was chosen because it allows to obtain the aromatic diammonium salt **61**, instead of the aromatic diamine, which is supposed to be less stable in air. In order for the reduction to work, it is necessary to provide 6 electrons (e^-) and 6 protons (H^+) for each nitro group, as depicted in Scheme 14, and their source is the oxidation of tin chloride.

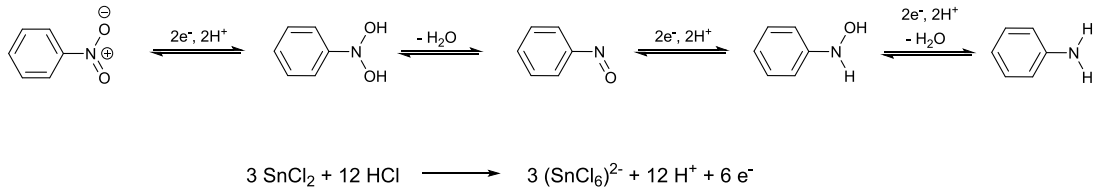

Scheme 14 – On the top, reduction of nitrobenzene to aniline. On the bottom, oxidation of tin chloride.

The first attempts of synthesising compound **61** were unsuccessful, likely because of the high water content of tin chloride. After several attempts, full conversion (judged by TLC) was achieved by doubling the amount of tin chloride (16 equivalents instead of the reported 8). Due to the high level of dryness required for the next reaction and the low stability in air, compound **61** was reprecipitated from methanol several times before being briefly dried under vacuum.

- Synthesis of compound **62**

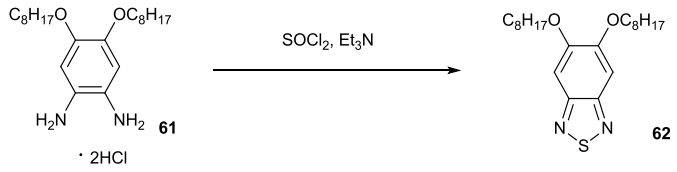

Compound **62** was synthesised following a slight modification of an existing procedure.[167] Crude compound **61** was first basified with triethylamine, before the cyclization could take place, as shown in Scheme 15.

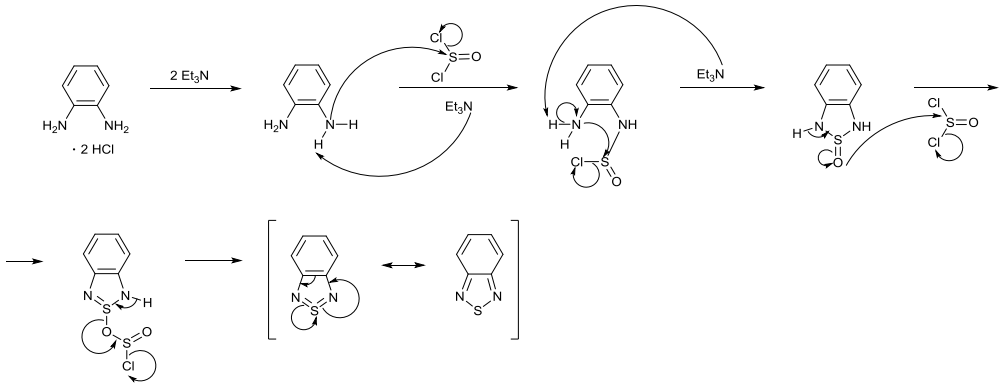

Scheme 15 – Proposed mechanism for the formation of BT.

As mentioned above, it is very important that the starting material is as dry as possible, since water would react with $SOCl_2$, generating SO_2 and compromising the yield of the reaction. The final yield for **62** of 72% (65% on average), over two steps, proves the effectiveness of the purification method used for compound **61**.

- Synthesis of compound **63**

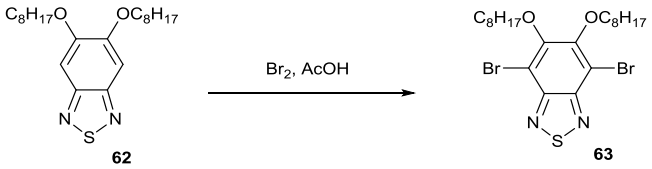

For this reaction an existing protocol was followed.[169] The conditions for this bromination are milder than the ones used for the synthesis of compound **46**. This is due to the alkoxy-chains in position C(5) and C(6) which activate the aromatic ring towards the electrophilic aromatic substitution.

- Synthesis of compound **64**

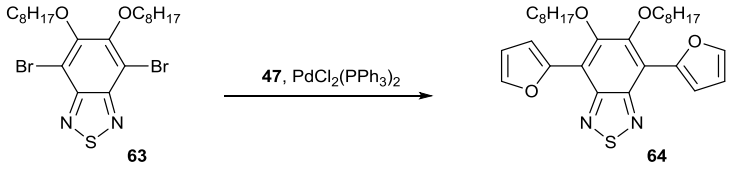

This Stille coupling was carried out according to an existing protocol.[170] Unlike in the protocol seen for obtaining compound **48**, the palladium catalyst used for this reaction is deactivated ($Pd^{(II)}$). This means that before taking part in the catalytic cycle it needs to be reduced *in situ* by two molecules of the stannane (Scheme 16).

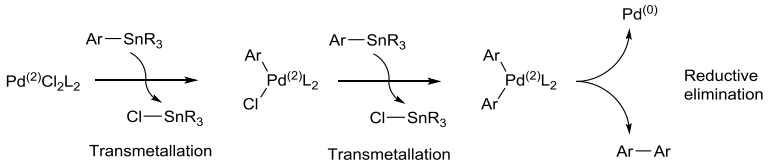

Scheme 16 – Proposed mechanism for *in situ* the generation of $Pd^{(0)}$. L and Ar are generic phosphine ligand and aryl group respectively.

The disadvantage of obtaining some homocoupling by-product is balanced by the better stability in air of $Pd^{(II)}$ catalyst than the $Pd^{(0)}$ counterpart. Compound **64** was afforded in 95% yield.

- Synthesis of compound **39**

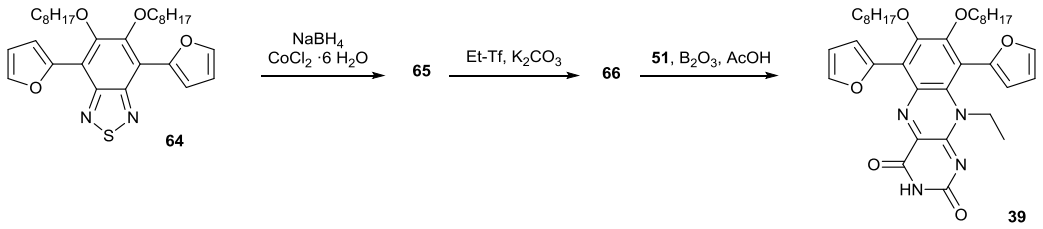

The reaction steps for making compound **39** from compound **64** are the same described previously for making compound **52** from **48**. However, the overall yield was only 5%, which is very poor when compared with that of compounds **52** and **54**. This might be due to greater reactivity of the aromatic diamine **65** towards alkylation. Another hypothesis would be connected to the effectiveness of the alloxan cyclization, as mentioned above.

- Analysis and characterisation of compound **39**

Compound **39** was characterised both optically and electrochemically, and the results were compared with those of flavin **38**. Fig. 61 highlights the differences in the UV-Vis absorption spectra of the two compounds: the presence of a bathochromic shift, of roughly 10 nm, in the absorption of compound **39** is certainly due to the inductive effect provided by the alkoxy side-chains. Another significant difference is the absence of the ICT band, present in flavin **38**. This could suggest that the two side-chains interfere with the conjugation of the two furans with the isoalloxazine unit, because of their steric hindrance, unlike predicted by the DFT simulations. Unfortunately, the distortion of the molecule was impossible to verify by X-ray diffractometry, as flavin **39** is a waxy solid. The absence of the ICT band is

responsible for the hypsochromic shift of the onset wavelength to 600 nm, however compound **39** shows a stronger absorption than **38** in the region between 400 and 500 nm.

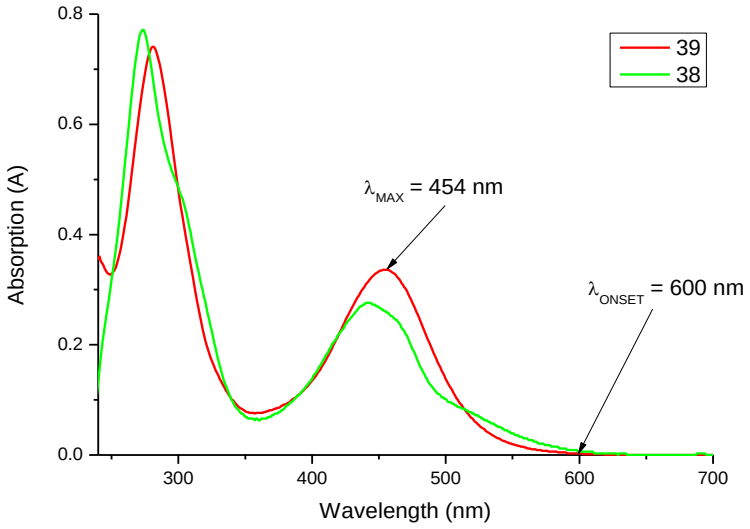

Figure 61 – UV-Vis absorption spectra of compounds **38** and **39**, in solution (C = 10^{-5} M, in DCM).

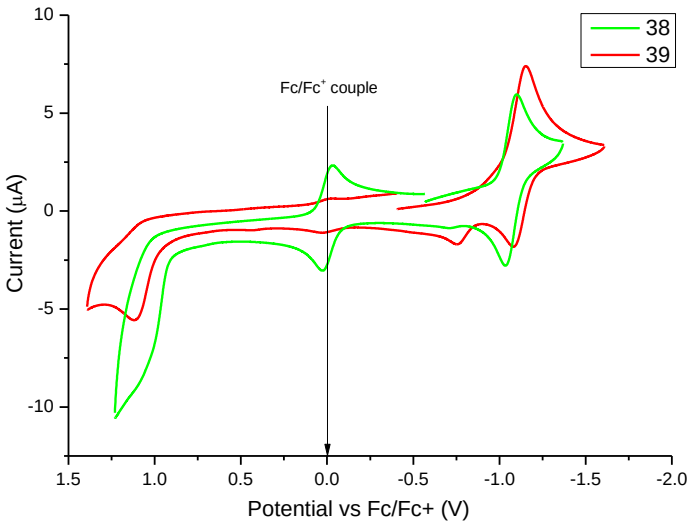

Figure 62 – CV plots of compounds **38** and **39** in solution (C = 10^{-3} M, in DCM), performed using a Pt disk working electrode, a Pt wire counter electrode and a Ag wire reference electrode. $TBAPF_6$ (0.1 M) was used as supporting electrolyte and the redox potential of the Fc/Fc^+ couple as internal standard.

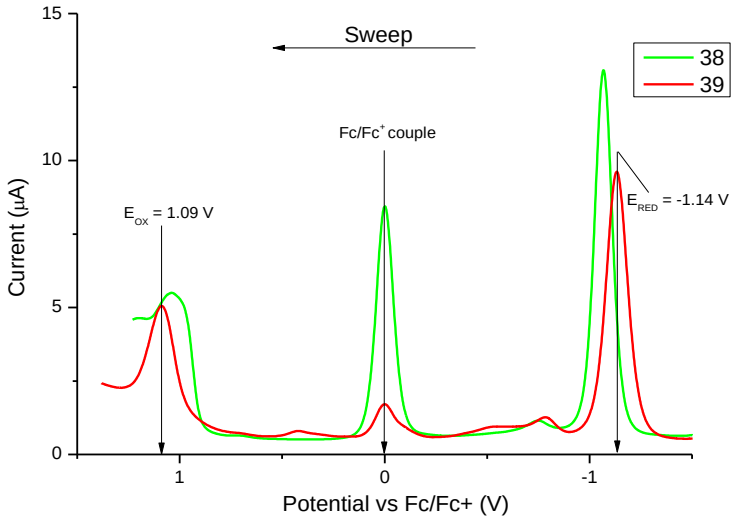

Figure 63 – SWV plots of compounds **38** and **39** in solution (C = 10^{-3} M, in DCM), performed using a Pt disk working electrode, a Pt wire counter electrode and a Ag wire reference electrode. $TBAPF_6$ (0.1 M) was used as supporting electrolyte and the redox potential of the Fc/Fc^+ couple as internal standard.

CV (Fig. 62) and SWV (Fig. 63) of compound **39** were carried out in order to study its electronic properties. Like **38**, flavin **39** possesses a reversible reduction wave and a non-reversible oxidation wave, at –1.14 V and 1.09 V, respectively. As expected from the absorption spectrum, the fundamental band gap of compound **39** is larger than that of flavin **38**. Table 6 summarises the electronic properties of **39**, in comparison with those of **38**.

Compound	I_P (eV)	E_A (eV)	$E_{G,fund}$ (eV)	$E_{G,opt}$ (eV)
38	–5.83	–3.73	2.10	1.99
39	–5.89	–3.66	2.23	2.07

Table 6 – Electronic properties of compounds **38** and **39**.

2.4.2 Fully conjugated TPT-Flavins

- Synthesis of compound **69**

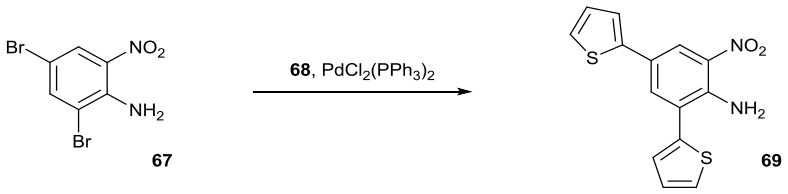

For this Stille coupling the same conditions seen above for synthesising compound **64** were applied. The product was found to be unstable in air so, after a quick work-

up, it was used for the next reaction without any further purification.

- Synthesis of compound **70**

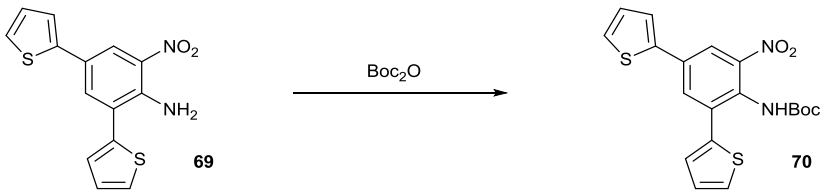

First attempts to synthesise compound **70**, using the literature conditions[171, 172] for the Boc protection of aniline, were unsuccessful. After few attempts, the best conditions were found by using a catalytic amount of DMAP as catalyst and THF as solvent (Scheme 17).

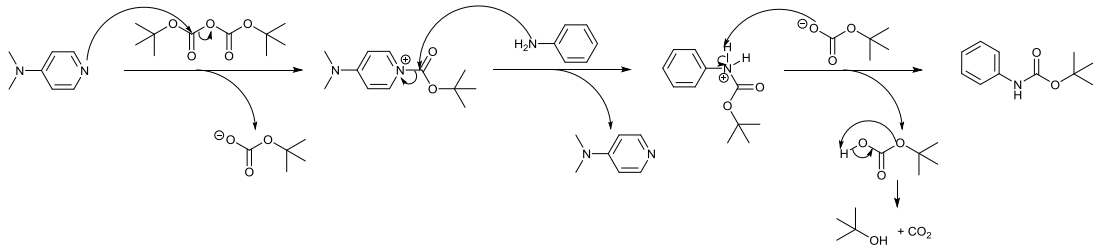

Scheme 17 – Proposed reaction mechanism for the Boc protection of aniline.[173]

However, the final product of this reaction was found to be the disubstituted carbamate **83** (Fig. 64).

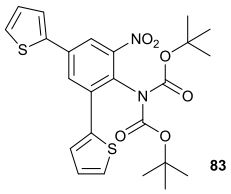

Figure 64 – Chemical structure of compound **83**.

A first attempt to use compound **83** straight for the next reactions did not work, likely for the large steric hindrance of the two Boc groups, so a partial deprotection was necessary. Compound **83** was then treated with 3 equivalents of potassium carbonate, affording **70** in an overall 68% yield (2 steps synthesis). The reaction mechanism could be a slight modification of the two possible mechanisms proposed by Martin and co-workers[174] (Scheme 18), although a different reagent is used. Both of them are based on the formation of a six-membered chelate system between the two Boc groups and a metal cation (in this case K^+), explaining the uneffectiveness

of the total Boc deprotection.

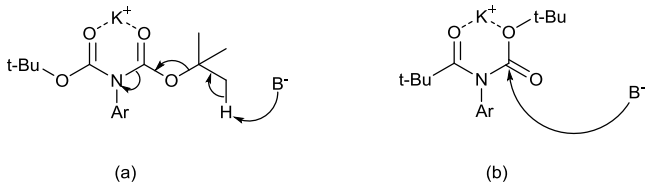

Scheme 18 – Proposed mechanisms for the selective deprotection of Boc groups. Ar and B are generic aromatic system and base, respectively.

- Synthesis of compound **71**

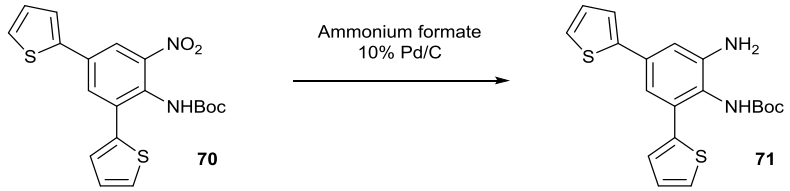

The reduction of compound **70** was carried out in mild conditions, using ammonium formate and palladium on activated charcoal, according to the general procedure reported by Ram and Ehrenkaufer in 1984.[175] The reaction is based on the decomposition of ammonium formate, in presence of palladium, to form ammonia, carbon dioxide and hydrogen. The latter is adsorbed on the surface of the catalyst, generating two moles of protons and two moles of free electrons for each mole of ammonium formate. As seen previously, for reducing nitrobenzene to aniline $6H^+$ and $6e^-$. This means that at least three equivalents of ammonium formate are needed. The reaction was carried out using an excess of formate, and the product, after a quick work-up, was used straight for the next reaction because of its poor stability in air.

- Synthesis of compound **72**

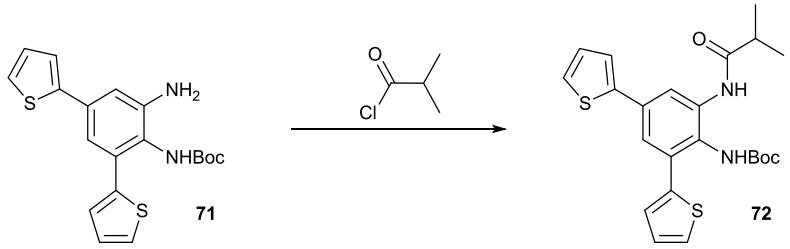

First attempts of making compound **72** were carried out using DMAP as catalyst and

dry THF as solvent, but they were unsuccessful. Surprisingly, further attempts replacing DMAP with triethylamine resulted in a successful conversion. Table 7 reports all the different conditions tried. A possible reaction mechanism is shown in Scheme 19.

Eq. DMAP	Eq. Et_3N	Solvent	Temperature	R. time (h)	Yield (%)
0.1	-	Dry THF	Room temp.	24	0
0.5	-	Dry THF	Reflux	24	0
-	1.5	Dry THF	Room temp.	24	53
-	1.5	Dry DCM	Room temp.	8	68

Table 7 – Reaction conditions tried for the acylation of compound **64**.

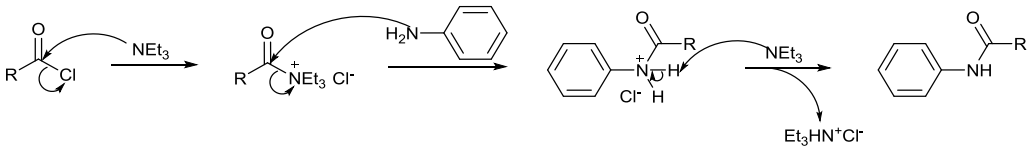

Scheme 19 – Proposed mechanism for the acylation of aniline.

- Synthesis of compound **73**

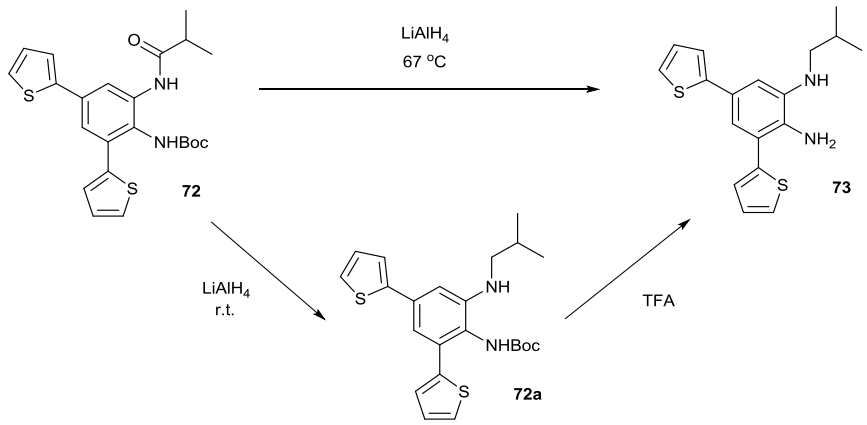

Two different strategies were tried for the amide reduction and Boc cleavage: the first one consisted of a one-pot step, carrying out the reduction reaction with $LiAlH_4$, at reflux in THF. The ^{1}H-NMR spectrum of the crude product showed no trace of the t-Bu singlet belonging to the Boc group. However, the product could not be detected by mass spectrometry. The crude compound was used without further analysis for the alloxan cyclization, to afford compound **40** (Scheme 6), but the reaction was unsuccessful, as the starting material was insoluble in acetic acid, even when heated up to 80 °C. Milder conditions for the reduction were then tried, using $LiAlH_4$ at room temperature. The ^{1}H-NMR spectrum of crude compound **72a** showed the

partial conversion of the amide and the unreacted Boc group, which was cleaved afterwards by treating intermediate **72a** with a TFA solution. Also in this case, the ^{1}H-NMR and mass spectra gave conflicting results.

There could be several reasons why these final steps of the synthesis do not work. Of course, one of the possible reasons can be attributed to unpredictability of alloxan reaction, as discussed above. In this case, the only way to sort the problem out would be a change in the synthetic approach. A possible synthetic path (Scheme 20) would be to start from the commercially available 3,5-dichloroaniline **84**, which would be coupled with **68** to get **85**. *N*-alkylation followed by reaction with 6-chlorouracil **77** would give the final flavin **40**.

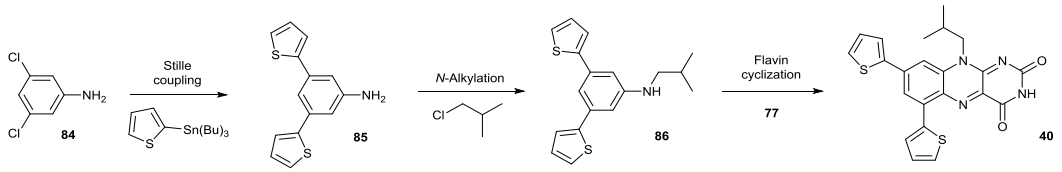

Scheme 20 – Proposed alternative synthetic protocol for the synthesis of flavin **40**.

In this case the flavin cyclization would be obtained *via* Yoneda's route.[176] Developed in the late 70's, it is a convenient way to synthesise isoalloxazines, starting from a *N*-alkylated aniline **71**, and consists of a *nitrative* cyclization of 6-(*N*-alkylanilino)uracil precursors **72**, followed by the consecutive alkene nitration to get **73** and of the benzene ring, affording **74**, which undergoes dehydration and deoxygenation to get the final flavin **76** (Scheme 21).

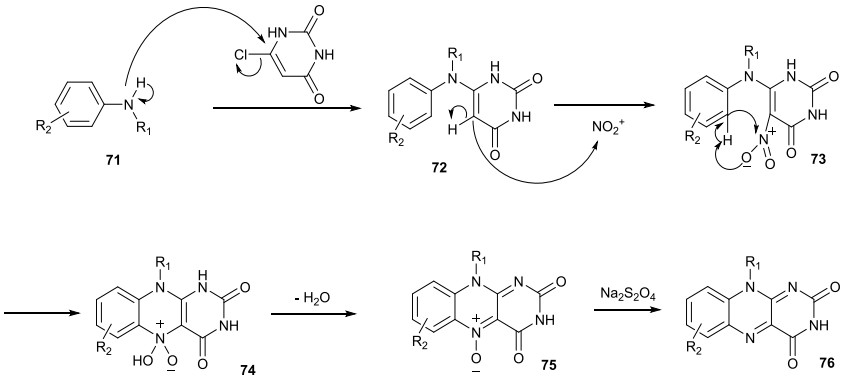

Scheme 21 – Proposed synthetic protocol for the Yoneda's route.[176]

Unfortunately, due to the time constraints of this project, the remainder of the synthesis will be carried out by somebody else within the Cooke group.

2.4.3 *bis*-Flavins

- Synthesis of compound **75**

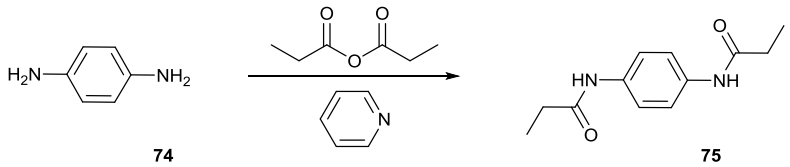

For this synthesis, a protocol already described in the literature was employed.[177] The reaction was carried out in THF, at reflux, using acetic anhydride as coupling agent and pyridine as base, and the yield for compound **75** was quantitative. The proposed mechanism for this reaction is depicted in Scheme 22: a first nucleophilic addition of pyridine to one of the carbonyl groups of the anhydride takes place, followed by the nucleophilic addition of aniline to the same carbonyl group with the release of pyridinium as leaving group.

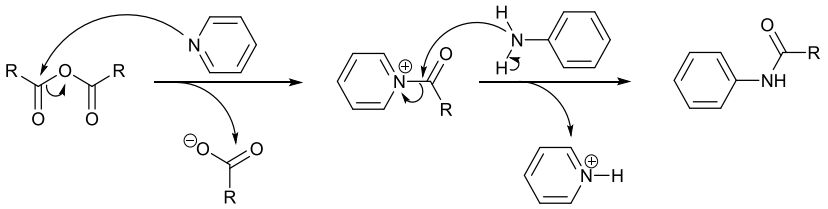

Scheme 22 – Proposed mechanism for the acylation of aniline.

- Synthesis of compound **76**

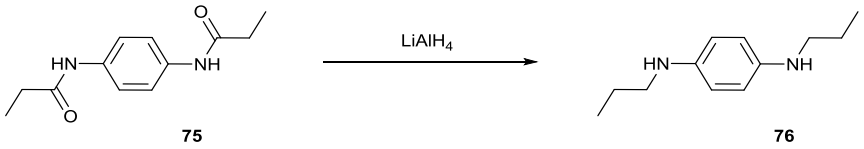

The reduction of compound **75** was carried out in THF, at reflux using $LiAlH_4$ as reducing agent, by adapting the procedure described for the synthesis of compound **73**. Compound **76** was afforded in quantitative yield.

- Synthesis of compound **77**

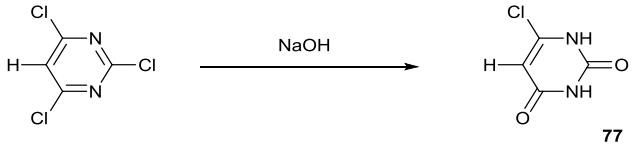

6-Chlorouracil **77** was synthesised starting from 2,4,6-trichloropyrimidine, according to a procedure described in the literature.[178] The reaction was carried out at reflux, in

an aqueous solution of 2.5 M NaOH and afforded **77** in 83% yield, after recrystallization from water.

- Synthesis of compound **78**

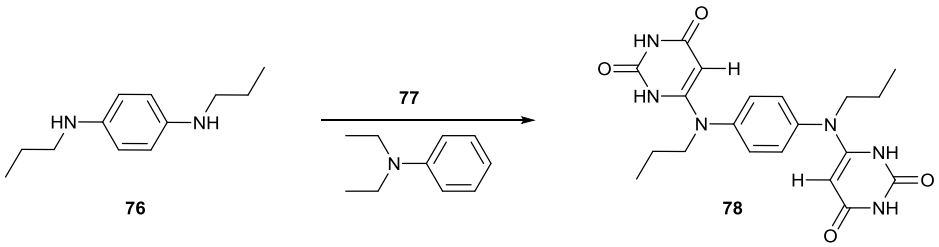

A first attempt to synthesise compound **78**, following a protocol described in the literature[179] was unsuccessful and ended up with the monosubstituted compound **87** (Fig. 65) in 84% yield.

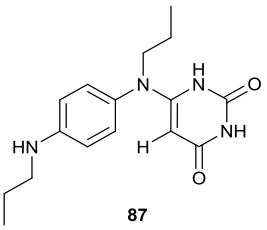

Figure 65 – Chemical structure of compound **87**.

Further attempts of synthesising compound **78** using the same strategy did not work, likely because of the degradation of *N*,*N*-diethylaniline, which was used as solvent. In fact, after the first use the colourless liquid turned dark yellow, suggesting decomposition. In the future, the same reaction should be tried by using a freshly distilled diethylaniline or using a more suitable solvent. The role of *N*,*N*-diethylaniline is dual (Scheme 23): first, it deprotonates the aromatic cation resulting from the nucleophilic addition of the starting material **76** to 6-chlorouracil; second, thanks to its high boiling point, it allows the reaction to be carried out at high temperature (180 ºC). A possible solution to investigate would be the use of neutral and high boiling point solvents, such as NMP, with the addition of an inorganic mild base, Na_2CO_3 for instance.

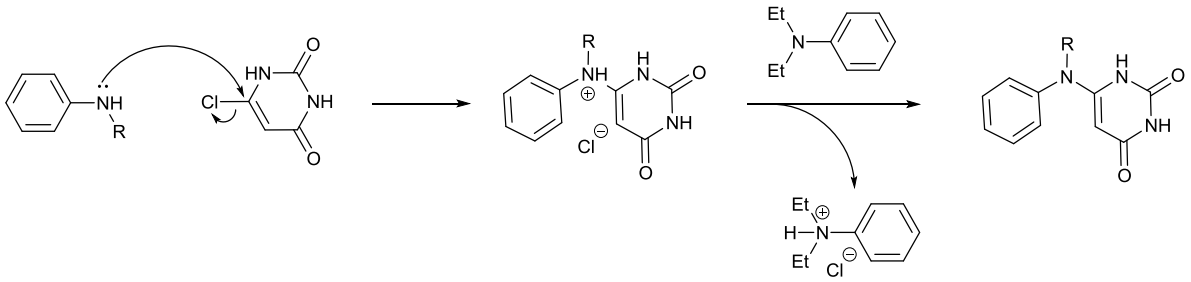

Scheme 23 – Proposed mechanism for the formation of compound **78.**

- Synthesis of compound **80**

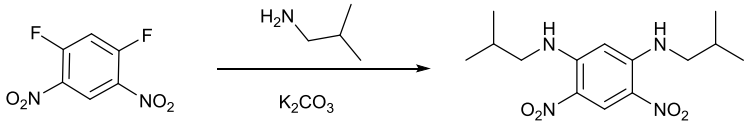

79 **80**

This reaction step involves two Nucleophilic Aromatic Substitutions (S_NAr), replacing each fluorine of compound **79** with an isopropylamine group. The reaction was carried out at reflux, in ethanol, and using K_2CO_3 as base, in order to deprotonate the resulting dication. Compound **80** was afforded in quantitative yield.

- Synthesis of compound **42**

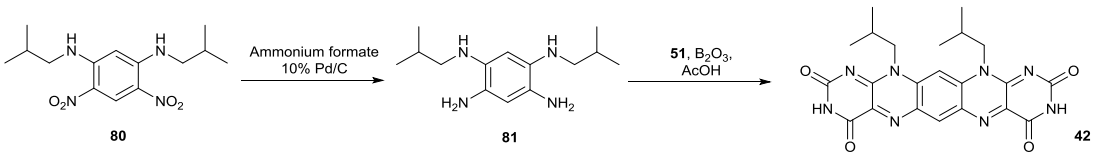

80 **81** **42**

The synthesis of compound **42** involved a two-step reaction: in the first instance compound **80** was reduced with 6 equivalents of ammonium formate, in the presence of palladium on activated charcoal, according to the procedure seen for the synthesis of compound **71**. The reaction was stopped after all compound **80** was consumed (according to TLC), and after a quick work-up and evaporation of the solvent, the crude compound was used for the alloxan cyclization, assuming compound **81** to be unstable in air, as most aromatic electron-rich amines are. The final reaction was conducted according to the standard alloxan cyclization procedure, but ended up with compound **88** (Fig. 66) in 48% yield, suggesting that the reduction worked only partially.

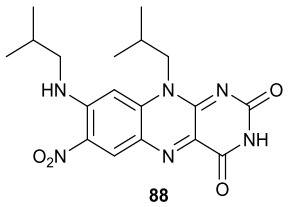

88

Figure 66 – Chemical structure of compound **88**.

A second reduction of compound **88** was attempted, by applying the same reaction conditions, but it led to the decomposition of the starting material. The reduction of compound **80** was tried further two times, using an excess of formate (12 equivalents), and using $LiAlH_4$ instead of formate/Pd. For both cases, mass spectrometry confirmed that the reaction worked, but the following alloxan cyclization was unsuccessful, although several solvents and different ranges of temperatures were tried. Due to time constrains, we decided to focus on different synthetic targets, which are also discussed within this thesis. However, current members of the group have been working on furthering this work.

- Analysis and characterisation of compound **88**

Compound **88** was characterised, both optically and electrochemically, showing peculiar properties. Fig. 67 shows the UV-Vis absorption of compound **88** in comparison with that of flavin **38** in the same experimental conditions: four main bands cover the whole light spectrum from the UV range up to the yellow (550 nm). The most intense band is that belonging to the isoalloxazine chromophore: the molar extinction factor associated to its maximum is almost double than that associated to the same peak in flavin **38**. The optical bandgap, calculated from the onset of the absorption is 2.26 eV; this is as expected, considering the absence of long push-pull conjugated systems. The CV plot of compound **88** (Fig. 68) shows the characteristic reversible reduction wave associated to the isoalloxazine, and other non-reversible reduction waves at more negative potentials.

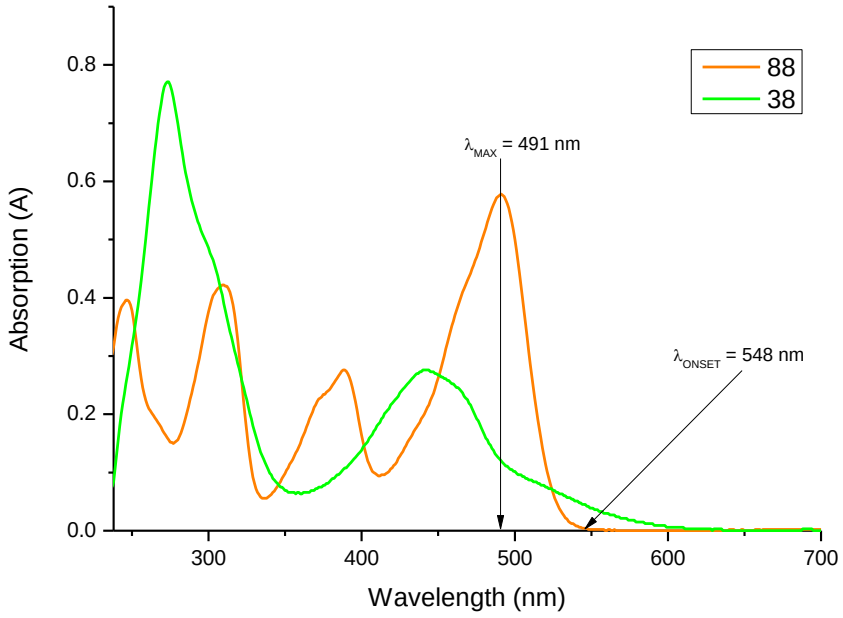

Figure 67 – UV-Vis absorption spectra of compounds **38** and **88** in solution (C = 10^{-5} M, in DCM).

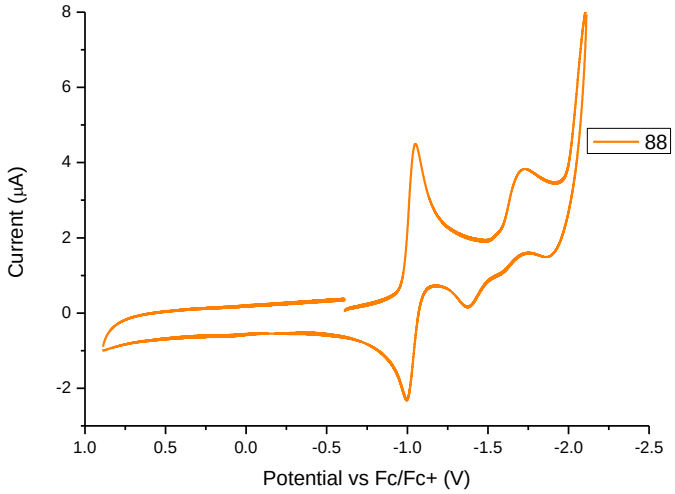

Figure 68 – CV plot of compound **88** in solution (C = 10^{-3} M, in DCM), performed using a Pt disk working electrode, a Pt wire counter electrode and a Ag wire reference electrode. $TBAPF_6$ (0.1 M) was used as supporting electrolyte and the redox potential of the Fc/Fc^+ couple as external standard.

Unfortunately, it was not possible to determine the position of the oxidation peak, likely because it is out of the range allowed by the solvent system. The SWV plot (Fig. 69) allowed to determine the position of the reduction peak, at –0.98 V, in line with the values found for the other flavins already synthesised.

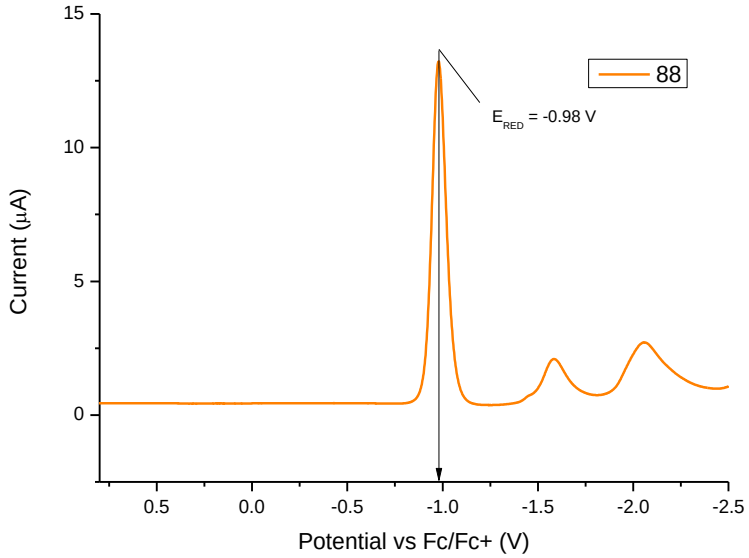

Figure 69 – SWV plot of compound **88** in solution (C = 10^{-3} M, in DCM), performed using a Pt disk working electrode, a Pt wire counter electrode and a Ag wire reference electrode. $TBAPF_6$ (0.1 M) was used as supporting electrolyte and the redox potential of the Fc/Fc^+ couple as external standard.

2.5 Conclusions and future work

The synthesis of two FPF-Flavins (**38** and **39**, Fig. 70) was successfully completed and flavin **38** was used to synthesise polymer **57**.

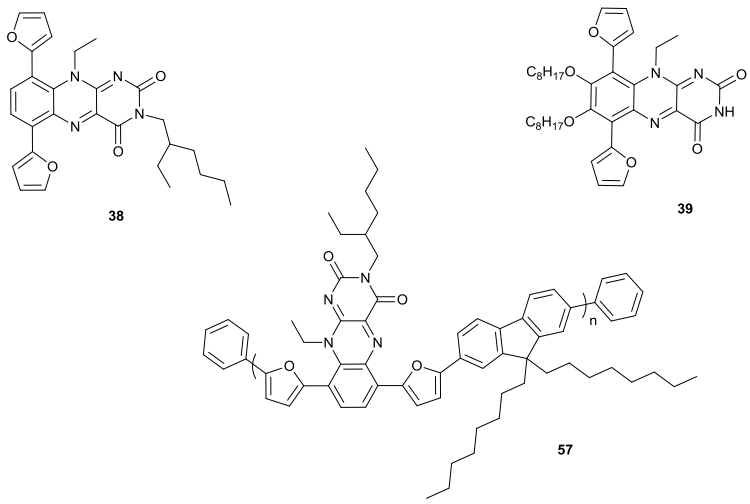

Figure 70 – Chemical structure of compounds **38**, **39** and **57**.

Compared to its TPT analogue, compound **38** has a slightly red-shifted absorption spectrum and, more importantly, a smaller gap between the optical and the fundamental bandgaps (11 meV for **38** against 42 meV for **43**, Fig. 45), meaning a better delocalization of the excitations. Polymer **57** showed a strong shift of the

absorption towards the NIR region of the electromagnetic spectrum which, together with the optimal position of I_P and E_A (both of them slightly above the HOMO and LUMO levels of PCBM[154]), suggest potential use as donor unit for BHJ devices. Further studies in this direction will be undertaken: in particular, a fluorescence quenching measurement of the polymer in solution with PCBM will give an indication about the effectiveness of the intermolecular charge transfer properties.

Compound **39** was synthesised in order to exploit the imide unit as non-covalent binding group, for molecular recognition, preserving the solubility that the alkylation of N(3) confers to the molecule. The two alkoxy chains in positions C(7) and C(8) give the molecule high solubility and a bathochromic shift of the absorption, due to the inductive effect. On the other hand their steric hindrance increases the non-planarity of the molecule, resulting in the absence of the ICT band and in the enlargement of the optical bandgap, as a consequence. This effect was confirmed by voltammetry studies. Further studies will be undertaken in order to study the potential ability of the imide functionality to bind TiO_2 particles, in order to use flavins as potential acceptor units for sensitisers in DSSCs.

Three novel flavin derivatives (**40** – **42**, Fig. 71) were designed and their synthesis was attempted. The reason behind the synthesis of compound **40** is the theoretically more enhanced conjugation between the two thiophene arms and the isoalloxazine unit. This should lead to an increase of the charge carriers mobility and of the intensity of the ICT absorption band. Unfortunately, the last step of the synthesis (Scheme 6) was unsuccessful, leading to a revision of the synthetic approach (Scheme 40). Compounds **41** and **42** were designed because of their potential employment as non-fullerene acceptors for BHJ devices, as supported by the DFT calculations. Their synthesis was started and will likely be completed by other members of the Cooke group.

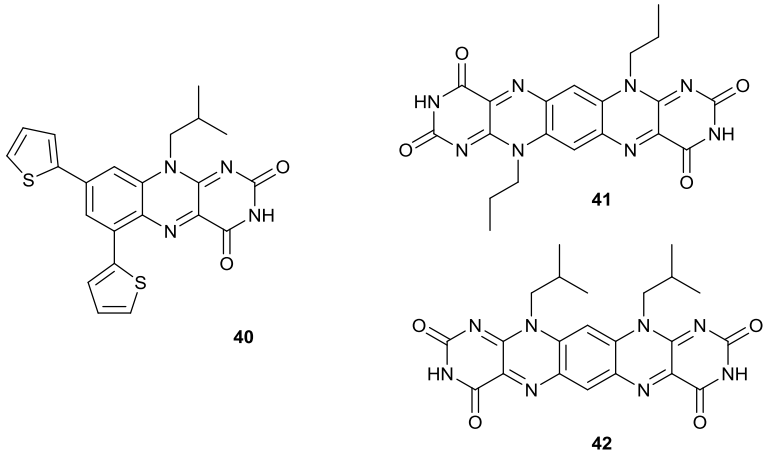

Figure 71 – Chemical structure of compounds **40**, **41** and **42**.

Chapter 3: Synthesis of benzothiadiazole derivatives

3.1 Introduction

BT is an aromatic heterocyclic molecule with a planar molecular structure which has been extensively used in a variety of applications, such as in fungicides,[180] herbicides, antibacterials,[181] plant growth and protection,[182] gene regulation,[183] and, of course, optoelectronics. More recently, it was shown that BT derivatives can even act as potent anti-HIV agents.[184] BT owes its properties to thiadiazole, of which it is a derivative. Thiadiazole is a heterocyclic five-membered aromatic compound containing two nitrogen atoms and one sulfur atom. Four possible isomeric structures exist, depending on the relative position of heteroatoms (Fig. 72): 1,2,3-thiadiazole, 1,2,5-thiadiazole, 1,2,4-thiadiazole and 1,3,4-thiadiazole, with the former two isomers being the most investigated.

Figure 72 – Chemical structure of thiadiazole isomers.

Bak *et al.*[185] analysed the microwave spectra of 1,3,4-thiadiazole, 1,2,5-thiadiazole and compared the results with those of thiophene and pyrrole: by evaluating the difference between the measured bond lengths and covalent radii, it was concluded that the aromatic character, as measured by the π-electron delocalization decreases in the order 1,2,5-thiadiazole > thiophene > 1,3,4- thiadiazole > pyrrole. Furthermore, it was found that 1,2,5-thiadiazole has a stronger aromatic character than the corresponding 1,2,5-oxadiazole.

It is not clear who first synthesised BT: as far as our records can go, in 1945, McGinty and Bywater[186] first reported the use of BT as precursor for antithyroidal drugs while, three years later, Luzzati[187] reported its X-ray structure. To the best of our knowledge, the first synthesis of BT was reported in 1950 by Khaletskii and Pesin,[188] who managed to make BT by coupling benzene-1,2-diamine with $SOCl_2$; although several synthetic procedures have been developed since then, their route is still one of the most employed.

3.2 Properties and applications of BT in PV applications

BT is one of the most employed acceptor units for photovoltaic materials, due to its particular electron withdrawing ability. In fact, compared to other acceptor groups (such as thienopyrazine, thienothiadiazole, etc.) BT can preserve a relative low-positioned HOMO energy level in the resulting polymers: this ensures a gain in terms of V_{OC} (see Par. 1.4.1.1) of the resulting device, and a higher stability of the molecule.[189] Since Dhanabalan *et al.*[190] first reported the utilization of a BT-based push-pull conjugated polymer as the donor unit for BHJ devices, BT has been extensively used as an acceptor unit to construct push–pull conjugated polymers for photovoltaic applications. For instance, in 2013 Hou *et al.*[191] reported the synthesis of polymer **88** (Fig. 73) which, used as active material in blend with $PC_{71}BM$, could deliver a PCE of 8.1%. Another significant example is the vacuum-processable small molecule **89** (Fig. 73), reported by Hong *et. al*,[192] which could deliver 4.1%, in blend with C_{70}.

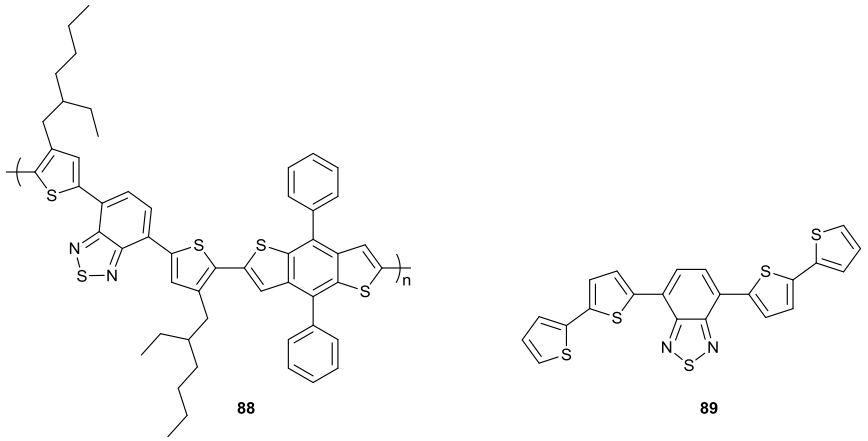

Figure 73 – Chemical structure of compounds **88** and **89**.

The success of BT in constructing highly efficient push–pull narrow bandgap conjugated copolymers for BHJ devices inspired chemists to exploit its analogues as building blocks for new photovoltaic donor polymers. Generally, there are two ways of modifying BT: the first is by introducing a significant change in the skeleton of the molecule, for instance by replacing the sulphur atom with other heteroatoms, such as oxygen, selenium and nitrogen, or with carbon, or by replacing the benzene ring of BT with more electron-deficient heterocycles, such as pyridine and pyridazine. Notably, these modifications would actually lead to new heterocyclic units and result in great changes in the conjugated backbones, having substantial effects on the optical and electronic properties of the resulting polymers.

In 2008, Leclerc *et al.*[193] compared the performance of several *push-pull* polymers containing the same carbazole unit as a donor and different modifications of BT (**90** – **93**, Fig. 74), finding out that polycarbazoles including pyridine-based thiadiazole or oxadiazole as acceptor (**92** and **93**) had a stronger and wider absorption than the parent benzene-based polymers (**90** and **91**). However, the latter show a better structural organization and better charge carrier mobilities that compromise the PV performance of the final devices. In 2014, Wong *et al.*[194] reported the results of their studies about the influence of the chalcogen atom in benzochalcogenodiazole-based vacuum-processable small molecules for large-area OPVs (**94** – **96**, Fig. 74). In particular, they found out a relationship between the atomic number of the chalcogen atom and the physical properties of the resulting molecules, and ideally **94** should give the best performance because of its higher planarity and stronger and more red-shifted absorption. However, the devices fabricated by blending the three molecules with C_{70} showed an opposite trend of performance, and this was explained by the high molecular recombination shown by **94**.

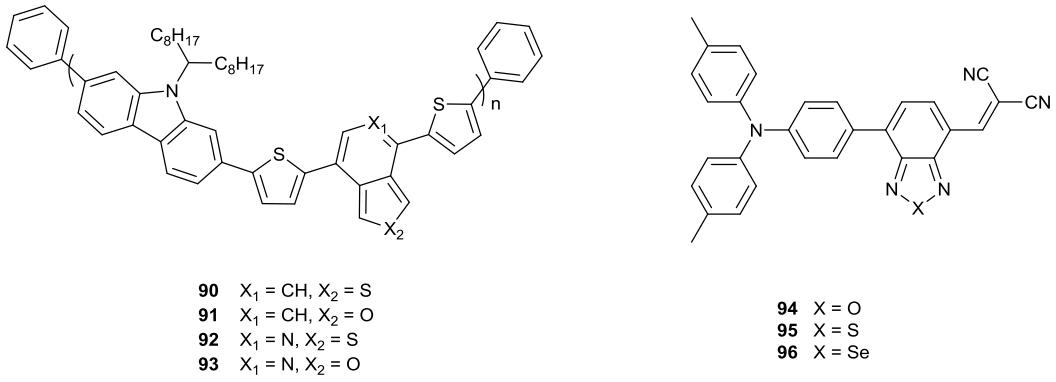

90 X_1 = CH, X_2 = S
91 X_1 = CH, X_2 = O
92 X_1 = N, X_2 = S
93 X_1 = N, X_2 = O

94 X = O
95 X = S
96 X = Se

Figure 74 – Chemical structure of compounds **90 – 96**.

Another widely explored way of modify BT is the introduction of functionalities on the C(5) and C(6) positions. In fact, it has been demonstrated that the functionalisation of this positions can lead to significant changes in the photovoltaic properties, although the intrinsic structure of BT does not change. As mentioned above (Par. 1.4.1.2.1), You *at al.*[53] demonstrated that simply by replacing the two hydrogen atoms of BT with fluorine atoms (**2**, Fig. 75), the performance of the resulting device increased from 5.0% to 7.2%. With respect to its non-fluorinated counterpart, in fact, polymer **2** showed a smaller E_G and deeper HOMO/LUMO levels. In 2009, Zhang *et al.*[195] revisited the work of Leclerc[193] by synthesising a new

polycarbazole, containing alkoxy-functionalised BT (**97**, Fig. 75), delivering a PCE of 5.4% (versus 3.6% for **90**) with the same conditions of fabrication. In particular, they obtained a better J_{SC} (9.6 mA/cm^2 for **97** against 6.9 mA/cm^2 for **90**) which was attributed to the better solubility and closer packing of the polymer in the solid state.

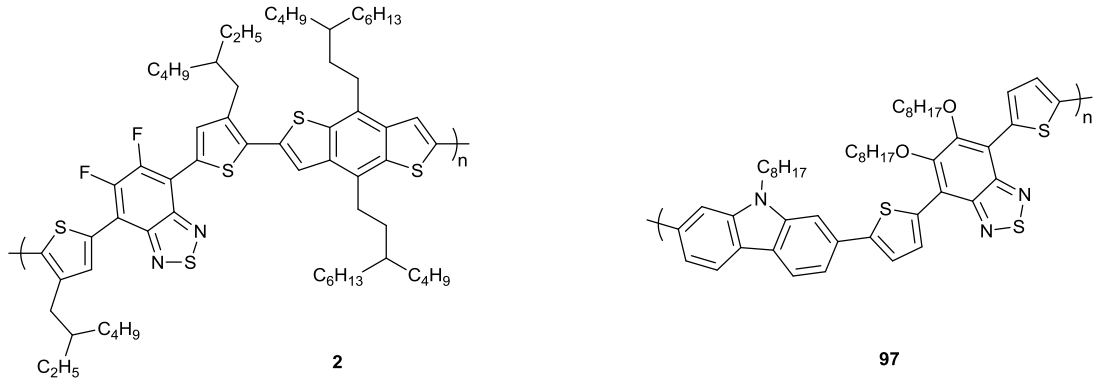

Figure 75 – Chemical structure of polymers **2** and **97**.

The high demand for NIR absorber materials has pushed the research to explore more "exotic" and stronger acceptors, in order to increase the strength of the *push-pull* system, thus decreasing the bandgap. The extension of the heterocyclic core of BT is a promising strategy that goes into this direction. Ting *et al.*[196] reported the synthesis of low-bandgap copolymers for exploiting the NIR absorption, based on hetero-annulated BT (**98** and **99**, Fig. 76) and the performance of the devices were compared with those obtained by using the BT parent compound **100** (Fig. 76).

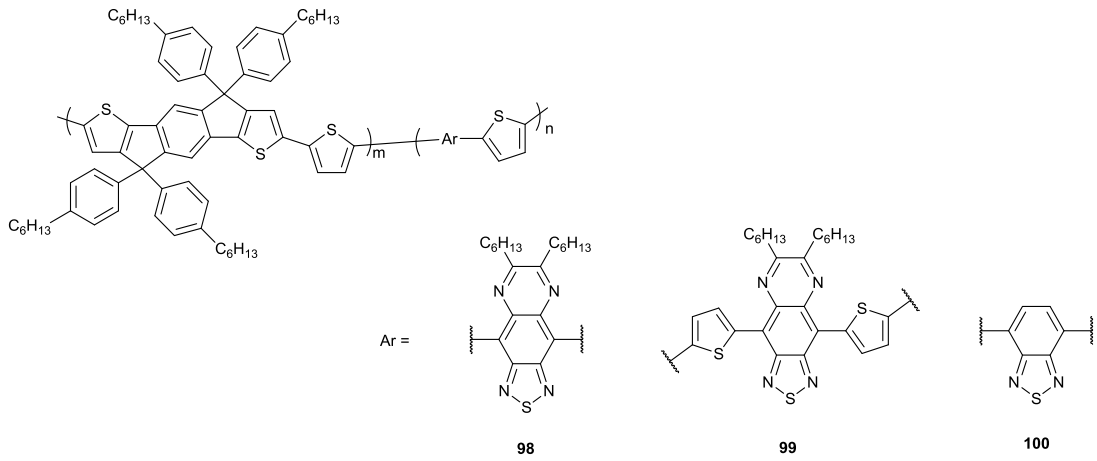

Figure 76 – Chemical structure of compounds **98** – **100**.

Although **98** and **99** showed a broader absorption, extending up to 1300 nm, the performance of devices made by blending them with $PC_{71}BM$ were very poor (PCEs of 0.5% and 0.8% respectively), not even comparable with those of polymer **100**

(PCE of 4.3%). This is likely due to the non-perfect match of the energy levels of the polymers with those of the acceptor.

BT has also been widely employed as acceptor unit in sensitisers for DSSCs. As shown in chapter 1.4.2.1, some of the most performing dyes are based on D-A-D-A or D-D-A-A architectures, in order to exploit the *push-pull* character for a better and broader absorption. Dyes **28** and **29** (Fig. 30) are an example of this strategy. Cao *et al.*[197] reported the results of a comparative study made on dipentyldithieno quinoxaline-based organic dyes (**101** – **103**, Fig. 77). They found that the incorporation of an acceptor or a donor unit (BT and EDOT, respectively) resulted in a significant improvement of the optical properties with a more intense and red shifted absorption. However, while the introduction of EDOT upshifted the HOMO level of dye **103** and resulted in a decrease of the electron lifetime, the incorporation of BT resulted in better electron transition properties and more effective suppression of recombination. A PCE of 6. 8% was achieved with dye **102** in contrast with the 4.0% achieved with both dyes **101** and **103** respectively.

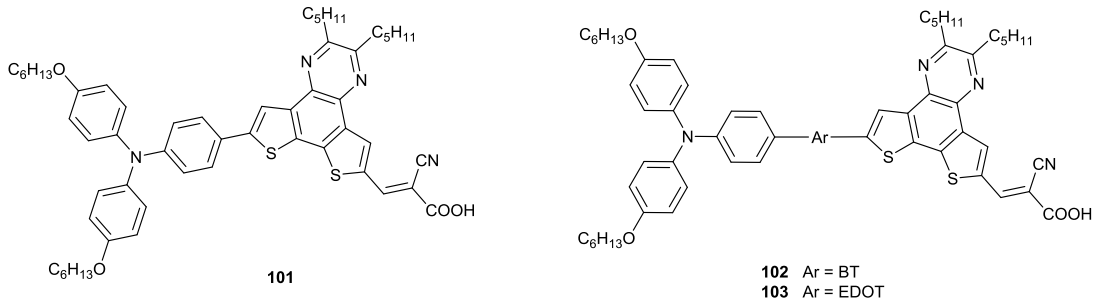

Figure 77 – Chemical structure of dyes **101** – **103**.

3.3 Aims

This chapter reports the synthesis of several BT derivatives (Fig. 78), designed to be used as P-type semiconductors in BHJ devices or as sensitisers in DSSCs. Among these, compound **107** contains an alkoxy-functionalised analogue of BT in order to increase the solubility of the whole molecule, while polymer **110**, designed for absorbing in the NIR, contains a benzo-*bis*-thiadiazole (BbT) unit, in order to enhance the strength of the *push-pull* character. Furthermore, the series of dyes **104** – **106** constitutes one of the first examples of dyes for DSSCs containing Fc as donor unit, reported to date.

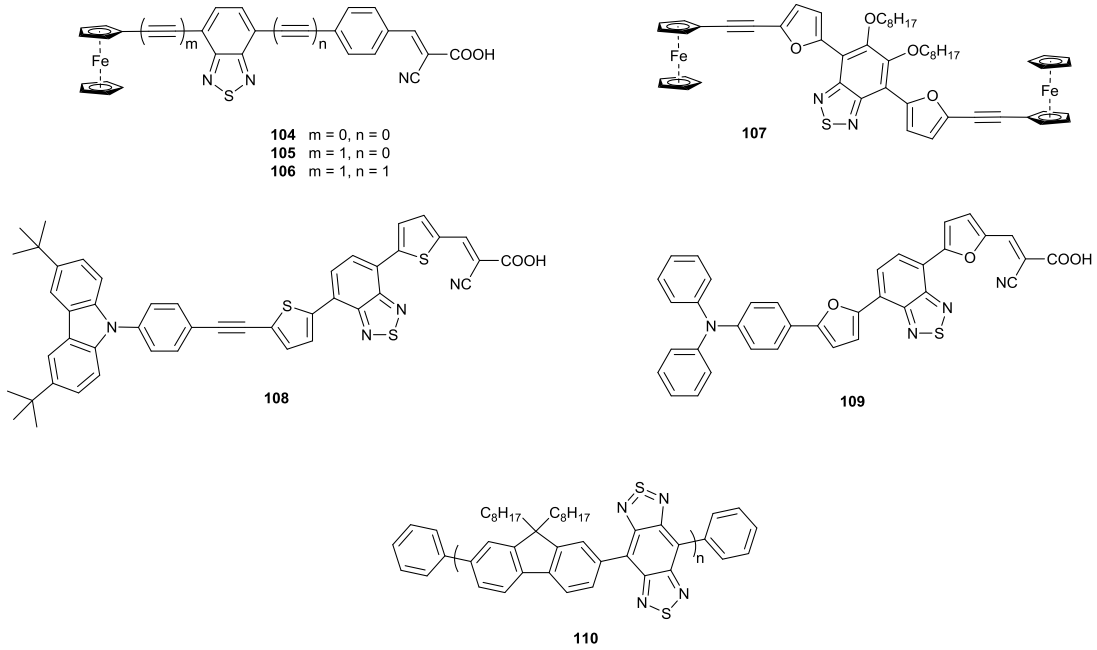

Figure 78 – Chemical structures of compounds **104** – **110**.

For dyes **104** – **106**, as well as for compound **107**, ferrocene (Fc) was chosen as donor unit since it is known to be an electron donor with absorption in the visible region, and it has interesting redox properties. Fc is a relatively cheap material which was unintentionally prepared, in 1951, by Pauson and Kealy[198] by reacting cyclopentadienyl magnesium bromide with ferric chloride. Its "sandwich" structure was assigned by Wilkinson *et al.*,[199] after a long controversial debate on it. This discovery allowed them to earn the Nobel Prize in 1973. Made of two aromatic cyclopentadiene rings (each of them contributing 5 electrons to the complex) and a Fe^{2+} (providing all its 8 shell electrons), Fc is considered as an 18-electrons aromatic compound and due to its high electron density, it reacts readily with electrophiles.[200, 201] The low potential at which it undergoes oxidation[202] (+ 0.4 V vs SCE, in MeCN, with $TBAPF_6$ 0.1M as electrolyte) gives an idea of its electron-richness. Furthermore, the Alfrey-Price *e* parameter of vinylferrocene (Fig. 79a), which gives a semi-empirical indication of the electron donating character of a molecule toward a conjugated vinyl group, was found to be –2.1.[203, 204] This value was compared to –1.37 for p-*N*,*N'*-dimethylaminostyrene (Fig. 79a), indicating that Fc should ideally be a better electron donor moiety than p-*N*,*N'*-dimethylaniline (a known donor in DSSC[205]). Another key factor taken into account was its "ideal" electrochemistry; in fact, the electrochemical transformation from Fc to Fc^+ is fully reversible (Fig. 79b), and this would play an important role if the final compounds keep the reversibility.[202]

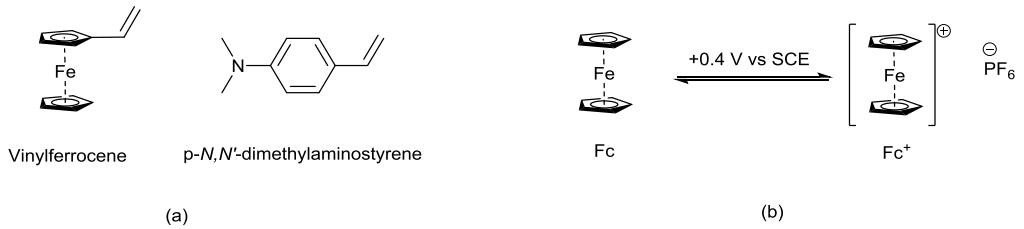

Figure 79 – (a) Chemical structure of Vinylferrocene and p-*N*,*N*'-dimethylaminostyrene; (b) electrochemical transformation of Fc to Fc^+.

The theoretical interest in this novel compound may now be added to the practical interest arising from its usefulness in several fields, such as catalysis, materials science (anti-smoke fuel additive[206]) and medicinal science (anticancer and antimalarial activity[207]). Most importantly the fully reversible one electron oxidation of Fc is often used as a standard in cyclic voltammetry to characterise the redox potential of other organic compounds.[208]

Despite the low cost and ideal optical and electrochemical properties that make Fc a serious candidate as donor unit, it is surprising that the photovoltaic properties have only received limited attention. In 2011, Spiccia *et al.*[209] used the Fc/Fc^+ redox couple as replacement of the corrosive iodide electrolyte as HTM in DSSCs, reporting a significant improvement of the V_{OC} and of the overall PCEs. Only in 2014, Sirbu *et al.*[210] reported a trisubstituted Fc-based porphyrin derivative (**111**, Fig. 80) with a cobalt (II/III) electrolyte for DSSCs but its DSSC performance was rather limited (J_{sc} = 0.068 mA/cm^2, V_{oc} = 283 mV, FF = 0.42, PCE = 0.008%) because of the close proximity of Fc to the TiO_2 surface and unmatched electron exchange kinetics between the dye and the electrolyte.

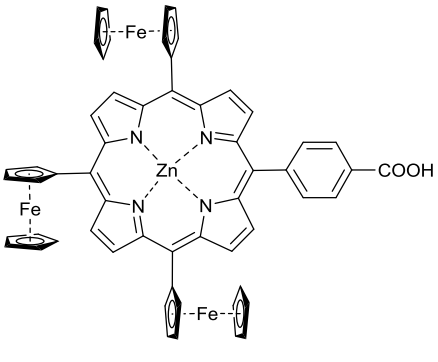

111

Figure 80 – Chemical structure of dye **111**.

The idea behind the synthesis of dyes **104** – **106** was the design of low-cost sensitisers with a very simple structure and an optimised match of energy levels

between the dye and the HTM. For this reason a D-A-π-A architecture was chosen, with BT as middle acceptor, for its low positioned HOMO level and its affordability. The three dyes differ in alkyne linkers between Fc and BT and between BT and benzene. The variation in linkers will provide a study of the performances of the devices with respect to varying the planarity of the sensitisers. The proposed strategy for the synthesis of dye **104** (Scheme 24) would start with the synthesis of compound **113**, *via* Suzuki coupling between ferrocene boronic acid **112** and 4,7-dibromobenzo[*c*][1,2,5]thiadiazole **46**, followed by another Suzuki coupling with 4-formylphenylboronic acid **114**, affording compound **115**. This would finally undergo a Knoevenagel condensation with cyanoacetic acid **116**, affording the target dye **104**.

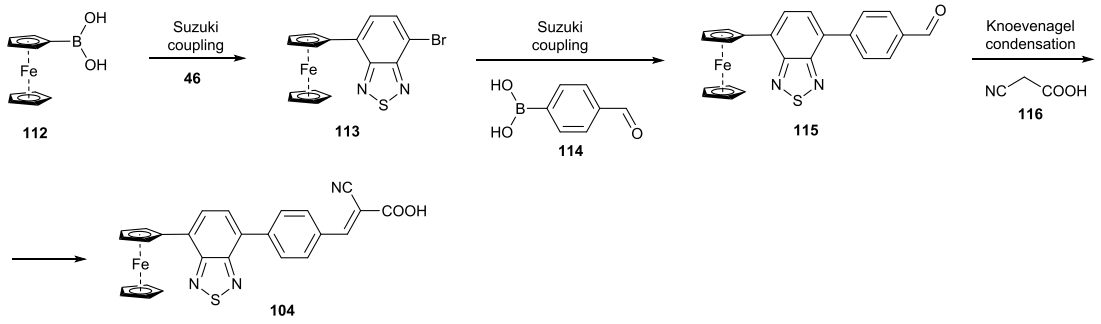

Scheme 24 – Proposed strategy towards the synthesis of dye **104**.

The protocol adopted for the synthesis of dye **105** is reported in Scheme 25. Commercially available ethynylferrocene **117** would be coupled with **46**, *via* Sonogashira coupling, affording **118**, which would be coupled with **114**, affording **119**. The final dye **105** would be obtained by Knoevenagel condensation with **116**.

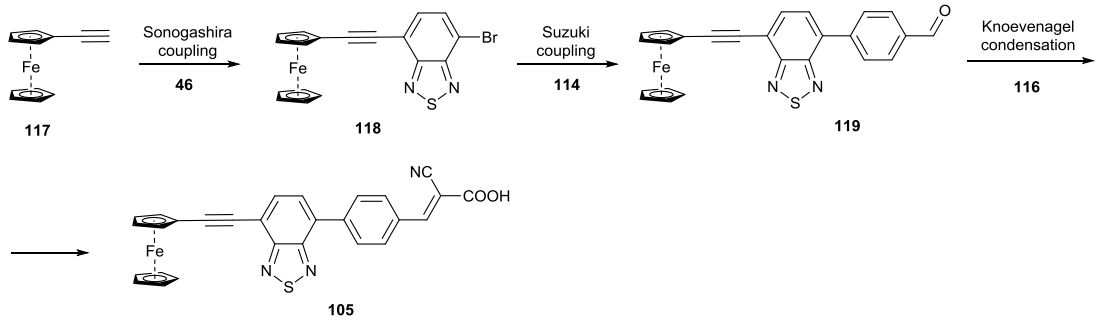

Scheme 25 – Proposed strategy towards the synthesis of dye **105**.

In Scheme 26 the proposed strategy for the synthesis of dye **106** is presented. Compound **118** would undergo a Sonogashira coupling with 4-ethynylbenzaldehyde **120**, affording compound **121**, which would be coupled with **116** through Knoevenagel reaction, affording the target dye **106**.

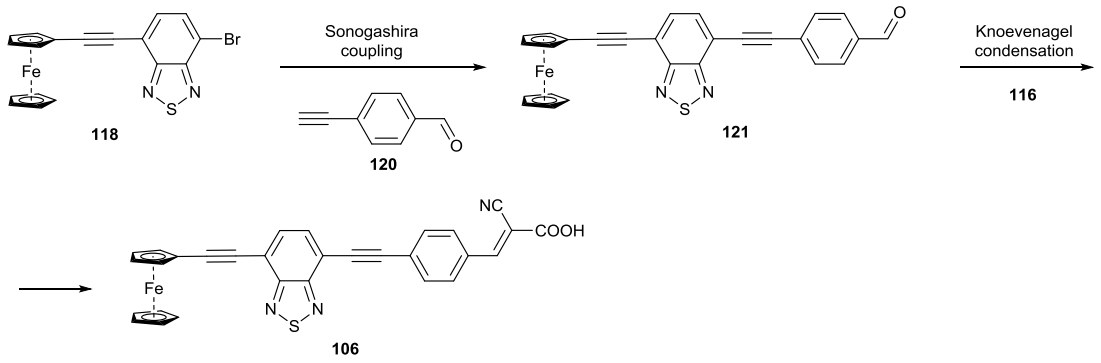

Scheme 26 – Proposed strategy towards the synthesis of dye **106**.

The employment of Fc in BHJ devices was also explored by synthesising derivative **107** which would be used as small-molecule donor. Also in this case, what makes Fc attractive is the reversibility of its oxidation, which would translate into a high hole-mobility. The central difuran benzothiadiazole would work both as chromophore and as solubilising group, due to the octyloxy side-chains on the BT unit. Furthermore, BT would contribute to lower the HOMO of the molecule, in terms of energy. The synthetic route (Scheme 27) would start from the previously made compound **64** (Scheme 4), which would undergo a dibromination, affording compound **122**, followed by a Sonogashira dicoupling with ethynylferrocene **117**, affording the target compound **107**.

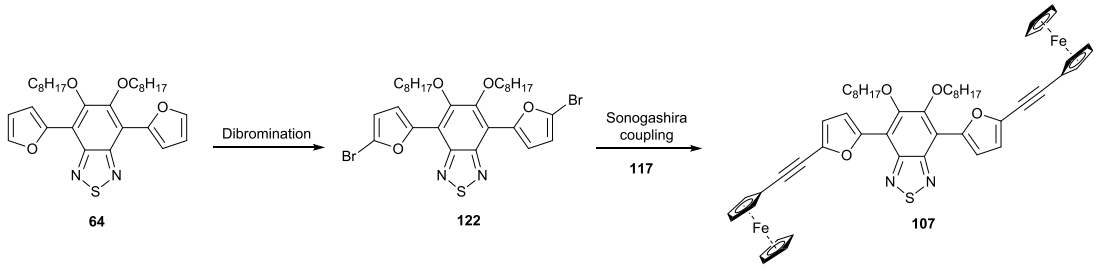

Scheme 27 – Proposed strategy towards the synthesis of compound **107**.

BT was also used as middle acceptor for the two D-A-π-A dyes **108** and **109**. The two molecules were designed basing on a previously published work by De Angelis *et al.*,[211] who synthesised a series of BT-based sensitisers, including dye **123** (Fig. 81), which delivered a PCE of 5.7%.

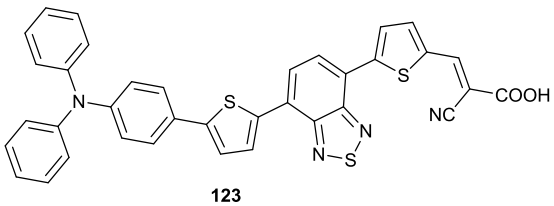

Figure 81 – Chemical structure of dye 123.

In particular, dye **108** was designed in order to understand whether or not a more planar geometry of the donor could improve the performance of the devices by facilitating the electron injection from the donor to the π-bridge. For this reason, the two peripheral phenyl unit were bridged to form a carbazole unit, and an alkyne linker was introduced between the donor and the first thiophene ring. Two alkyl side-chains were introduced on the carbazole unit, in order to prevent dye aggregation.

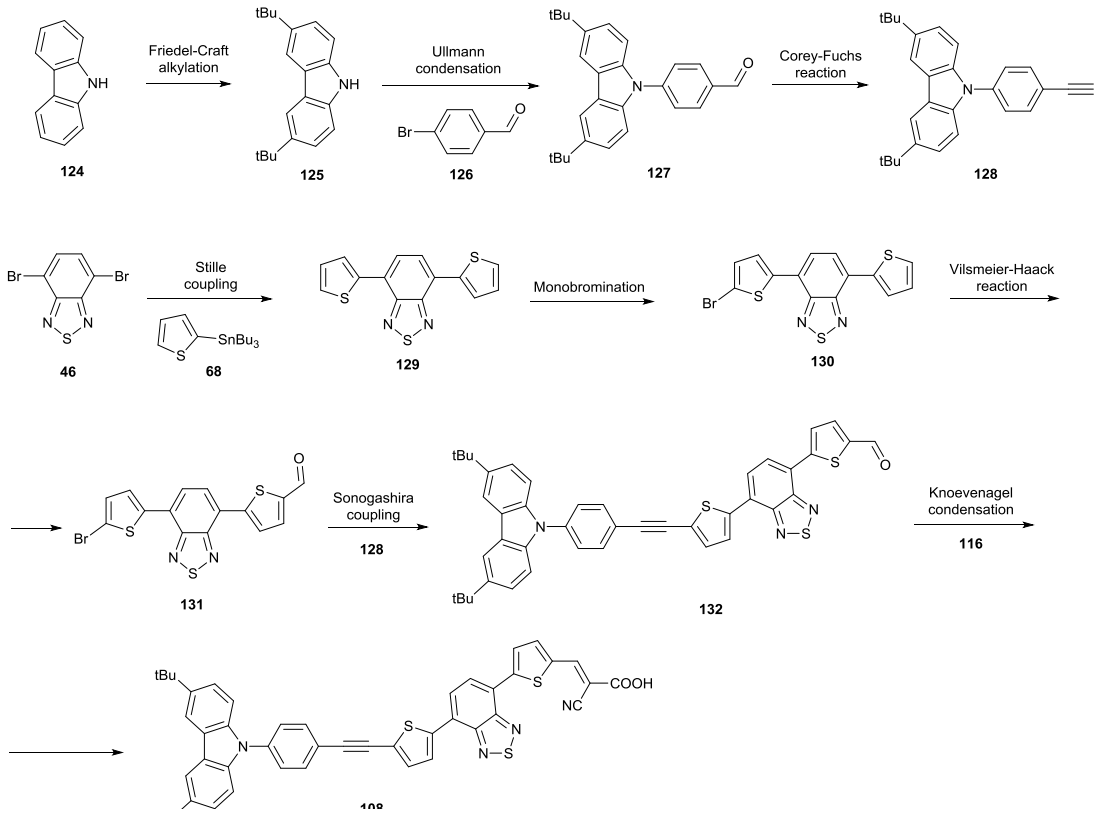

Scheme 28 – Proposed strategy towards the synthesis of dye **108**.

The proposed synthetic strategy (Scheme 28) would start from the alkylation of commercially available carbazole **124**, affording **125**, which would be coupled with 4-bromobenzaldehyde **126** to afford compound **127**. This would undergo a Corey-Fuchs reaction to afford **128**. The synthesis of the second building block would start from the Stille coupling between 4,7-dibromobenzo[*c*][1,2,5]thiadiazole **46** and 2-(tributylstannyl)thiophene **68**, to afford compound **129**, which would undergo a monobromination (**130**), followed by a Vilsmeier-Haack formylation to afford compound **131**. The two building blocks, **128** and **131**, would be coupled via Sonogashira cross-coupling, affording **132**, which would undergo a Knoevenagel reaction with cyanoacetic acid **116**, affording the target compound **108**.

Dye **109** was designed in order to explore the use of furan instead of thiophene. Indeed, due to its smaller resonance energy than thiophene (16 kcal/mol and 29 kcal/mol, respectively), furan is expected to be more efficient (see Par. 2.3).[152] Peng *et al.*[92] reported the results of their comparative study on thiophene, furan and selenophene when incorporated in a sensitiser: they found that furan could slightly improve the overall PCE when replacing thiophene. Furthermore, furan derivatives can be obtained from a variety of natural products, thus a large scale production of dyes containing furans could be considered more sustainable. The proposed synthetic strategy (Scheme 29) would start from previously made compound **48**, which would be monobrominated (**133**) and then formylated to get compound **134**. This would undergo a Suzuki reaction with the boronic acid **135**, affording compound **136**, which would be treated with **116**, via Knoevenagel condensation, affording the target dye **109**.

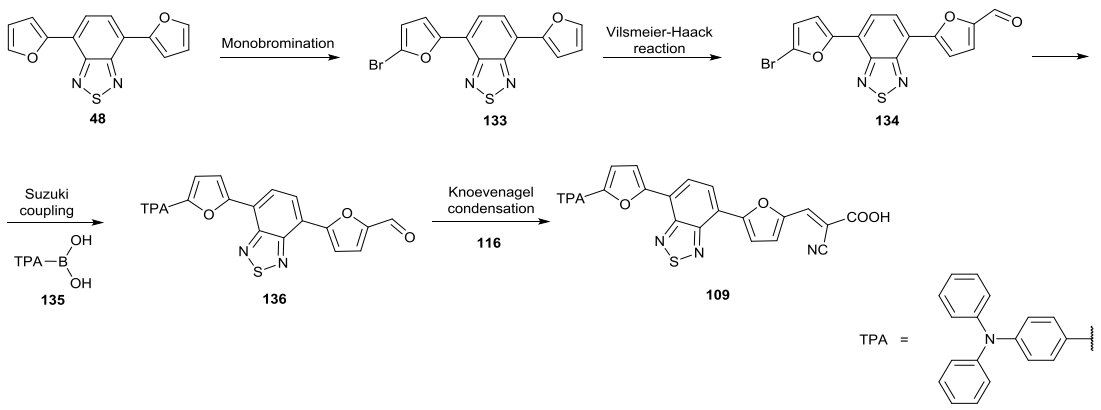

Scheme 29 – Proposed strategy towards the synthesis of dye **109**.

Finally, with the synthesis of polymer **110**, the use of benzo[1,2-c:4,5-c']*bis*[1,2,5]thiadiazole (BbT) was explored as potential acceptor unit for *push-pull* structures in order to shift the absorption of the active material to the NIR. In 1995, Yamashita *et al.*[212] first developed a synthetic route to BbT derivatives, inspired by the intriguing valence-bond representation in which there is a formally tetravalent sulfur atom in an aromatic 14 π-electron ring system, as well as the formation of the quinoid form (Fig. 82), which is expected since more stable 1,2,5-thiadiazole rings are generated in this form. This peculiarity of BbT facilitated a bandgap of 0.5 eV for polymer **137** (Fig. 82), with a bathochromic absorption of about 250 nm, compared to the parent BT-based polymer **138** (Fig. 82).

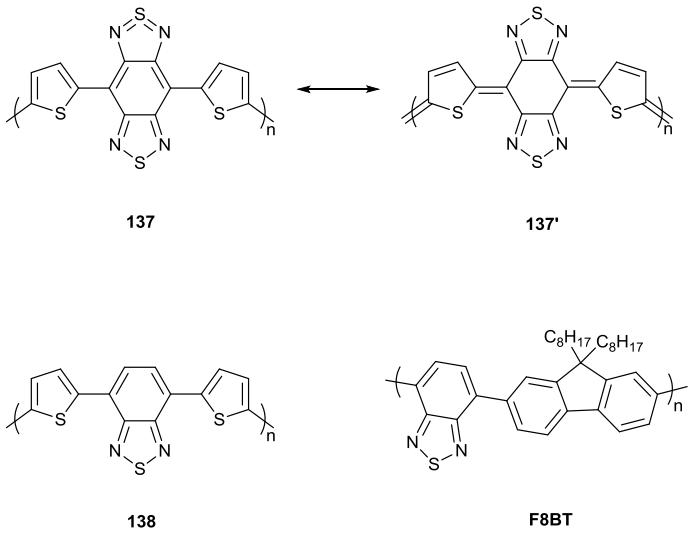

Figure 82 – Chemical structures of polymers **137**, with its quinoidal form **137'**, and **138**.

The idea behind the design of polymer **110** was to exploit the good hole mobility of F8BT (Fig. 82), a known polymer[213] used for a variety of electronic applications, and to replace the BT unit with a more accepting BbT, in order to shift its absorption from the blue range towards the NIR. The proposed synthetic route to **110** is shown in Scheme 30. Previously made compound **46** would be dinitrated in positions C(5) and C(6) (**139**) and then reduced to the parent diamine **140**, which would undergo a cyclization to form **141**. This would polymerise with **142**, via Suzuki cross-coupling, obtaining **110**, after end-capping procedure.

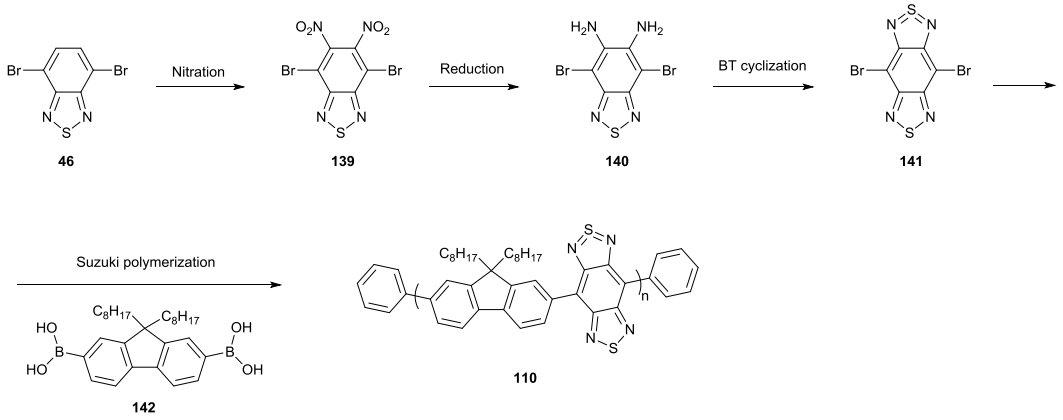

Scheme 30 – Proposed strategy towards the synthesis of polymer **110**.

3.4 Results and discussion

3.4.1 FcBT-Dyes for DSSCs

- Synthesis of compound **113**

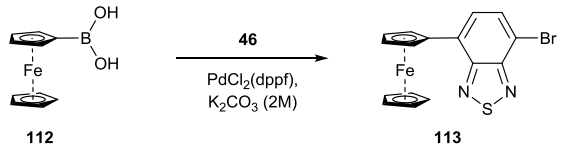

This Suzuki coupling was carried out using a different Pd catalyst than that used for the synthesis of compound **57** (Scheme 9). These conditions resulted from a reaction optimisation in order to get the best possible yield. The use of $Pd^{(II)}$ implies the consumption of two moles of boronic acid for each mole of catalyst, generating the reactive $Pd^{(0)}$ and the boronic acid homocoupling side-product, in analogy with that seen in Scheme 12 for stannanes. In order to avoid dicoupling, a slight excess of compound **46** and high dilutions were used. The reaction was carried out in Ar, at reflux for 14 hours, affording compound **113** in 46% yield.

- <u>Synthesis of compound **118**</u>

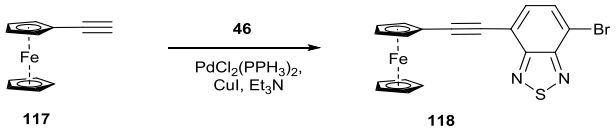

For the synthesis of compound **118**, a previously reported Sonogashira cross-coupling procedure was followed.[214] This reaction involves the formation of a C-C single bond between a terminal alkyne and a halide in the presence of a palladium catalyst, a copper co-catalyst and a base. It was developed in 1975 by Kenkichi Sonogashira and co-workers,[215] and has the great advantage of working under mild conditions and of extending the conjugation of the molecule by adding an alkyne unit, which ensures the planarity of the system. Although it is still debated, the reaction mechanism is thought to proceed according to the two-catalytic cycle mechanism shown in Scheme 31. The palladium catalyst undergoes oxidative addition with the aryl halide to form a $Pd^{(II)}$ complex, which further undergoes transmetallation with a copper acetylide species, which is the product of the copper cycle. Finally, after *trans*/*cis* isomerisation the palladium complex undergoes reductive elimination, in which the target product is obtained, and $Pd^{(II)}$ is reduced to $Pd^{(0)}$ to start the cycle again. The copper cycle starts with a copper halide, which forms a complex with the terminal alkyne, making the terminal proton more acidic. This would react with the amine, leading to the formation of the copper acetylide.

The Sonogashira cross-coupling reaction is very sensitive to the presence of oxygen, which can promote the competing Glaser coupling.[216]

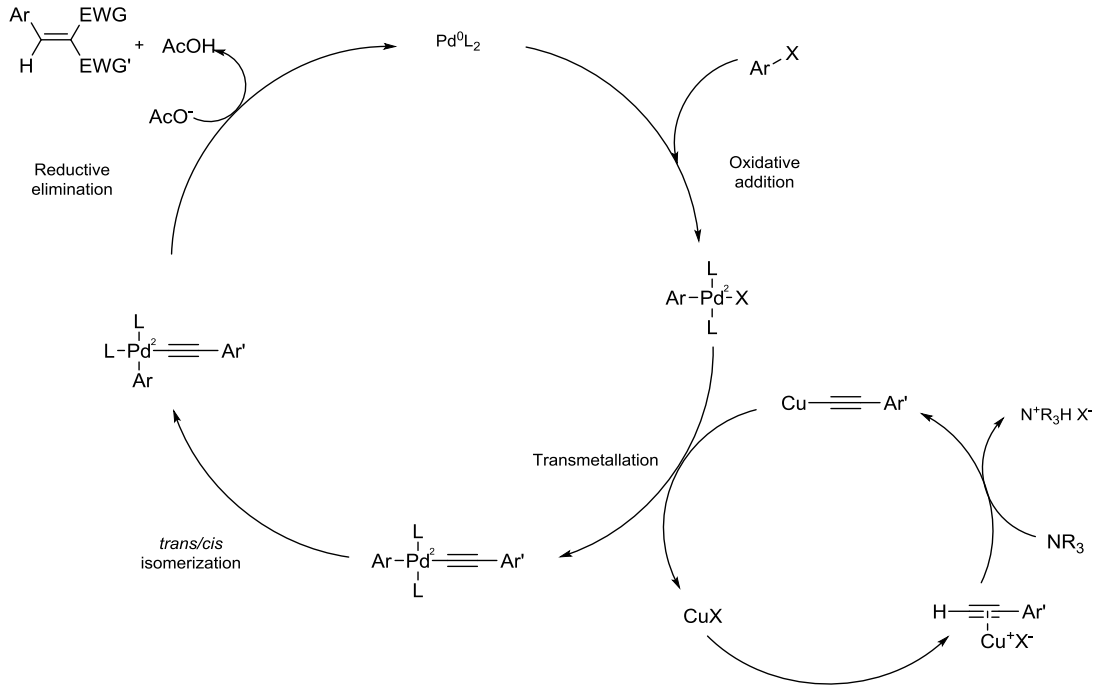

Scheme 31 – Catalytic cycle of the Sonogashira cross-coupling. L denotes a phosphine ligand, Ar and Ar' are generic aromatic groups and NR_3 is an aliphatic amine.

For this reaction, the copper co-catalyst and the base used were CuI and Et_3N, respectively, while $Pd^{(II)}$ was used as catalyst: this is reduced *in situ* to $Pd^{(0)}$ either by transmetallation of two copper acetylides (giving the homocoupling butadiyne side-product, as shown in Scheme 6 for stannanes) or by the amine, generating the oxidised iminium ion, as shown in Scheme 32. The reaction was carried out for 6 hours in dry THF, at 60°C, affording compound **118** was in 89% yield.

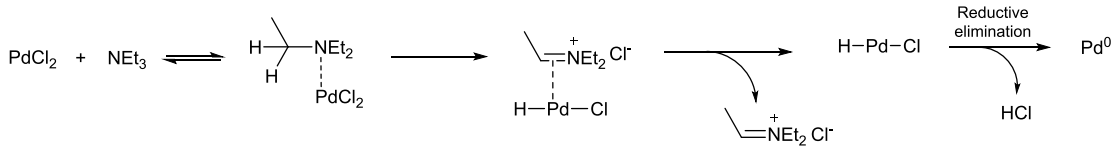

Scheme 32 – Proposed mechanism for the Pd-catalyst activation.

- Synthesis of compounds **115** and **119**

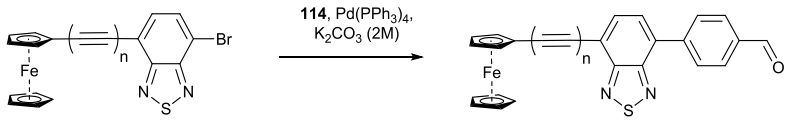

n = 0, **113**
n = 1, **118**

n = 0, **115**
n = 1, **119**

Compounds **115** and **119** were synthesised *via* Suzuki reactions, by coupling compounds **113** and **118**, respectively, with 4-formylphenylboronic acid **114**. For this step, the synthetic protocol seen for the synthesis of polymer **57** was used. Both reactions were carried out at reflux, under N_2, and compounds **115** and **119** were afforded in 84% and 86% yields, respectively.

- <u>Synthesis of compounds **121**</u>

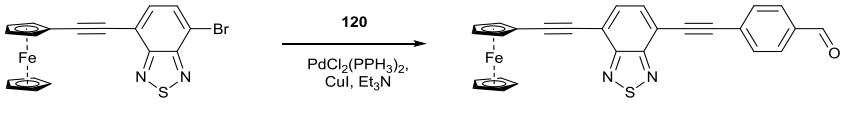

118

121

Compound **121** was synthesised *via* a Sonogashira cross-coupling reaction, by applying the same conditions described above for the synthesis of compound **118**. The target compound was afforded in a 45% yield, after purification by column chromatography.

- <u>Synthesis of compounds **104** – **106**</u>

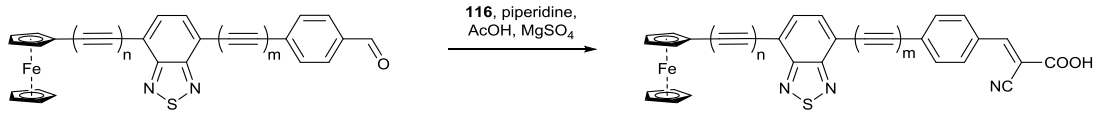

n = 0, m = 0, **115**
n = 1, m = 0, **119**
n = 0, m = 1, **121**

n = 0, m = 0, **104**
n = 1, m = 0, **105**
n = 0, m = 1, **106**

For this reaction a modified version of the Knoevenagel reaction was used: this is the condensation between carbonyl compounds and activated methylene compounds, catalysed by a base (generally amines), and was developed by Knoevenagel,[217] in 1898. The reaction involves the nucleophilic addition of an alpha-carbon to a carbonyl compound followed by elimination of a molecule of water (condensation) in the presence of a weak base such as piperidine (Scheme 33).

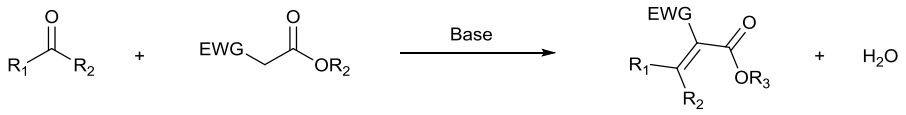

Scheme 33 – Knoevenagel condensation.

The conditions used in this work are a variation of the standard protocol: in particular, piperidine is used as a catalyst and acetic acid is used as a co-catalyst. The proposed mechanism consists of a catalytic cycle (Scheme 34), where piperidine undergoes a nucleophilic addition to the acid-activated aldehyde, followed by subsequent loss of a molecule of water leading to the formation of an iminium intermediate. This intermediate would undergo a nucleophilic addition with the base-activated hydrogen active species. Then, the elimination of a molecule of piperidine, acivated by acid, would give the target compound and allow the cycle to restart.

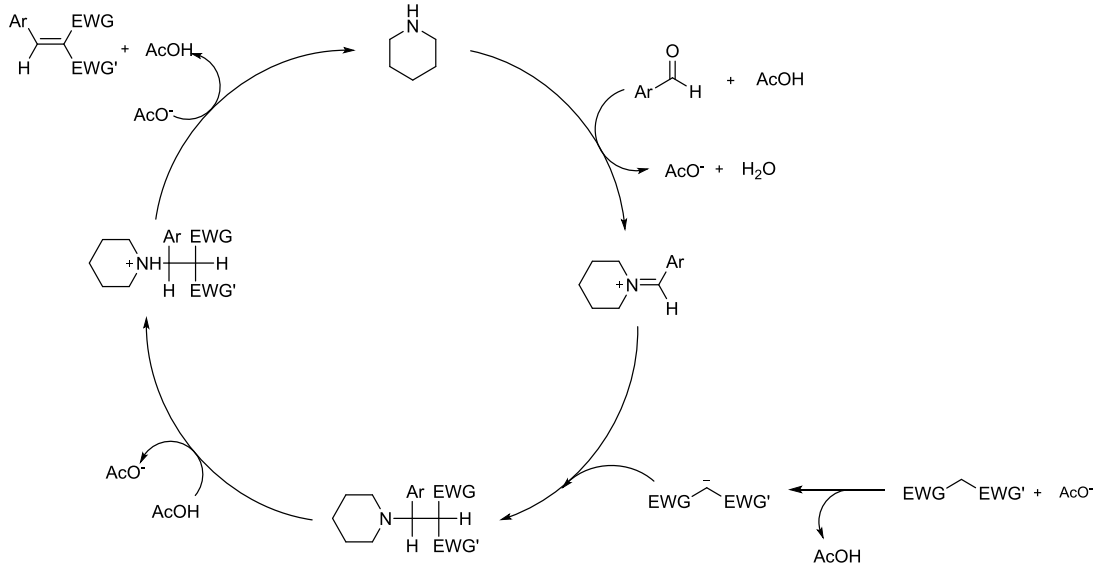

Scheme 34 – Proposed synthetic mechanism for the modified Knoevenagel condensation.

For the reaction dry toluene was used as solvent and $MgSO_4$ was used as water scavenger, keeping the system anhydrous in order to speed up the conversion. The reaction was carried out at reflux and the target dyes **104**, **105** and **106** were afforded in 71%, 96% and 44% yields, respectively.

- <u>Analysis and characterisation of dyes **104** – **106**</u>

Fig. 83 reports the results of DFT calculations performed on the three dyes. The optimised geometry shows the role of the acetylene units in maintaining the overall planarity of the structures. Specifically, going from dye **104** to dye **106** the sequential

addition of the acetylene unit makes the dihedral angles between the Fc and BT moieties and between the BT and phenyl ring moieties significantly decrease from 18.87° to 0.92° and from 33.23° to 2.12°, respectively. This is clearly due to the reduction of the steric hindrance between the aromatic rings. Fig. 83 also shows the electronic density distributions of the HOMO and LUMO of the three dyes. The HOMOs are mainly localized on the Fc moiety and are extended along to the BT moiety to the phenyl ring. The LUMOs are localised on the BT and cyanoacrylate residues. The significant overlap between HOMOs and LUMOs suggests that efficient ICT likely occurs from the donor to the terminal acceptor group which anchors to the TiO_2 surface.[218]

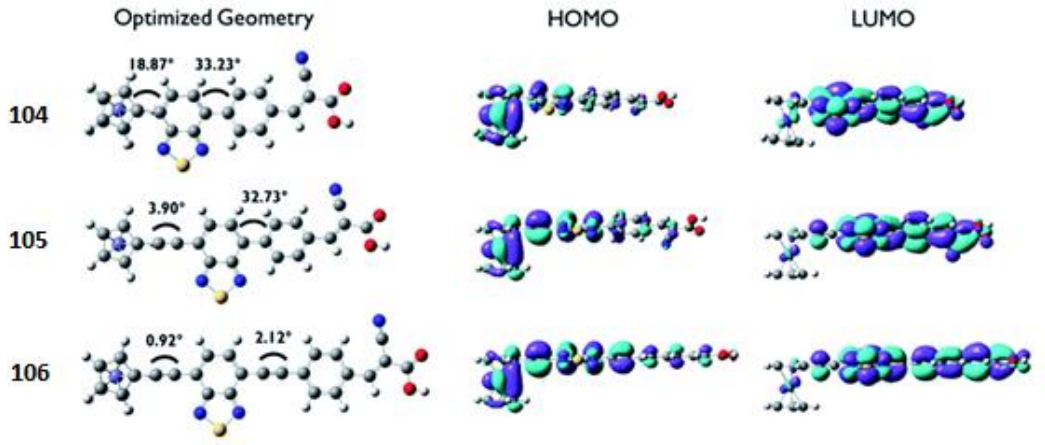

Figure 83 – Ground state optimized geometry and electron density distribution representations of dyes **104**, **105** and **106**. Calculations were run using B3LYP functional and 6-311+G(d,p) basis set for H, C, N, O, S and LanL2DZ functional for Fe, under vacuum.[218]

The UV-Vis spectra of the three compounds in solution are reported in Fig. 84. The absorption band around 300 nm is likely due to n-π* transition of BT or π-π* transition of the conjugated aromatic moieties, whilst that between 350 nm and 450 nm corresponds to the ICT between donor and acceptor groups. The connection between the length of conjugation and position of the maxima is evident. In particular, the addition of each acetylene unit corresponds to a red shift of 10 nm for the ICT maxima. The distinct absorption band around 550 nm in dye **104** might be attributed to the metal-acceptor (d-π*) charge transfer (CT). However, such d-π* CT band, which is sensitive to the adjacent acceptor strength, is not significantly observed as the conjugation length increases (**105** and **106**).[218]

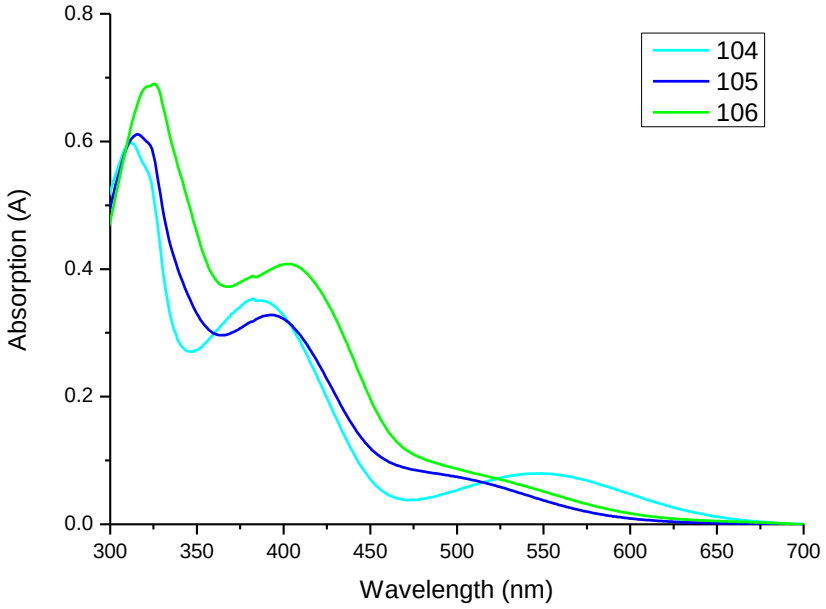

Figure 84 – UV-Vis absorption spectra of dyes **104** – **106** in solution (C = 10^{-5} M, in DMF).[218]

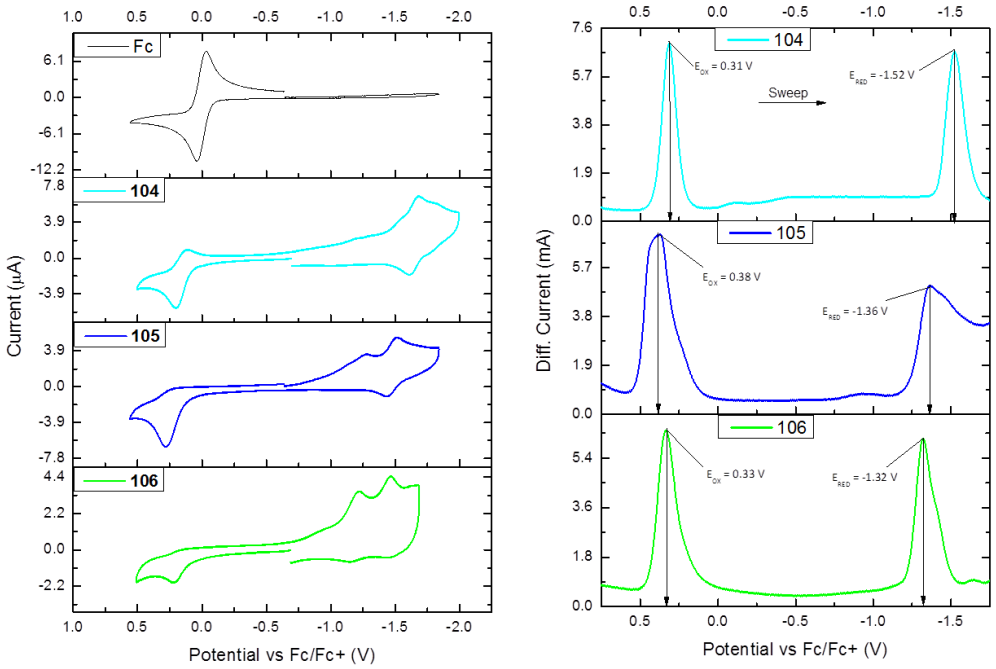

Figure 85 – CV (left) and SWV (right) plots of dyes **104 – 106** in solution (C = 10^{-3} M, in DMF), performed using a Pt disk working electrode, a Pt wire counter electrode and a Ag wire reference electrode. $TBAPF_6$ (0.1 M) was used as supporting electrolyte and the redox potential of the Fc/Fc^+ couple as external standard.

The electrochemical behaviour of the three dyes in DMF solution was explored by CV and SWV, and reported in Fig. 85. As expected, a shift of the oxidation potential

was observed, likely due to the presence of BT as strong acceptor. For all the dyes, this shift was between 300 and 400 mV. Unfortunately, the reversibility of the oxidation wave of Fc was not retained by the dyes. Unlike Fc, for the three dyes a reduction wave is observed, likely due to BT. The addition of acetylene units seems to shift the reduction potential towards more positive values, indicating that the BT is easier to reduce and resulting in a lower $E_{G,fund}$.

The observed E_A and I_P values, as well as the calculated HOMOs and LUMOs and the observed $E_{G,opt}$ values, are reported in Table 8. A summary of the position of energy levels of dyes is reported in in Fig. 86: while the E_A values are found to be almost 1 eV above the TiO_2 conduction band, all the I_P values are considerably above the I_2^{-rad}/I^- redox couple, making the regeneration of the dye energetically unfavourable.[218]

Dye	$E_{G,opt}$ (eV)	I_P (HOMO) (eV)	E_A (LUMO) (eV)	$E_{G,fund}$ (eV)
104	1.62	–5.11 (–5.41)	–3.28 (–2.85)	1.83
105	1.70	–5.18 (–5.45)	–3.44 (–2.91)	1.74
106	1.61	–5.13 (–5.42)	–3.48 (–3.03)	1.75

Table 8 – Summary of the electronic properties of dyes **104 – 106**. $E_{G,opt}$ was estimated from λ_{ONSET} of absorption; I_P and E_A were estimated by SWV. HOMO and LUMO were calculated by DFT and $E_{G,fund} = E_A - I_P$.

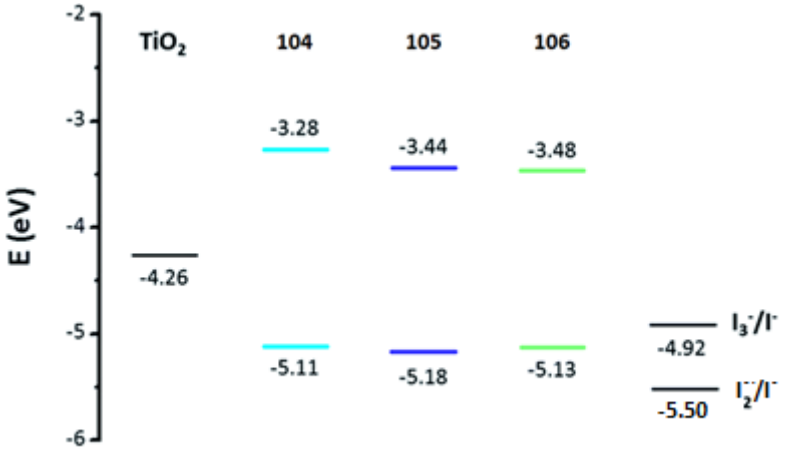

Figure 86 – Energy level diagram showing I_P and E_A of each dye, and their position relative to the TiO_2 conduction band and I^-/I_3^- redox potential.

DSSCs were fabricated, at the Chung-Ang University (S. Korea), using dyes **104** – **106** as sensitisers and the results are shown in Table 9. Two different electrolyte solutions were employed as HTM: AN-50 (Solaronix) as the classical iodide based redox electrolyte, and a hybrid HTM, obtained by mixing I^-/I_3^- and 2-Mercapto-5-

methyl-1,3,4-thiadiazole/1,2-Bis(5-methyl-1,3,4-thiathiazole-2-yl)sulphide (McMT^{-}/ BMT) in MeOH. The addition of the two acetylene bridging units in **106** resulted in better photovoltaic performance with the I^{-}/I_3^{-} redox couple than **104**: V_{OC} from 0.407 V to 0.434 V, J_{SC} from 0.730 mA cm^{-2} to 1.070 mA cm^{-2} and PCE from 0.180% to 0.279%. The PCE value of **106** compared to **104** is more than doubled which may be ascribed to the improvement of light harvesting efficiency or the electron injection efficiency of **106**.[218]

Dye (Electrolyte)	V_{OC} (V)	J_{SC} (mA cm^{-2})	FF (%)	PCE (%)
104 (AN-50)	0.407 ± 0.004	0.730 ± 0.049	58.4 ± 2.1	0.180 ± 0.009
104 (Hybrid)	0.405 ± 0.021	0.610 ± 0.046	61.2 ± 1.2	0.160 ± 0.019
105 (AN-50)	0.337 ± 0.014	0.590 ± 0.056	57.9 ± 2.0	0.115 ± 0.018
105 (Hybrid)	0.380 ± 0.010	0.770 ± 0.050	60.3 ± 1.9	0.190 ± 0.004
106 (AN-50)	0.434 ± 0.005	1.070 ± 0.052	57.5 ± 1.3	0.279 ± 0.023
106 (Hybrid)	0.494 ± 0.008	1.190 ± 0.057	54.1 ± 2.3	0.325 ± 0.005

Table 9 – Summary of devices performances using dyes **104 – 106** as sensitisers.[218]

The low values of J_{SC}, which drastically affect the overall PCE of the dyes, are likely due to a back charge recombination at the surface between dye and TiO_2, and dye and electrolyte solution. In order to demonstrate this electrochemical impedance spectroscopy (EIS) was performed for devices sensitised with dye **106** (Fig. 87). In the figure on the left (Fig. 87a) the imaginary part of impedence (Z") is reported on Y axis, while the real part (Z') is reported on the X-axis (*Nyquist Plot*). Each point on the Nyquist Plot is the impedance at one frequency and low frequency data are on the right side of the plot and higher frequencies are on the left side. The semicircle at higher frequency region represents the electron transfer process at the TiO_2/dye/electrolyte interface and its radius is related to the charge recombination rate, *i.e.* a larger radius indicates a slower charge recombination. The electron lifetime (τ_e) corresponding to the TiO_2/dye/electrolyte interface, could be estimated from the peak frequency (f_{peak}) in Fig. 87b, according to $\tau_e = 1/2\pi f_{peak}$. The calculated values of **106** (AN-50) and **106** (Hybrid) are 0.36 ms and 0.71 ms, respectively. This means that addition of the organic redox couple contributed to suppress the back charge recombination at the TiO_2/dye/electrolyte, but, unfortunately, the values for τ_e are 10^3 to 10^4 times lower than those associated with better performing dyes.[218]

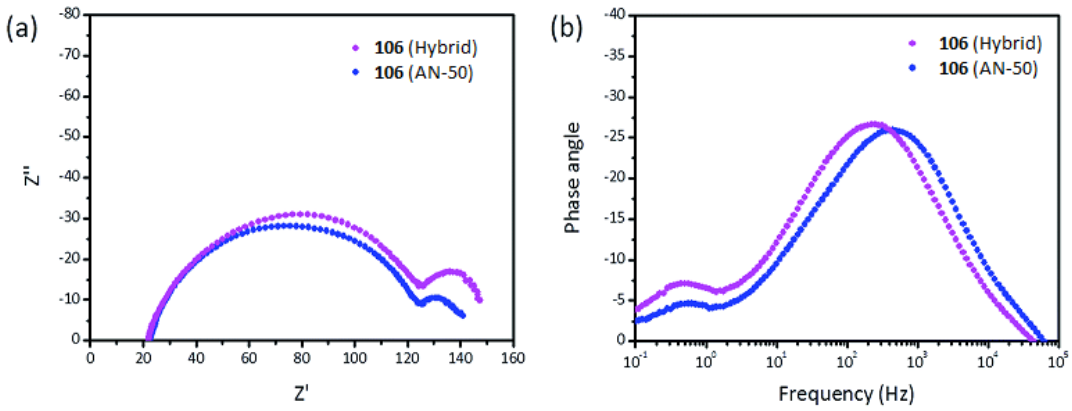

Figure 87 – EIS plots of the DSSC devices using dye **106** as sensitiser.[218]

3.4.2 Fc-Based donor for OPVs

- Synthesis of compound **122**

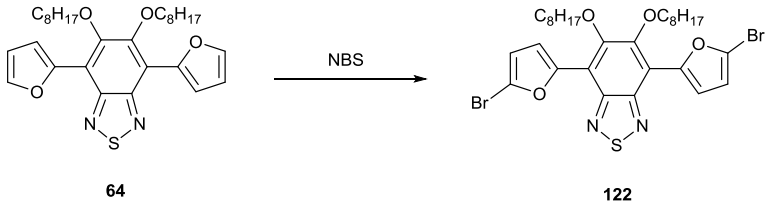

This reaction involved the dibromination of compound **64** by following a slight modification of the previously reported method:[170] these conditions were described above for the synthesis of compound **55**. Compound **122** was afforded in a 65% yield.

- Synthesis of compound **107**

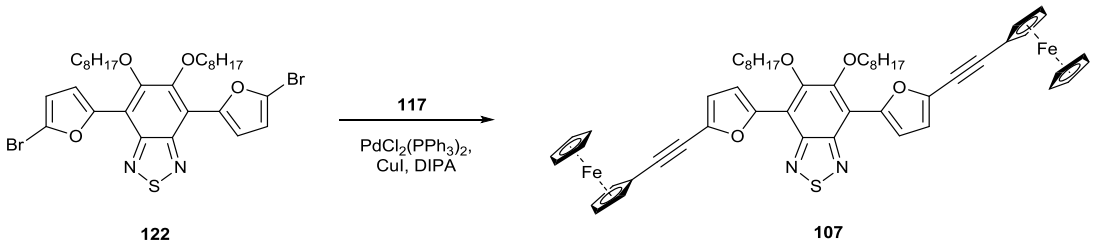

This reaction involved a Sonogashira dicoupling between compounds **122** and **117**. The general conditions described above for the synthesis of compound **118** were applied, except for the base. Diisopropylamine, instead of triethylamine was found to be a more effective base for this reaction. Compound **107** was afforded in 92% yield.

- Analysis and characterisation of compound **107**

In order to gain insight on the electronic structure and optical properties of compound **107**, DFT calculations were performed. The optimised geometry results, reported in Fig. 88a, shows a good overall planarity of the molecule, with a dihedral twist of 11.53° between BT and the two furan rings, and 0° between furan and the Cp ring of Fc (due to the acetylene suppressing the steric hindrance), with the two Fc's pointing towards opposite directions. Fig. 88b shows the distribution of the frontier energy levels. The HOMO level is more concentrated on the two Fc units and seems to correspond to the dz^2 of Fe. The LUMO is spread throughout the molecule, suggesting a good hole-mobility. The calculated HOMO and LUMO levels were –5.82 eV and –3.96 eV, respectively.

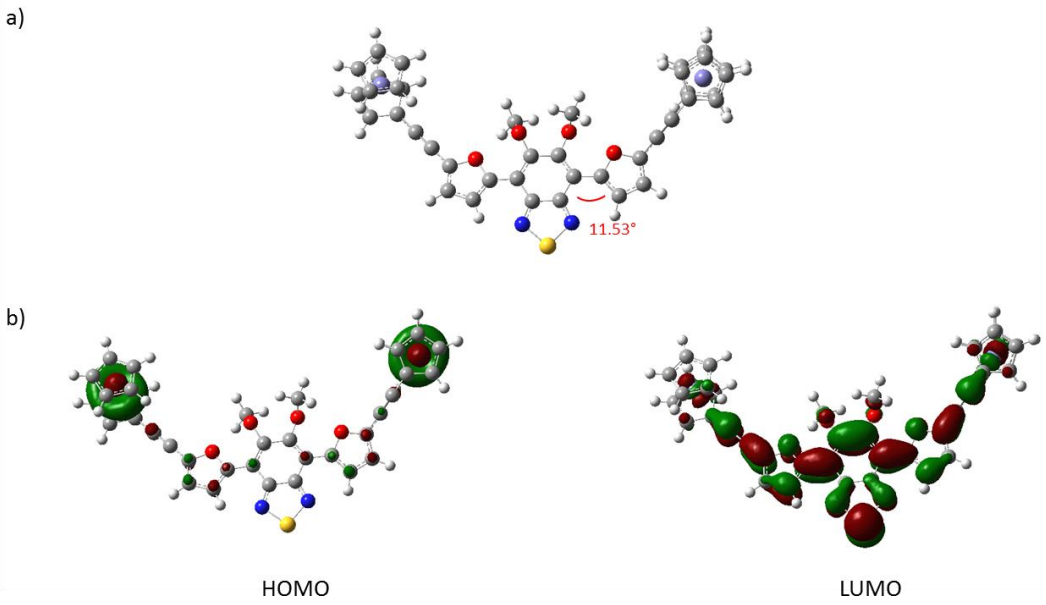

Figure 88 – (a) Optimised geometry and (b) energy level distribution for compound **107**. The calculations was run using B3LYP functional and 6-311+G(d) basis set for H, C, N, O, S and Lanl2DZ functional for Fe.

The absorption spectrum of compound **107,** reported in Fig. 89, shows the presence of two distinct bands: the one at around 350 nm is likely due to n-π* transition of BT or π-π* transition of the conjugated aromatic moieties, whilst that between 400 nm and 600 nm corresponds to the ICT between donor and acceptor groups. Due to the presence of the acetylene linkers, the band at higher λ, seen for dye **104** and relative to the metal-acceptor (d-π*) CT was not observed. The maximum intensity of the ICT band is observed at 481 nm, with a high molar extinction coefficient of about

5×10^4 $cm^{-1}M^{-1}$, while the onset of absorption is at 614 nm, corresponding to $E_{G,opt}$ = 2.02 eV.

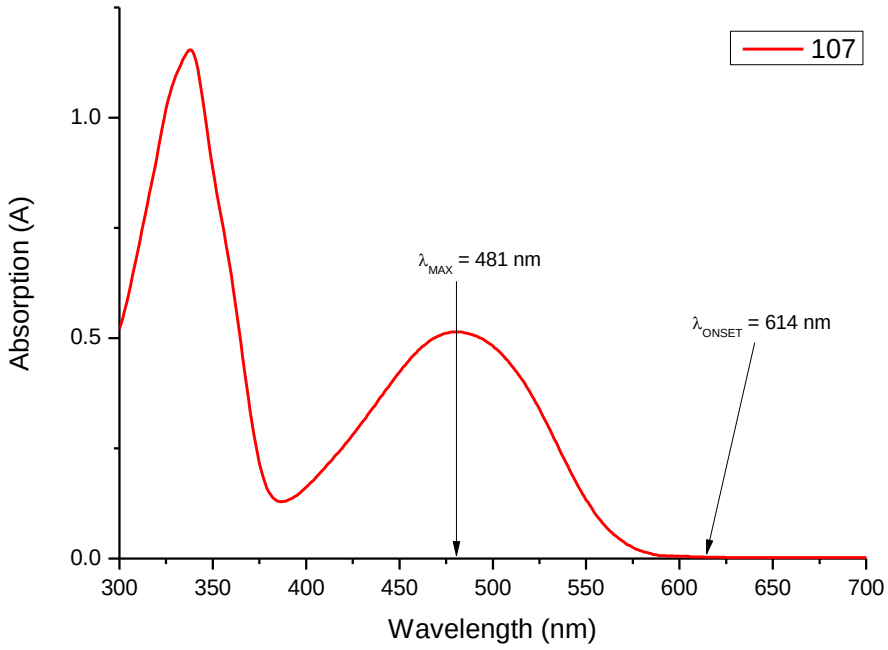

Figure 89 – Absorption spectrum of compound **107** (C = 10^{-5} M, in DCM).

The electrochemical properties of compound **107** were explored by CV and SWV. The CV plot, in Fig. 90, shows the presence of two distinct reversible waves corresponding to the oxidation and reduction potentials. Interestingly, the oxidation potential of Fc, was not only shifted by more than 800 mV but, unlike what was observed for dyes **104** – **106**, its reversibility was retained in the final compound. The two potentials were quantified by SWV (Fig. 91) as E_{OX} = +0.84 V and E_{RED} = –1.18 V. These values were converted to the corresponding I_P and E_A of –5.64 eV and –3.62 eV, respectively, in good accordance with the calculated HOMO and LUMO values, and both of them slightly above those of PCBM, suggesting that compound **107** could be an effective p-type semiconductor in BHJ devices. The estimated difference between E_A and I_P, $E_{G,fund}$ = 2.02 eV, coincides with the optical bandgap, meaning that the exciton binding energy would be very low.

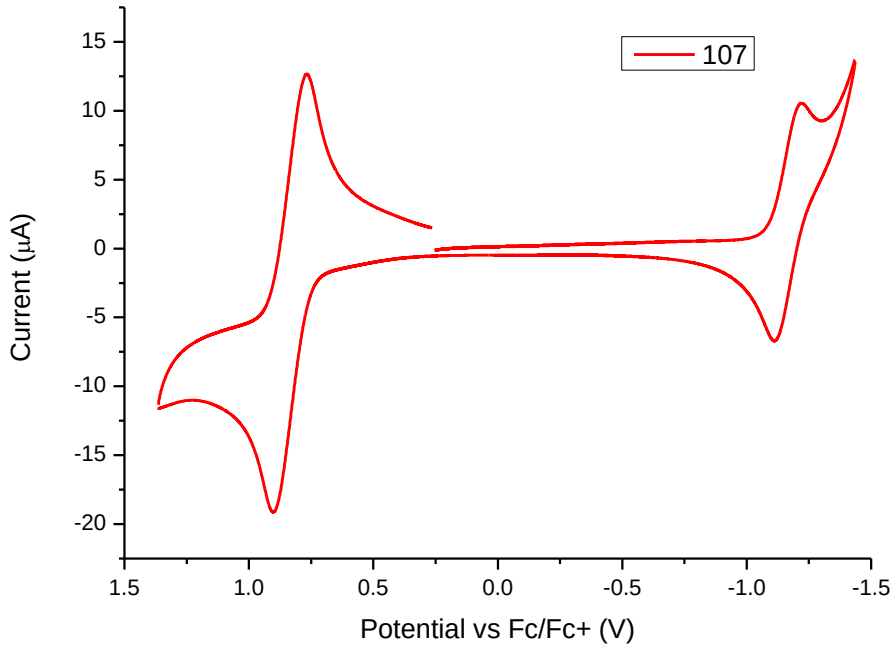

Figure 90 – CV plot of compound **107** in solution (C = 10^{-3} M, in DCM), performed using a Pt disk working electrode, a Pt wire counter electrode and a Ag wire reference electrode. $TBAPF_6$ (0.1 M) was used as supporting electrolyte and the redox potential of the Fc/Fc^+ couple as external standard.

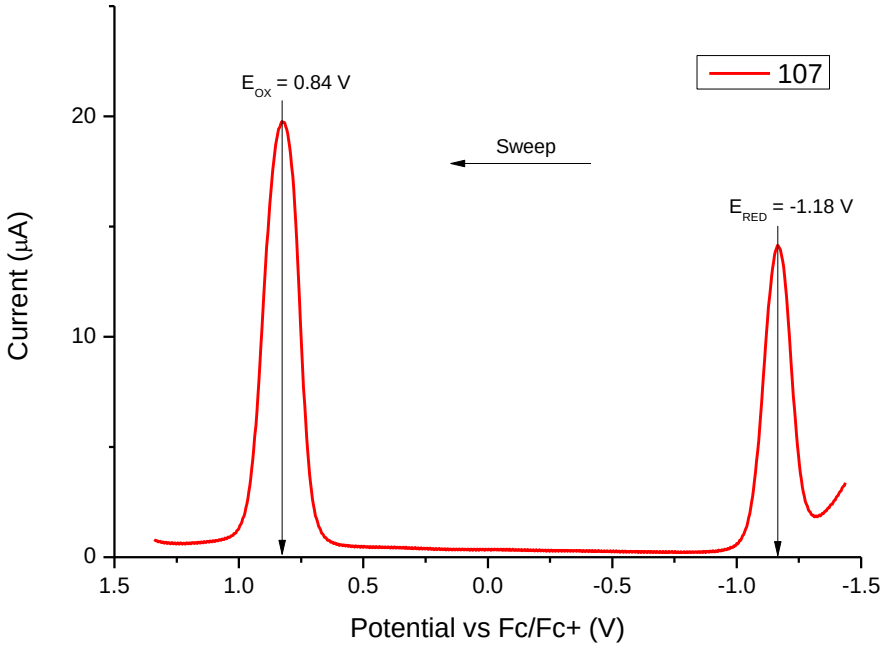

Figure 91 – SWV plot of compound **107** in solution (C = 10^{-3} M, in DCM), performed using a Pt disk working electrode, a Pt wire counter electrode and a Ag wire reference electrode. $TBAPF_6$ (0.1 M) was used as supporting electrolyte and the redox potential of the Fc/Fc^+ couple as external standard.

3.4.3 BT-Dyes for DSSCs

- Synthesis of compound **125**

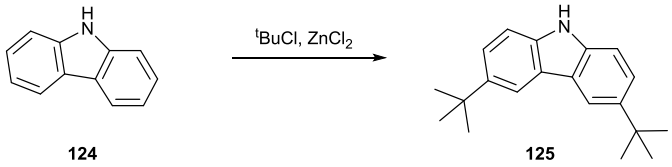

124 **125**

This reaction, involving an E_AS, was carried out by following a previously reported protocol.[219] In the case when the substrate is more reactive towards E_AS $ZnCl_2$ is preferred, instead of the more common $AlCl_3$, as it is a weaker Lewis acid. The reaction is expected to take place only in C(4) and C(7), due to the amine acting as a strong electron-donating, *para*-directing group. Indeed, compound **125** was afforded in 90% yield.

- Synthesis of compound **127**

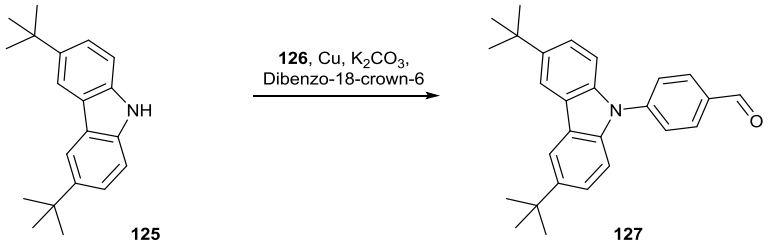

125 **127**

For this reaction, involving a Ullmann-type cross-coupling reaction, a previously reported protocol[220] was followed. The Ullmann reaction was developed in 1904 by Fritz Ullmann[221] and it consists in the synthesis of symmetric biaryls, mediated by Cu, starting from an aryl halide (Scheme 35).

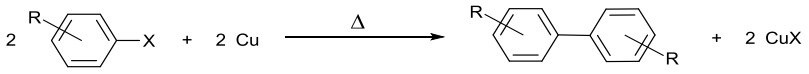

Scheme 35 – Ullmann reaction.

The Ullmann-type reaction is a modification of the classical protocol, and it was introduced two years later by Irma Goldberg:[222] it involves a Cu-mediated S_NAr between substituted anilines (or phenols) and aryl halides (Scheme 36). In particular, a first addition of the aryl halide to metallic Cu, takes place, with $Cu^{(0)}$ oxidising to $Cu^{(II)}$; this is then reduced to $Cu^{(I)}$ by another molecule of $Cu^{(0)}$. Then the addition of the deprotonated aniline occurs, with the formation of a $Cu^{(II)}$-complex, which

releases the target compound and $Cu^{(0)}$ by reductive elimination. The reaction takes place in a basic environment and with a stoichiometric amount of Cu.

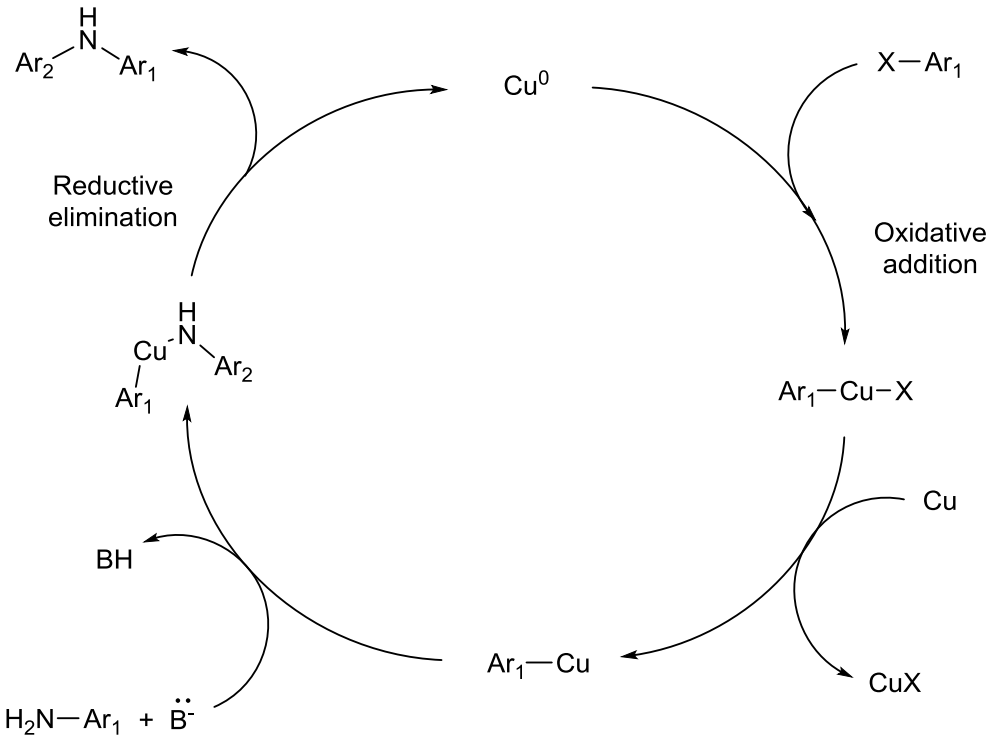

Scheme 36 – Proposed catalytic cycle for the Ullmann-type condensation.

For the synthesis of compound **127**, K_2CO_3 was used as base and a catalytic amount of dibenzo-18-crown-6 was used as K^+ scavenger, in order to facilitate the base dissociation in organic media. The reaction was carried out, under Ar, in anhydrous and degassed DMF at 150 °C, for 3 days, leading to the formation of compound **127** in 45% yield.

- <u>Synthesis of compound **128**</u>

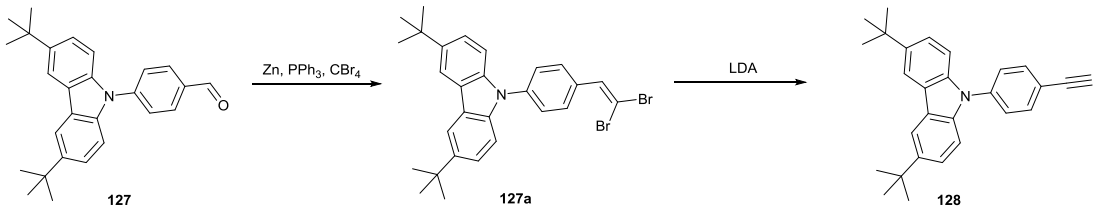

Compound **128** was synthesised according to the general mechanism of the Corey-Fuchs reaction. This was developed, in 1972, by Elias J. Corey and Philip L. Fuchs[223] and involves the one-carbon homologation of an aldehyde to a dibromoolefin, which is then treated with n-BuLi or LDA to produce a terminal alkyne. The proposed

mechanism, shown in Scheme 37, involves the formation of a phosphorus ylide from the reaction between triphenylphosphine and carbon tetrabromide. The addition of Zn powder helps to remove bromine (a side-product of the first reaction), by forming $ZnBr_2$. The ylide reacts with the aldehyde, according to the Wittig mechanism, forming the dibromoolefin and triphenylphosphine oxide, as side product. The final step is carried out in an excess of BuLi or LDA, which converts the olefin to an alkyne, by elimination of LiBr followed by debromination.

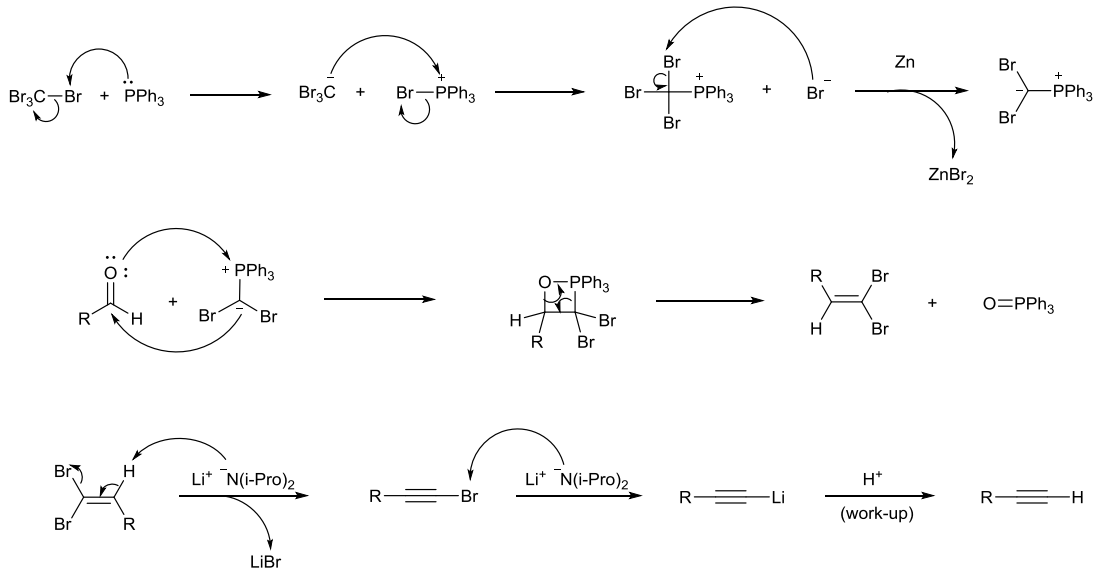

Scheme 37 – Corey-Fuchs reaction mechanism.

The first step was carried out in anhydrous DCM, at room temperature and under Ar, affording **127a** in 34% yield, after filtration through a pad of silica gel. The second step was carried out in anhydrous THF at –78 °C, using 10 equivalents of LDA: after 10 minutes compound **128** was afforded in quantitative yield.

- <u>Synthesis of compound **129**</u>

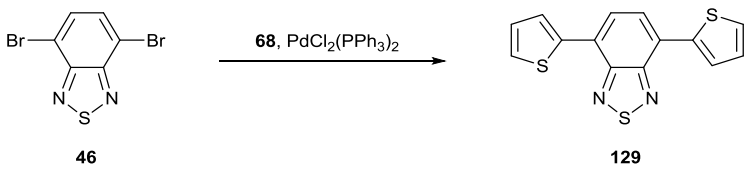

This Stille coupling was carried out according to an existing protocol.[224] Compound **129** was afforded in quantitative yield, after the remaining organo-tin reactant was quenched with an aqueous solution of KF.

- <u>Synthesis of compound **130**</u>

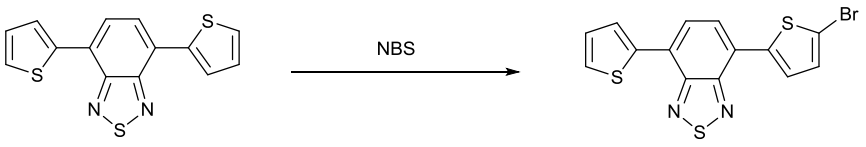

129 **130**

For the monobromination of compound **129** apreviously reported protocol was followed.[225] In order to minimise the rate of dibromination the reaction was carried out in high dilution and NBS was added portion-wise over 30 minutes at 0 °C, in the dark. Compound **130** was afforded in 65%.

- Synthesis of compound **131**

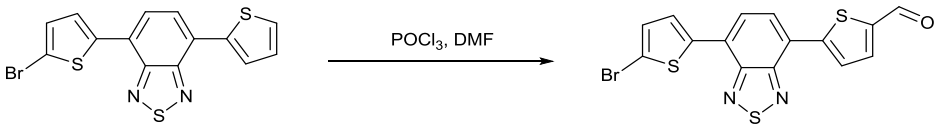

130 **131**

This step involves a formylation reaction using a slight modification of an existing protocol.[211] It consisted of a Vilsmeier-Haack reaction, which was developed in 1927, by Anton Vilsmeier and Albrecht Haack.[226] The reaction mechanism (Scheme 38) involves the formation of a substituted chloroiminium ion, as a mild formylating agent for electron-rich aromatic compounds. The chloroiminium ion, formed by reacting $POCl_3$ with DMF in anhydrous conditions, acts as the electrophile for the next E_AS, producing an iminium ion intermediate, which is then hydrolysed in a basic aqueous environment to give the target aromatic aldehyde.

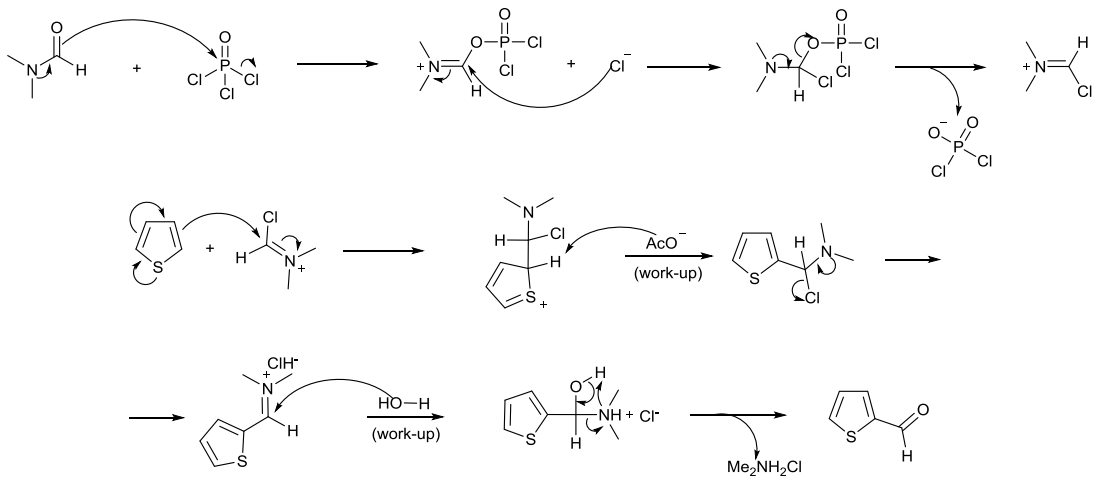

Scheme 38 – Vilsmeier-Haack reaction mechanism for the formylation of thiophene.

The reaction between **130** and the freshly made chloroiminium ion was carried out in 1,2-dichloroethane, at 80 ºC, under Ar, for 8 hours. This was followed by the reaction work-up, consisting of quenching the mixture with an aqueous solution of sodium acetate. Compound **131** was afforded in 86% yield.

- Synthesis of compound **132**

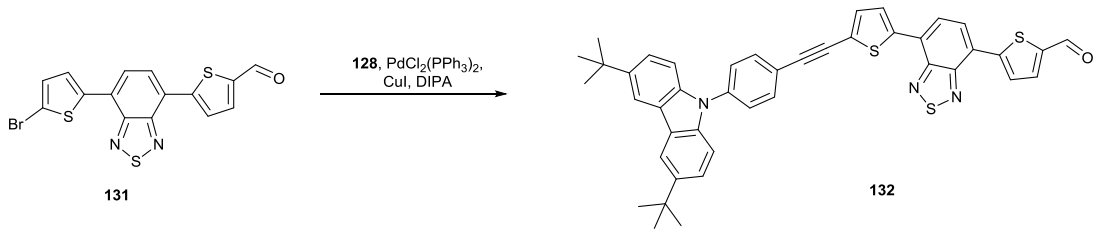

A first attempt of synthesising compound **132** using the standard Sonogashira coupling conditions employed above for synthesising compound **118** was unsuccessful, likely due to the low reactivity of compound **128**. However, compound **132** was successfully synthesised carrying out the reaction in anhydrous DMF, at 90 ºC, and with DIPA as base. The target compound was afforded in 55% yield.

- Synthesis of compound **108**

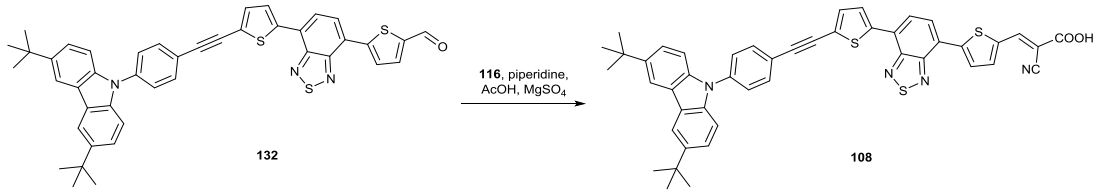

For this reaction, involving a Knoevenagel condensation, the standard conditions described above for the synthesis of dyes **104** – **106** were applied. Dye **108** was afforded in 87% yield, after multiple reprecipitations in different organic solvents.

- Synthesis of compound **133**

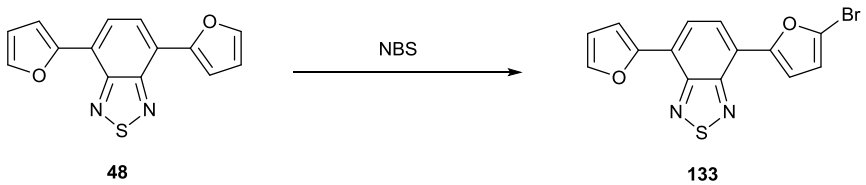

For this monobromination reaction, the same conditions described previously for the synthesis of compound **130** were applied. Compound **133** was afforded in 78% yield.

- Synthesis of compound **134**

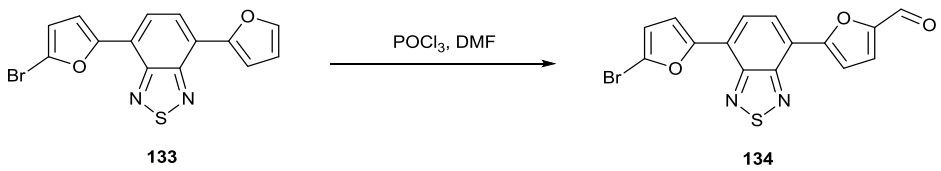

Compound **134** was synthesised by applying the same reaction conditions described above for the synthesis of compound **131**, involving a Vilsmeier-Haack reaction. The target compound was afforded in 91% yield.

- Synthesis of compound **136**

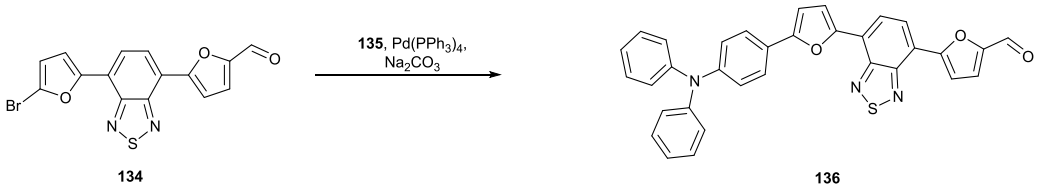

Compound **136** was synthesised *via* Suzuki cross-coupling reaction, using a mixture of toluene and EtOH as solvent. The reaction was carried out at reflux, affording the target compound in 69% yield.

- Synthesis of compound **109**

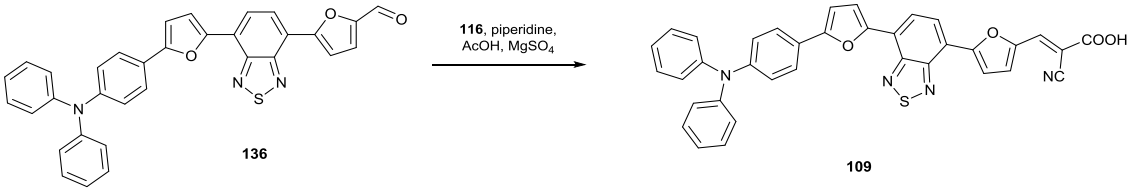

Dye **109** was synthesised *via* Knoevenagel condensation, using the same conditions employed for the synthesis of dyes **104** – **106**. The target compound was afforded in 84% yield, after purification by multiple reprecipitations from different organic solvents.

- Analysis and characterisation of dyes **108** and **109**

Fig. 92 reports the results of DFT calculations performed on the three dyes. The optimised geometry of dye **108** gives an idea of its planarity, with dihedral angles between BT and the two thiophene rings of less than 1° and with the cyanoacrylic unit lying on the same plane of thiophene. The acetylene linker ensures planarity between thiophene and benzene, while there is a dihedral angle between carbazole and benzene of about 45°, due to the steric interaction between benzene and the carbazole benzene rings. Changing from thiophene to furan leads to an unexpected change of geometry and structural conformation. Unlike thiophenes in dye **108**, furans of dye **109** are found to point the heteroaromatic atom towards the thiadiazole ring. This was verified by running the same DFT calculation on dye **109** with the two furans manually twisted of 180° but the calculation did not find convergence. Due to the repulsion between O, of furan, and N, of thiadiazole, the molecule resulted more twisted than dye **108** with dihedral angles between BT and furans of 10.2° and 25.6°. The absence of the acetylene unit between benzene and furan led to a twisting angle of 6.4°, while the change from carbazole to TPA led to a more twisted system. Although the lack of planarity means a less effective conjugation, it should improve the solubility of the molecule making aggregation less effective.

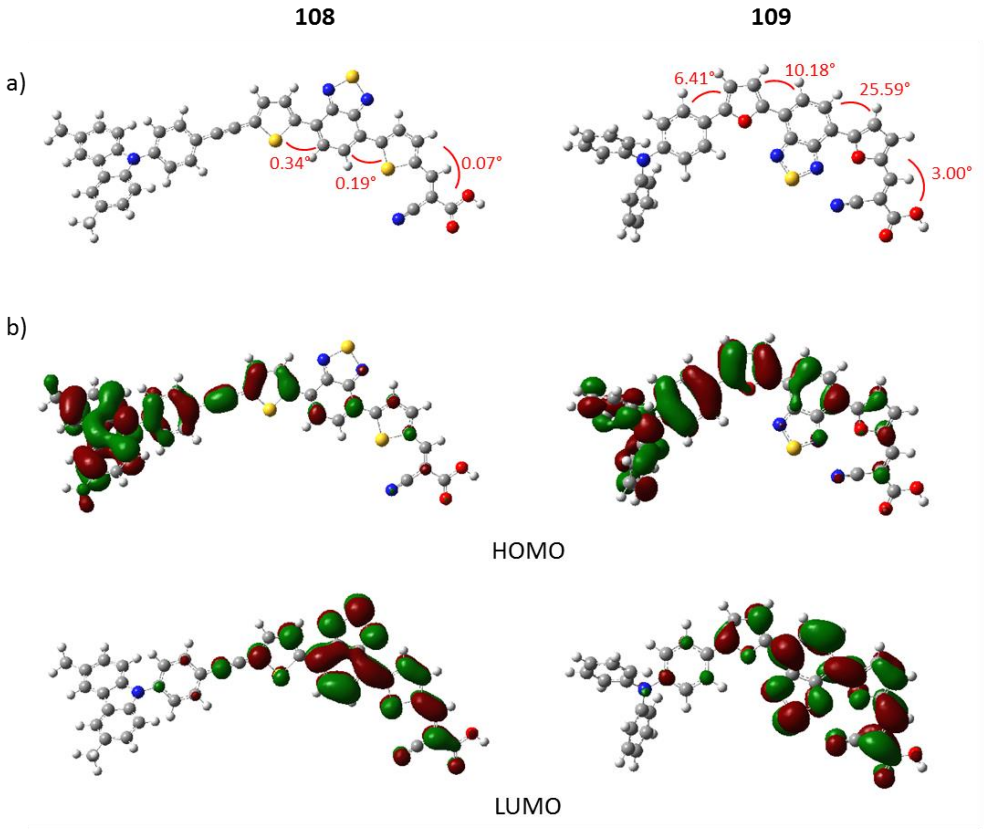

Figure 92 – (a) Optimised geometry and (b) frontier molecular orbital distributions for dyes **108** and **109**. Calculations were run using B3LYP functional and 6-311+G(d) basis set.

The UV-Vis spectra of the two dyes in solution are reported in Fig. 93. Both of them consist of two major bands: that between 300 nm and 400 nm is likely due to n-π* transition of BT or π-π* transition of the conjugated aromatic moieties, while that between 400 nm and 600 nm corresponds to the ICT between donor and acceptor groups. The onset absorption for both the molecules is at 719 nm, corresponding to $E_{G,opt}$ = 1.72 eV. It is evident from the position of the ICT maxima how planarity affects the strength of the conjugation. Indeed, the maximum absorption for dye **108** at 533 nm is 39 nm more red-shifted than that of dye **109** (494 nm).

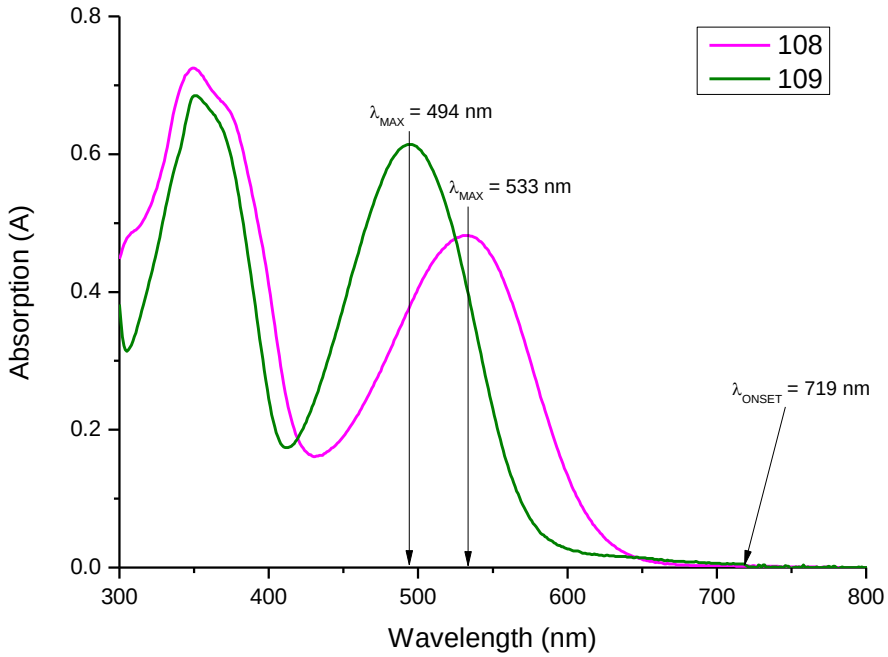

Figure 93 – Absorption spectra of dyes **108** and **109** (C = 10^{-5} M, in DMF).

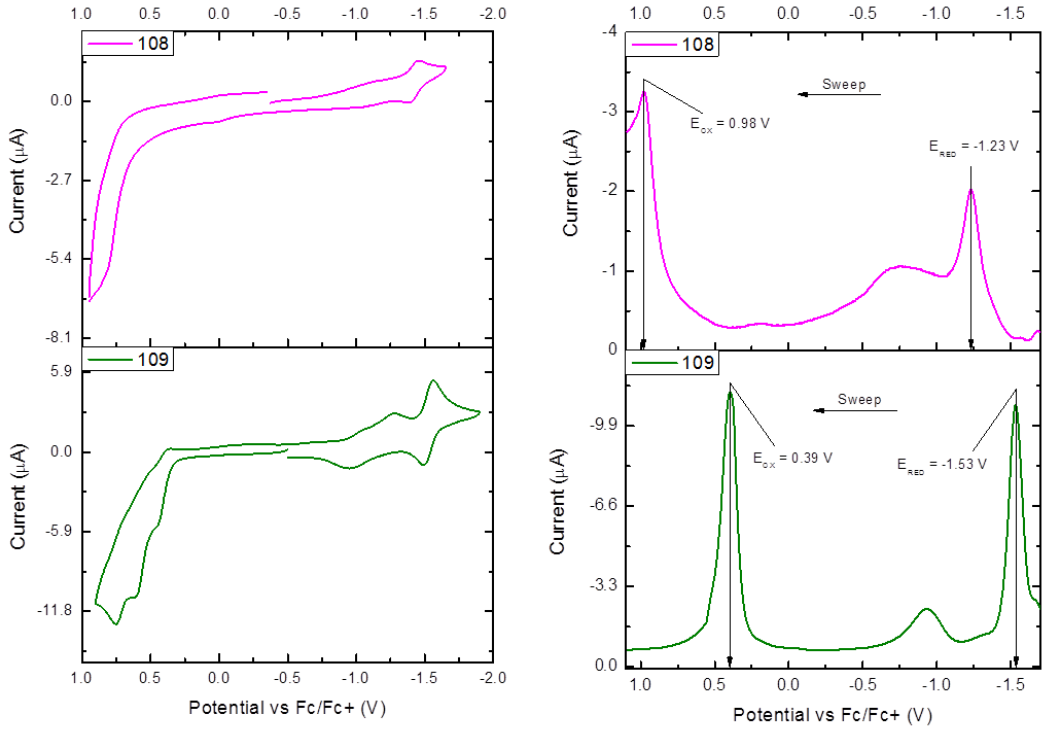

Figure 94 – CV (left) and SWV (right) plots of dyes **108** and **109** in solution (C = 10^{-3} M, in DMF), performed using a Pt disk working electrode, a Pt wire counter electrode and a Ag wire reference electrode. $TBAPF_6$ (0.1 M) was used as supporting electrolyte and the redox potential of the Fc/Fc^+ couple as external standard.

The electrochemical properties of both dyes **108** and **109** were explored by CV and SWV, and their plots are reported in Fig. 94. The two CV plots show a reversible reduction wave at around –1.5 V, and a non-reversible oxidation peak between 0.5 V and 1.0 V. There is also a non-reversible reduction peak at around –0.8 V and –0.9 V, respectively. The SWV plot shows that the position of oxidation peak of dye **109** is 0.59 V more shifted towards negative values respect to that of dye **108**. This shift is less evident (0.30 V) for the reduction peak and is likely due to the different aromaticity of furans and thiophenes. Indeed, as they are less aromatic, furans have a better donor effect on the *push-pull* system. The estimated E_A and I_P values, as well as the calculated HOMOs and LUMOs and the estimated $E_{G,opt}$ values, are reported in Table 10.

Dye	$E_{G,opt}$ (eV)	I_P (HOMO) (eV)	E_A (LUMO) (eV)	$E_{G,fund}$ (eV)
108	1.72	–5.78 (–5.50)	–3.57 (–3.56)	2.21
109	1.70	–5.19 (–5.17)	–3.27 (–3.14)	1.92

Table 10 – Summary of the electronic properties of dyes **108** and **109**. $E_{G,opt}$ values were estimated from λ_{ONSET} of absorption; I_P and E_A values were estimated by SWV. HOMOs and LUMOs were calculated by DFT and $E_{G,fund} = E_A - I_P$.

Fig. 95 reports a representation of energy levels of both the dyes respect to ETM and HTM: according to this scheme, dye **108** should perform better than **109**, as its E_A lies above the CB of TiO_2 while its I_P lies below the iodide-based HTM redox potential. However, the I_P of dye **109** was found to be slightly above the redox potential of the I_2^{-rad}/I^-, making the dye regeneration energetically unfavourable.

Figure 95 – Energy level diagram showing I_P and E_A values of each dye, and their position relative to the TiO_2 conduction band and I^-/I_3^- redox potential.

DSSCs were fabricated using the two dyes as sensitisers, at the École Polytechnique Fédérale de Lausanne (EPFL, Switzerland). Both of them were deposited by dip-coating on a 12 μm thick layer of mesoporous TiO_2 (15 nm particle size), with a Pt counter electrode and a I^-/I_3^- based electrolyte (Z960). Solubility issues were encountered, especially with dye **108** which forced us to use a 10 times more diluted solution than the optimum 10^{-3} M concentration, in plain DMSO and for longer dipping times. IV-curves of the preliminary devices are reported in Fig. 96, which also shows the variation of the electrical parameters as a function of the light intensity. The resulting parameters are reported in Table 11: the PCE for both the devices were poor, likely depending on the unfavourable thermodynamics for dye **109** and on the solubility and aggregation issues for dye **108**. This suggests that the use of anti-aggregation additives could help to improve the performances. Further studies towards this direction will be undertaken.

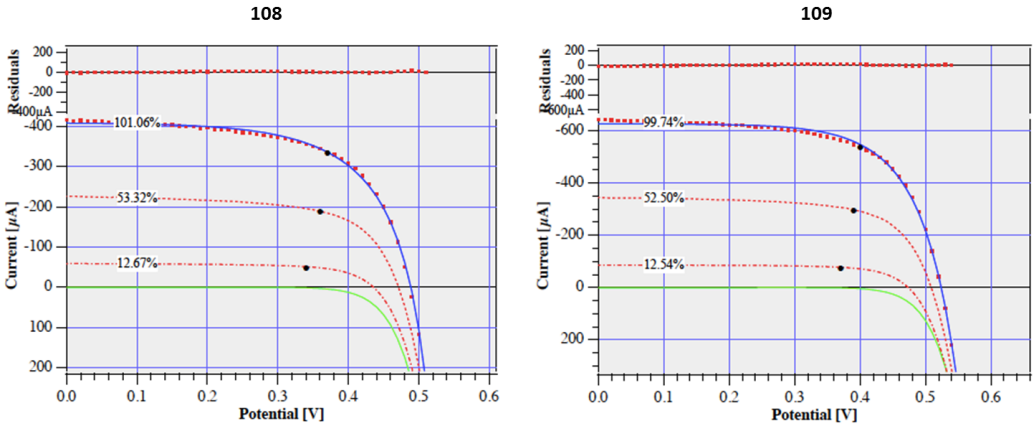

Figure 96 – IV-plots of DSSCs fabricated using dyes **108** (left) and **109** (right) as sensitisers.

Dye	J_{SC} (mA/cm^2)	V_{OC} (V)	FF	PCE (%)
108	–2.57	0.486	0.62	0.77
109	–4.03	0.522	0.64	1.35

Table 11 – Summary of devices performances using dyes **104 – 106** as sensitisers.

3.4.4 BbT-fluorene polymer

- Synthesis of compound **139**

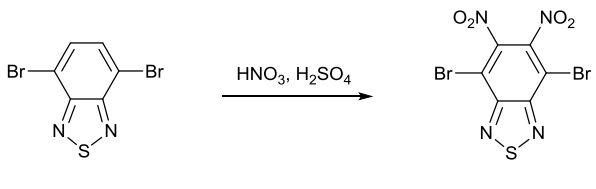

46 **139**

For this dinitration, an existing synthetic protocol was followed.[227] Unlike what was seen above for the synthesis of compound **60**, where mild conditions were used due to the "electron-richness" of the substrate, in this case the use of the "mixed acid" was required because of the deactivating effect of imines on the aromatic ring. The mixed acid was prepared by slowly adding sulfuric acid to fuming nitric acid at 0 °C, and compound **46** was added portion-wise. The reaction was carried out at 50 °C and compound **139** was afforded in 40% yield.

- Synthesis of compound **140**

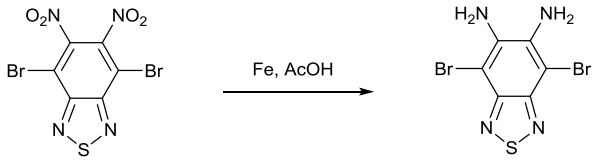

139 **140**

Compound **140** was synthesised according to a slight modification of an existing procedure.[228] The reaction involved a Béchamp reduction, which is the reduction of a nitro-group to an amine, by using metallic iron in an acidic environment. As seen above for the synthesis of compound **61**, the reduction of a single nitro-group requires 6 e^- and 6 H^+ (Scheme 10). The former are provided by the oxidation of metallic Fe to Fe^{2+} while the latter are provided by the acid. In order to reduce both nitro-groups, 6 equivalents of Fe would be necessary. The reducing mixture consisted of 7 equivalents of Fe in acetic acid and the reaction was carried out at 80 °C. After a basic work-up, the residual iron was separated from the product by Soxhlet extraction with EtOAc, leading to compound **140** in 56% yield.

- Synthesis of compound **141**

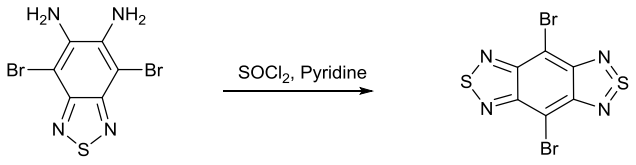

140 **141**

Compound **141** was synthesised according to a previously reported protocol.[228] The reaction mechanism is the same described above for the synthesis of compound **62**

(Scheme 11), involving the cyclization of the thiadiazole ring, using $SOCl_2$ and pyridine a base. Compound **141** was afforded in 69% yield, after reprecipitation.

- Synthesis of compound **110**

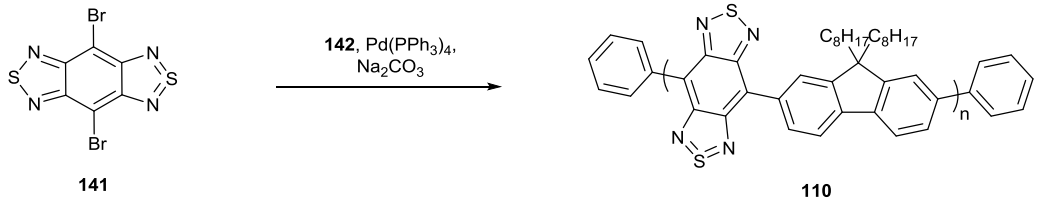

This reaction involved a Suzuki polymerization, applying the same conditions employed for the synthesis of polymer **57**. The polymerization was carried out in toluene, for 5 days, under Ar, and the end-capping agents were added afterwards, with a gap of 12 hours from each other. After the work-up, the mixture was purified *via* Soxhlet extraction, affording polymer **110** in 30% yield (calculated assuming the repeating unit as product).

- Analysis and characterisation of polymer **110**

The purification of polymer **110**, by Soxhlet extraction, led to the isolation of two batches with different molecular masses. The first fraction, with a lower M_n, was obtained by using $CHCl_3$ as extracting solvent, while for the second one THF was used. The two fractions were characterised by GPC in order to analyse the molecular weight distribution (Fig. 97) and, in both cases, a homogeneous distribution of the molecular weights was observed.

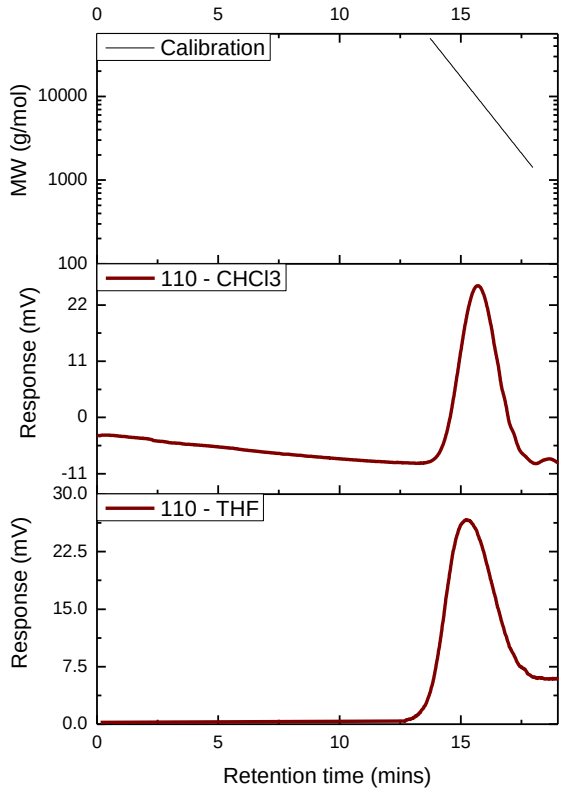

Figure 97 – GPC plots for the two isolated fractions of polymer **110**.

The parameters relative to both the fractions, provided in Table 12, suggest that the average number of repeating units in each molecule is between around 15 for the $CHCl_3$ fraction and around 23 for the THF one. In both the cases a very narrow polydispersity was observed.

Fraction	M_n (g/mol)	M_w (g/mol)	PDI
110 – $CHCl_3$	7566	10663	1.41
110 – THF	11234	15285	1.36

Table 12 – Significant parameters of polymer **110**.

The optimised structure of an oligomer of polymer **110** (Fig. 98a) was simulated by DFT calculation, featuring two repeating units. It showed a twisted structure with dihedral angles between BbT and fluorene units of around 30º, in line with the optimized structure of parent polymer F8BT.[229] Fig. 98b shows the frontier energy level distribution with the HOMO spread throughout the molecule and the LUMO localised on the BbT unit. This suggests that the polymer could be effective as p-type

semiconductor. The estimated HOMO and LUMO levels were –5.40 eV and –4.27 eV, suggesting that the bandgap would be approximately 1.1 eV.

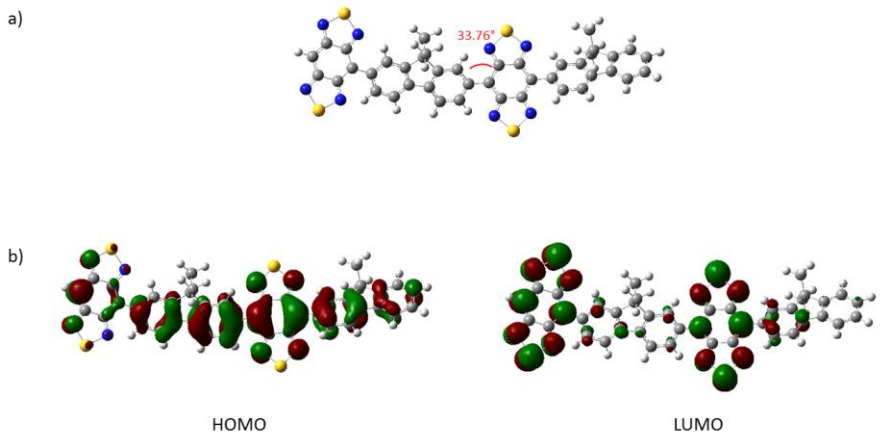

Figure 98 – (a) Optimised geometry and (b) energy level distribution for polymer **110** (two repeating units). Calculations were run using B3LYP functional and 6-311+G(d) basis set.

The absorption spectrum of polymer **110** in DCM solution is reported in Fig. 99. It consists of two main bands: one at around 350 nm, likely due to n-π* transition of BbT or π-π* transition of the conjugated aromatic moieties, whilst that between 500 nm and 800 nm corresponds to the ICT between donor and acceptor groups. The maximum of the ICT band is at 650 nm, almost 200 nm more shifted towards the NIR than that of parent F8BT (Fig. 100),[230] suggesting that replacing BT with BbT in conjugated systems could be an effective strategy for developing NIR absorbing polymers. The onset of absorption at λ = 773 nm corresponds to $E_{G,opt}$ = 1.60 eV.

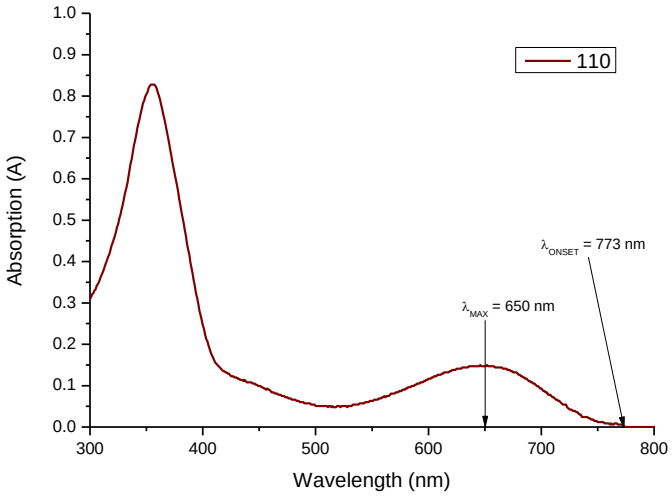

Figure 99 – UV-Vis absorption spectrum of polymer **110** in solution (C = 10^{-5} M, in DCM).

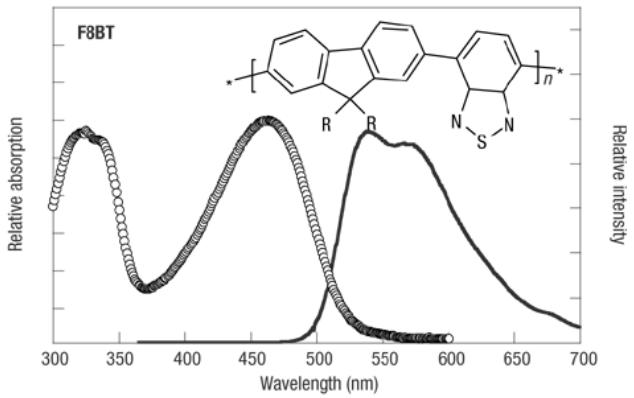

Figure 100 – Absorption and emission spectra of compound F8BT. The emission was recorded by exciting the sample at the maximum of absorption.[230]

F8BT is known for its emission properties, and in particular for its large Stokes shift of about 100 nm (Fig. 100), which allows green fluorescence while exciting with blue light. The emission spectrum of polymer **110** was recorded, by exciting a DCM solution of **110** with a light source at λ = 650 nm (Fig. 101).The polymer showed a fluorescence maximum at around 700 nm, therefore giving a Stokes shift of 50 nm.

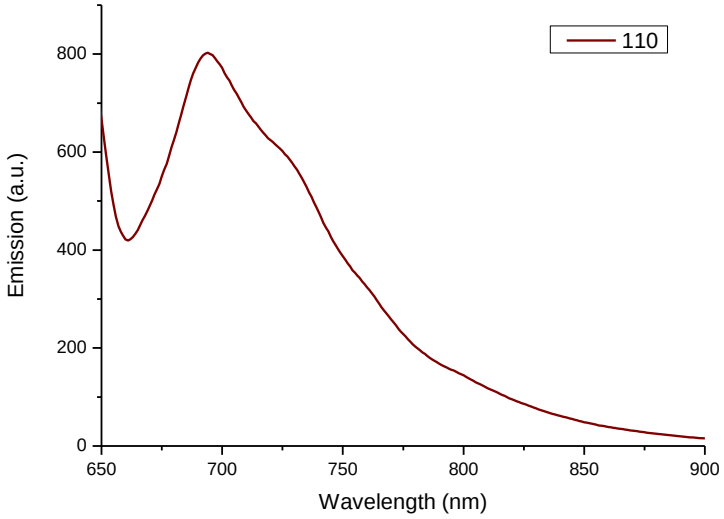

Figure 101 – Emission spectrum of polymer **110** in solution (C = 10^{-5} M, in DCM), using λ_{exc} = 650 nm.

The electrochemical properties of polymer **110** were explored by CV (Fig. 102) and SWV (Fig. 103). The CV plot showed a complex reduction side with the overlapping of two or more waves, with no trace of reversibility. From the SWV plot it was possible to estimate both E_{OX} and E_{RED} being equal to 0.66 V and –1.08 V, respectively. These were converted to the corresponding I_P = –5.46 eV and E_A = –

3.72 eV, which correspond to $E_{G,fund}$ = 1.74 eV, meaning that the exciton binding energy would be of around 140 meV. Also in this case, since both I_P and E_A of polymer **110** are slightly above those of PCBM, a possible application for this compound would be as p-type semiconductor for BHJ devices, blended with PCBM.

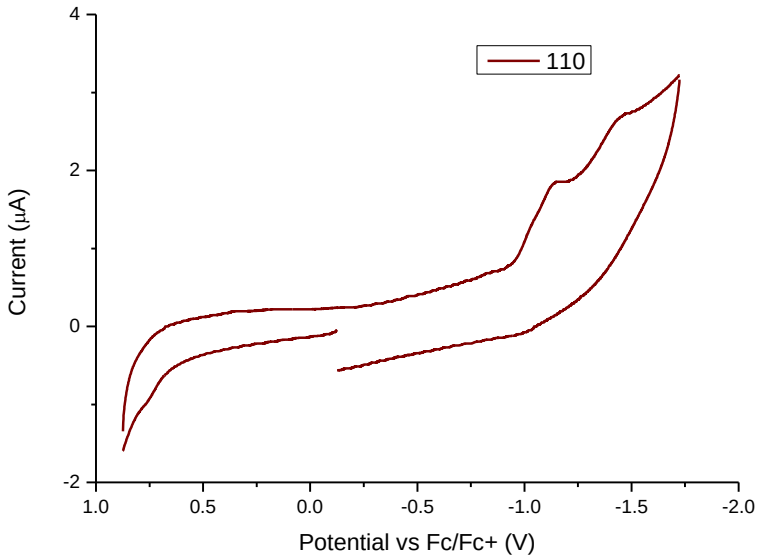

Figure 102 – CV plot of polymer **110** in solution (C = 10^{-3} M, in DCM), performed using a Pt disk working electrode, a Pt wire counter electrode and a Ag wire reference electrode. $TBAPF_6$ (0.1 M) was used as supporting electrolyte and the redox potential of the Fc/Fc^+ couple as external standard.

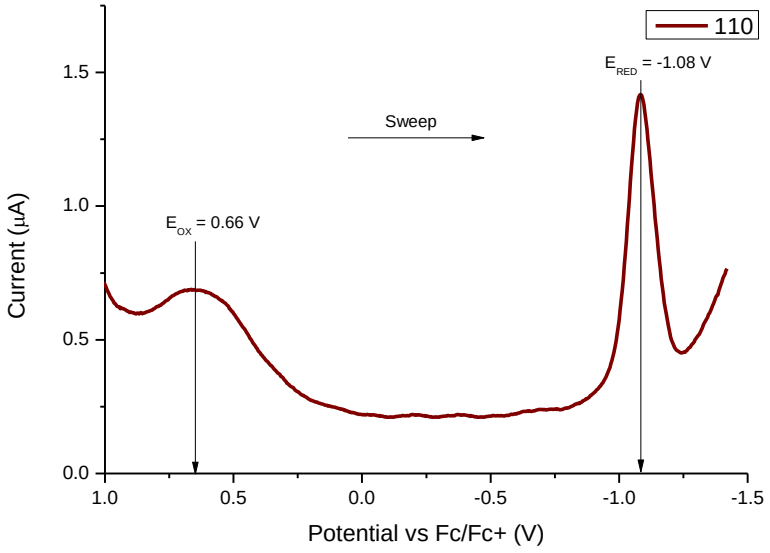

Figure 103 – SWV plot of polymer **110** in solution (C = 10^{-3} M, in DCM), performed using a Pt disk working electrode, a Pt wire counter electrode and a Ag wire reference electrode. $TBAPF_6$ (0.1 M) was used as supporting electrolyte and the redox potential of the Fc/Fc^+ couple as external standard.

Polymer **110** was tested as donor unit in BHJ devices in blend with $PC_{71}BM$, at the University of St. Andrews. A preliminary device was fabricated by spin-coating a mixture of **110** and $PC_{71}BM$ (1:1.5) on a ITO substrate, previously coated with PEDOT:PSS. An aluminium counter-electrode was then deposited by thermal vapour deposition. The IV-plot relative to the device is reported in Fig. 104, and the resulting parameters are provided in Table 13. The high value of V_{OC} is particularly interesting, since it is comparable to that reported by Foetig *et al.*,[231] using PTB7 in the same conditions. The low values of J_{SC} and FF are expected to increase by adjusting the blend ratio and using anti-aggregating co-solvents, such as 1,8-diiodooctane. Further studies will be undertaken in this direction.

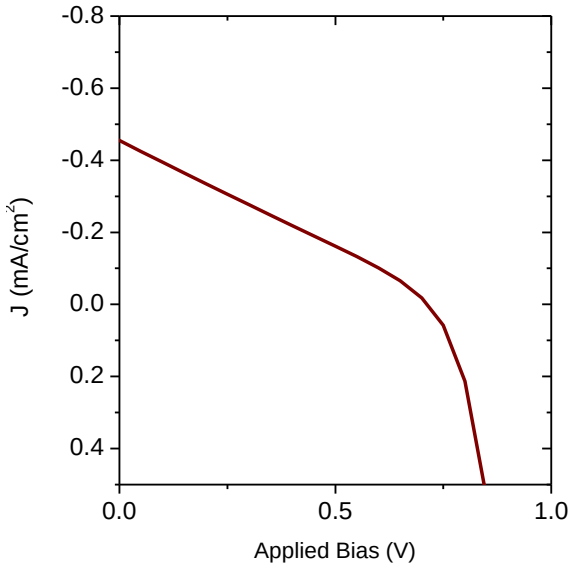

Figure 104 – IV-plot of BHJ device fabricated using a **110**:$PC_{71}BM$ blend as active material.

J_{SC} (mA/cm^2)	V_{OC} (V)	FF	PCE (%)
0.46	0.71	0.27	0.09

Table 13 – Summary of performances of BHJ devices using the **110**:$PC_{71}BM$ blend as active layer.

3.5 Conclusions and future work

Several BT-based compounds were successfully synthesised (Fig. 105). FcBT-based dyes **104** – **106** were used as sensitisers in DSSCs (fabricated at Chung-Ang University, S.Korea), providing a study of the influence of the acetylene linkers on the overall performances of the devices, and the results were published.[218] FcBT-

based compound **107** was also synthesised and characterised. Its interesting electrochemical properties, such as the reversible oxidation and reduction peaks, make it suitable as a potential donor unit for BHJ devices and as HTM in perovskite solar cells and will be tested in the future. Furthermore, the two dyes **108** and **109** were synthesised, characterised and used as sensitisers for DSSCs, fabricated by myself at EPFL (Switzerland). Unfortunately, both of them were affected by solubility issues which resulted in poor performances. Further attempts of increasing the PCE will be undertaken by adding anti-aggregating additives and changing HTM. Another possible solution would be to change their chemical structure by adding alkyl side chains, in order to improve the solubility. Finally, polymer **110** was synthesised and isolated with a good PDI. This compound, characterised by a broad UV-Vis absorption covering part of the NIR spectrum, was tested as donor unit for BHJs in blend with $PC_{71}BM$, at the University of St. Andrews. The preliminary device showed an encouragingly high V_{OC}, and further studies will be undertaken in order to improve J_{SC} and FF. Particularly, the low values of J_{SC} suggest that the molecule suffers of low charge-mobility. This may be due to the lack of planarity of the polymer structure. A possible way to make the polymer more planar could be the insertion of a spacer, such as a five-membered aromatic ring or an alkyne.

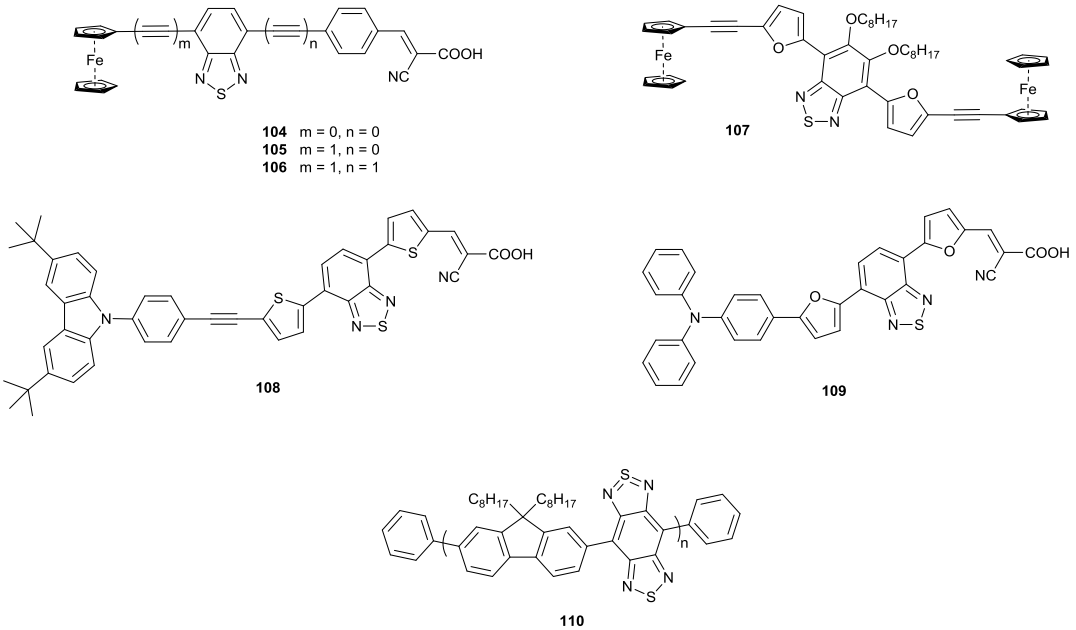

Figure 105 – Chemical structure of compounds **104** – **110**.

Chapter 4: Synthesis of tetrathiafulvalene derivatives

4.1 Introduction

Tetrathiafulvalene (TTF, Fig. 106) is a key heterocyclic compound. It was synthesised in 1970 by Wudl *et al.*[232] and since then it has been among the most studied heterocyclic systems. In 1973, for instance, Cowan *et al.*[233] found out that the charge-transfer complex TTF-TCNQ (TCNQ: tetracyanoquinodimethane, Fig. 106) had metallic conductive properties and, one year later, Engler and Patel[234] reported the synthesis of the selenium TTF analogue TSeF (Fig. 106), as the first example of an organic superconductor. Consequently, TTF and its derivatives, due to their unique π-donor properties, are successfully used as versatile building blocks for charge-transfer salts, giving rise to a multitude of organic conductors and superconductors.[235]

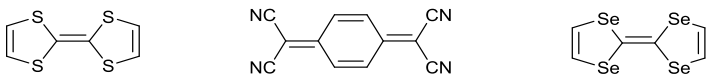

Figure 106 – Chemical structure of TTF, TCNQ and compound **141**.

The key property of the electron rich TTF unit is its ability to act as a unique π-electron donor. TTF can be oxidised in two one-electron steps to yield the thermodynamically stable radical cation $TTF^{\bullet+}$ and dication TTF^{2+} (Fig. 107). This was shown by the action of chlorine gas on a carbon tetrachloride solution of TTF.[236] When treated with one equivalent of chlorine, an unusually stable purple radical cation was formed. Addition of excess chlorine yielded the stable yellow dication. The stability of the radical cation and dication was found to be due to the sequential formation of six-π–electron aromatic dithiolium cation with each successive one-electron oxidation. The two successive one-electron oxidations are clearly observed in the CV at $E^{1/2}$ = +0.34 V and $E^{1/2}$ = +0.71 V (vs. Ag/AgCl in MeCN) and are completely reversible.

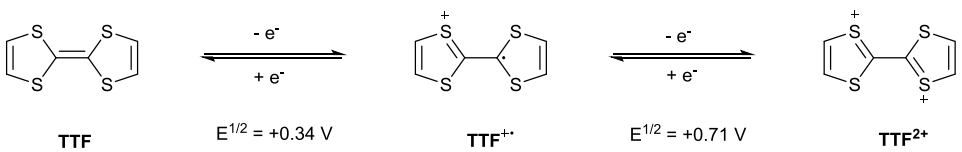

Figure 107 – The redox chemistry of TTF.

Neutral TTF shows a highly flexible structure, easily interconverting from a planar to a boat-like conformation (Fig. 108); while the radical cation adopts a nearly planar form.[237] The dication again shows more flexibility and its twisted conformation (with a torsion angle of 60°) is more favoured, but it is also found in a more planar form due to packing interactions.[238] The contribution from 6-π-electron heteroaromaticity in the 1,3-dithiolium cations explains structural changes as well as the relatively low oxidation potentials of the oxidized states. The interesting properties of TTF-based compounds are usually related to changes in oxidation state, and these changes bring about remarkable modifications in both the molecular and the electronic structure.[237]

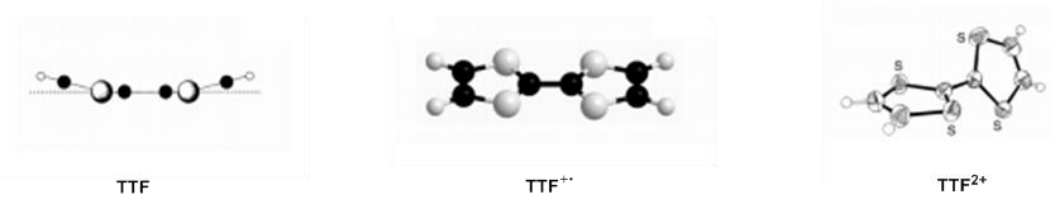

Figure 108 – Structural conformations of TTF redox states (boat-like, planar, gauche-like twisted).[237]

In the solid state, TTF derivatives readily form highly ordered stacks (Fig. 109) or two-dimensional sheets, which are stabilized by intermolecular π-π interactions and non-bonded S-S interactions. These short contacts allow the formation of a band structure. Consequently, partial oxidation of the TTF species in the stacks generates the charge carriers for the conducting properties, due to the resulting partially filled LUMO level.

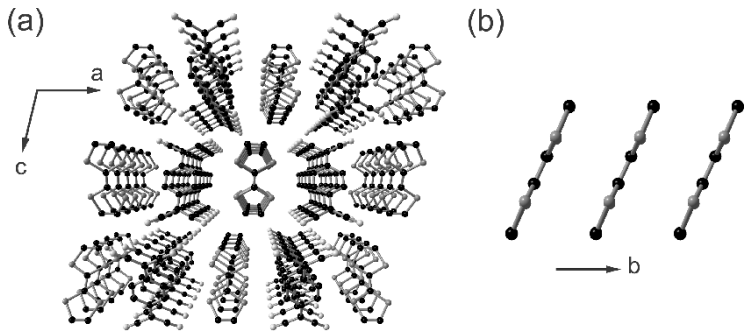

Figure 109 – Crystal structure of TTF-TCNQ. Cell parameters: $P2_1/c$, a = 1.2298 nm, b = 0.3819, c = 1.8468 nm. (a) Perspective view along the stacking *b*-axis and (b) view along the *a*-axis of a TTF stack.[239]

4.2 Applications in organic optoelectronics

TTFs are interesting building blocks which form supramolecular aggregates in the solid state with interesting conducting and magnetic properties. TTFs are strong

electron donors that form stable open-shell species by transferring one π-electron from the HOMO. Moreover, these molecules promote stacking as a consequence of the π–π orbital overlap. TTF is also a versatile unit, which can easily be substituted in C(2), C(3), C(6) and C(7) positions, modifying not only the electronic but also the supramolecular characteristics of the TTF derivative. These properties, together with the exceptional reversibility of its electrochemistry, have encouraged researchers to explore TTF and its derivatives as potential candidates for organic optoelectronic applications. In 2004, Rovira *et al.*[240] reported the fabrication of single-crystal organic field-effect transistors (OFETs) based on dithiophene-tetrathiafulvalene (DT-TTF, Fig. 110), observing a hole mobility of 1.4 cm^2/Vs, one of the highest reported at the time for organic semiconductors, and of the same order of magnitude of amorphous silicon, widely used in solar cells and flat screen displays.

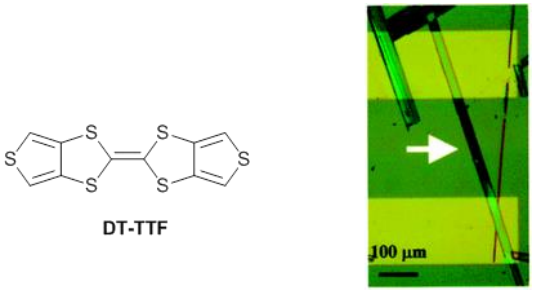

Figure 110 – Structure of DT-TTF (left) and DT-TTF crystal formed on microfabricated electrodes (right).[240]

One year later, Martin *et al.*[241] reported the results of their study about photoluminescence quenching for the donor-acceptor dyad system made of a TTF derivative (ex-TTF) and fullerene C_{60} (Fig. 111). In particular, they observed an effective ICT that caused photoluminescence quenching and triplet-triplet absorption, concluding that the ex-TTF-C_{60} dyad could act as photovoltaic active material in thin-film devices showing extended absorption range as compared to pristine C_{60}.

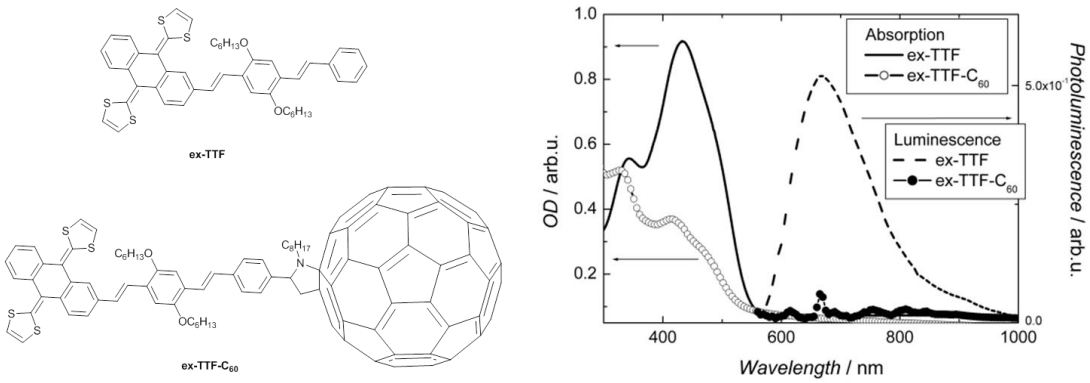

Figure 111 – Chemical structure of ex-TTF and ex-TTF-C_{60} dyad (left) and their absorption and luminescence on spin cast film.[241]

Despite the high potential of TTF as donor unit, there are only few examples in the literature, regarding the use of this unit in photovoltaics. Very recently, Skabara *et al.*[242] reported the synthesis of a DPP-based polymer (**142**, Fig. 112), containing a TTF derivative as donor unit, which is so far the only example of TTF-containing polymer for OPVs. A PCE of 1.8% was achieved for the BHJ device made from a blend of polymer **142** and $PC_{71}BM$, while in a single material organic solar cell (SMOC) the polymer **142** showed a PCE of 0.3%, marking it as a promising structure to develop for SMOCs.

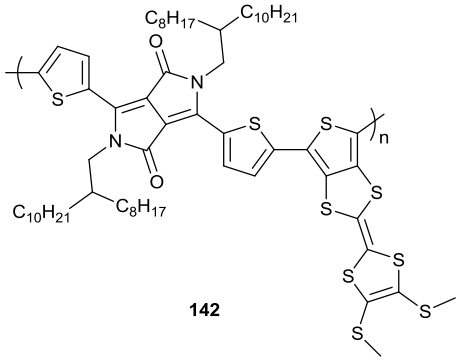

Figure 112 – Chemical structure of polymer **142**.

Regarding DSSCs, in 2012 Kloo *et al.*[243] investigated the use of TTF as an iodine-free redox shuttle, with modest results, mainly due to the high recombination rate between HTM and TiO_2. TTF derivatives have also been used as donor units for the synthesis of sensitisers. In 2010, Robertson *et al.*[244] developed the Ru-based dye **143** (Fig. 113) containing TTF as donor unit. Unfortunately, due to the inefficient charge regeneration the device performances were poor (PCE = 0.006%). Better results were achieved in 2014 by Graetzel et al.[245] who reported the synthesis of a fused quinoxaline-TTF dye (**144**, Fig. 113), which showed a PCE of 6.5%.

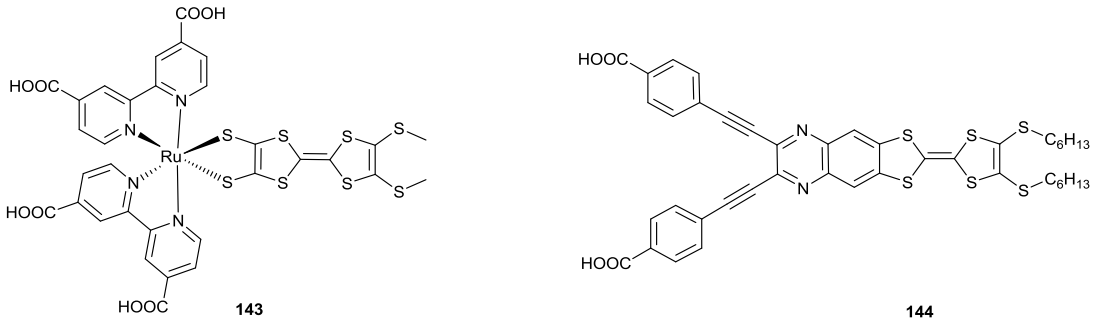

Figure 113 – Chemical structure of compounds **143** and **144**.

4.3 Aims

This chapter reports the synthesis of several TTF derivatives (Fig. 114), designed to be used as donor materials in BHJ devices (eg **147** and **148**) or as sensitisers in DSSCs (eg **145** and **146**).

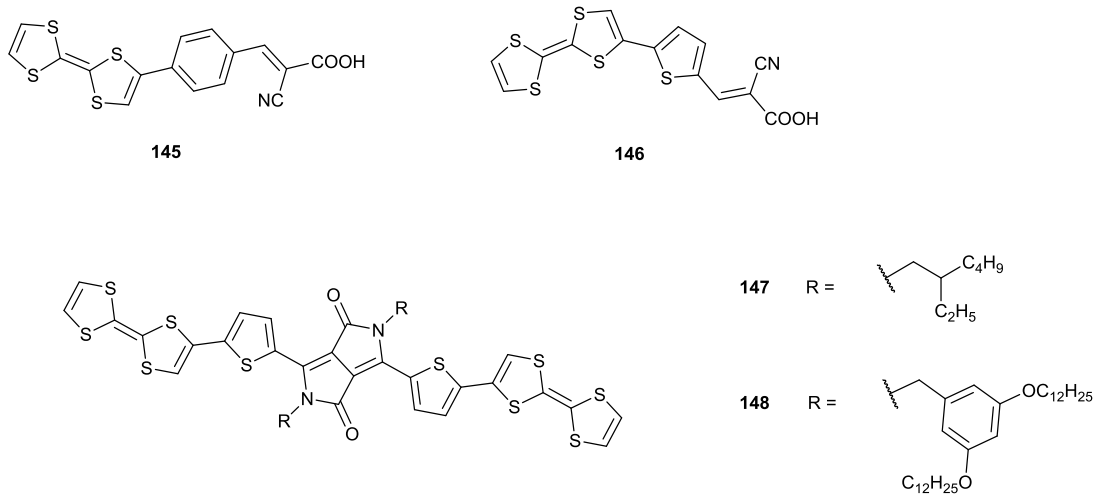

Figure 114 – Chemical structure of compounds **145** – **148**.

The idea behind the synthesis of dyes **145** and **146** was the design of very simple sensitisers for DSSCs, in order to explore the potential application of TTF as donor unit, by comparing the performances of the resulting devices with the known TPA-based analogues **149**[246] and **150**[91] (Fig. 115), which deliver PCEs of 4.1% and 2.8%, respectively.

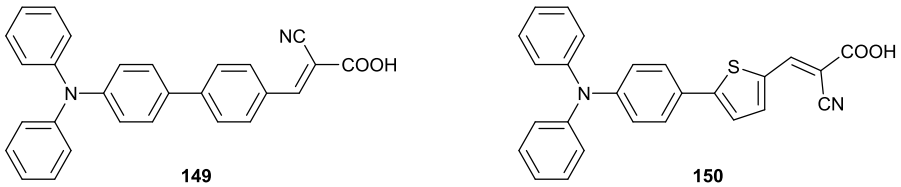

Figure 115 – Chemical structure of dyes **149** and **150**.

Comparable performances would prove the effectiveness of TTF as donor unit and the potential development of more complex molecules containing chromophoric π-bridges. The synthesis of the two compounds (Scheme 39) started with the functionalisation of commercially available TTF to make the corresponding organo-tin compound **151**, *via* lithiation. Then, compound **151** would be coupled with the two aromatic bromide aldehydes (**152** and **153**), *via* Stille coupling, to give the

corresponding aldehydes **154** and **155**. These would be treated with cyanoacetic acid **116**, in a Knoevenagel condensation to give the final compounds **145** and **146**.

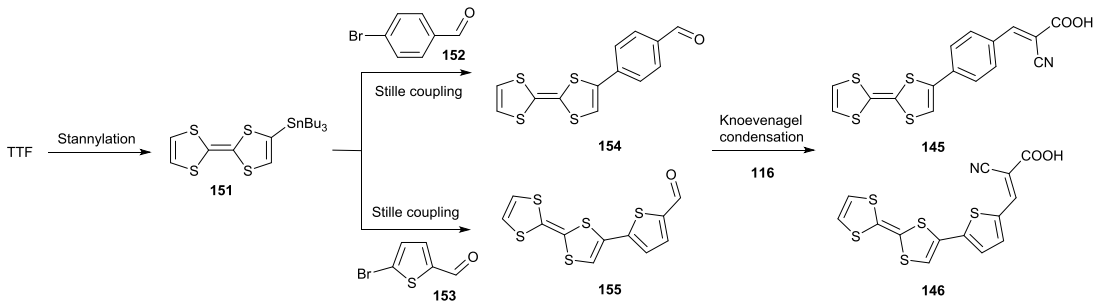

Scheme 39 – Proposed strategy towards the synthesis of dyes **145** and **146**.

The application of TTF as donor unit for small molecule OPVs was explored with the synthesis of compounds **147** and **148**. The DPP central core was chosen for its powerful and broad absorption in the UV-Vis range, as well as for its good charge mobility. Two different side chains were used in order to test how the film smoothness and crystallinity can vary. The proposed synthetic strategy (Scheme 40) starts with the *N*-alkylation of commercially available compound **156**, leading to compounds **157** and **158**, depending on the alkylating agent. Then, the DPP core would undergo dibromination of the thiophene moieties' at C(5), followed by Stille reaction with compound **151**, to afford the target compounds **147** and **148**.

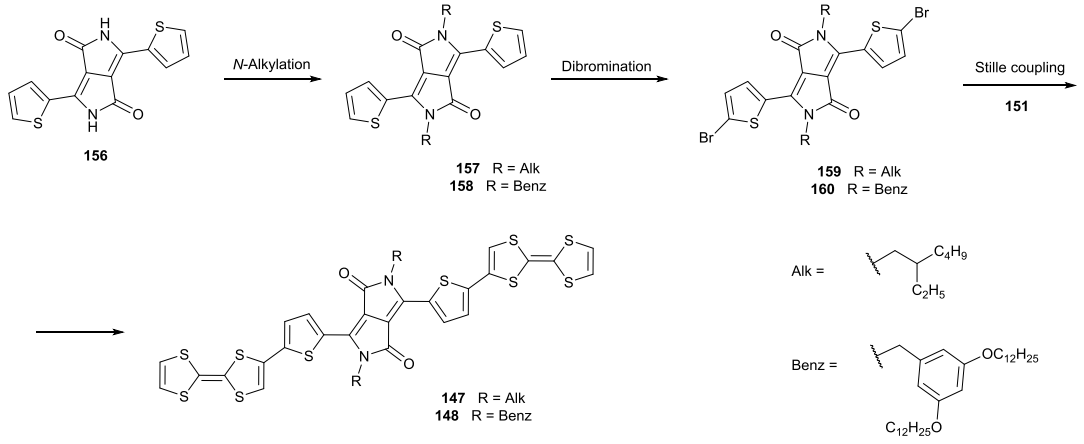

Scheme 40 – Proposed strategy towards the synthesis of compounds **147** and **148**.

Compound **157** would be obtained by using 2-ethylhexylbromide as alkylating agent, while for the alkylation of compound **158**, the synthesis of the benzylic bromide **163** would be required (Scheme 41). This would start from commercially available

compound **161**, which would first undergo a Williamson reaction, leading to compound **162**, followed by Appel reaction, affording the target compound **163**.

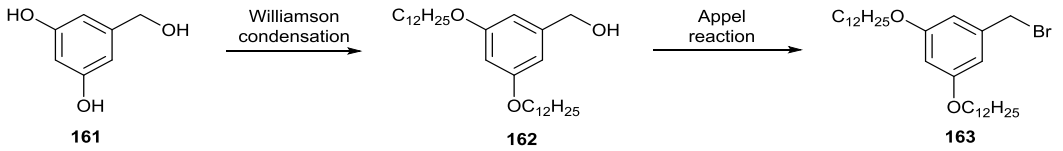

Scheme 41 – Proposed strategy towards the synthesis of compound **163**.

4.4 Results and discussion

4.4.1 TTF-based dyes for DSSCs

- Synthesis of compound **151**

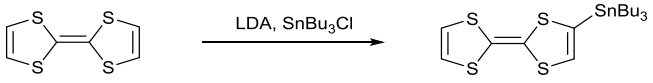

Compound **151** was synthesised according to a slight modification of a previously reported protocol.[247] The reaction involves the use of a lithiating agent in order to substitute one or more hydrogens of the substrate with a suitable functionality. In 1977, Green[248] first reported the synthesis of the monofunctionalised TTF derivatives, directly prepared from 4-lithiotetrathiafulvalene, and showed that the formation of the TTF anion could be accomplished via the action of butyllithium or LDA in Et_2O at –78 °C. At temperatures above –78 °C disproportionation of monolithiated species is more likely to occur, leading to multisubstituted products; thus, it is necessary to keep temperature control at all time during the reaction.

In order to maximise the reaction yield a slight excess of a freshly titrated LDA solution, in THF, was added drop-wise to a solution of TTF in Et_2O at –78 °C. The solution was stirred at the same temperature until a lemon-yellow precipitate was observed, and then one equivalent of the tin-reagent was added. This choice of conditions led to the isolation of the product in 67% yield with exceptionally high NMR grade purity, after a purification procedure consisting of multiple extractions, using MeCN and PE.

- Synthesis of compounds **154** and **155**

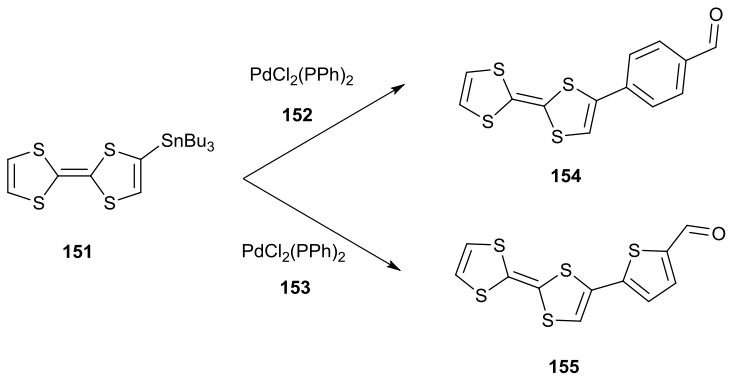

The synthesis of compounds **154** and **155** involved a Stille coupling between compound **151** and the corresponding halide aromatic aldehydes **152** and **153**. The reaction was carried out following the procedure described above, using toluene as solvent and a $Pd^{(II)}$ catalyst. Compounds **154** and **155** were afforded in 85% and 82% yield, respectively.

- Synthesis of compounds **145** and **146**

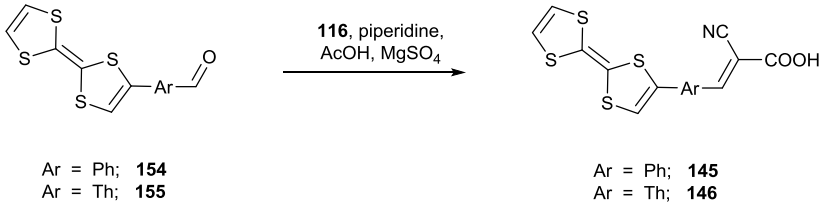

The synthesis of dyes **145** and **146** was accomplished by a Knoevenagel condensation, applying the reaction conditions described above. The two dyes were isolated in 91% and 87% yield, respectively.

- Analysis and characterisation of dyes **145** and **146**

The geometry and electronic properties of dyes **145** and **146** were explored by DFT calculations. The optimised geometry results, reported in Fig. 116a, show that there is a dihedral angle of 28.5° between TTF and benzene for **145**, and of 19.9° between TTF and thiophene for **146**. In both cases, the TTF moiety is almost planar, with the two 5-membered rings slightly tilted towards each other in a boat configuration. The distribution of frontier molecular orbitals, shown in Fig. 116b, reveals that in both dyes the HOMO level is localised on TTF, while the LUMO is spread throughout the remainder of the molecule and touches part of TTF, ensuring the overlap of the two frontier orbitals.

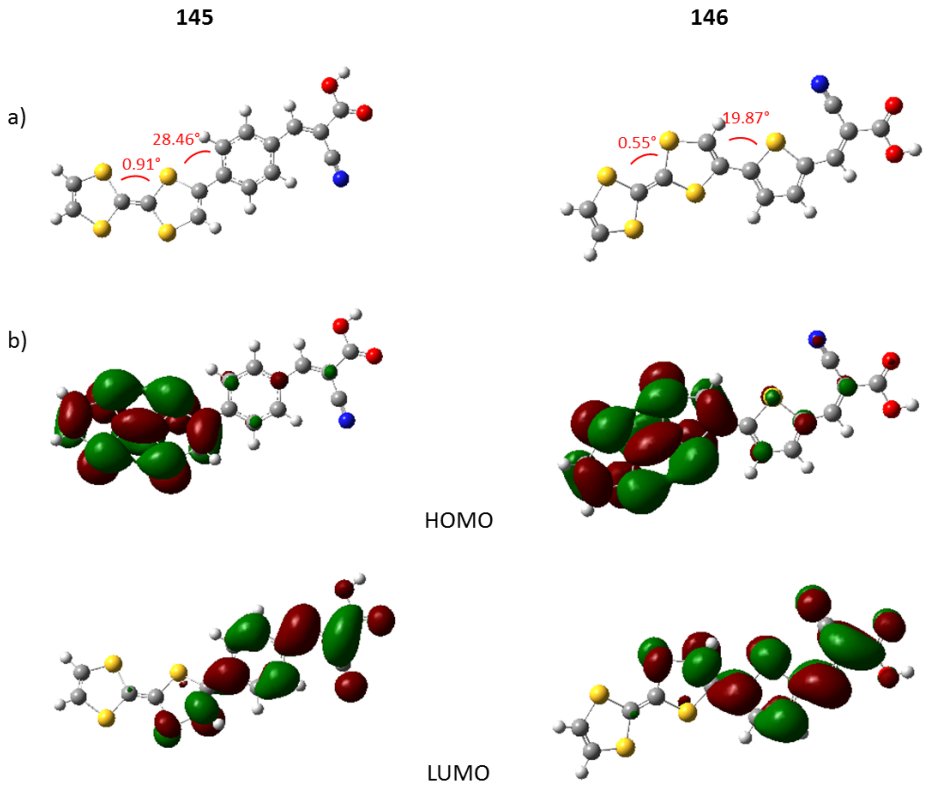

Figure 116 – (a) Optimised geometry and (b) frontier molecular orbital distributions for dyes **145** and **146**. Calculations were run using the B3LYP functional and the 6-311+G(d) basis set.

Fig. 117 reports the UV-Vis absorption spectrum of the two dyes in solution. Both of them consist of two main bands: the most intense of them are in the range between 300 nm and 400 nm and are likely due to the π-π* transitions of the aromatic units. The bands in the range between 400 nm and 700 nm are most probably due to the ICT between donor and acceptor units. Their low intensity is mainly attributable to the lack of a strong *push-pull* system and to the distorted structure which hampers the charge flow. The absorption spectrum of dye **146** is shifted by around 50 nm towards higher wavelengths, compared to that of dye **145**, with the ICT maxima at 478 nm and 529 nm for dyes **145** and **146**, respectively. The red-shift is also reflected by the onset of absorption, at 707 nm and 750 nm respectively, corresponding to optical bandgaps of 1.75 eV and 1.65 eV.

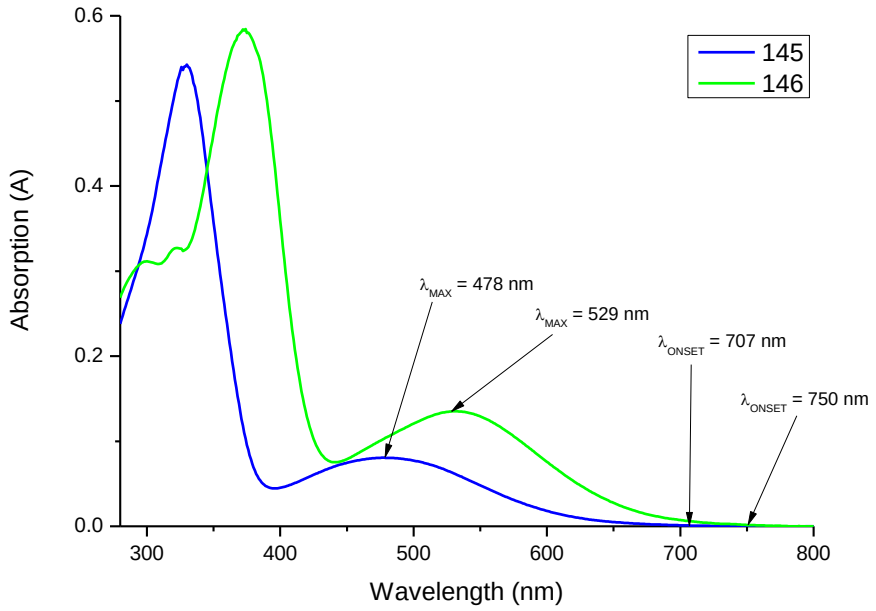

Figure 117 – UV-Vis absorption spectrum of dyes **145** and **146** in solution (C = 10^{-5} M, in DMF).

The CVs (Fig. 118) show the presence of two reversible oxidation waves for each dye. These correspond to the typical CV pattern of TTF, with the first wave corresponding to the oxidation from TTF to $TTF^{\bullet+}$ and the second to the oxidation process which leads to TTF^{2+}. Also, the reduction part of the plot is very similar for both dyes, with a non-reversible peak at around –1.5 V and a quasi-reversible wave at around –2.0 V. The SWV plots (Fig. 118) show that the position of the first oxidation peak for both dyes is 0.01 V respect to Fc/Fc^{+} which would suggest a high-positioned I_P of –4.81 eV. Also the values of E_{RED} are very similar, respectively at –2.09 V and –2.01 V, corresponding to E_A values of –3.14 eV for dye **145** and –3.21 eV for dye **146**.

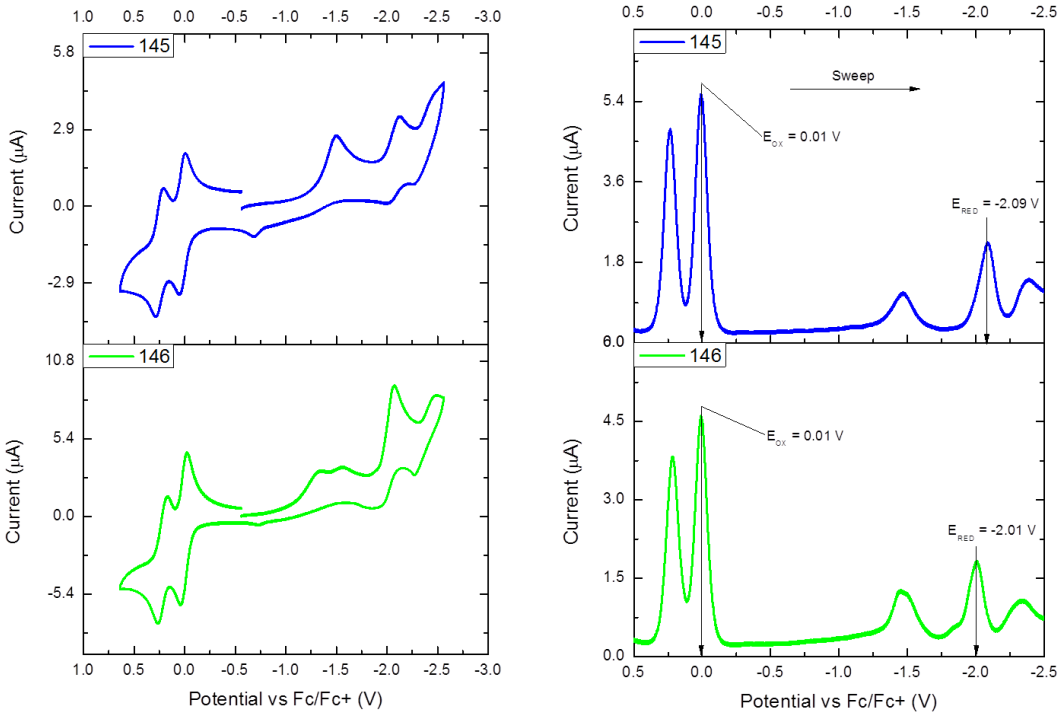

Figure 118 – CV (left) and SWV (right) plots of dyes **145** and **146** in solution (C = 10^{-3} M, in DMF), performed using a Pt disk working electrode, a Pt wire counter electrode and a Ag wire reference electrode. $TBAPF_6$ (0.1 M) was used as supporting electrolyte and the redox potential of the Fc/Fc^+ couple as external standard.

DSSCs were fabricated by our collaborators, at Bangor University, using dyes **145** and **146** as sensitisers and the results are shown in Table 14. For both the devices, a 0.5M LiI solution in MeCN was used as the redox shuttle.

Dye	J_{SC} (mA/cm^2)	V_{OC} (V)	FF	PCE (%)
145	1.34	0.45	0.58	0.4
146	1.11	0.38	0.52	0.2

Table 14 – Summary of devices performances using dyes **145** and **146** as sensitisers.

There could be several reasons for such poor efficiencies. In the first instance, the I_P values are slightly higher in energy than the I^-/I_3^- redox couple, suggesting that a better electrolyte system – such as Fc/Fc^+ – has to be explored. Also the E_A values lie at almost 1.0 eV above the CB of TiO_2, facilitating the charge recombination processes. One possible solution for both the problems would be a redesign of the dyes, with the incorporation of a *push-pull* structure in the π-bridge, in order to lower the bandgap, and the addition of an acceptor unit after TTF in order to pull down the HOMO level. Another issue arising with these systems is aggregation. Fig. 119 reports the absorption spectra of the two dyes after dip-coating onto TiO_2 substrates.

Surprisingly, the plots show the loss of the peaks in the visible range and new and intense peaks around 1200 nm. This may be explained with the formation of crystalline domains. Further studies will be undertaken towards this direction.

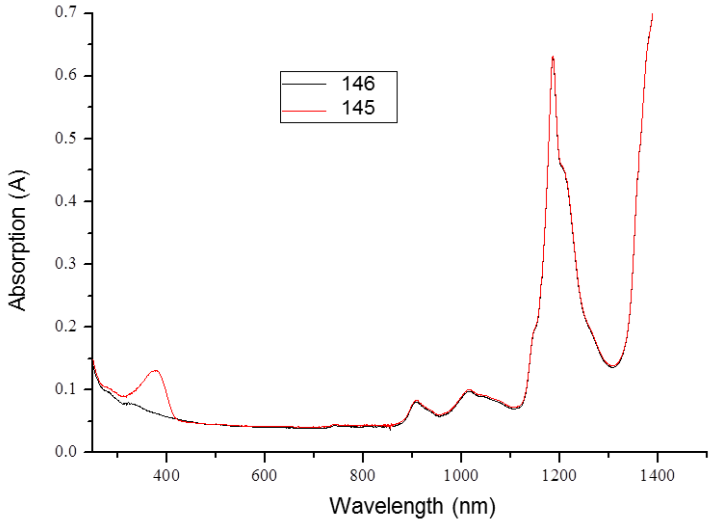

Figure 119 – Absorption spectrum of dyes **145** and **146**, adsorbed on TiO_2 surface.

4.4.2 TTF-based small *push-pull* molecules

- Synthesis of compound **162**

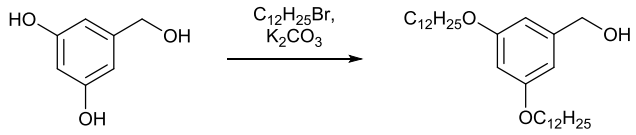

161 **162**

Compound **162** was synthesised *via* a Williamson synthesis, following a previously reported method.[249] The reaction was carried out over 3 days in acetone, affording the target compound in 67% yield.

- Synthesis of compound **163**

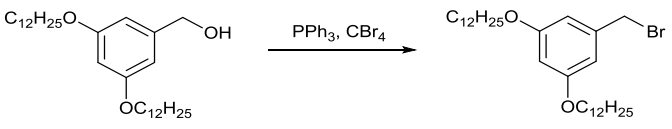

162 **163**

Compound **163** was synthesised, *via* an Appel reaction, according to a published protocol.[250] This procedure allows the synthesis of aliphatic halides starting from the corresponding alcohol (Scheme 42), using the same reagents seen above for the Corey-Fuchs reaction.

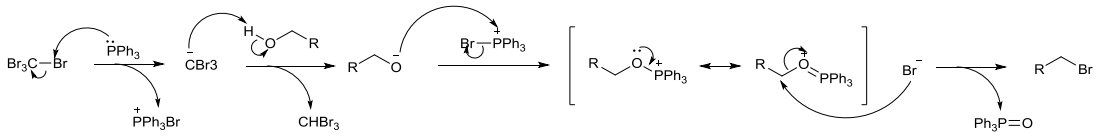

Scheme 42 – Proposed Appel reaction mechanism.

The reaction was carried out in dry THF for 15 minutes, and the target compound was isolated in quantitative yield.

- Synthesis of compound **157**

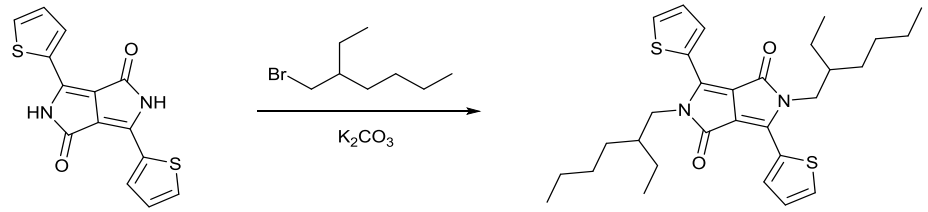

156 **157**

Compound **157** was synthesised according to a slight modification of a reported procedure.[251] First attempts to perform this *N*-alkylation, using K_2CO_3 as base and dry DMF as solvent, resulted in very low yields, below 20%, which could be improved by around 5% upon addition of catalytic amounts of 18-crown-6, as a K^+ scavenger. The main issue with this reaction was the purification step, involving multiple chromatographic columns due to the presence of side-product **164** (Fig. 120) eluting at very similar R_f, resulting as the major product of the reaction.

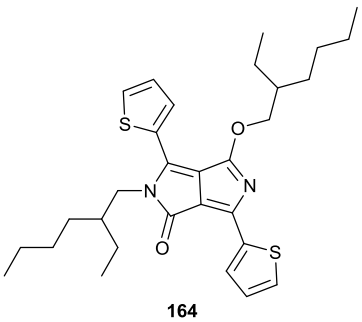

164

Figure 120 – Chemical structure of compound **161**.

The mechanism towards the formation of compound **164**, described by Ouyang *et al.*,[252] involves the tautomerization (Scheme 43) of deprotonated DPP to form the thermodynamically stable enolate, which leads to the *O*-alkylation.

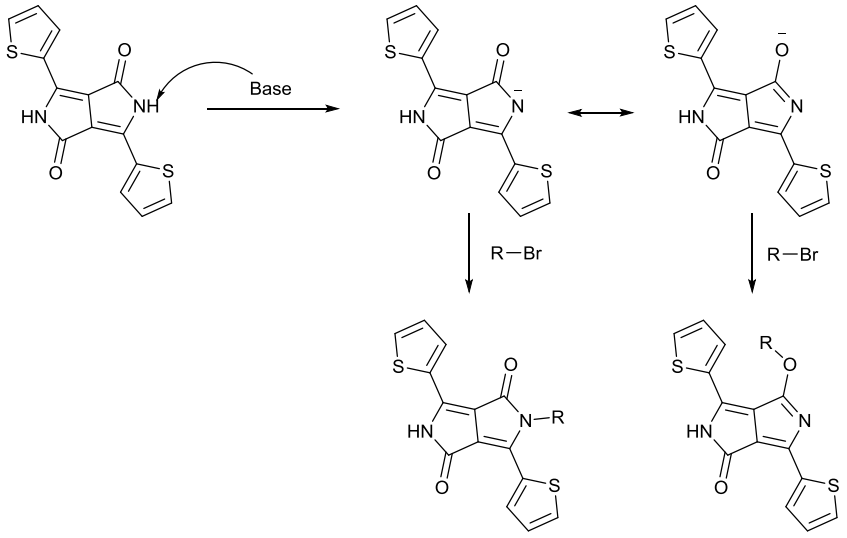

Scheme 43 – Proposed mechanism towards the formation of compound **161**.

Further attempts performed by decreasing the reaction temperature to 100 ºC, from reported 145 ºC, and increasing the reaction time to 36 hours, instead of 12 hours, led to the isolation of compound **157** in 52% yield.

- Synthesis of compound **158**

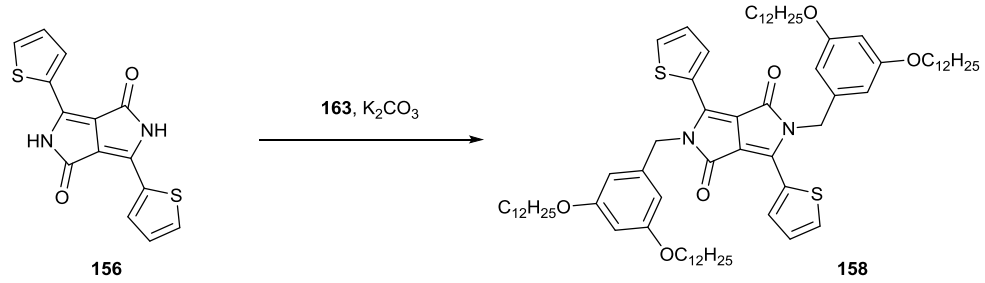

156 **158**

Compound **158** was synthesised similarly to compound **157**. Dry NMP, instead of DMF was used, and the reaction was carried out at 80 ºC, for 5 days. Compound **158** was isolated in 44% yield, and no trace of the *O*-benzylated isomer was observed.

- Synthesis of compounds **159** and **160**

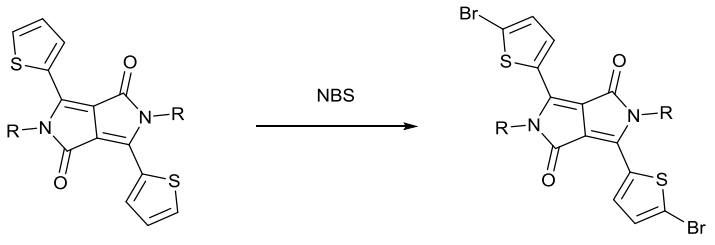

157 R = Alk
158 R = Benz

159 R = Alk
160 R = Benz

For the bromination of both compounds **157** and **158**, the conditions described above for bromination with NBS where applied. Compound **159** was isolated in 97% yield, while the synthesis of compound **160** was unsuccessful. Indeed, due to the activating effect of the alkoxy-chains on the benzyl-group, this resulted to be more activated towards electrophilic substitution than thiophene and the reaction ended up with compounds **165** – **167** (Fig. 121) which were isolated in 9%, 40% and 26% yields, respectively.

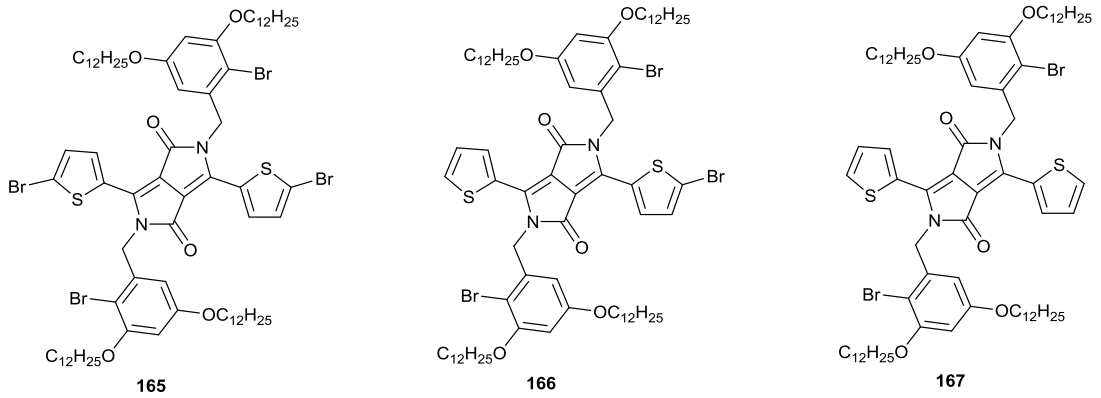

Figure 121 – Chemical structure of compounds **165** – **167**.

Unfortunately, due to the time constraints of this project, the remainder of the synthesis will be carried out by other researchers within the Cooke group.

- <u>Synthesis of compound **147**</u>

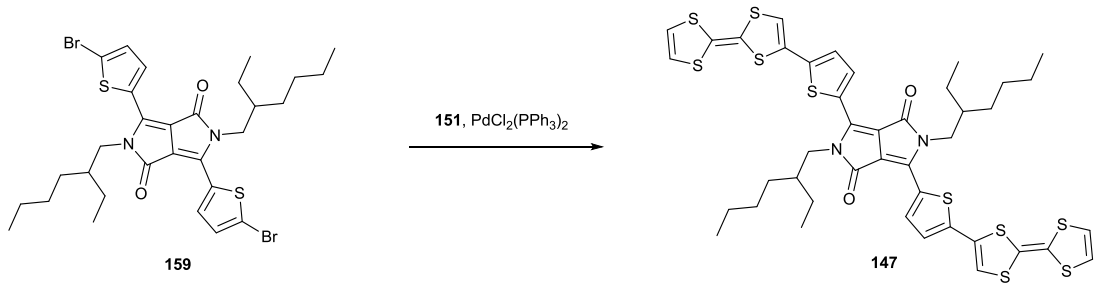

Compound **147** was synthesised *via* Stille cross-coupling of compound **159** with two equivalents of compound **151**. First attempts of purifying the target compound were unsuccessful, due to its instability on silica gel and in presence of chlorinated solvents, making it impossible to purify with conventional techniques. After reprecipitation from MeOH, followed by a Soxhlet extraction with hexane, the raw compound was adsorbed on celite and placed on the top of a pad of silica gel; PE was passed through the pad in order to wash away the impurities until the washings were

colourless. Thereafter, the celite part was recovered and extracted with EtOAc, affording compound **147** in 83% yield.

- Analysis and characterisation of compound **147**

Fig. 122a reports the DFT optimised geometry of compound **147**. The aromatic backbone of the molecule is almost planar with dihedral angles of around 2° between the aromatic units. Again, TTF adopts a boat-like configuration. The HOMO/LUMO distribution, depicted in Fig. 122b, shows that the HOMO is mainly distributed over the peripheral TTF units, whilst the LUMO is spread over the central DPP unit. The calculated values are –5.21 eV for the HOMO and –3.19 eV for the LUMO.

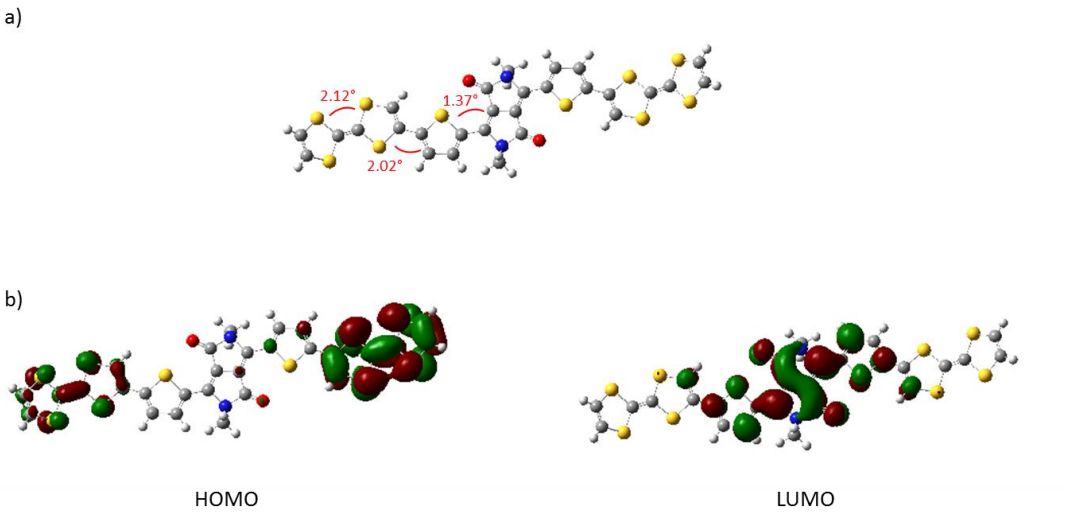

Figure 122 – (a) Optimised geometry and (b) frontier molecular orbital distributions for compound **147**. Calculations were run using the B3LYP functional and the 6-311+G(d) basis set.

The UV-Vis absorption of compound **147**, reported in Fig. 123, shows the presence of two absorption bands: the first, below 400 nm, is due to the π-π* transitions of the aromatic units, while the second and more intense, between 500 nm and 900 nm, is due to ICT between the donor and the acceptor moieties. The absorption maximum at 647 nm gives rise to the compound a blue colour. The absorption onset is at 909 nm, corresponding to an optical bandgap of 1.36 eV.

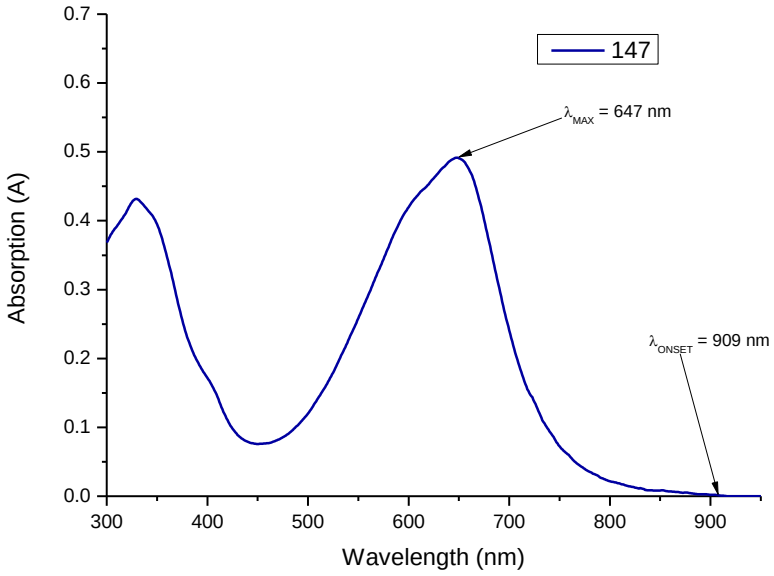

Figure 123 – UV-Vis absorption spectrum of compound **147** in solution (C = 10^{-5} M, in $CHCl_3$).

The CV plot (Fig. 124) shows the existence of multiple oxidation waves, between 0.5 V and 1.0 V, corresponding to a broad peak in the SWV plot at 0.57 V. This peak, in the latter, is likely made up of superimposition of several peaks. The SWV plot also shows the presence of a reduction peak at –0.86 V. These two values correspond to IP = –5.37 eV and EA = –3.94, leading to a bandgap of 1.46 eV.

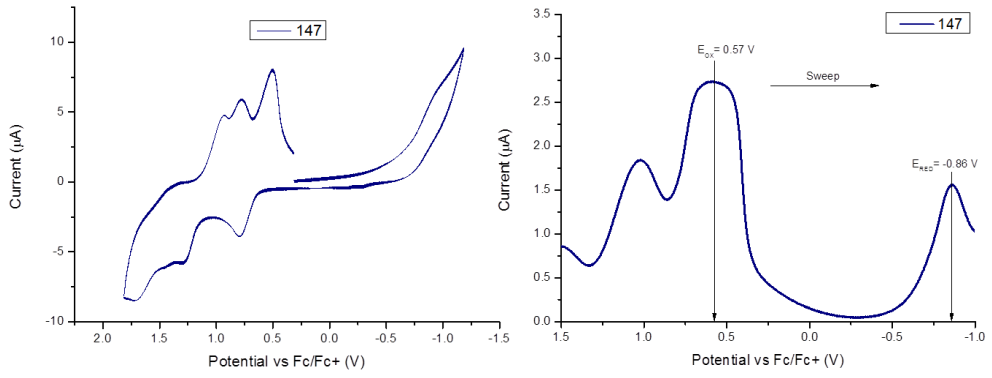

Figure 124 – CV (left) and SWV (right) plots of compound **147** in solution (C = 10^{-3} M, in $CHCl_3$), performed using a Pt disk working electrode, a Pt wire counter electrode and a Ag wire reference electrode. $TBAPF_6$ (0.1 M) was used as supporting electrolyte and the redox potential of the Fc/Fc^+ couple as external standard.

The small bandgap of compound **147** makes it an attractive material to be employed as donor unit for BHJ solar cells and further investigations will be undertaken in this direction. Although it has a strong absorption in the UV-Vis, the I_P value of –5.37 eV makes it a possible candidate as HTM for perovskite solar cells. This possibility was

explored at the EPFL, where compound **147** was used as solid HTM in $MAPbI_3$-based devices, reporting the results shown in Table 15. Several solvents concentrations and doping additives were explored, and the best performances were obtained with a HTM concentration of 30 mM (instead of the standard 60 mM concentration, due to solubility limits) with no additives, with an overall PCE of 7.7% (Fig. 125a). Surprisingly, the addition of Li-TFSI led to worse performances with an overall PCE of 5.6% and a much less uniform IV curve (Fig. 125b). The generally low performances are due to the non-optimal morphology of the HTM film, which seems to form clusters on the perovskite surface. This was due to the poor solubility and led to the design of compound **148**, which, with the long-alkylated benzyl rings, would provide higher solubility and better processability.

HTM	J_{SC} (mA/cm^2)	V_{OC} (V)	FF	PCE (%)
147	14.4	0.785	0.68	7.7
147:Li-TFSI	12.8	0.663	0.65	5.6

Table 15 – Summary of device performances using compound **147** as HTM for perovskite solar cells.

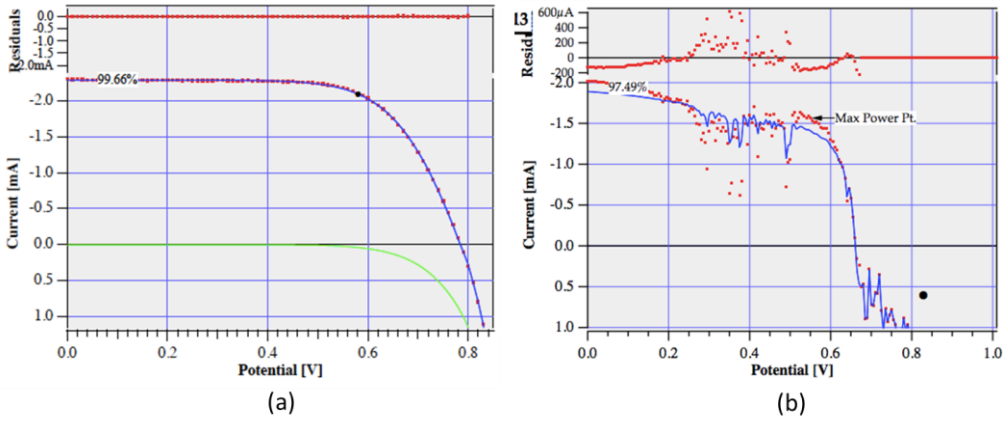

Figure 125 – IV-plots of perovskite solar cells fabricated using pristine compound **147** (left) and compound **147** doped with Li-TFSI (right) as solid HTM.

4.5 Case study: TTF dehalogenation and halogen dance

In 1986, while attempting to synthese 2,3-dihydrotetrathiafulvalene **171** by treating TTF bromide **168** with LDA (Scheme 44), Nakayama *et al.*[253] reported the unexpected *halogen dance* (HD), with the formation of **172** and **173** by halide migration. The same base-catalysed reaction was observed using t-BuOK instead of LDA.

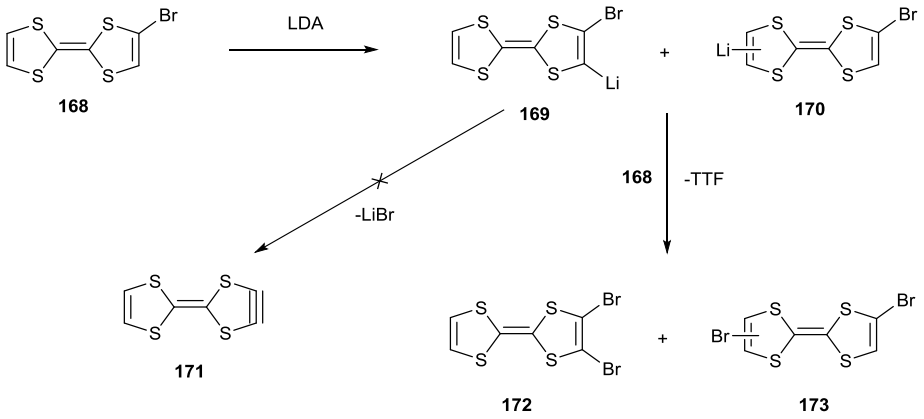

Scheme 44 – Halogen dance taking place on TTF bromide **168**.

The HD in aromatic compounds is well documented[254] and several reaction conditions and mechanisms have been reported to date. However, HD reactions for non-aromatic compounds are unusual.

In an attempt to synthesise aryne-like compound **171**, base-catalysed reactions (using different conditions) were performed, starting from TTF chloride **174** and TTF iodide **175**, prepared according to Scheme 45.

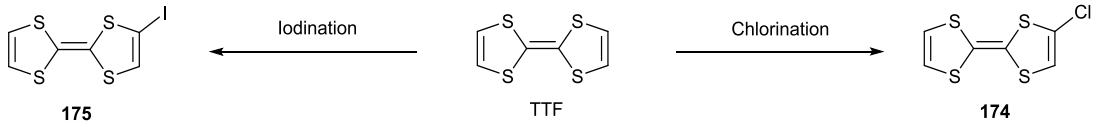

Scheme 45 – Proposed strategy towards the synthesis of compounds **174** and **175**.

- <u>Synthesis of compound **174**</u>

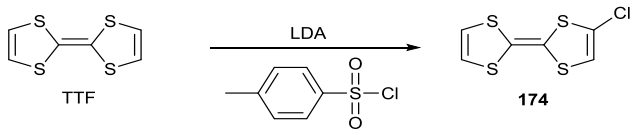

Compound **174** was synthesised according to a slight modification of a previously reported method.[255] This procedure involved the deprotonation of TTF *via* lithiation with LDA (Scheme 46) and successive addition of a chlorinating agent, specifically *p*-toluenesulfonyl chloride (TsCl). A first lithiation took place by adding LDA to TTF in dry Et_2O, at –78 ºC, then 0.9 equivalents of TsCl were added, in order to avoid multiple chlorinations. The target compound was afforded in 63% yield, with respect to TTF.

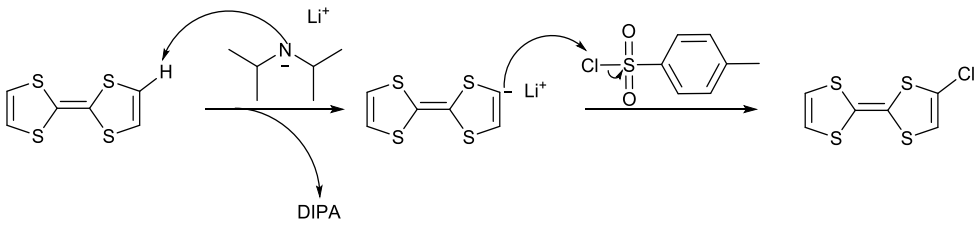

Scheme 46 – Proposed reaction mechanism towards the chlorination of TTF.

- Synthesis of compound **175**

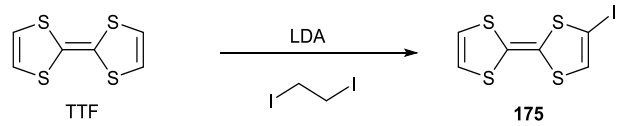

For this reaction a previously reported protocol[256] was followed. A first lithiation of TTF, followed by addition of 1,2-diiodoethane, led to compound **175**, according to the mechanism proposed in Scheme 47.

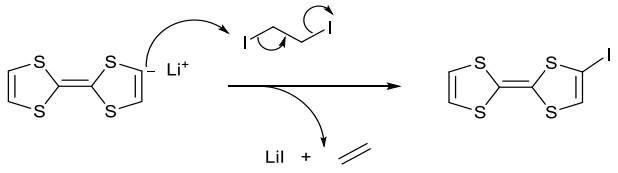

Scheme 47 – Proposed reaction mechanism towards the iodination of TTF.

Compound **175** was particularly unstable in the reaction mixture, and longer reaction times resulted in the formation of an insoluble black solid. For this reason, monitoring the reaction and quenching it with sodium thiocyanate, when the formation of the black solid on the wall of the reaction flask was observed, was crucial for the reaction success. The target compound was afforded in 80% yield.

- Results and discussion

Compound **175** was treated with MeONa under various conditions, as reported in Table 16. The reaction performed in MeOH at room temperature did not lead to any changes and unreacted starting material was recovered. However, carrying out the reaction at 65 °C a quantitative conversion of **175** to TTF occurred in 5 minutes. The same results were obtained using DMF instead of MeOH, while the reaction occurred at room temperature when using MeCN as solvent. Different results were observed when using THF as solvent. In fact, at 65 °C, after 6 hours, 50% of the starting

material was converted to TTF and a mixture of TTF diiodide isomers, **176** and **177** (Fig. 126), in 0.22 : 0.78 ratio. Both isomers were isolated and characterised by NMR and MS. The same experiments were repeated using TTF chloride **174** as substrate but no reactions were observed.

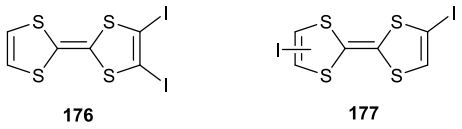

Figure 126 – Chemical structure of compounds **176** and **177**.

Solvent	Temperature	Reaction time	Products
MeOH	r.t.	15 h	No reaction
MeOH	65 °C	5 mins	TTF
DMF	r.t.	15 h	No reaction
DMF	65 °C	5 mins	TTF
MeCN	r.t.	5 mins	TTF
THF	r.t.	15 h	No reaction
THF	65 °C	6 h	TTF + **175** + **176** + **177**

Table 16 – Reaction conditions for the treatment of compound **175** with MeONa.

A possible mechanism explaining the HD on TTF is shown in Scheme 48. A first deprotonation would take place on compound **175**, with formation of MeOH. Then, the deprotonated species would attack the halogen of a second molecule of **175**, leading to the formation of **176** and a TTF anion, which would deprotonate a third molecule of **175**, forming TTF and the active deprotonated species **175**$^{-}$, making the reaction cyclic (Scheme 49).

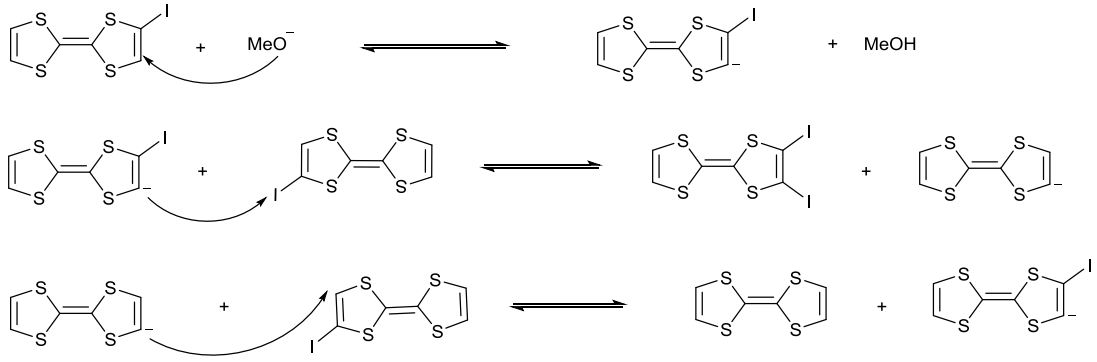

Scheme 48 – Proposed mechanism of TTF HD.

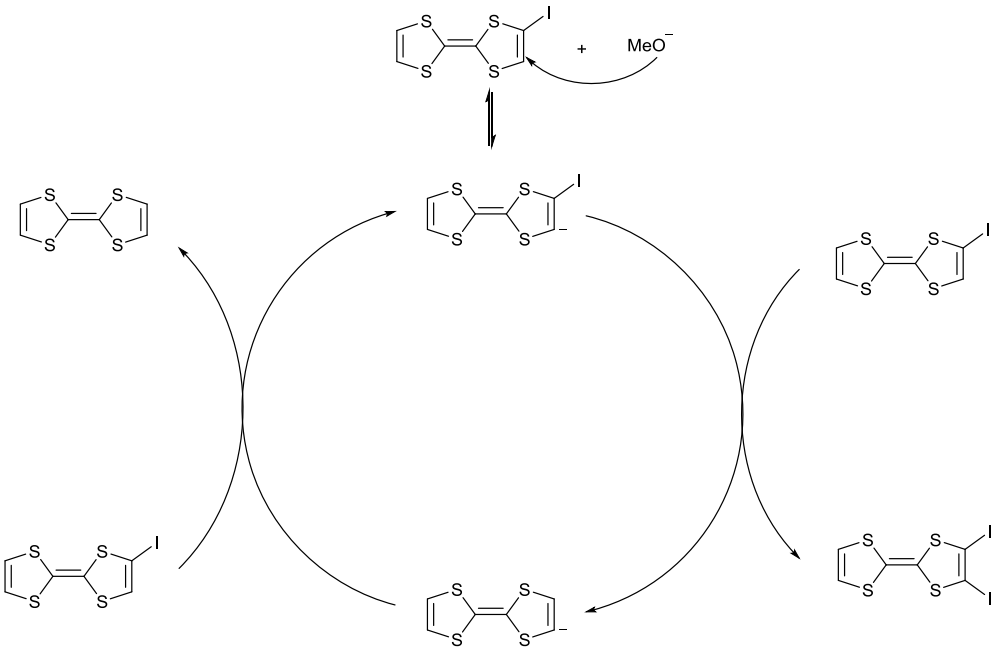

Scheme 49 – Cyclic representation of TTF HD.

Concerning the deiodination reactions, there are few examples in the literature regarding the dehalogenation of aromatic iodides. For instance, in 2011, Lane *et al.*[257] reported the photo-induced dehalogenation of 2-iodothiophene *via* a radical reaction, using a UV-light source. One year later, Stephenson *et al.*[258] achieved the same result, using visible light and a catalytic amount of an Ir-based initiator. As mentioned above, although TTF itself is not aromatic, it gains aromaticity *via* oxidation. It is reasonable that if the corresponding radical cation of **175** (**175**$^{\bullet+}$) is in solution, it will act as substrate and radical initiator. Electronic Paramagnetic Resonance (EPR) spectroscopy was performed on a sample of **175** in MeCN, a signal was observed, confirming the presence of a radical species. This signal corresponded to that of the radical **175**$^{\bullet+}$ obtained by simulation (Fig. 127). A quantitative EPR experiment, using a 0.1 mM solution of (2,2,6,6-tetramethylpiperidin-1-yl)oxyl (TEMPO) as standard, determined the concentration of **175**$^{\bullet+}$ to be 0.087%. The addition of MeONa to the sample resulted in the instantaneous disappearance of the EPR signal, obtaining pristine TTF. Interestingly, no EPR signals were observed for compound **174** in MeCN. Further studies will be undertaken in order to better understand the mechanism behind the formation of the radical species as well as the following dehalogenation.

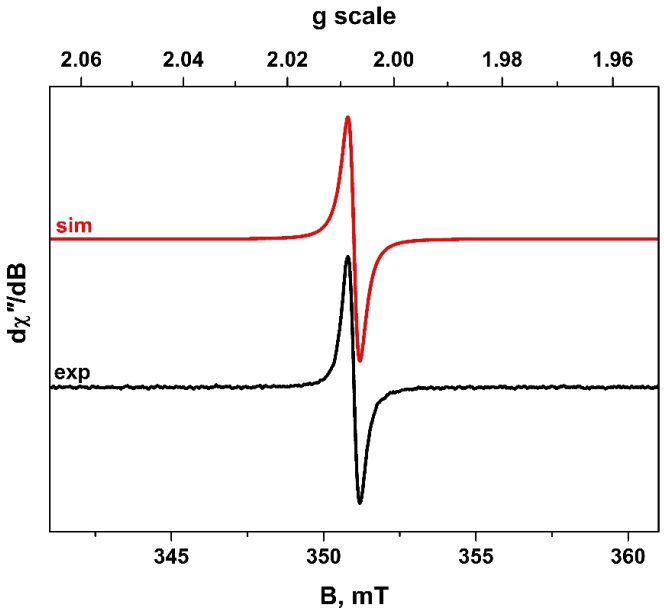

Figure 127 – Experimental EPR spectrum of **175** in MeCN (black) and simulated EPR spectrum of **175**$^{\bullet+}$ (red). Experimental conditions: frequency, 9.8619 GHz; power, 10 mW; modulation, 0.2 mT; temperature 293 K.

4.6 Conclusions and future work

Two new TTF-based dyes **145** and **146** (Fig. 128) were successfully synthesised and used as sensitisers for DSSCs, fabricated by our collaborators at Bangor University. To the best of our knowledge, they represent the first examples of dyes based on pure TTF. Problems arising from the low absorption coefficient and aggregation limited their performances, suggesting that a better design, including an alkylated chromophore unit in the π-bridge and a strong acceptor unit after TTF, could significantly increase the performances.

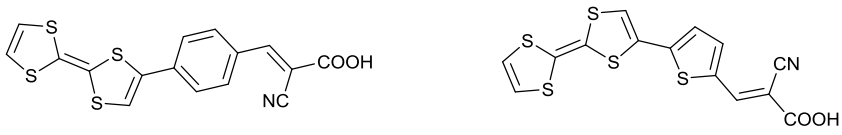

145 **146**

Figure 128 – Chemical structre of dyes **145** and **146**.

A symmetric small molecule (**147**, Fig. 129) containing a DPP core and peripheral TTF units was also successfully synthesised. This compound was used as HTM for perovskite solar cells, fabricated by myself at EPFL. Low performances were recorded, due to solubility issues which affected the morphology of the HTM film. A better response was obtained without doping the HTM. In order to increase the solubility and processability of compound **147**, a slight modification of its structure

was planned with the introduction of alkylated benzyl groups instead of the 2-ethylhexyl chains, leading to compound **148** (Fig. 129).

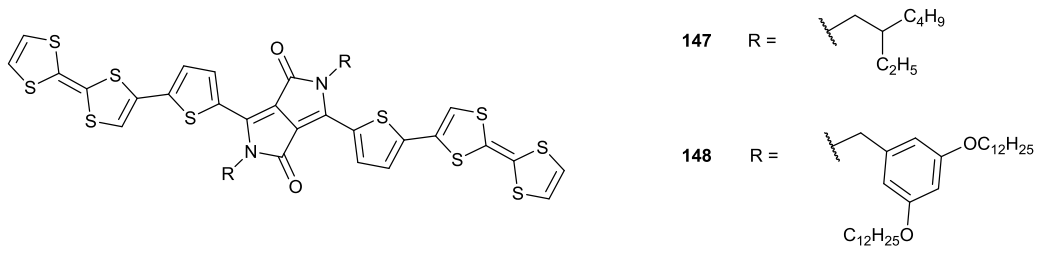

Figure 129 – Chemical structure of compounds **147** and **148**.

Unfortunately, its synthesis was unsuccessful due to higher reactivity of benzyl groups towards bromination. A possible solution would be the selective lithiation of position C(5) of thiophenes with LDA, with successive functionalisation with halogens or boronic esters (Scheme 51).

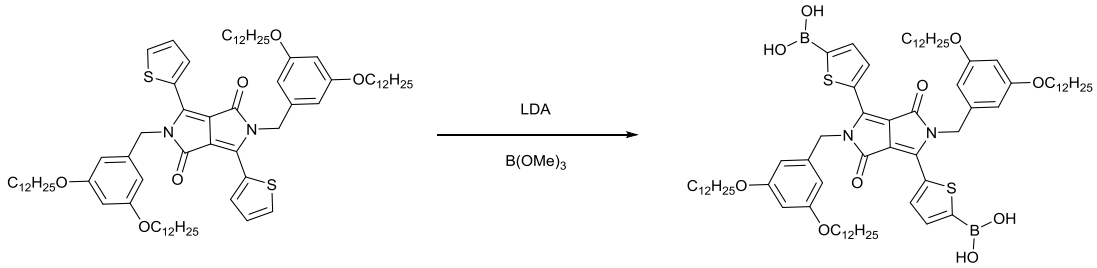

Scheme 50 – Proposed reaction scheme towards the borylation of benzylated DPP unit.

The base-catalysed halogen dance and dehalogenation of TTF was studied. In particular, it has been observed that TTF iodide **175** (Scheme 52) undergoes HD when treated with MeONa in THF at reflux while, under the same reaction conditions, in MeOH or DMF (or at room temperature in MeCN), it rapidly forms TTF in quantitative yield. A proposed mechanism for both reactions was provided, and further studies will be undertaken in order to confirm it. This results indicate that compound **175** may be a poor reagent for base-mediated reactions (e.g. Suzuki coupling).

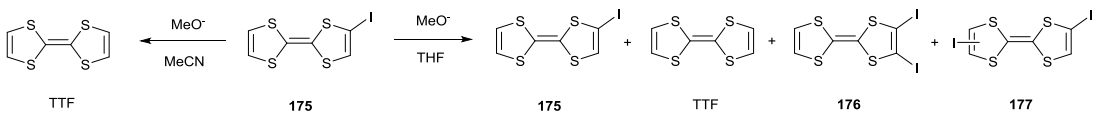

Scheme 51 – TTF dehalogenation and HD.

Chapter 5: Experimental

5.1. General experimental

Experimental terms and methods

All the reagents were purchased from either Sigma Aldrich®, TCI®, Alfa Aesar®, Acros® and Fisher Scientific®. Column chromatography was carried out using silica gel (Sigma-Aldrich) 40 – 63 nm 60 Å. The solvent system is specified in each experiment. TLCs were performed using Merck silica gel 60 covered aluminium plates F254. Dry solvents were obtained either Innovative Technology inc. Pure Solv 400-5-MD solvent purification system (activated alumina columns) or Sigma Aldrich®.

Reaction temperatures: room temperature refers to 20 – 25 ºC. Other temperatures were obtained using ice-water bath for 0 ºC and acetone-dry ice bath for −78 ºC.

Analytical methods

Mass spectrometry and elemental analysis were obtained from the mass spectrometry service at the University of Glasgow or the EPSRC UK National Mass Spectrometry Facility at Swansea University**.** Melting points (mp) were recorded on a SMP-10 Stuart Scientific melting point machine. Melting points are uncorrected. NMRs were recorded on either Bruker Avance III 400 or Bruker Avance III 500 spectrometers. The ^{1}H and ^{13}C spectra were recorded at 400 or 500 MHz and 100 or 125 MHz, respectively, with TMS as internal standard. NMR spectra were analysed using either SpinWorks 3.1.8.1. free software or iNMR 5.0 (licensed edition). Signals in ^{1}H-NMR spectra are described as singlet (s), doublet (d), triplet (t), quartet (q), quintet (quint), multiplet (m), broad (b) or a combination of these, which refers to the spin-spin coupling pattern observed. DEPTQ, and two-dimensional (COSY, HSQC) NMR spectroscopy were used where appropriate to assist the assignment of signals in the ^{1}H and ^{13}C NMR spectra. Electrochemistry was performed using a CH Instrument Electrochemical Workstation (CHI 440a), Austin, TX, USA. Samples were analysed at 1.0 mM concentrations with a scan rate of 0.1 V/s, unless specified, using $TBAPF_6$ (0.1 M in corresponding solvent) as the supporting electrolyte. A platinum disk working electrode, a platinum wire counter electrode and a silver wire reference were

used for all measurements. The reduction potentials are referred to ferrocene (internal or external reference) with the Fc/Fc^+ redox couple adjusted to 0.00 V. Absorbance spectrometry was performed using a Shimadzu UV-3600 UV-Vis-NIR spectrophotometer and a Perkin Elmer Lambda 25 UV/Vis Spectrometer. Qualitative fluorescence spectroscopy was performed using a Shimadzu RF-5301PC spectro-fluorimeter. All the spectroscopic and electrochemical data were processed using Origin Pro 8.5 software suite.

Computational methods

Calculations were performed using either Spartan ’08 or Gaussian ‘09 software suites. Molecular geometries were initially optimized semi-empirically (AM1) and then re-optimized by DFT. Energy minima were confirmed by the absence of imaginary frequencies from vibrational frequency calculations. To facilitate the convergence of the geometry optimizations, in molecules where long alkyl chains such as 2-ethylhexyl side chains were present the alkyl chains were replaced by methyl units.

5.2 Experimental details

4,7-Dibromobenzo[*c*][1,2,5]thiadiazole[155] **46**

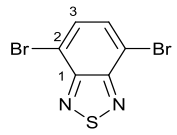

Benzo[*c*][1,2,5]thiadiazole **45** (5.00 g, 36.8 mmol) was dissolved in an aqueous solution of 48% HBr (80 mL). Br_2 (5.67 mL, 0.110 mol), previously dissolved in an aqueous solution of 48% HBr (50mL), was added drop-wise. The mixture was then stirred at reflux. During the reaction, an orange precipitate was observed. After 6 hours, the mixture was allowed to cool to room temperature, and quenched with an aqueous solution of saturated $Na_2S_2O_3$ (300 mL). The resulting suspension was stirred for further 1 hour and then filtered. The solid was washed with water (200 mL) and purified by recrystallization from MeCN, affording the title compound as a yellowish needle-shaped solid (8.42 g, 78%); mp 189 – 190 °C [lit. 188 – 189 °C]; δ_H (400 MHz, $CDCl_3$, TMS) 7.73 (s, 2H). δ_C (100 MHz, $CDCl_3$, TMS) 152.6 C(1), 132.1 C(3), 113.6 C(2); MS (EI^+, *m/z*): $[M]^+$ found 293.8.

4,7-Di(furan-2-yl)benzo[*c*][1,2,5]thiadiazole[158] **48**

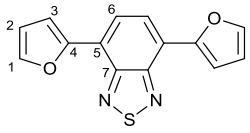

Compound **46** (5.00 g, 17.0 mmol) and tributyl-furan-2-yl-stannane **47** (13.0 mL, 40.0 mmol) were dissolved in dry THF (80 mL). The solution was degassed for 30 minutes with N_2, then $Pd(PPh_3)_4$ (0.800 g, 0.680 mmol) was added. The resulting mixture was stirred at reflux, under N_2, and was monitored by TLC. After 24 hours, the mixture was allowed to cool to room temperature and poured into an aqueous solution of 1M KF (200 mL). The suspension was stirred for further 1 hour, then the organic layer was extracted with DCM (3 × 150 mL). The combined organic extracts were dried over $MgSO_4$, filtered and concentrated under vacuum. The crude compound was purified by column chromatography (SiO_2; PE:DCM; 9:1) to afford the title compound as an orange solid (4.50 g, 93%); mp 189 – 190 °C; δ_H (400 MHz, $CDCl_3$, TMS) 7.99 (s, 2H, C(6)H), 7.62 (d, *J* 1.7, 2H, C(1)H), 7.52 (d, *J* 1.7, 2H, C(3)H), 6.57 (dd, *J* 1.7, 1.7, 2H, C(2)H); δ_C (100 MHz, $CDCl_3$, TMS) 154.6 C(7), 153.1 C(4), 142.0 C(1),129.9 C(5), 128.3 C(6), 110.3 C(3), 104.6 C(2); MS (EI^+, *m/z*): $[M]^+$ found 268.0.

3,6-Di(furan-2-yl)benzene-1,2-diamine **49**

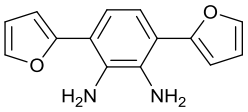

Compound **48** (1.00 g, 3.73 mmol) and $CoCl_2 \cdot 6H_2O$ (0.180 g, 0.740 mmol) were dissolved in EtOH (150 mL). $NaBH_4$ (0.420 g, 11.2 mmol) was slowly added, then the mixture was stirred at reflux for 2 hours. The white mixture was then allowed to cool to room temperature and filtered through celite. The residue was washed with Et_2O (100 mL) and the resulting filtrate was poured into water (200 mL) and extracted with Et_2O (3 × 100 mL). The combined organic extracts were dried over $MgSO_4$, filtered and concentrated under vacuum. The crude title compound was used for the next reaction, without further purification (unstable).

N^1-Methyl-3,6-di(furan-2-yl)benzene-1,2-diamine **50**

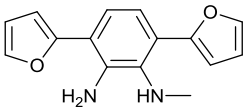

Compound **49** (4.48 g, 18.7 mmol) and K_2CO_3 (3.86 g, 28.0 mmol) were dissolved in dry Et_2O (150 mL). After cooling to 0 °C, methyl triflate (2.11 mL, 18.7 mmol) was added drop-wise. The mixture was stirred at 0 °C, under N_2, and was monitored by TLC. After 24 hours, the mixture was poured into water (200 mL), and extracted with Et_2O (3 × 100 mL). The combined organic extracts were dried over $MgSO_4$, filtered and concentrated under vacuum. The crude compound was used for the next reaction, without further purification (unstable).

6,9-Di(furan-2-yl)-10-methylbenzo[*g*]pteridine-2,4(3*H*,10*H*)-dione **52**

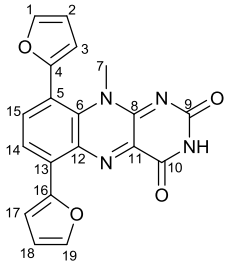

Compound **50** (4.75 g, 18.7 mmol), alloxan monohydrate **51** (2.65 g, 18.7 mmol) and B_2O_3 (2.61 g, 37.3 mmol) were dissolved in glacial AcOH (150 mL). The mixture was stirred at room temperature under N_2 and was monitored by TLC. After 24 hours, the mixture was poured into water (100 mL). The precipitate was filtered and washed with MeOH and the crude compound was purified by recrystallization from DMF, affording the title compound as a brownish red solid (3.07 g, 45% over three steps); mp > 300 °C; δ_H (400 MHz, DMSO-d_6, TMS) 11.52 (s, 1H, NH), 8.01 (d, *J* 8.1, 1H, C(14)H), 7.97 (d, *J* 1.8, 1H, C(19)H), 7.96-7.93 (m, 2H, C(15, 17)H), 7.91 (d, *J* 1.8, 1H, C(1)H), 6.84 (d, *J* 1.8, 1H, C(3)H), 6.81 (dd, *J* 3.5, 1.8, 1H, C(18)H), 6.74 (dd, *J* 3.5, 1.8, 1H, C(2)H), 3.38 (s, 2H, C(7)H); δ_C (100 MHz, DMSO-d_6, TMS) 159.8, 155.7 C(9, 10), 152.6, 150.5, 148.7 C(4, 8, 11), 144.6 C(19), 143.9 C(1), 138.0 C(15), 137.7 C(16), 133.3, 131.2, 130.9 C(6, 12, 13), 120.6 C(14), 118.4 C(5), 116.6 C(17), 113.2 C(18), 112.5 C(2), 110.0 C(3), 37.2 C(7); HRMS (ESI^+, *m/z*): $[M+Na]^+$ found 383.0740; calc. for ($C_{19}H_{12}N_4NaO_4^+$) 383.0751.

N^1-Ethyl-3,6-di(furan-2-yl)benzene-1,2-diamine **53**

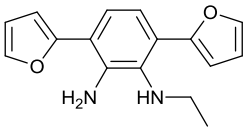

Compound **49** (0.895 g, 3.73 mmol) and K_2CO_3 (0.770 g, 5.60 mmol) were dissolved in dry Et_2O (450 mL). After cooling to 0 °C, a solution of ethyl triflate (480 µL, 3.73 mmol) in dry Et_2O (50 mL) was added drop-wise. The mixture was stirred at 0 °C under N_2 and was monitored by TLC. After 6 hours, the mixture was poured into water (500 mL) and extracted. The water layer was extracted with Et_2O (2 × 200 mL) and the combined organic extracts were dried over $MgSO_4$, filtered and concentrated under vacuum. The crude compound was used for the next reaction, without further purification (unstable).

10-Ethyl-6,9-di(furan-2-yl)benzo[*g*]pteridine-2,4(3*H*,10*H*)-dione **54**

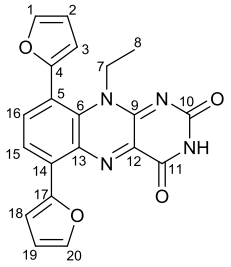

Compound **53** (1.00 g, 3.73 mmol), compound **51** (0.530 g, 3.73 mmol) and B_2O_3 (0.520 g, 7.46 mmol) were dissolved in glacial AcOH (50 mL). The mixture was stirred at room temperature under N_2 and was monitored by TLC. After 24 hours, the mixture was poured into water (100 mL) and extracted with DCM (3 × 100 mL). The combined organic extracts were dried over $MgSO_4$, filtered and concentrated under vacuum. The crude compound was further washed with PE (50 mL) and filtered. Finally, it was purified by column chromatography (SiO_2; DCM:EtOAc; 9:1), affording the title compound as a brownish red solid (0.460 g, 33% over three steps); mp > 300 °C; δ_H (400 MHz, DMSO-d_6, TMS) 11.50 (s, 1H, N<u>H</u>), 8.01 (d, *J* 8.1, 1H, C(15 or 16)<u>H</u>), 7.99 – 7.96 (m, 2H, C(18, 20)<u>H</u>), 7.90 (d, *J* 1.9, 1H, C(1)<u>H</u>), 7.87 (d, *J* 8.1, 1H, C(15 or 16)<u>H</u>), 6.86 (d, *J* 3.4, 1H, C(3)<u>H</u>), 6.81 (b, 1H, C(19)<u>H</u>), 6.74 (b, 1H, C(2)<u>H</u>), 4.06 (b, 2H, C(7)<u>H</u>), 0.98 (t, *J* 7.0, 3H, C(8)<u>H</u>); δ_C (100 MHz, DMSO-d_6, TMS) 159.9, 155.8 <u>C</u>(10, 11), 151.8, 150.4, 148.8 <u>C</u>(4, 9, 12), 144.6 <u>C</u>(20), 143.8 <u>C</u>(1), 139.4 <u>C</u>(16), 137.9 <u>C</u>(17), 132.2, 131.9, 131.5 <u>C</u>(6, 13, 14), 120.6 <u>C</u>(15), 118.0 <u>C</u>(5), 116.9 <u>C</u>(18), 113.3 <u>C</u>(19), 112.3 <u>C</u>(2), 110.1 <u>C</u>(3), 41.7 <u>C</u>(7), 13.2 <u>C</u>(8); HRMS (EI$^-$, *m/z*): $[M\text{-}H]^-$ found 373.0952; calc. for ($C_{20}H_{13}N_4O_4^-$) 373.0942.

10-Ethyl-3-(2-ethylhexyl)-6,9-di(furan-2-yl)benzo[*g*]pteridine-2,4(3*H*,10*H*)-dione **38**

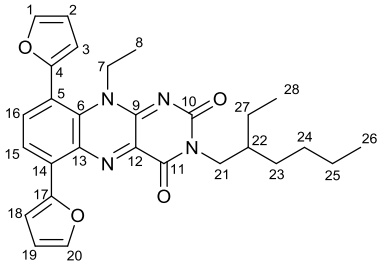

Compound **54** (0.500 g, 1.34 mmol), K_2CO_3 (0.370 g, 2.68 mmol) and 18-crown-6 (71.0 mg, 0.27 mmol) were dissolved in dry DMF (50 mL). The mixture was degassed for 30 minutes with N_2, then 2-ethyl-hexylbromide (470 μL, 2.68 mmol) was added. The solution was stirred at 50 °C, under N_2, and was monitored by TLC. After 7 days, the mixture was allowed to cool to room temperature, and poured into an aqueous solution of 5% HCl (100 mL). The precipitate was collected by filtration and washed with water (100 mL) and cold MeOH (50 mL). The crude product was purified by column chromatography (SiO_2, DCM), affording the title compound as an orange solid (0.350 g, 54%); mp 183 – 184 °C; δ_H (400 MHz, $CDCl_3$, TMS) 8.09 (d, *J* 3.1, 1H, C(18)H), 8.01 (d, *J* 8.1, 1H, C(15)H), 7.74 (d, *J* 8.1, 1H, C(16)H), 7.60 – 7.54 (m, 2H, C(1, 20)H), 6.66 (dd, *J* 3.5, 1.8, 1H, C(19)H), 6.61 – 6.57 (m, 2H, C(2, 3)H), 4.27 (b, 2H, C(7)H), 4.08 – 3.98 (m, 2H, C(21)H), 2.02 – 1.93 (m, 1H, C(22)H), 1.46 – 1.16 (m, 10H, C(23, 24, 25, 27)H), 1.07 (t, *J* 7.0, 3H, C(8)H), 0.96 – 0.86 (m, 6H, C(26, 28)H); δ_C (100 MHz, $CDCl_3$, TMS) 159.9, 156.3 C(10, 11), 150.8, 150.1, 149.0 C(4, 9, 12), 143.9 C(1), 143.3 C(20), 140.4 C(16), 135.6, 133.9, 132.8, 132.5 C(6, 13, 14, 17), 121.5 C(15), 118.4 C(18), 118.0 C(5), 113.8 C(19), 112.2, 110.1 C(2, 3), 46.0 C(21), 42.4 C(7), 37.7, 30.7, 28.8, 24.0, 23.2 C(22, 23, 24, 25, 27), 14.2 C(28), 13.9 C(8), 10.7 C(26); HRMS (ESI^+, *m/z*): $[M+Na]^+$ found 509.2148; calc. for ($C_{28}H_{30}N_4NaO_4^+$) 509.2159.

6,9-*bis*(5-Bromofuran-2-yl)-10-ethyl-3-(2-ethylhexyl)benzo[*g*]pteridine-2,4(*3H,10H*)-dione **55**

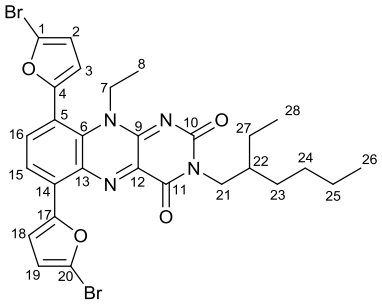

Compound **38** (0.240 g, 0.49 mmol) was dissolved in dry DCM (40 mL) and the solution was stirred at 0 °C. NBS (0.176 g, 1.00 mmol) was added portion-wise over 30 minutes in the dark. The mixture was allowed to warm to room temperature and stirred in the dark for 6 hours, then it was poured into an aqueous solution of 5% $Na_2S_2O_3$ (150 mL) and stirred for further 1 hour. The organic fraction was extracted with DCM (100 mL), washed with water (3 × 150 mL), dried over $MgSO_4$, filtered and concentrated under vacuum. The crude product was purified by column chromatography (SiO_2, DCM) affording the title compound as an orange solid (0.260 g, 83%); mp 251 – 252 ºC; δ_H (400 MHz, $CDCl_3$, TMS) 8.07 (d, *J* 3.6, 1H, C(18)H), 7.98 (d, *J* 8.1, 1H, C(15)H), 7.73 (d, *J* 8.1, 1H, C(16)H), 6.59 (d, *J* 3.3, 1H, C(3)H), 6.57 (d, *J* 3.6, 1H, C(19)H), 6.52 (d, *J* 3.3 Hz, 1H, C(2)H), 4.36 (b, 2H, C(7)H), 4.09 – 3.98 (m, 2H, C(21)H), 2.02 – 1.92 (m, 1H, C(22)H), 1.41 – 1.27 (m, 8H, C(23, 24, 25, 27)H), 1.15 (t, *J* 7.0, 3H, C(8)H), 0.95 – 0.85 (m, 6H, C(26, 28)H); δ_C (100 MHz, $CDCl_3$, TMS) 159.8, 156.1 C(10, 11), 152.7, 151.2, 150.2 C(4, 9, 12), 140.4 C(16), 135.9, 133.2, 132.6, 132.4 C(6, 13, 14, 17), 125.1, 123.4 C(1, 20), 121.2 C(15), 121.2 C(18), 117.1 C(5), 115.8 C(19), 113.8 C(2), 112.6 C(3), 46.1 C(21), 42.7 C(7), 37.8 C(22), 30.8, 28.8, 24.1, 23.2 C(23, 24, 25, 27), 14.2 C(26 or 28), 13.8 C(8), 10.7 C(26 or 28); HRMS (ESI^+, *m/z*): $[M+H]^+$ found 645.0530; calc. for ($C_{28}H_{29}N_4O_4Br_2^+$) 645.0530.

Poly[(9,9-di-*n*-octylfluorenyl-2,7-diyl)-*alt*-5-(6,9-*bis*(furan-2-yl)-10-ethyl-3-(2-ethylhexyl)benzo[*g*]pteridine-2,4(*3H,10H*)-dione)] **57**

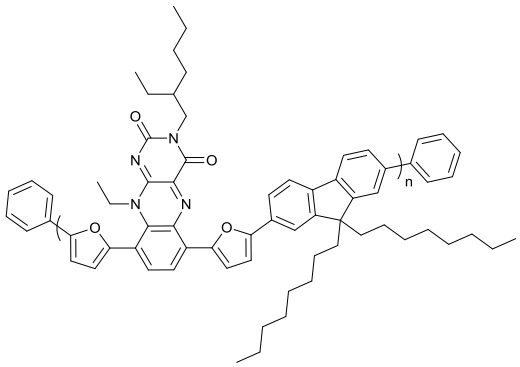

Compound **55** (0.155 g, 0.240 mmol), 9,9-dioctylfluorene-2,7-diboronic acid *bis*(1,3-propanediol) ester **56** (0.138 g, 0.240 mmol) and $Pd(PPh_3)_4$ (8.0 mg, 7.0 μmol) were placed in a flask. The system was evacuated and refilled with N_2 3 times, then degassed toluene (15 mL) was added. A degassed aqueous solution of 2 M Na_2CO_3 (2.50 mL, 4.97 mmol) was added and the resulting mixture was stirred at reflux, under N_2, and was monitored by GPC. After 4 days bromobenzene (25.0 μL, 0.240 mmol) was added, followed by phenylboronic acid (30.0 mg, 0.240 mmol) 4 hours later. After further 12 hours the mixture was allowed to cool to room temperature and poured into water (100 mL). The mixture was extracted with toluene (3 × 100 mL) and concentrated under vacuum. The crude polymer was purified by Soxhlet extraction, using hexane, MeOH, and $CHCl_3$, consecutively, affording the title polymer as a black solid (0.122 g, 58%) of M_n = 9.00 kDa and M_w = 13.5 (PDI = 1.5).

1,2-*bis*(Octyloxy)benzene[167] **59**

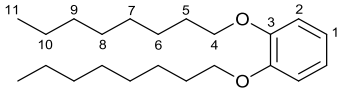

Pyrocatechol **58** (10.0 g, 90.8 mmol) and NaOH (7.99 g, 0.200 mol) were dissolved in acetone (150 mL). 1-Bromooctane (34.8 mL, 0.200 mol) was slowly added. The mixture was stirred at reflux and monitored by TLC. After 24 hours, the solution was allowed to cool to room temperature, poured into an aqueous solution of saturated NH_4Cl (200 mL), and extracted with DCM (3 × 150 mL). The combined organic extracts were dried over $MgSO_4$, filtered and concentrated under vacuum. The crude compound was purified by distillation, affording the title compound as a colourless oil (30.3 g, 99%); δ_H (400 MHz, $CDCl_3$, TMS) 6.88 (s, 4H, C(1)H and C(2)H), 3.98 (t, 4H, *J* 6.5, C(4)H), 1.89-1.26 (m, 24H, C(5, 6, 7, 8, 9, 10)H), 0.90 (t, *J* 6.6, 6H, C(11)H); δ_C (100 MHz, $CDCl_3$, TMS) 149.3 C(3), 121.0 C(1), 114.2 C(2), 69.3 C(4), 31.9, 29.7, 29.5, 29.4, 26.1, 22.7 C(5, 6, 7, 8, 9, 10), 14.1 C(11). MS (EI^+, *m/z*): $[M]^+$ found 334.3.

1,2-Dinitro-4,5-*bis*(octyloxy)benzene[167] **60**

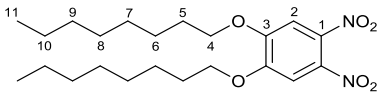

Compound **59** (10.0 g, 29.9 mmol) was dissolved in a mixture of AcOH (100 mL) and DCM (100 mL). The mixture was cooled to 0 °C, then HNO_3 (70%, 25 mL) was added drop-wise. The mixture was then allowed to warm to room temperature. After 1 hour, the mixture was cooled again to 0 °C and fuming HNO_3 (50 mL) was added drop-wise. The resulting mixture was allowed to warm to room temperature, and stirred for further 2 days. Afterwards, the mixture was poured into iced-water (500 mL). The yellow precipitate was filtered and washed with an aqueous solution of saturated $NaHCO_3$ (300 mL) and water (300 mL) respectively. The raw solid was purified by recrystallization from MeOH, affording the title compound, as a yellow solid (11.5 g, 90%); mp 87 – 88 °C [lit. 87 – 87.5 °C]; δ_H (400 MHz, $CDCl_3$, TMS) 7.30 (s, 2H, C(2)H), 4.12 (t, 4H, *J* 6.5, C(4)H), 1.95-1.82 (m, 4H, C(5)H), 1.57-1.18 (m, 20H, C(6, 7, 8, 9, 10)H), 0.89 (t, *J* 6.6, 6H, C(11)H); δ_C (100 MHz, $CDCl_3$, TMS) 151.8 C(3), 136.5 C(1), 107.9 C(2), 70.2 C(4), 31.9 C(5), 29.7, 29.5, 29.1, 25.9, 22.7 C(6, 7, 8, 9, 10), 14.1 C(11); MS (ESI^+, *m/z*): $[M+H]^+$ found 425.3.

4,5-*bis*(Octyloxy)benzene-1,2-diamine dihydrochloride[167] **61**

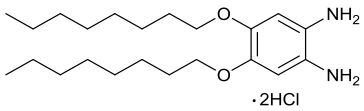

Compound **60** (1.50 g, 3.54 mmol) and $SnCl_2$ (10.8 g, 56.6 mmol) were dissolved in a mixture of HCl (37%, 30 mL) and EtOH (70 mL). The mixture was stirred at reflux under N_2 and was monitored by TLC. After 12 hours, the mixture was cooled to 0°C and the white precipitate was filtered off under vacuum and washed with water (50 mL). It was then suspended in MeOH (50 mL) and filtered after and finally dried under vacuum. The crude product was used for the next reaction, without further purification (unstable).

5,6-*bis*(Octyloxy)benzo[*c*][1,2,5]thiadiazole[167] **62**

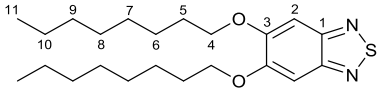

Compound **61** (1.54 g, 3.54 mmol) was dissolved in dry DCM (100 mL). Et_3N (4.90 mL, 47.0 mmol) was added and the solution was stirred for 5 minutes. Then $SOCl_2$ (0.680 mL, 9.40 mmol), diluted in dry DCM (25 mL), was added drop-wise. The mixture was stirred at reflux, for 18 hours. Afterwards, the mixture was allowed to cool to room temperature, poured into an aqueous solution of 5% HCl (200 mL) and extracted with DCM (3 × 100 mL). The combined organic extracts were dried over $MgSO_4$, filtered and concentrated under vacuum. The crude compound was purified by recrystallization from MeOH, affording the title compound as a white solid (1.00 g, 72% over 2 steps); mp 94 – 95 °C [lit. 97.1 – 97.5 °C]; δ_H (400 MHz, $CDCl_3$, TMS) 7.14 (s, 2H, C(2)H), 4.10 (t, 4H, *J* 6.5, C(4)H), 2.04 – 1.78 (m, 4H, C(5)H), 1.58 – 1.15 (m, 20H, C(6, 7, 8, 9, 10)H), 0.90 (t, *J* 6.6, 6H, C(11)H); δ_C (100 MHz, $CDCl_3$, TMS) 154.2 C(1), 151.4 C(3), 98.4 C(2), 69.1 C(4), 31.9 C(5), 29.7, 29.4, 28.9, 26.0, 22.7 C(6, 7, 8, 9, 10), 14.1 C(11). MS (EI^+, *m/z*): $[M]^+$ found 392.2.

4,7-Dibromo-5,6-*bis*(octyloxy)benzo[*c*][1,2,5]thiadiazole[169] **63**

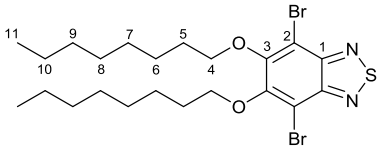

Compound **62** (0.500 g, 1.27 mmol) was dissolved in a mixture of AcOH (15 mL) and DCM (40 mL). Br_2 (0.196 mL, 3.81 mmol), diluted in AcOH (15 mL), was added drop-wise, and the mixture was stirred at room temperature for 2 days. Afterwards, the mixture was poured into an aqueous solution of saturated $Na_2S_2O_3$ (200 mL) and stirred for further 1 hour. The mixture was then extracted with DCM (3 × 100 mL), dried over $MgSO_4$, filtered and concentrated under vacuum. The crude product was purified by recrystallization from MeOH, affording the title compound as a yellowish white solid (0.500 g, 71%); mp 44 – 45 °C [lit. 44.5 – 44.6 °C]; δ_H (400 MHz, $CDCl_3$, TMS) 4.16 (t, 4H, *J* 6.5, C(4)H), 1.96-1.82 (m, 4H, C(5)H), 1.62-1.20 (m, 20H, C(6, 7, 8, 9, 10)H), 0.89 (t, *J* 6.6, 6H, C(11)H); δ_C (100 MHz, $CDCl_3$, TMS) 154.5 C(1), 150.4 C(3), 106.2 C(2), 75.1 C(4), 31.9 C(5), 29.7, 29.4, 29.3, 26.0, 22.7 C(6, 7, 8, 9, 10), 14.1 C(11). MS (EI^+, *m/z*): $[M]^+$ found 550.0.

4,7-Di(furan-2-yl)-5,6-*bis*(octyloxy)benzo[*c*][1,2,5]thiadiazole[170] **64**

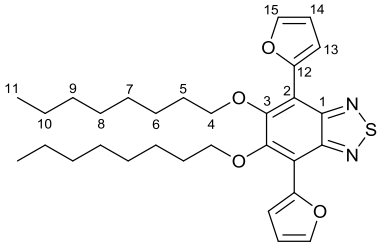

Compounds **63** (0.300 g, 0.540 mmol) and tributyl-furan-2-yl-stannane **47** (0.430 mL, 1.35 mmol) were dissolved in dry toluene (20 mL). The solution was degassed for 30 minutes with N_2, then, $PdCl_2(PPh_3)_2$ (15.0 mg, 21.3 μmol) was added and the mixture was stirred at reflux under N_2 and was monitored by TLC. After 24 hours, the mixture was allowed to cool to room temperature, poured into an aqueous solution of 1M KF (150 mL) and stirred for 1 hour. The organic layer was extracted with EtOAc (3 × 100 mL) and the combined organic extracts were dried over $MgSO_4$, filtered and concentrated under vacuum. The crude compound was purified by column chromatography (SiO_2, PE:DCM; 3:1), affording the title compound as an orange waxy solid (0.286 g, 95%); δ_H (400 MHz, $CDCl_3$, TMS) 7.69 (dd, *J* 1.8, 0.8, 2H, C(15)H), 7.42 (dd, *J* 3.4, 0.8, 2H, C(13)H), 6.65 (dd, *J* 3.4, 1.8, 2H, C(14)H), 4.10 (t, 4H, C(4)H), 1.84 (quint, *J* 6.8, 4H, C(5)H), 1.40 – 1.25 (m, 20H, C(6, 7, 8, 9, 10)H), 0.92 (t, *J* 6.8, 6H, C(11)H); δ_C (100 MHz, $CDCl_3$, TMS) 152.6 C(1), 149.6, 149.5 C(3, 12), 143.2 C(15), 122.9 C(2), 113.6 C(13), 113.4 C(14), 75.2 C(4), 31.8 C(5), 30.3, 29.6, 29.3, 26.1, 22.7 C(6, 7, 8, 9, 10), 14.1 C(11); MS (EI^+, *m/z*): $[M]^+$ found 524.3.

3,6-Di(furan-2-yl)-4,5-*bis*(octyloxy)benzene-1,2-diamine **65**

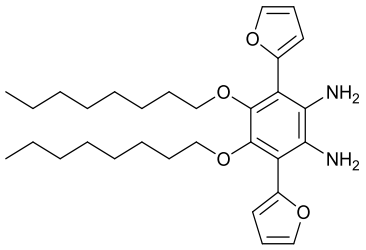

Compound **64** (1.00 g, 1.91 mmol) and $CoCl_2$ (90.0 mg, 0.380 mmol) were dissolved in EtOH (150 mL). $NaBH_4$ (0.217 g, 5.73 mmol) was slowly added, then the mixture was stirred at reflux 2 hours. The white mixture was allowed to cool to room temperature, filtered through celite and the residue washed with Et_2O. The filtrate was poured into water (300 mL) and extracted with Et_2O (3 × 300 mL). The combined organic extracts were dried over $MgSO_4$, filtered and concentrated under vacuum. The crude compound was used for the next reaction, without further purification (unstable).

N^1-Ethyl-3,6-di(furan-2-yl)-4,5-*bis*(octyloxy)benzene-1,2-diamine **66**

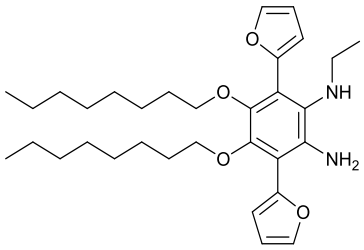

Compound **65** (0.950 g, 1.91 mmol) and K_2CO_3 (0.397 g, 2.87 mmol) were dissolved in dry Et_2O (100 mL). The mixture was cooled to 0 °C, then ethyl triflate (0.25 mL, 1.91 mmol) was added drop-wise. The mixture was allowed to warm to room temperature and stirred under N_2. After 24 hours, the mixture was poured into water (200 mL), and extracted with Et_2O (3 × 100 mL), dried over $MgSO_4$, filtered and concentrated under vacuum. The crude compound was used for the next reaction, without further purification (unstable).

10-ethyl-6,9-di(furan-2-yl)-7,8-*bis*(octyloxy)benzo[*g*]pteridine-2,4(3*H*,10*H*)-dione

39

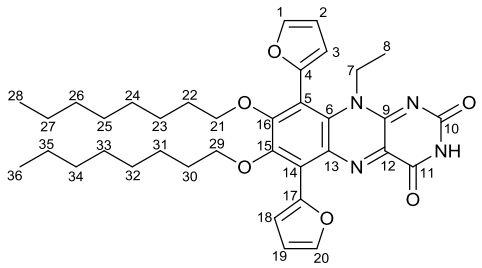

Compound **66** (0.975 g, 1.91 mmol), compound **51** (0.271 g, 1.91 mmol) and B_2O_3 (0.267 g, 3.82 mmol) were dissolved in glacial AcOH (50 mL). The mixture was stirred at room temperature under N_2 and was monitored by TLC. After 24 hours, the mixture was poured into water (100 mL) and extracted with DCM (3 × 100 mL). The combined organic extracts were dried over $MgSO_4$, filtered and concentrated under vacuum. The crude product was purified by column chromatography (SiO_2, DCM:EtOAc; 9:1), affording the title compound as an orange waxy solid (60.0 mg, 5% over three steps); δ_H (500 MHz, $CDCl_3$, TMS) 8.60 (s, 1H, N<u>H</u>), 7.70 (d, *J* 1.0, 1H, C(20)<u>H</u>), 7.63 (d, *J* 1.0, 1H, C(1)<u>H</u>), 7.29 (d, *J* 3.3, 1H, C(18)<u>H</u>), 6.68 (dd, *J* 3.4, 1.7, 1H, C(19)<u>H</u>), 6.62 – 6.58 (m, 2H, C(2, 3)<u>H</u>), 4.25 – 4.01 (m, 4H, C(7, 21 or 29)<u>H</u>), 3.86 (t, *J* 6.6, 2H, C(21 or 29)<u>H</u>), 1.71 – 1.66 (m, 2H, C(22 or 30)<u>H</u>), 1.55 – 1.51 (m, 2H, C(22 or 30)<u>H</u>), 1.35 – 1.15 (m, 20H, C(23, 24, 25, 26, 27, 31, 32, 32, 33, 34, 35)<u>H</u>), 1.10 (t, *J* 6.9, 3H, C(8)<u>H</u>), 0.90 – 0.86 (m, 6H, C(28, 36)<u>H</u>); δ_C (125 MHz, $CDCl_3$, TMS) 161.7, 159.4, 155.7 <u>C</u>(10, 11, 16), 151.4, 148.8, 145.7, 144.7 <u>C</u>(4, 9, 12, 15), 144.2 <u>C</u>(20), 143.3 <u>C</u>(1), 134.4, 131.9, 131.8, 128.5 <u>C</u>(6, 13, 14, 17), 118.2 <u>C</u>(18), 113.5 <u>C</u>(5), 112.9 <u>C</u>(2 or 3), 112.4 <u>C</u>(19), 112.0 <u>C</u>(2 or 3), 75.9, 74.8 <u>C</u>(21, 29), 43.3 <u>C</u>(7), 31.9, 31.9, 30.5, 30.3, 30.2, 29.8, 29.5, 29.4, 29.4, 29.3, 26.1, 25.8 <u>C</u>(22, 23, 24, 25, 26, 27, 30, 31, 32, 32, 33, 34, 35), 22.8 <u>C</u>(8), 14.2, 13.8 <u>C</u>(28, 36); HRMS (EI$^-$, *m/z*): $[M-H]^-$ found 630.3336; calc. for ($C_{35}H_{43}N_4O_6^-$) 630.3345.

2-Nitro-4,6-di(thiophen-2-yl)aniline **69**

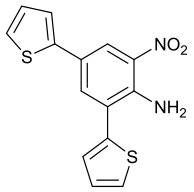

2,4-Dibromo-6-nitroaniline **67** (0.500 g, 1.69 mmol) and tributyl-thiophen-2-yl-stannane **68** (1.07 mL, 3.38 mmol) were dissolved in dry toluene (20 mL). The mixture was degassed for 30 minutes with N_2, then $PdCl_2(PPh_3)_2$ (59.3 mg, 0.084 mmol) was added. The resulting mixture was stirred at reflux under N_2 and was monitored by TLC. After 12 hours, the mixture was allowed to cool to room temperature and poured into an aqueous solution of 1M KF (100 mL). The slurry was stirred for further 1 hour, extracted with EtOAc (80 mL) and washed with brine (150 mL) and water (150 mL), respectively. The organic fraction was dried over $MgSO_4$, filtered and concentrated under vacuum. The crude compound was used for the next reaction, without further purification (unstable).

tert-Butyl (2-nitro-4,6-di(thiophen-2-yl)phenyl)carbamate **70**

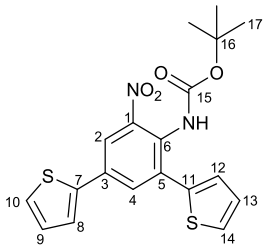

Compound **69** (0.511 g, 1.69 mmol), was dissolved in dry THF (20 mL). Di-*tert*-butyl dicarbonate (1.11 g, 5.07 mmol) and DMAP (20.7 mg, 0.169 mmol) were added. The resulting mixture was stirred at reflux under Ar and was monitored by TLC. After 12 hours, the mixture was allowed to cool to room temperature, poured into an aqueous solution of 0.5 M HCl (100 mL) and extracted with EtOAc (3 × 100 mL). The combined organic extracts were dried over $MgSO_4$, filtered and concentrated under vacuum. The crude compound was suspended in MeOH (50 mL) and K_2CO_3 (700 mg, 5.07 mmol) was added. The mixture was stirred at reflux for 3 hours, then it was allowed to cool to room temperature, poured into water (100 mL) and extracted with DCM (3 × 100 mL). The combined organic extracts were dried over $MgSO_4$, filtered and concentrated under vacuum. The crude product was purified by column chromatography (SiO_2, PE:DCM; gradient from 9:1 to 1:1), affording the title compound as a pale yellow solid (0.463 g, 68% over 2 steps); mp 135 – 136 ºC; δ_H (500 MHz, $CDCl_3$, TMS) 8.10 (d, *J* 2.1, 1H, C(2)H), 7.90 (d, *J* 2.1, 1H, C(4)H), 7.45 (dd, *J* 5.1, 1.1, 1H, C(10)H), 7.45 – 7.00 (b, 1H, C(6)NH) 7.40 – 7.35 (m, 2H, C(12, 14)H), 7.32 (d, *J* 2.9 Hz, 1H, C(8)H), 7.16 – 7.10 (m, 2H, C(9, 13)H), 1.36 (s, 9H, C(17)H); δ_C (125 MHz, $CDCl_3$, TMS) 152.2 C(15), 141.0, 138.7 C(7, 11), 132.1 C(4), 128.6 C(9 or 13), 127.8 C(3), 127.7 C(9 or 13), 127.4 C(8), 127.2 C(10), 127.2 C(5), 126.7, 125.0 C(12, 14), 121.3 C(2), 77.7 C(16), 28.1 C(17); HRMS (EI^+, *m/z*): $[M]^+$ found, 402.0713; calc. for ($C_{19}H_{18}N_2O_3S_2^+$), 402.0708.

tert-Butyl (2-amino-4,6-di(thiophen-2-yl)phenyl)carbamate **71**

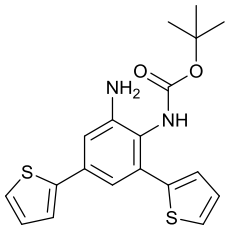

Compound **70** (0.300 g, 0.746 mmol) was dissolved in MeOH (50 mL). Ammonium formate (0.235 g, 3.73 mmol) was added, followed by 10% Pd/C (78.3 mg, 74.6 μmol) portion-wise. The mixture was stirred at reflux under Ar. After 6 hours it was allowed to cool to room temperature and filtered through celite. The filtrate was diluted with DCM (100 mL) and washed with water (3 × 100 mL). The organic layer was dried over $MgSO_4$, filtered and concentrated under vacuum. The crude compound was used for the next reaction, without further purification (unstable).

tert-Butyl (2-isobutyramido-4,6-di(thiophen-2-yl)phenyl)carbamate **72**

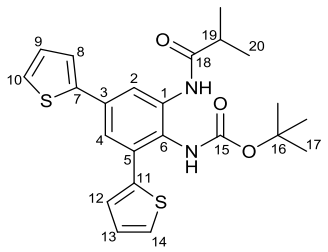

Compound **71** (0.280 g, 0.752 mmol) was dissolved in dry DCM (20 mL). Et_3N (0.115 mL, 0.827 mmol) was added and the resulting solution was stirred at 0 ºC. A solution of isobutyroyl chloride (86.6 μL, 0.827 mmol) in dry DCM (15 mL) was added drop-wise and the resulting mixture was allowed to warm to room temperature under Ar. After 8 hours, it was poured into an aqueous solution of saturated NH_4Cl (200 mL) and extracted with DCM (3 × 150 mL). The combined organic extracts were dried over $MgSO_4$, filtered and concentrated under vacuum. The crude product was purified by reprecipitation from hexane, affording the title compound as a pink solid (0.226 g, 68%); mp 95 – 96 ºC; δ_H (500 MHz, $CDCl_3$, TMS) 8.52 (bs, 1H, C(1)N<u>H</u>), 8.15 (bs, 1H, C(4)<u>H</u>), 7.50 (d, *J* 2.1, 1H, C(2)<u>H</u>), 7.44 (dd, *J* 5.0, 1.2, 1H, C(14)<u>H</u>), 7.35 (dd, *J* 3.6, 0.9, 1H, C(8)<u>H</u>), 7.29 (dd, *J* 5.1, 1.0, 1H, C(10)<u>H</u>), 7.17 (dd, *J* 3.6, 1.0, 1H, C(12)<u>H</u>), 7.15 (dd, *J* 5.0, 3.6, 1H, C(13)<u>H</u>), 7.07 (dd, *J* 5.1, 3.6, 1H, C(9)<u>H</u>), 6.24 (bs, 1H, C(6)N<u>H</u>), 2.60 – 2.54 (m, 1H, C(19)<u>H</u>), 1.52 (s, 9H, C(17)<u>H</u>), 1.29 (d, *J* 6.9, 6H, C(20)<u>H</u>); δ_C (125 MHz, $CDCl_3$, TMS) 175.7 <u>C</u>(18), 154.9 <u>C</u>(15), 143.1, 139.5 <u>C</u>(7, 11), 130.2 <u>C</u>(6), 128.2 <u>C</u>(3), 127.7 <u>C</u>(13), 127.3 <u>C</u>(12), 127.2 <u>C</u>(4), 127.0 <u>C</u>(14), 126.9 <u>C</u>(1), 125.5 <u>C</u>(10), 124.4 <u>C</u>(2), 124.2 <u>C</u>(8), 122.6 <u>C</u>(5), 81.8 <u>C</u>(16), 36.8 <u>C</u>(19), 28.4 <u>C</u>(17), 19.7 <u>C</u>(20); HRMS (EI^+, *m/z*): $[M]^+$ found, 442.1383 calc. for ($C_{23}H_{26}N_2O_3S_2^+$), 442.1385.

N,*N*'-(1,4-Phenylene)dipropionamide[259] **75**

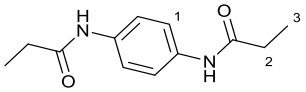

Benzene-1,4-diamine **74** (2.00 g, 18.5 mmol) and pyridine (3.28 mL, 40.7 mmol) were dissolved in THF (50 mL). Acetic anhydride (14.2 mL, 0.111 mol) was slowly added. The mixture was stirred at reflux and was monitored by TLC. After 20 hours the solvent was removed under vacuum and the residue was washed with water. The crude material was filtered and purified by recrystallisation from $CHCl_3$, affording the title compound as a white solid (4.00 g, 100%); mp 143 – 144 °C [lit.[260] 139 – 140 °C]; δ_H (400 MHz, DMSO-d_6, TMS) 9.75 (s, 2H, N<u>H</u>), 7.48 (s, 4H, C(1)<u>H</u>), 2.28 (q, *J* 7.6, 4H, C(2)<u>H</u>), 1.07 (t, *J* 7.6, 6H, C(3)<u>H</u>); MS (ESI$^-$, *m/z*): $[M-H]^-$ found 219.1.

N^1,N^4-Dipropylbenzene-1,4-diamine **76**

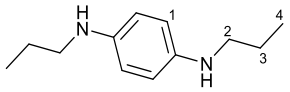

$LiAlH_4$ (4.23 g, 0.111 mol) was dissolved in dry THF (100 mL) and was added *via* canula to a solution of compound **75** (4.00 g, 18.6 mmol) in dry THF (200 mL). The resulting mixture was stirred at reflux under N_2 and was monitored by TLC. After 8 hours, the mixture was allowed to cool to room temperature, and was slowly poured into ice-water (300 mL). The resulting suspension was stirred for further 1 hour, and filtered. The filtrate was extracted with EtOAc (3 × 200 mL). The combined organic extracts were dried over $MgSO_4$, filtered and concentrated under vacuum, affording the pure title compound as brown oil (3.57 g, 100%); δ_H (400 MHz, $CDCl_3$, TMS) 6.55 (b, 4H, C(1)H), 3.02 (b, 4H, C(2)H), 1.66 – 1.56 (m, 4H, C(3)H), 0.98 (t, *J* 7.4, 6H, C(4)H); MS (EI^+, *m/z*): $[M]^+$ found 192.2.[261]

6-Chlorouracil[178] **77**

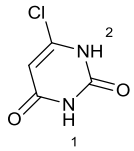

2,4,6-Trichloropyrimidine (5.00 g, 27.3 mmol) was suspended in an aqueous solution of 2.5 M NaOH (40.0 mL, 0.100 mol). The mixture was stirred at reflux for 2 hours, then it was cooled to 0 °C. An aqueous solution of 37% HCl was slowly added, while stirring, until pH = 2 was reached, then the resulting precipitate was filtered and purified by recrystallisation from water, affording the title compound as a white solid (3.30 g, 83%); mp > 300 °C [lit. 300 °C (decomp.)]; δ_H (400 MHz, DMSO-d_6, TMS) 12.04 (b, 1H, N(1)H), 11.29 (b, 1H, N(2)H), 5.75 (s, 1H, CH); MS (ESI^-, *m/z*): $[M-H]^-$ found 145.0.

N^1,N^3-Diisobutyl-4,6-dinitrobenzene-1,3-diamine **73**

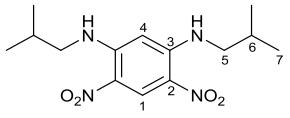

1,5-Difluoro-2,4-dinitrobenzene **72** (2.00 g, 9.80 mmol) and K_2CO_3 (2.97 g, 21.6 mmol) were dissolved in EtOH (100 mL). Isopropylamine (2.14 mL, 21.6 mmol) was added drop-wise, then the mixture was stirred at reflux and was monitored by TLC. After 12 hours, the mixture was allowed to cool to room temperature, poured into water (200 mL) and extracted with DCM (3 × 200 mL). The combined organic extracts were dried over $MgSO_4$, filtered and concentrated under vacuum. The title compound was obtained, as a cream solid, without further purification (2.80 g, 100%); mp 132 – 133 °C; δ_H (400 MHz, $CDCl_3$, TMS) 9.26 (s, 1H, C(1)H), 8.44 (b, 2H, NH), 5.63 (s, 1H, C(4)H), 3.12 (dd, *J* 7.0, 5.1 4H, C(5)H), 2.14 – 2.00 (m, 2H, C(6)H), 1.08 (d, *J* 7.0,12H, C(7)H); δ_C (100 MHz, $CDCl_3$, TMS) 148.8 C(2), 129.7 C(3), 124.2 C(1), 90.2 C(4), 52.0 C(5), 27.8 C(6), 20.1 C(7); HRMS (ESI^+, *m/z*): $[M+Na]^+$ found 333.1539; calc. for ($C_{14}H_{22}N_4NaO_4^+$) 333.1533.

4-Bromo-7-ferrocenylbenzo[*c*][1,2,5]thiadiazole[218] **113**

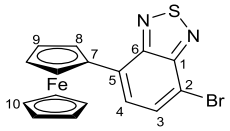

Ferroceneboronic acid **112** (0.500 g, 2.17 mmol) and compound **46** (0.960 g, 3.26 mmol) were dissolved in 1,4-dioxane (15 mL). An aqueous solution of 2M K_2CO_3 (10.9 mL, 21.7 mmol) was added, and the solution was degassed for 30 minutes with N_2. Then Pd(dppf)Cl_2 (0.791 g, 0.110 mmol) was added and the resulting mixture was stirred at reflux under N_2 and was monitored by TLC. After 14 hours, the mixture was allowed to cool to room temperature, poured into water (100 mL) and extracted with DCM (3 × 100 mL). The combined organic extracts were dried over $MgSO_4$, filtered and concentrated under vacuum. The crude product was purified by column chromatography (SiO_2, PE:Toluene; 1:1), affording the title compound as a purple solid (0.393 g, 46%); mp 165-166 °C; δ_H (400 MHz, $CDCl_3$, TMS) 7.73 (d, *J* 7.7, 1 H, C(3)H), 7.55 (d, *J* 7.7, 1 H, C(4)H), 5.24 (t, *J* 1.9, 2 H, C(8)H), 4.51 (t, *J* 1.9, 2 H, C(9)H), 4.03 (s, 5 H, C(10)H); δ_C (100 MHz, $CDCl_3$, TMS) 154.2, 153.1 C(1,6), 134.1 C(5), 132.4 C(3), 125.2 C(4), 110.5 C(2), 80.4 C(7), 70.3 C(9), 70.0 C(10), 68.8 C(8); HRMS (EI^+, *m/z*): $[M]^+$ found, 397.9155; calc. for ($C_{16}H_{11}BrFeN_2S^+$), 397.9170.

4-(7-Ferrocenyl-2,1,3-benzothiadiazol-4-yl)-benzaldehyde[218] **115**

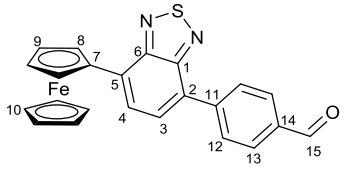

Compound **113** (0.390 g, 0.980 mmol) and 4-formylphenylboronic acid **114** (0.177 g, 1.18 mmol) were dissolved in THF (15 mL). An aqueous solution of 2M K_2CO_3 (4.90 mL, 9.80 mmol) was added, and the mixture was degassed for 30 minutes with N_2. Then $Pd(PPh_3)_4$ (57.0 mg, 49.3 μmol) was added and the resulting mixture was stirred at reflux under N_2 and was monitored by TLC. After 48 hours, the mixture was allowed to cool to room temperature, poured into water (100 mL) and extracted with DCM (3 × 100 mL). The combined organic extracts were dried over $MgSO_4$, filtered and concentrated under vacuum. The crude compound was purified by column chromatography (SiO_2, Toluene), affording the title compound as a purple solid (0.355 g, 84%); mp > 300 °C; δ_H (400 MHz, $CDCl_3$, TMS) 10.11 (s, 1 H, C(15)H), 8.17 (d, *J* 8.2, 2 H, C(12)H), 8.05 (d, *J* 8.2, 2 H, C(13)H), 7.80 (d, *J* 7.5, 1 H, C(3)H), 7.70 (d, *J* 7.5, 1 H, C(4)H), 5.34 (t, *J* 1.9, 2 H, C(8)H), 4.55 (t, *J* 1.9, 2 H, C(9)H), 4.07 (s, 5 H, C(10)H); δ_C (100 MHz, $CDCl_3$, TMS) 192.1 C(15), 154.1, 153.9 C(1, 6), 143.9 C(14), 135.7, 134.8 C(5, 11), 130.1 C(13), 129.7 C(12), 129.5 C(2), 129.1 C(4), 125.0 C(3), 80.8 C(7), 70.3 C(9), 70.1 C(10), 69.0 C(8); HRMS (EI^+, *m/z*): $[M]^+$ found, 424.0331; calc. for ($C_{23}H_{16}FeN_2OS^+$), 424.0333.

2-Cyano-3-(4-(7-ferrocenylbenzo[*c*][1,2,5]thiadiazol-4-yl)phenyl)acrylic acid[218] **104**

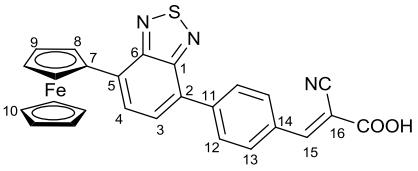

Compound **115** (0.332 mg, 0.780 mmol) and cyanoacetic acid **116** (89.9 mg, 0.940 mmol) were dissolved in dry toluene (50 mL). $MgSO_4$ (40.0 mg, 0.160 mmol), piperidine (7.70 μL, 78.0 μmol) and AcOH (26.7 μL, 0.468 mmol) were added, then the mixture was stirred at 100 °C under N_2 and was monitored by TLC. After 6 hours, the solvent was removed under vacuum and the crude product was purified by column chromatography (SiO_2, DCM:MeOH; 9:1), affording the title compound as a green solid (0.270 g, 71%); mp > 300 °C; δ_H (500 MHz, DMSO-d_6, TMS) 8.18 (d, *J* 8.4, 2 H, C(12)H), 8.05 (d, *J* 8.4, 3 H, C(13, 15)H), 8.01 (d, *J* 7.5, 1 H, C(3)H), 7.90 (d, *J* 7.5, 1 H, C(4)H), 5.41 (t, *J* 1.9, 2 H, C(8)H), 4.57 (t, *J* 1.9, 2 H, C(9)H), 4.06 (s, 5 H, C(10)H). HRMS (ESI$^-$, *m/z*): $[M-H]^-$ found, 490.0315; calc. for ($C_{26}H_{16}FeN_3O_2S^-$), 490.0318; anal. calc. for ($C_{26}H_{17}FeN_3O_2S$): C, 63.56; H, 3.49; N, 8.55; found C, 64.12; H, 3.28; N, 8.83.

4-Bromo-7-(ferrocenyl)ethynylbenzo[*c*][1,2,5]thiadiazole[214] **118**

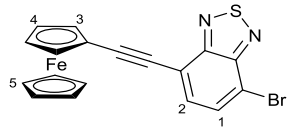

Ethynylferrocene **117** (0.157 g, 0.747 mmol), and compound **46** (0.200 g, 0.680 mmol) were dissolved in a mixture of dry THF (10 mL) and dry Et_3N (10 mL). The mixture was degassed for 30 minutes with N_2, then $Pd(PPh_3)_2Cl_2$ (23.8 mg, 34.0 μmol) and CuI (7.46 mg, 34.0 μmol) were added. The resulting mixture was stirred at 60 °C under N_2, and was monitored by TLC. After 6 hours, the mixture was allowed to cool to room temperature, poured into an aqueous solution of 5% HCl (100 mL) and extracted with DCM (3 × 100 mL). The combined organic extracts were dried over $MgSO_4$, filtered and concentrated under vacuum. The crude product was purified by column chromatography (SiO_2, PE:DCM; 9:1), affording the title compound as a red solid (0.255 g, 89%); mp 169 – 170 °C [lit. 170.5-171.2 °C]; δ_H (400 MHz, $CDCl_3$, TMS) 7.81 (d, 1H, *J* 7.6, C(1)H), 7.61 (d, 1H, *J* 7.6, C(2)H), 4.63 (t, 2H, *J* 1.9, C(3)H), 4.32 (t, *J* 1.9, 2H, C(4)H), 4.30 (s, 5H C(5)H); MS (EI^+, *m/z*): $[M]^+$ found 421.9.

4-(7-(Ferrocenyl)ethynylbenzo[*c*][1,2,5]thiadiazol-4-yl)benzaldehyde[218] **119**

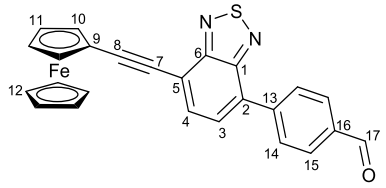

Compounds **118** (0.200 g, 0.474 mmol) and **114** (85.3 mg, 0.569 mmol) were dissolved in THF (20 mL). An aqueous solution of 2M K_2CO_3 (2.37 mL, 4.74 mmol) was added, and the mixture was degassed for 30 minutes with N_2. Then $Pd(PPh_3)_4$ (32.8 mg, 28.4 μmol) was added and the resulting mixture was stirred at reflux under N_2 and was monitored by TLC. After 6 hours, the mixture was allowed to cool to room temperature, poured into water (100 mL) and extracted with DCM (3 × 100 mL). The combined organic extracts were dried over $MgSO_4$, filtered and concentrated under vacuum. The crude product was purified by column chromatography (SiO_2, PE:DCM; 1:1), affording the title compound as a brown solid (0.180 g, 86%); mp > 300 °C; δ_H (400 MHz, $CDCl_3$, TMS) 10.11 (s, 1 H, C(17)H), 8.15 (d, *J* 8.5, 2 H, C(14)H), 8.05 (d, *J* 8.5, 2 H, C(15)H), 7.87 (d, *J* 7.4, 1 H, C(3)H), 7.77 (d, *J* 7.4, 1 H, C(4)H), 4.67 (t, *J* 1.9, 2 H, C(11)H), 4.34 (t, *J* 1.9, 2 H, C(10)H), 4.32 (s, 5 H, C(12)H); δ_C (100 MHz, TCE-d_2, TMS) 192.4 C(17), 155.6, 153.2 C(1, 6), 143.3 C(16), 136.0 C(13), 132.5 C(3), 132.2 C(5), 130.3 C(15), 130.1 C(14), 129.0 C(4), 118.3 C(2), 97.3 C(8), 82.2 C(7), 72.3 C(10), 70.7 C(12), 69.9 C(11), 64.5 C(9); HRMS (EI^+, *m/z*): $[M]^+$ found, 448.0331; calc. for ($C_{25}H_{16}FeN_2OS^+$), 448.0333.

2-Cyano-3-(4-(7-(ferrocenyl)ethynylbenzo[*c*][1,2,5]thiadiazol-4-yl)phenyl)acrylic acid[218] **105**

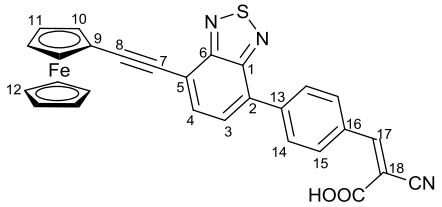

Compounds **119** (0.130 g, 0.290 mmol) and **116** (29.6 mg, 0.348 mmol) were dissolved in dry toluene (20 mL). Piperidine (2.86 μL, 29.0 μmol), AcOH (9.95 μL, 0.174 mmol) and $MgSO_4$ (14 mg, 0.06 mmol) were added, then the mixture was stirred at reflux under N_2 and was monitored by TLC. After 12 hours, the solvent was removed under vacuum and the crude product was purified by column chromatography (SiO_2, DCM:MeOH; 9:1), affording the title compound as a dark brown solid (0.144 g, 96%); mp > 300 °C; δ_H (500 MHz, d_6-DMSO, TMS) 8.17 (d, *J* 8.5, 2 H, C(15)H), 8.05 (d, *J* 8.5, 2 H, C(14)H), 8.02 (s, 1 H, C(3, 4)H), 7.98 (s, 2 H, C(15)H), 4.70 (t, *J* 1.9, 2 H, C(10)H), 4.44 (t, *J* 1.9, 2 H, C(11)H), 4.35 (s, 5 H, C(12)H); HRMS (ESI$^-$, *m/z*): $[M-H]^-$ found, 514.0295; calc. for ($C_{28}H_{16}FeN_3O_2S^-$), 514.0318; anal. calc. for ($C_{28}H_{17}FeN_3O_2S$): C, 65.26; H, 3.33; N, 8.15; found C, 65.32; H, 3.19; N, 8.35.

4-((7-(Ferrocenyl)ethynylbenzo[*c*][1,2,5]thiadiazol-4-yl)ethynyl)benzaldehyde[218]

121

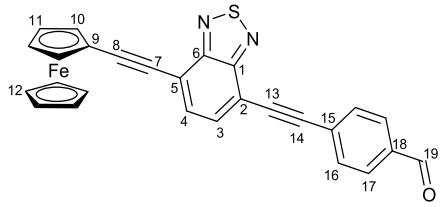

Compound **118** (0.280 g, 0.663 mmol) and 4-ethynylbenzaldehyde **120** (94.8 mg, 0.729 mmol) were dissolved in a mixture of dry THF (10 mL) and dry Et_3N (10 mL). The mixture was degassed for 30 minutes with N_2, then $Pd(PPh_3)_2Cl_2$ (23.3 mg, 33.1 μmol) and CuI (6.30 mg, 33.1 μmol) were added. The resulting mixture was stirred at room temperature under N_2 and was monitored by TLC. After 6 hours, the mixture was poured into an aqueous solution of saturated NH_4Cl (100 mL) and extracted with DCM (3 × 100 mL). The combined organic extracts were dried over $MgSO_4$, filtered and concentrated under vacuum. The crude product was purified by column chromatography (SiO_2, Toluene:Et_2O; 9:1), affording the title compound as an orange solid (0.140 g, 45%); mp > 300 °C; δ_H (500 MHz, $CDCl_3$, TMS) 10.05 (s, 1 H, C(19)H), 7.92 (d, *J* 8.4, 2 H, C(16)H), 7.82 (d, *J* 8.4, 2 H, C(17)H), 7.80 (d, *J* 7.4, 1 H, C(3)H), 7.75 (d, *J* 7.4, 1 H, C(4)H), 4.66 (t, *J* 1.9, 2 H, C(10)H), 4.35 (t, *J* 1.9, 2 H, C(11)H), 4.31 (s, 5 H, C(12)H); δ_C (125 MHz, $CDCl_3$, TMS) 191.5 C(19), 154.5 C(1, 6), 136.1 C(18), 133.3 C(3), 132.6 C(16), 131.7 C(4), 129.8 C(17), 129.0 C(2), 119.1, 115.5 C(5, 15), 98.8, 95.9 C(8, 14), 89.4, 82.1 C(7, 13), 72.2 C(10), 70.4 C(12), 69.8 C(11), 64.1 C(9); HRMS (EI^+, *m/z*): $[M]^+$ found, 472.0328; calc. for ($C_{27}H_{16}FeN_2OS^+$), 472.0333.

2-Cyano-3-(4-((7-(ferrocenyl)ethynylbenzo[*c*][1,2,5]thiadiazol-4-yl)ethynyl)phenyl) acrylic acid[218] **106**

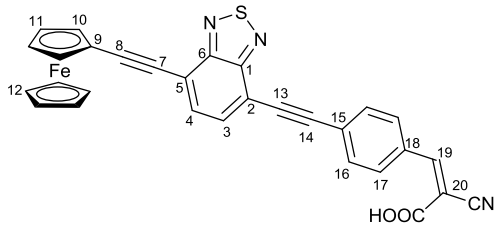

Compounds **121** (0.140 g, 0.297 mmol) and **116** (30.2 mg, 0.356 mmol) were dissolved in dry toluene (20 mL). $MgSO_4$ (14.6 mg, 59.4 μmol), piperidine (2.93 μL, 29.7 μmol) and AcOH (10.2 μL, 0.178 mmol) were added, then the mixture stirred at 100°C under N_2 and was monitored by TLC. After 6 hours, the solvent was removed under vacuum. The crude product was purified by column chromatography (SiO_2, DCM:MeOH; 9:1), affording the title compound as an orange solid (0.190 g, 44%); mp > 300 °C; δ_H (400 MHz, d_6-DMSO, TMS) 8.07 (b, 1 H, C(19)H), 8.02 (d, *J* 8.2, 2 H, C(17)H), 7.98 (d, *J* 7.4, 1 H, C(16)H), 7.90 (d, *J* 7.4, 1 H, C(3)H), 7.78 (d, *J* 8.2, 2 H, C(4)H), 4.70 (t, *J* 1.9, 2 H, C(10)H), 4.45 (t, *J* 1.9, 2 H, C(11)H), 4.34 (s, 5 H, C(12)H); HRMS (ESI$^-$, *m/z*): $[M-H]^-$ found, 538.0326; calc. for ($C_{30}H_{16}FeN_3O_2S$), 538.0318. anal. calc. for ($C_{30}H_{17}FeN_3O_2S$): C, 66.80; H, 3.18; N, 7.79; found C, 66.59; H, 3.28; N, 7.92.

4,7-*bis*(5-Bromofuran-2-yl)-5,6-bis(octyloxy)benzo[*c*][1,2,5]thiadiazole[170] **122**

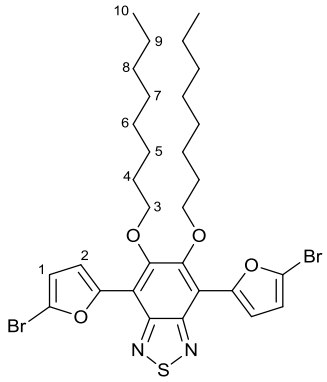

Compound **64** (0.560 g, 1.07 mmol) was dissolved in a mixture of DCM (20 mL) and acetic acid (20 mL) and the solution was cooled to 0 °C and kept in the dark. NBS (0.199 g, 1.12 mmol) was added in small portions over 30 minutes. The resulting mixture was stirred at room temperature and monitored by TLC. After 12 hours, the mixture was poured into water (200 mL) and the mixture was extracted with DCM (3 × 100 mL), dried over $MgSO_4$, filtered and concentrated under vacuum. The crude compound was purified by column chromatography (SiO_2, PE:DCM; 20:1) affording the title compound as yellow waxy solid (0.475 g, 65%); δ_H (400 MHz, $CDCl_3$, TMS) 7.48 (d, *J* 3.6, 2H, C(2)H), 6.56 (d, *J* 3.6, 2H, C(1)H), 4.10 (t, *J* 6.8, 4H, C(3)H), 1.84 (quint, *J* 6.8, 4H, C(5)H), 1.40–1.25 (m, 20H, C(6, 7, 8, 9, 10)H), 0.92 (t, *J* 6.8, 6H, C(11)H); MS (EI^+, *m/z*): $[M]^+$ found 682.1.

4,7-*bis*(5-(Ferrocenylethynyl)furan-2-yl)-5,6-*bis*(Octyloxy)-benzo[*c*][1,2,5] thiadiazole **107**

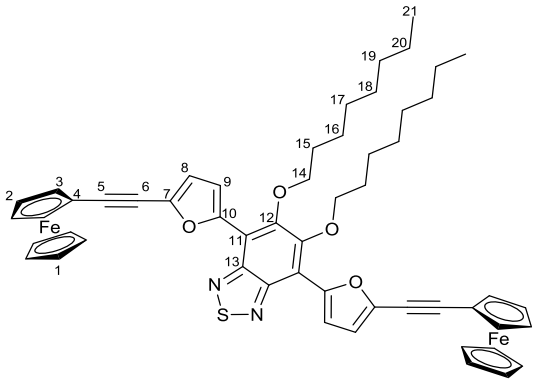

Compounds **122** (0.300 g, 0.442 mmol) and **64** (0.231 mg, 1.11 mmol) were dissolved in a mixture of dry THF (20 mL) and dry DIPA (20 mL). The mixture was degassed for 30 minutes with Ar, then $PdCl_2(PPh_3)_2$ (15.5 mg, 22.1 μmol) and CuI (4.20 mg, 22.1 μmol) were added. The resulting mixture was stirred at 50 °C under Ar and was monitored by TLC. After 8 hours, it was allowed to cool to room temperature, poured into an aqueous solution of saturated NH_4Cl (150 mL) and extracted with DCM (3 × 150 mL). The combined organic extracts were dried over $MgSO_4$, filtered and concentrated under vacuum. The crude product was purified by column chromatography (SiO_2, PE:DCM; 4:1), affording the title compound as a red waxy solid (0.380 g, 92%); δ_H (400 MHz, $CDCl_3$, TMS) 7.56 (d, *J* 3.6, 2H, C(9)H), 6.81 (d, *J* 3.6, 2H, C(8)H), 4.54 (t, *J* 6.8, 4H, C(3)H), 4.32 – 4.24 (m, 14H, C(1, 2)H), 4.17 (t, *J* 6.8, 4H, C(14)H), 2.05 – 1.94 (m, 4H, C(15)H), 1.60 – 1.49 (m, 4H, C(16)H), 1.45 – 1.21 (m, 16H, C(17, 18, 19, 20)H), 0.88 (t, *J* 6.8, 6H, C(21)H); δ_C (100 MHz, $CDCl_3$, TMS) 153.1 C(13), 150.1, 148.1, 138.0, 116.6 C(7, 10, 11, 12), 115.6 C(8), 114.2 C(9), 94.4, 76.4, 75.4 C(4, 5, 6), 71.7 C(2), 70.3 C(1), 69.3 C(3), 64.2 C(14), 32.1 C(15), 30.5 C(16), 29.8, 29.5, 26.4, 22.8 C(17, 18, 19, 20), 14.3 C(21); HRMS (ESI^+, *m/z*): $[M+H]^+$ found, 941.2752; calc. for ($C_{54}H_{57}Fe_2N_2O_4S^+$), 941.2732; anal. calc. for ($C_{54}H_{56}Fe_2N_2O_4S$): C, 68.94; H, 6.00; N, 2.98; found C, 68.41; H, 6.08; N, 3.04.

3,6-Di-*tert*-butyl-9*H*-carbazole[219] **125**

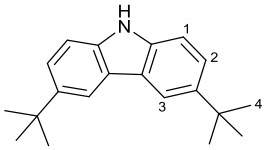

9H-Carbazole **124** (5.00 g, 29.9 mmol), and $ZnCl_2$ (12.1 g, 88.8 mmol) were dissolved in nitromethane (150 mL) under Ar. *tert*-Butyl chloride (6.51 mL, 59.7 mmol) was added drop-wise and the resulting mixture was stirred at room temperature, for 5 hours. Then it was poured into water (300 mL), extracted with DCM (300 mL) and washed with water (3 × 300 mL). The organic extract was dried over $MgSO_4$, filtered and concentrated under vacuum. The title compound was afforded as a white solid (7.51 g, 90%); mp 229 – 230 °C [lit. 233 – 235 °C]; δ_H (500 MHz, $CDCl_3$, TMS) 8.08 (d, *J* 1.8, 2H, C(3)H), 7.85 (bs, 1H, NH), 7.46 (dd, *J* 8.5, 1.8, 2H, C(1)H), 7.34 (d, *J* 8.5, 2H, C(2)H), 1.45 (s, 18H, C(4)H); MS (ESI^+, *m/z*): $[M+H]^+$ 280.2.

4-(3,6-Di-*tert*-butyl-9*H*-carbazol-9-yl)benzaldehyde[220] **127**

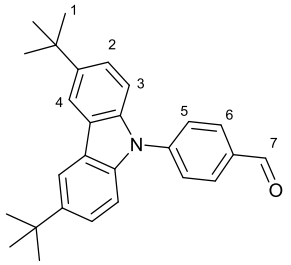

Compound **125** (1.50 g, 5.37 mmol), 4-bromobenzaldehyde **126** (0.99 g, 5.37 mmol), copper powder (0.684 g, 10.7 mmol), K_2CO_3 (2.93 g, 21.5 mmol) and dibenzo-18-crown-6 (0.193 g, 0.537 mmol) were dissolved in dry and degassed DMF (25 mL). The mixture was stirred at 150 °C under Ar for 3 days. Then, the mixture was allowed to cool to room temperature and filtered and the filtrate was poured into water (100 mL) and stirred for further 1 hour. The crude product was collected by filtration and purified by column chromatography (SiO_2, DCM/PE; 9:1), affording the title compound as a yellow solid (0.922 g, 45%); mp 156 – 157 °C [lit. 159 – 160 °C]; δ_H (400 MHz, $CDCl_3$, TMS) 10.12 (s, 1H, C(7)H), 8.23 (dd, *J* 1.8, 0.5, 2H, C(4)H), 8.13 (d, *J* 8.6, 2H, C(5)H), 7.82 (d, *J* 8.6, 2H, C(6)H), 7.50-7.55 (m, 4H, C(2)H, C(3)H), 1.55 (s, 18H, C(1)H); MS (EI^+, *m/z*): $[M]^+$ found 383.2.

3,6-Di-*tert*-butyl-9-(4-(2,2-dibromovinyl)phenyl)-9*H*-carbazole **127a**

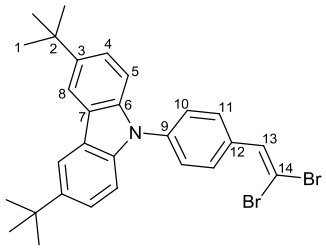

Zinc powder (0.292 g, 4.46 mmol), PPh_3 (1.48 g, 4.46 mmol) and CBr_4 (1.17 g, 4.46 mmol) were dissolved in dry DCM and stirred at room temperature under Ar for 1 hour. A solution of compound **127** (0.570 g, 1.48 mmol) in dry DCM (5 mL) was added, and the resulting mixture was stirred at room temperature under Ar and was monitored by TLC. After 2 days, the mixture was filtered through celite and the residue was washed with DCM (50 mL). The filtrate was concentrated under vacuum and was purified by column chromatography (SiO_2, PE:DCM; 4:1), affording the title compound as a pale green waxy solid (0.273 g, 34%); δ_H (500 MHz, $CDCl_3$, TMS) 8.15 (d, *J* 1.8, 2H, C(8)H), 7.78 (d, *J* 8.4, 2H, C(10)H), 7.59 (d, *J* 8.4, 2H, C(11)H) 7.58 (s, 1H, C(13)H), 7.47 (dd, *J* 8.6, 1.8, 2H, C(5)H), 7.40 (d, *J* 8.6, 2H, C(4)H), 1.48 (s, 18H, C(1)H); δ_C (125 MHz, $CDCl_3$, TMS) 143.3, 139.0, 138.4 C(3, 6, 9), 136.2 C(13), 133.7 C(12), 130.0 C(11), 126.4 C(8), 123.8 C(10), 123.7 C(4), 116.4 C(7), 109.4 C(5), 90.1 C(14), 34.9 C(2), 32.1 C(1); HRMS (EI^+, *m/z*): $[M]^+$ found, 539.0643; calc. for ($C_{28}H_{29}Br_2N^+$), 539.0646.

3,6-Di-*tert*-butyl-9-(4-ethynylphenyl)-9*H*-carbazole **128**

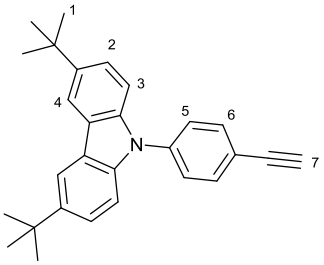

Compound **127a** (0.270 mg, 0.503 mmol) was dissolved in dry THF (20 mL). The mixture was cooled to –78 °C and a solution of 0.93 M LDA in THF (5.37 mL, 5.01 mmol) was added drop-wise. After stirring for 10 minutes, the mixture was allowed to warm to room temperature, poured into an aqueous solution of saturated NH_4Cl (100 mL) and extracted with DCM (3 × 100 mL), dried over $MgSO_4$, filtered and concentrated under vacuum. The crude compound was filtered through a pad of silica, eluting with PE, affording the title compound as a white shining solid (0.189 g, 100%); mp 133 – 134 °C [lit.[262] 135 °C]; δ_H (400 MHz, $CDCl_3$, TMS) 8.16 (d, *J* 1.5, 2H, C(4)H), 7.72 (d, *J* 8.6, 2H, C(5)H), 7.56 (d, *J* 8.6, 2H, C(6)H), 7.49 (dd, *J* 8.6, 1.5, 2H, C(3)H), 7.38 (dd, *J* 8.6, 1.5, 2H, C(2)H), 3.18 (s, 1H, C(7)H), 1.49 (s, 18H, C(1)H); MS (EI^+, *m/z*): $[M]^+$ found 379.2.

4,7-Di(thiophen-2-yl)benzo[*c*][1,2,5]thiadiazole[224] **129**

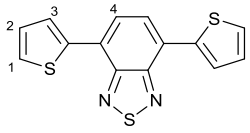

Compounds **46** (3.00 g, 10.1 mmol) and **68** (7.02 mL, 22.1 mmol) were dissolved in dry THF (80 mL). The solution was degassed for 30 minutes with Ar, then $PdCl_2(PPh_3)_2$ (0.420 g, 0.606 mmol) was added and the resulting mixture was stirred at reflux under Ar and was monitored by TLC. After 12 hours, the mixture was allowed to cool to room temperature and poured into an aqueous solution of 1 M KF (200 mL) and stirred for 1 hour. The mixture was extracted with DCM (3 × 150 mL), dried over $MgSO_4$, filtered and concentrated under vacuum. The crude product was purified by column chromatography (SiO_2; PE:DCM; 9:1) affording the title compound as an orange solid (3.15 g, 100%); mp 124 – 125 °C [lit. 124 – 125 °C]. δ_H (400 MHz, $CDCl_3$, TMS) 8.13 (d, *J* 3.7, 2H, C(1)H), 7.89 (s, 2H, C(4)H), 7.46 (d, *J* 5.1, 2H, C(3)H), 7.22 (dd, *J* 5.1, 3.7, 2H, C(2)H); MS (EI^+, *m/z*): $[M]^+$ found 300.0.

4-(5-bromothiophen-2-yl)-7-(thiophen-2-yl)benzo[*c*][1,2,5]thiadiazole[225] **130**

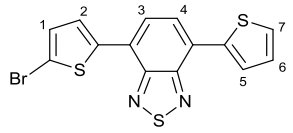

Compound **129** (1.00 g, 3.33 mmol) was dissolved in a mixture of DCM (100 mL) and acetic acid (100 mL) and the solution was cooled to 0 °C and kept in the dark. NBS (0.590 g, 3.33 mmol) was added in small portions over 30 minutes. The resulting mixture was stirred at room temperature and monitored by TLC. After 12 hours, the mixture was poured into water (200 mL) and the mixture was extracted with DCM (3 × 100 mL), dried over $MgSO_4$, filtered and concentrated under vacuum. The crude compound was purified by column chromatography (SiO_2, PE:DCM; 9:1) affording the title compound as an orange solid (0.823 g, 65%); mp 123 – 124 °C [lit. 126 °C]; δ_H (500 MHz, $CDCl_3$, TMS) 8.12 (dd, *J* 3.7, 1.0, 1H, C(7)H), 7.85 (d, *J* 7.6, 1H, C(3 or 4)H), 7.80 – 7.77 (m, 2H, C(2, 3 or 4)H), 7.47 (dd, *J* 5.1, 1.0, 1H, C(5)H), 7.21 (dd, *J* 5.1, 3.7, 1H, C(6)H), 7.15 (d, *J* 4.0, 1H, C(1)H); MS (EI^+, *m/z*): $[M]^+$ found 377.9.

5-(7-(5-Bromothiophen-2-yl)benzo[*c*][1,2,5]thiadiazol-4-yl)thiophene-2-carbaldehyde[211] **131**

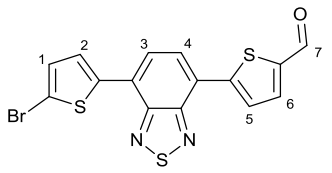

$POCl_3$ (0.135 mL, 1.32 mmol) was added to dry DMF (5 mL) at 0 ºC under Ar. Then, the mixture was allowed to warm to room temperature and stirred for 30 minutes. Afterwards, it was cooled back to 0 ºC and a solution of compound **130** (0.500 g, 1.32 mmol) in 1,2-dichloroethane (50 mL) was slowly added. The resulting mixture was stirred at 80 ºC under Ar and was monitored by TLC. After 8 hours, the mixture was allowed to cool to room temperature and poured into an aqueous solution of 1M NaOAc (200 mL). The resulting suspension was stirred for further 1 hour and extracted with DCM (3 × 200 mL). The combined organic extracts were dried over $MgSO_4$, filtered and concentrated under vacuum. The crude product was purified by column chromatography (SiO_2, PE:DCM; 2:1) affording the title compound as an orange solid (0.462 g, 86%); mp 207 – 208 ºC; δ_H (400 MHz, $CDCl_3$, TMS) 9.97 (s, 1H, C(7)H), 8.21 – 8.18 (m, 2H, C(3, 4)H), 8.00 (d, *J* 8.7, 1H, C(6)H), 7.91 (d, *J* 8.7, 1H, C(5)H), 7.84 (d, *J* 8.4, 1H, C(2)H), 7.50 (d, *J* 8.4, 1H, C(1)H); MS (EI^+, *m/z*): $[M]^+$ found 405.9.

5-(7-(5-((4-(3,6-Di-*tert*-butyl-9*H*-carbazol-9-yl)phenyl)ethynyl)thiophen-2-yl)benzo[*c*][1,2,5]thiadiazol-4-yl)thiophene-2-carbaldehyde **132**

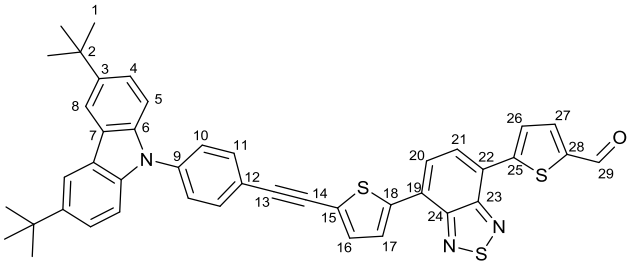

Compounds **128** (0.210 g, 0.552 mmol) and **131** (0.150 g, 0.373 mmol) were dissolved in a mixture of dry DMF (5 mL) and dry DIPA (1 mL). The mixture was degassed for 30 minutes with Ar then $PdCl_2(PPh_3)_2$ (7.85 mg, 0.011 mmol) and CuI (2.09 mg, 0.011 mmol) were added. The resulting mixture was stirred at 90 ºC under Ar and was monitored by TLC. After 10 hours, it was allowed to cool to room temperature and poured into water (100 mL). The precipitate was filtered and washed with water (100 mL) and cold MeOH (50 mL) respectively. The crude product was purified by column chromatography (SiO_2, PE:DCM; 1:1) and recrystallized from MeOH, affording the title compound as a red solid (0.144 g, 55%); mp 256 – 257 ºC; δ_H (400 MHz, $CDCl_3$, TMS) 9.99 (s, 1H, C(29)H), 8.25 (d, *J* 3.9, 1H, C(27)H), 8.14 (d, *J* 1.8, 2H, C(8)H), 8.11 (d, *J* 3.9, 1H, C(26)H), 8.04 (d, *J* 7.7, 1H, C(20)H), 7.95 (d, *J* 7.7, 1H, C(21)H), 7.87 (d, *J* 4.0, 1H, C(17)H), 7.76 (d, *J* 8.6, 2H, C(10)H), 7.60 (d, *J* 8.6, 2H, C(11)H), 7.49 (dd, *J* 8.6, 1.8, 2H, C(5)H), 7.44 – 7.37 (m, 3H, C(4, 16)H), 1.47 (s, 18H, C(1)H); δ_C (100 MHz, $CDCl_3$, TMS) 177.5 C(29), 155.1, 152.1 C(23, 24), 151.8, 151.7, 150.8 C(19, 22, 28), 143.3, 139.5, 139.2, 139.1 C(3, 6, 9, 25), 133.6 C(27), 133.1 C(11), 128.5 C(20), 126.5 C(21), 124.3 C(8), 123.9 C(4), 123.6 C(16), 123.2 C(26), 120.3 C(17), 116.5, 116.1, 114.8 C(7, 12, 15), 114.4 C(10), 109.1 C(5), 93.1, 90.3 C(13, 14), 34.9 C(2), 32.1 C(1); HRMS (EI^+, *m/z*): $[M]^+$ found, 705.1947; calc. for ($C_{43}H_{35}N_3OS_3^+$), 705.1942.

3-(5-(7-(5-((4-(3,6-di-*tert*-butyl-9*H*-carbazol-9-yl)phenyl)ethynyl)thiophen-2-yl) benzo[*c*][1,2,5]thiadiazol-4-yl)thiophen-2-yl)-2-isocyanoacrylic acid **108**

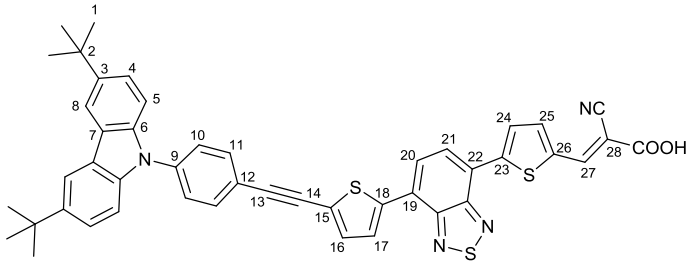

Compounds **132** (0.175 g, 0.251 mmol) and **116** (25.6 mg, 0.301 mmol) were dissolved in dry toluene (5 mL). $MgSO_4$ (12 mg, 50.2 μmol), piperidine (2.48 μL, 25.1 mmol) and acetic acid (8.61 μL, 0.151 mmol) were added and the resulting mixture was stirred under Ar at 100 ºC, for 6 hours. The mixture was allowed to cool to room temperature and the crude product was left to precipitate overnight at 0 ºC in the mother solution. The precipitate was filtered and washed with cold toluene (50 mL), PE (50 mL), Et_2O (50 mL), water (50 mL) and cold MeOH (50 mL) respectively, affording the title compound as a dark purple powder (0.168 g, 87%); mp > 300 °C; δ_H (500 MHz, DMSO-d_6, TMS) 8.36 – 8.17 (m, 6H), 7.89 – 7.89 (m, 3H), 7.75 – 7.60 (m, 4H), 7.45 – 7.37 (m, 4H), 1.43 (s, 18H); HRMS (FAB$^-$, *m/z*): [M-H]$^-$ found, 771.1937; calc. for ($C_{46}H_{35}N_4O_2S_3^-$), 771.1928; anal. calc. for ($C_{46}H_{36}N_4O_2S_3$): C, 71.48; H, 4.69; N, 7.25; found C, 71.35; H, 4.58; N, 7.18.

4-(5-Bromofuran-2-yl)-7-(furan-2-yl)benzo[*c*][1,2,5]thiadiazole **133**

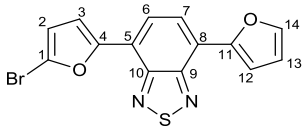

Compound **48** (1.00 g, 3.72 mmol) was dissolved in $CHCl_3$ (50 mL) and stirred at 0 ºC. NBS (0.663 g, 3.72 mmol) was added portion-wise, over 30 minutes, in the dark. The mixture was allowed to warm to room temperature and stirred in the dark for 12 hours. It was then poured into an aqueous solution of 5% $Na_2S_2O_3$ (150 mL) and stirred for further 1 hour. The organic fraction was extracted with DCM (100 mL), washed with water (3 × 150 mL), dried over $MgSO_4$, filtered and concentrated under vacuum. The crude product was purified by column chromatography (SiO_2, PE:DCM; 9:1) affording the title compound as an orange solid (1.01 g, 78%); mp 110 – 111 ºC; δ_H (500 MHz, $CDCl_3$, TMS) 8.02 (s, 2H), C(6, 7)H), 7.69 (d, *J* 3.4, 1H, C(14)H), 7.63 (d, *J* 3.4, 1H, C(12)H), 7.59 (d, *J* 1.2, 1H, C(3)H), 6.63 (dd, *J* 3.4, 1.8, 1H, C(13)H), 6.54 (d, *J* 3.4, 1H, C(2)H); δ_C (125 MHz, $CDCl_3$, TMS) 152.3, 151.4 C(9, 10), 151.0, 150.2 C(4, 11), 143.1 C(14), 123.7, 123.5 C(6, 7), 123.2, 122.3 C(5, 8), 120.7 C(1), 114.7 C(2), 114.5 C(3), 112.7 C(13), 112.6 C(12); HRMS (EI$^+$, *m/z*): $[M]^+$ found, 345.9412; calc. for ($C_{14}H_7BrN_2O_2S^+$), 345.9405.

5-(7-(5-Bromofuran-2-yl)benzo[*c*][1,2,5]thiadiazol-4-yl)furan-2-carbaldehyde **134**

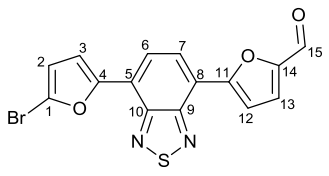

$POCl_3$ (0.300 mL, 3.21 mmol) was added to dry DMF (10 mL) at 0 ºC under Ar. Then, the mixture was allowed to warm to room temperature and stirred for 30 minutes. Afterwards, the mixture was cooled back to 0 ºC and a solution of compound **133** (1.01 g, 2.92 mmol) in 1,2-dichloroethane (90 mL) was slowly added. The resulting mixture was stirred at 80 ºC under Ar and monitored by TLC. After 6 hours, the mixture was allowed to cool to room temperature and poured into an aqueous solution of 1M NaOAc (300 mL). The resulting suspension was stirred for further 1 hour and extracted with DCM (3 × 200 mL), dried over $MgSO_4$, filtered and concentrated under vacuum. The crude product was purified by column chromatography (SiO_2, PE:DCM; 2:1) affording the title compound as an orange solid (1.00 g, 91%); mp 215 – 216 ºC; δ_H (500 MHz, $CDCl_3$, TMS) 9.74 (s, 1H, C(15)H), 8.33 (d, *J* 7.7, 1H, C(7)H), 8.07 (d, *J* 7.7, 1H, C(6)H), 7.90 (d, *J* 3.5, 1H, C(13)H), 7.73 (d, *J* 3.5, 1H, C(12)H), 7.45 (d, *J* 3.5, 1H, C(3)H), 6.58 (d, *J* 3.5, 1H, C(2)H); δ_C (125 MHz, TCE-d_2, TMS) 177.8 C(15), 155.5, 155.4 C(9, 10), 152.0, 151.8, 151.3 C(4, 11, 14), 145.0, 144.0 C(5, 8), 126.8 C(6), 124.3 C(7), 123.3 C(1), 119.9 C(13), 114.5 C(12), 114.2 C(2), 113.2 C(3); HRMS (EI^+, *m/z*): $[M]^+$ found, 373.9360; calc. for ($C_{15}H_7BrN_2O_3S^+$), 373.9361.

5-(7-(5-(4-(Diphenylamino)phenyl)furan-2-yl)benzo[*c*][1,2,5]thiadiazol-4-yl)furan-2-carbaldehyde **136**

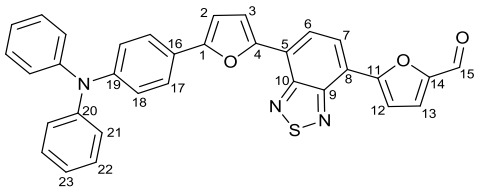

Compounds **134** (0.300 g, 0.800 mmol) and **135** (0.255 g, 0.879 mmol) were dissolved in a mixture of toluene (30 mL) and EtOH (5 mL). An aqueous solution of 2 M Na_2CO_3 (1.20 mL, 2.40 mmol) was added, and the mixture was degassed for 30 minutes, with Ar. $Pd(PPh)_4$ (46.2 mg, 40.0 μmol) was added, and the resulting mixture was stirred at reflux under Ar and was monitored by TLC. After 4 hours, the mixture was allowed to cool to room temperature, poured into an aqueous solution of saturated NH_4Cl (200 mL) and extracted with DCM (3× 200 mL). The combined organic extracts were dried over $MgSO_4$, filtered and concentrated under vacuum. The crude product was purified by column chromatography (SiO_2, toluene) and reprecipitated from MeOH, affording the title compound as a purple solid (0.300 g, 69%); mp 198 – 199 ºC; δ_H (400 MHz, $CDCl_3$, TMS) 9.72 (s, 1H, C(15)H), 8.34 (d, *J* 7.8, 1H, C(7)H), 8.11 (d, *J* 7.8, 1H, C(6)H), 7.88 (dd, *J* 8.7, 3.7, 2H, C(18)H), 7.72 – 7.67 (m, 2H, C(17)H), 7.45 (d, *J* 3.8, 1H, C(12)H), 7.32 – 7.27 (m, 4H, C(22)H), 7.17 – 7.14 (m, 6H, C(3, 13, 21)H), 7.10 – 7.04 (m, 2H, C(23)H), 6.80 (d, *J* 3.6, 1H, C(2)H); δ_C (100 MHz, $CDCl_3$, TMS) 177.4 C(15), 155.5, 155.3 C(9, 10), 152.0, 151.9, 151.3, 148.9, 148.1 C(1, 4, 11, 14, 19), 147.5 C(20), 129.5 C(22), 126.8 C(6), 125.4 C(17), 125.0 C(5), 124.9 C(21), 124.1, 124.1 C(6, 7), 123.6 C(23), 123.3 C(18), 122.3 C(13), 119.3 C(8), 116.7 C(12), 114.0 C(3), 107.5 C(2); HRMS (EI^+, *m/z*): $[M]^+$ found, 539.1306; calc. for ($C_{33}H_{21}N_3O_3S^+$), 539.1304.

2-Cyano-3-(5-(7-(5-(4-(diphenylamino)phenyl)furan-2-yl)benzo[*c*][1,2,5]thiadiazol-4-yl)furan-2-yl)acrylic acid **109**

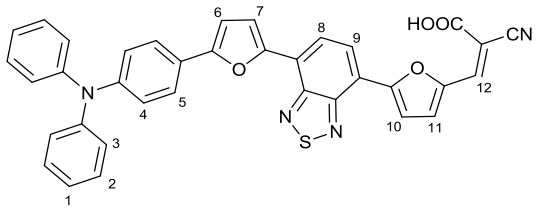

Compounds **136** (0.270 mg, 0.500 mmol) and **116** (51.0 mg, 0.600 mmol) were dissolved in dry toluene (20 mL). $MgSO_4$ (0.247 g, 0.100 mmol), piperidine (5.93 μL, 50.0 μmol) and acetic acid (17.2 μL, 0.300 mmol) were added and the resulting mixture was stirred under Ar at 100 ºC for 6 hours. The mixture was then allowed to cool to room temperature and the crude product was left to precipitate overnight at 0 ºC from the mother solution. The precipitate was filtered and washed with cold toluene (50 mL), PE (50 mL), Et_2O (50 mL), water (50 mL) and cold MeOH (50 mL) respectively, affording the title compound as a black powder (0.255 g, 84%); mp 256 – 257 °C; δ_H (400 MHz, DMSO-d_6, TMS) 13.71 (s, 1H, COOH), 8.27 (d, *J* 7.8, 2H, C(8, 9)H), 8.14 (s, 1H, C(12)H), 7.89 – 7.80 (m, 3H, C(4, 11)H), 7.80 (d, *J* 3.6, 1H, C(10)H), 7.64 (d, *J* 3.7, 1H, C(7)H), 7.39 – 7.32 (m, 4H, C(3)H), 7.15 – 7.07 (m, 7H, C(2, 5, 6)H), 7.01 (d, *J* 8.8, 2H, C(1)H); HRMS (ESI$^-$, *m/z*): $[M-H]^-$ found, 605.1293; calc. for ($C_{36}H_{21}N_4O_4S^-$), 605.1289; anal. calc. for ($C_{36}H_{22}N_4O_4S$): C, 71.28; H, 3.66; N, 9.24; found C, 71.35; H, 3.49; N, 9.12.

4,7-Dibromo-5,6-dinitrobenzo[*c*][1,2,5]thiadiazole[227] **139**

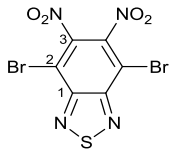

Sulfuric acid (150 mL) was slowly added to fuming nitric acid (150 mL) at 0 °C. 4,7-Compound **46** (10.0 g, 34.0 mmol) was added portion-wise and the resulting mixture was stirred at 50 °C for 24 hours. The mixture was allowed to cool to room temperature, poured into iced water and stirred for further 4 hours. The precipitate was collected by filtration, washed with water (100 mL), cold MeOH (50 mL) and PE (50 mL) consecutively, affording the title compound as a pale yellow solid (5.25 g, 40%); mp 198 – 199 °C [lit. 201 °C]; δ_H (500 MHz, DMSO-d_6, TMS) no peaks found; δ_C (500 MHz, DMSO-d_6, TMS) 151.7 C(1), 144.1 C(3), 111.8 C(2).

4,7-Dibromobenzo[*c*][1,2,5]thiadiazole-5,6-diamine[228] **140**

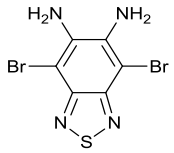

Iron powder (5.00 g, 89.2 mmol) was suspended in glacial AcOH (100 mL). To this suspension, compound **139** (5.00 g, 13.02 mmol) was added, and the resulting mixture was stirred at 80 °C, for 1 hour. It was then allowed to cool to room temperature and poured into an aqueous solution of 5% NaOH (200 mL). The precipitate was collected by filtration and washed with water (50 mL). Then it was purified by Soxhlet extraction for 3 hours with EtOAc, affording the title compound as a yellow solid (2.38 g, 56%); MS (ESI^+, *m/z*): $[M+H]^+$ found 324.9.

4,8-Dibromo-benzo[1,2-*c*;4,5-*c*']*bis*[1,2,5]thiadiazole[228] **141**

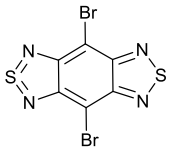

Compound **140** (2.38 g, 7.33 mmol) and pyridine (0.342 mL, 4.26 mmol) were dissolved in dry $CHCl_3$ (150 mL). A solution of $SOCl_2$ (0.164 mL, 2.13 mmol) in $CHCl_3$ (50 mL) was added drop-wise, and the resulting mixture was stirred at reflux for 10 hours. The mixture was then allowed to cool to room temperature, poured into water (200 mL) and the organic layer was separated, washed with water (2 × 200 mL), dried over $MgSO_4$, filtered and concentrated under vacuum. The crude product was purified by reprecipitation from a mixture of MeOH and DCM (1:1), affording the title compound as a red solid (2.18 g, 69%); δ_H (500 MHz, DMSO-d_6, TMS) no peaks found; MS (EI^+, *m/z*) $[M]^+$ found 351.8.

Poly[(9,9-di-*n*-octylfluorenyl-2,7-diyl)-*alt*-(benzo[1,2-*c*;4,5-*c*']*bis*[1,2,5]thiadiazol-4,8-diyl)] **110**

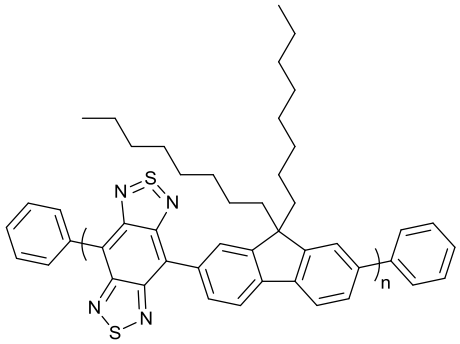

Compound **141** (0.413 g, 1.17 mmol), compound **142** (0.510 g, 1.23 mmol) and $Pd(PPh_3)_4$ (0.164 g, 0.117 mmol) were placed in a flask. The system was evacuated and refilled with Ar 3 times, then degassed toluene (70 mL) was added. A degassed aqueous solution of 2 M Na_2CO_3 (10.5 mL, 21.3 mmol) was added and the resulting mixture was stirred at reflux under Ar and was monitored by GPC. After 5 days bromobenzene (0.223 g, 1.42 mmol) was added, followed by phenylboronic acid (0.173 g, 1.42 mmol) 12 hours later. After further 12 hours the mixture was allowed to cool to room temperature and poured into water (200 mL). The mixture was extracted with toluene (3 × 150 mL) and concentrated under vacuum. The crude polymer was purified by Soxhlet extraction, using hexane, MeOH, acetone, $CHCl_3$ and THF, consecutively, affording the title polymer as a greenish blue solid in two batches of M_n = 10 kDa (PDI = 1.3, 0.125 g) and M_n = 12 kDa (PDI = 1.3, 83 mg), respectively.

[2,2'-Bi(1,3-dithiolylidene)]-4-yltributylstannane[247] **151**

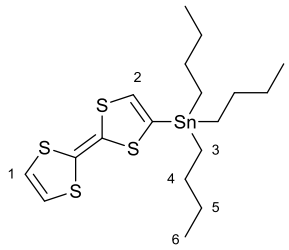

TTF (1.00 g, 4.90 mmol) was dissolved in dry Et_2O (100 mL), under N_2. After cooling the solution to –78 °C, a solution of 1.95 M LDA in THF (2.76 mL, 5.39 mmol) was added drop-wise and the resulting mixture was stirred at –78 ºC, for 1 hour, when a lemon yellow precipitate was observed. Tributyltin chloride (1.33 mL, 4.90 mmol) was then added and the mixture was stirred at –78 °C, for 1 hour and then for a further 1 hour at room temperature. The mixture was then poured into water (200 mL), extracted with Et_2O (3 × 100 mL). The combined organic extracts were dried over $MgSO_4$, filtered and concentrated under vacuum. The crude product was dissolved in hexane (100 mL) and washed with MeCN (4 × 100 mL). The hexane layer was then collected and concentrated under vacuum, affording the title compound as a yellow oil (1.62 g, 67%); δ_H (400 MHz, $CDCl_3$, TMS) 6.28 (d, *J* 1.4 Hz, 2H, C(1)H), 6.11 (s, 1H, C(2)H), 1.59 – 1.49 (m, 6H, C(3)H), 1.35 – 1.27 (m, 6H, C(4)H), 1.14 – 1.00 (m, 6H, C(5)H), 0.90 (t, *J* 7.3 Hz, 9H, C(6)H); MS (EI^+, *m/z*): $[M]^+$ found 494.0.

4-([2,2'-Bi(1,3-Dithiolylidene)]-4-yl)benzaldehyde[263] **154**

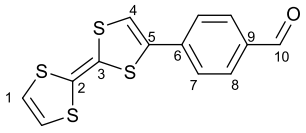

Compound **151** (1.00 g, 2.03 mmol) and 4-bromobenzaldehyde **152** (0.414 g, 2.24 mmol) were dissolved in dry toluene (50 mL) and the mixture was degassed for 30 minutes with N_2. $Pd(PPh_3)_2Cl_2$ (0.142 g, 0.203 mmol) was added and the resulting mixture was stirred at reflux under N_2 and was monitored by TLC. After 12 hours, the solution was allowed to cool to room temperature and poured into an aqueous solution of 1M KF (200 mL). The slurry was stirred for a further 1 hour, then it was extracted with DCM (200 mL) and washed with brine (200 mL) and water (200 mL) respectively. The organic fraction was dried over $MgSO_4$, filtered and concentrated under vacuum. The crude product was purified by column chromatography (SiO_2, PE:DCM; 3:2) affording the title compound as a dark red solid (0.532 g, 85%); δ_H (400 MHz, $CDCl_3$, TMS) 10.00 (s, 1H, C(10)H), 7.87 (d, *J* 8.5, 2H, C(8)H), 7.55 (d, *J* 8.5, 2H, C(7)H), 6.75 (s, 1H, C(4)H), 6.35 (s, 2H, C(1)H); MS (ESI^+, *m/z*): $[M+Na]^+$ found 330.9.

3-(4-([2,2'-Bi(1,3-dithiolylidene)]-4-yl)phenyl)-2-cyanoacrylic acid **145**

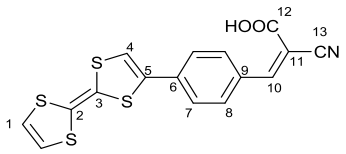

Compounds **154** (0.345 g, 1.12 mmol) and **116** (0.114 mg, 1.34 mmol) were dissolved in dry toluene (50 mL). $MgSO_4$ (55.2 mg, 0.224 mmol), piperidine (11.0 µL, 0.112 mmol) and AcOH (40 µL, 0.67 mmol) were added and the resulting mixture was stirred at reflux under N_2 for 5 hours. The reaction was then allowed to cool to room temperature and the crude product was left to precipitate overnight at 0 ºC from the mother solution. The precipitate was filtered and washed with PE (50 mL), water (50 mL) and MeOH (50 mL), affording the title compound as a bluish green powder (0.382 g, 91%); mp 226 – 227 °C; δ_H (500 MHz, DMSO-d_6, TMS) 14.03 (s, 1H, COOH), 8.31 (s, 1H, C(10)H), 8.07 (d, *J* 8.5, 2H, C(8)H), 7.66 (d, *J* 8.5, 2H, C(7)H), 7.57 (s, 1H, C(4)H), 6.78 (s, 2H, C(1)H); δ_C (125 MHz, DMSO-d_6, TMS) 163.7 C(12), 153.5 C(10), 135.8, 133.9 C(6, 9), 131.8 C(7), 131.6, 129.4 C(3, 5), 126.9 C(8), 120.7 C(1), 120.5 C(4), 120.4 C(13), 113.4 C(2), 106.5 C(11); HRMS (ESI$^-$, *m/z*): $[M-H]^-$ found, 373.9434; calc. for ($C_{16}H_8NO_2S_4^-$), 373.9443.

5-([2,2'-Bi(1,3-dithiolylidene)]-4-yl)thiophene-2-carbaldehyde **155**

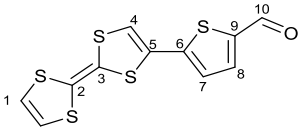

Compound **151** (1.00 g, 2.03 mmol) was dissolved in dry toluene (50 mL), and 5-bromo-2-thiophenecarboxaldehyde (0.260 mL, 2.24 mmol), was added. The mixture was degassed for 30 minutes with N_2, then $Pd(PPh_3)_2Cl_2$ (0.140 g, 0.203 mmol) was added. The resulting mixture was stirred at reflux under N_2 and was monitored by TLC. After 12 hours, the mixture was allowed to cool to room temperature and poured into an aqueous solution of 1M KF (200 mL). The slurry was stirred for a further 1 hour, extracted with DCM (200 mL) and washed with brine (200 mL) and water (200 mL), respectively. The organic fraction was dried over $MgSO_4$, filtered and concentrated under vacuum. The crude product was purified by column chromatography (SiO_2, PE:DCM; 3:1) affording the title compound as a purple solid (0.523 g, 82%); mp 141 – 142 °C; δ_H (500 MHz, $CDCl_3$, TMS) 9.86 (s, 1H, C(10)H), 7.64 (d, *J* 4.0, 1H, C(8)H), 7.05 (d, *J* 4.0, 1H, C(7)H), 6.72 (s, 1H, C(4)H), 6.36 (s, 2H, C(1)H). δ_C (125 MHz, $CDCl_3$, TMS) 182.3 C(10), 143.7, 142.3 C(6, 9), 136.6 C(8), 128.2, 127.5 C(3, 5), 126.5 C(7), 125.9 C(2), 119.0 C(1), 118.5 C(4); HRMS (ESI^+, *m/z*): $[M+Na]^+$ found, 336.8914; calc. for ($C_{11}H_6NaOS_5^+$), 336.8914.

3-(5-([2,2'-Bi(1,3-dithiolylidene)]-4-yl)thiophen-2-yl)-2-cyanoacrylic acid **146**

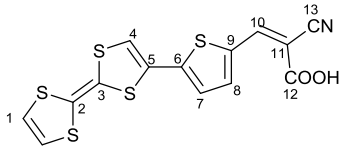

Compounds **155** (0.570 g, 1.82 mmol) and **116** (0.185 g, 2.17 mmol) were dissolved in dry toluene (60 mL). $MgSO_4$ (90.0 mg, 0.364 mmol), piperidine (18.0 µL, 0.182 mmol) and AcOH (62.0 µL, 1.09 mmol) were added and the resulting mixture was stirred at reflux under N_2 for 5 hours. The mixture was then allowed to cool to room temperature and the crude product was left to precipitate overnight at 0 ºC from the mother solution. The precipitate was filtered and washed with PE (50 mL), water (50 mL) and MeOH (50 mL), respectively, affording the title compound as a violet powder (0.603 g, 87%); mp 227 – 228 °C; δ_H (400 MHz, DMSO-d_6, TMS) 13.84 (s, 1H, COO<u>H</u>), 8.49 (s, 1H, C(10)<u>H</u>), 7.95 (d, *J* 4.3, 1H, C(7)<u>H</u>), 7.52 (s, 1H, C(4)<u>H</u>), 7.41 (d, *J* 4.3, 1H, C(8)<u>H</u>), 6.79 (s, 2H, C(1)<u>H</u>); δ_C (100 MHz, DMSO-d_6, TMS) 163.3 <u>C</u>(12), 146.2 <u>C</u>(10), 142.0, 140.7 <u>C</u>(6, 9), 134.9 <u>C</u>(8), 133.7 <u>C</u>(5), 126.7 <u>C</u>(7), 126.3 <u>C</u>(3), 121.4 <u>C</u>(4), 120.2 <u>C</u>(1), 116.3 <u>C</u>(13), 114.5 <u>C</u>(2), 105.0 <u>C</u>(11); HRMS (ESI$^-$, *m/z*): $[M-H]^-$ found, 373.8992; calc. for ($C_{14}H_6NO_2S_5^-$), 379.9008.

2,5-*bis*(2-Ethylhexyl)-3,6-di(thiophen-2-yl)pyrrolo[3,4-c]pyrrole-1,4(2H,5H)-dione **157**

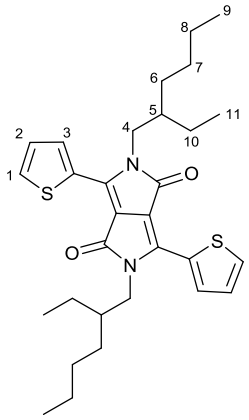

2,5-*bis*(2-Ethylhexyl)-3,6-di(thiophen-2-yl)pyrrolo[3,4-c]pyrrole-1,4(2H,5H)-dione **156** (2.00 g, 6.66 mmol), 18-crown-6 (44.9 mg, 0.17 mmol) and K_2CO_3 (2.30 g, 16.7 mmol) were dissolved in dry DMF (30 mL), and stirred at 100 ºC for 30 minutes under Ar. 2-Ethylhexylbromide (2.97 mL, 16.7 mmol) was then added and the resulting mixture was stirred at 100 ºC for further 36 hours. The mixture was allowed to cool to room temperature, poured into iced water (200 mL) and stirred for a further 1 hour. The precipitate was collected by filtration and purified by column chromatography (SiO_2, PE:$CHCl_3$; 1:1), affording the title compound as a dark red solid (1.82 g, 52%); mp 123 – 124 ºC [lit.[251] 127 ºC]; δ_H (400 MHz, $CDCl_3$, TMS) 8.89 (dd, *J* 3.9, 1.1, 2H, C(3)H), 7.62 (dd, *J* 5.0, 1.1, 2H, C(1)H), 7.27 (dd, *J* 5.0, 3.9, 2H, C(2)H), 4.03 (m, 4H, C(4)H), 1.86 (m, 2H, C(5)H), 1.41 – 1.18 (m, 16H, C(6, 7, 8, 10)H), 0.86 (m, 12H, C(9, 11)H); MS (EI^+, *m/z*): $[M]^+$ found 524.3.

3,6-*bis*(5-Bromothiophen-2-yl)-2,5-*bis*(2-ethylhexyl)pyrrolo[3,4-c]pyrrole-1,4(2H, 5H)-dione[251] **159**

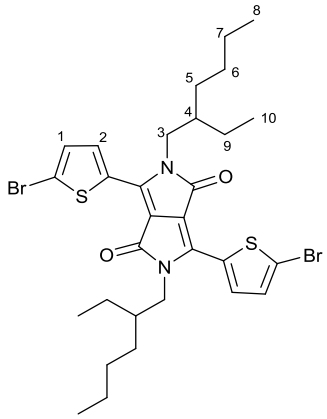

Compound **157** (1.00 g, 1.91 mmol) was dissolved in $CHCl_3$ (30 mL) at 0 ºC, in the dark. NBS (0.693 g, 3.89 mmol) was added to the mixture in portions over 30 minutes and the mixture was stirred at 0 ºC for a further 1 hour. The mixture was then washed with water (2 × 30 mL) and brine (30 mL). The organic fraction was separated, dried over $MgSO_4$, filtered and concentrated under vacuum, affording the title compound as a purple solid (2.97 g, 97%); mp 165 – 166 ºC; δ_H (400 MHz, $CDCl_3$, TMS) 8.64 (d, *J* 4.1, 2H, C(3)H), 7,22 (d, *J* 4.1, 2H, C(2)H), 3.93 (m, 4H, C(3)H), 1.84 (m, 2H, C(4)H), 1.20 – 1.39 (m, 16H, C(5, 6, 7, 9)H), 0.87 (m, 12H, C(8, 10)H); MS (EI^+, *m/z*): $[M]^+$ found 682.0.

3,6-*bis*(5-([2,2'-bi(1,3-dithiolylidene)]-4-yl)thiophen-2-yl)-2,5-*bis*(2-ethylhexyl) pyrrolo[3,4-c]pyrrole-1,4(2H,5H)-dione **147**

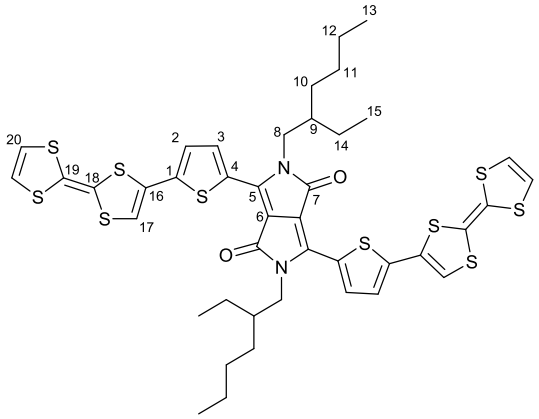

Compounds **159** (0.175 g, 0.263 mmol) and **151** (0.506 g, 1.03 mmol) were dissolved in dry toluene (30 mL). The mixture was degassed for 30 minutes with Ar, then $PdCl_2(PPh_3)_2$ (18.4 mg, 26.3 μmol) was added. The resulting mixture was stirred at reflux under Ar and was monitored by TLC. After 8 hours, the mixture was allowed to cool to room temperature and poured into an aqueous solution of 1M KF (100 mL). The resulting slurry was stirred for further 1 hour, then the mixture was extracted with EtOAc (3 × 100 mL) and the organic extracts were dried over $MgSO_4$, filtered and concentrated under vacuum. The crude product was reprecipitated from MeOH, and purified by Soxhlet extraction, using hexane. The filtrate was adsorbed on celite and placed over a pad of SiO_2. The impurities were washed off with PE while the pure product remained adsorbed unto celite. The celite layer was then removed while taking care to avoid collection of silica. Finally the title compound was recovered from the celite by washing the celite with EtOAc. The title compound was afforded as a blue solid, after evaporation of the solvent (0.177 g, 83%); mp 218 – 219 ºC; δ_H (400 MHz, $CDCl_3$, TMS) 8.88 (d, *J* 4.2, 2H, C(3)H), 7.35 (d, *J* 4.2, 2H, C(2)H), 6.66 (s, 2H, C(17)H), 6.35 (d, *J* 1.3, 4H, C(20)H), 4.02 – 3.96 (m, 4H, C(8)H), 1.90 – 1.84 (m, 2H, C(9)H), 1.38 – 1.21 (m, 16H, C(10, 11, 12, 14)H), 0.91 – 0.83 (m, 12H, C(13, 15)H); δ_C (100 MHz, $CDCl_3$, TMS) 161.6 C(7), 139.6, 135.5 C(4, 5), 131.6, 131.3 C(18, 19), 130.2 C(17), 119.1 C(20), 119.1 C(16), 117.8 C(3), 115.3 C(2), 114.7 C(1), 108.2 C(6), 46.2 C(8), 39.2 C(9), 30.3, 28.5, 23.7, 23.2 C(10, 11, 12, 14), 14.2, 10.6 C(13, 15); HRMS (ESI^+, *m/z*): $[M+H]^+$ found, 929.0682; calc. for ($C_{42}H_{45}N_2O_2S_{10}^+$), 929.0683.

(3,5-*bis*(Dodecyloxy)phenyl)methanol **162**

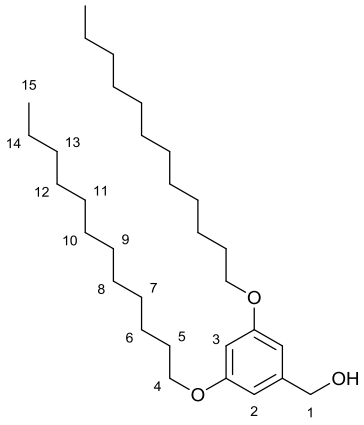

5-(Hydroxymethyl)benzene-1,3-diol **161** (1.00 g, 7.14 mmol) and K_2CO_3 (3.95 g, 28.55 mmol) were dissolved in acetone (30 mL). 1-Dodecylbromide (3.61 mL, 15.0 mmol) was added and the mixture was stirred at reflux and was monitored by TLC. After 3 days, the solution was allowed to cool to room temperature, poured into an aqueous solution of 10% HCl (150 mL) and extracted with DCM (3 × 150 mL). The combined organic extracts were dried over $MgSO_4$, filtered and concentrated under vacuum. The crude product was purified by column chromatography (SiO_2, PE:DCM; 1:1) affording the title compound as a pale yellow solid (2.27 g, 67%); mp 38 – 39 ºC [lit.[249] 41 ºC]; δ_H (400 MHz, $CDCl_3$, TMS) 6.50 (d, *J* 2.3, 2H, C(2)H), 6.38 (t, *J* 2.3, 1H, C(3)H), 4.61 (s, 2H, C(1)H), 3.93 (t, *J* 6.6, 4H, C(4)H), 1.80 – 1.72 (m, 4H, C(5)H), 1.48 – 1.40 (m, 4H, C(6)H), 1.40 – 1.19 (m, 32H, C(7, 8, 9, 10, 11, 12, 13, 14)H), 0.88 (t, *J* 6.6, 6H, C(15)H); MS (EI^+, *m/z*): $[M]^+$ found 476.4.

1-(Bromomethyl)-3,5-*bis*(dodecyloxy)benzene[250] **163**

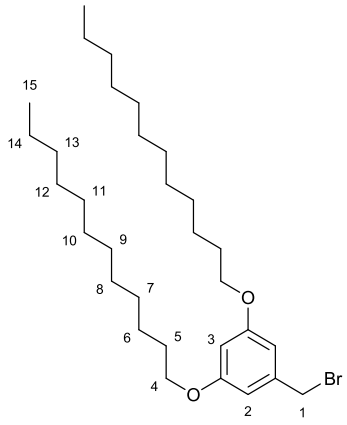

Compound **162** and CBr_4 (2.37 g, 7.14 mmol) were dissolved in dry THF (10 mL). PPh_3 (1.87 g, 7.14 mmol) was added and the mixture was stirred at room temperature under Ar for 15 minutes. Then, it was poured into water (100 mL) and extracted with DCM (3 × 100 mL). The combined organic extracts were dried over $MgSO_4$, filtered and concentrated under vacuum. The crude product was diluted in DCM and filtered through a pad of silica, to afford the title compound as a yellowish white solid (2.43 g, 100%); mp 48 – 49 ºC [lit. 48 – 49 ºC]; δ_H (400 MHz, $CDCl_3$, TMS) 6.51 (d, *J* 2.2, 2H, C(2)H), 6.38 (t, *J* 2.2, 1H, C(3)H), 4.40 (s, 2H, C(1)H), 3.92 (t, *J* 6.6, 4H, C(4)H), 1.80 – 1.72 (m, 4H, C(5)H), 1.48 – 1.40 (m, 4H, C(6)H), 1.37 – 1.24 (m, 32H, C(7, 8, 9, 10, 11, 12, 13, 14)H), 0.88 (t, *J* 6.9, 6H, C(15)H); MS (ESI^+, *m/z*): $[M+H]^+$ found 539.3.

2,5-*bis*(3,5-*bis*(Dodecyloxy)benzyl)-3,6-di(thiophen-2-yl)pyrrolo[3,4-c]pyrrole-1,4(2H,5H)-dione **158**

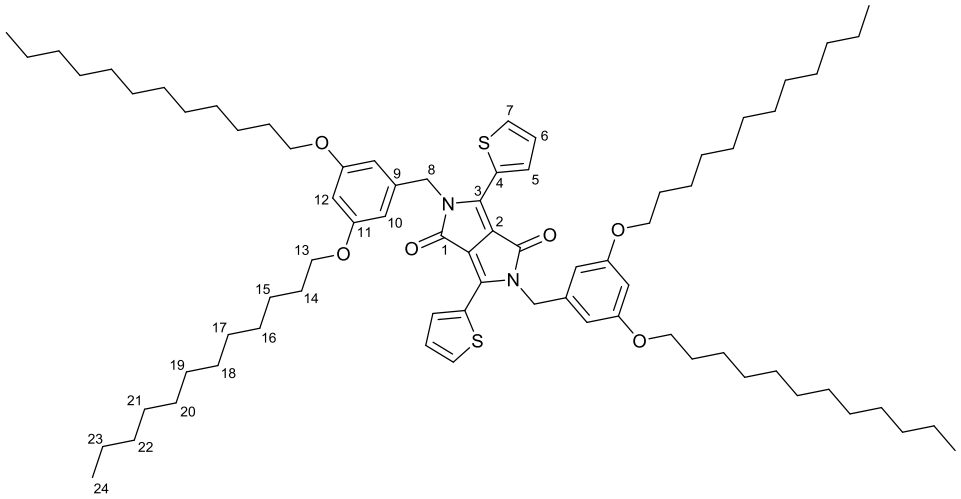

Compound **156** (0.616 g, 2.05 mmol), and K_2CO_3 (1.13 g, 8.20 mmol) were dissolved in dry NMP (60 mL), and stirred at 60 ºC for 30 minutes under Ar. A solution of compound **163** (3.15 g, 6.15 mmol) in dry NMP (10 mL) was then added and the resulting mixture was stirred at 80 ºC under Ar and was monitored by TLC. After 5 days, the mixture was allowed to cool to room temperature, poured into water (200 mL) and extracted with DCM (3 × 200 mL). The combined organic extracts were dried over $MgSO_4$, filtered and concentrated under vacuum. The crude product was reprecipitated from MeOH and purified by column chromatography (SiO_2, toluene) affording the title compound as a purple solid (1.12 g, 44%); mp 95 – 96 ºC; δ_H (500 MHz, $CDCl_3$, TMS) 8.67 (dd, *J* 3.9, 1.1, 2H, C(5)H), 7.55 (dd, *J* 5.0, 1.1, 2H, C(7)H), 7.18 (dd, *J* 5.0, 4.0, 2H, C(6)H), 6.37 (d, *J* 2.1, 4H, C(10)H), 6.32 (t, *J* 2.1, 2H, C(12)H), 5.27 (s, 4H, C(8)H), 3.88 (t, *J* 6.6, 8H, C(13)H), 1.73 (m, 8H, C(14)H), 1.43 – 1.38 (m, 8H, C(15)H), 1.31 – 1.24 (m, 64H, C(16, 17, 18, 19, 20, 21, 22, 23)H), 0.88 (t, *J* 7.0, 12H, C(24)H); δ_C (125 MHz, $CDCl_3$, TMS) 161.6, 160.8 C(1, 11), 140.6, 139.3, 135.0 C(3, 4, 9), 131.5 C(7), 129.8 C(5), 128.6 C(6), 107.7 C(2), 104.8 C(10), 99.9 C(12), 68.2 C(13), 45.6 C(8), 32.1 C(14), 29.8, 29.8, 29.8, 29.7, 29.6, 29.5, 29.4, 26.2, 22.8 C(15, 16, 17, 18, 19, 20, 21, 22, 23), 14.3 C(24); HRMS (ESI^+, *m/z*): $[M+H]^+$ found, 1217.8351; calc. for ($C_{76}H_{117}N_2O_6S_2^+$), 1217.8348.

4-Chlorotetrathiafulvalene[255] **174**

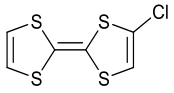

TTF (0.500 g, 2.45 mmol) was dissolved in dry Et_2O (100 mL) under Ar. After cooling the solution to –78 °C, a solution of 0.96 M LDA in THF (3.07 mL, 2.94 mmol) was added drop-wise and the resulting mixture was stirred at –78 ºC, for 1 hour, when a lemon yellow precipitate was observed. *p*-Toluenesulfonyl chloride (0.420 g, 2.21 mmol), previously dissolved in dry Et_2O (5 mL) was added and the mixture maintained at –78 °C for 3 hours and then allowed to warm to room temperature and stirred for further 10 hours. The mixture was then poured into water (100 mL), and the organic layer was separated, dried over $MgSO_4$, filtered and concentrated under vacuum. The crude compound was purified by column chromatography (SiO_2, PE), affording the target compound as an orange solid (0.369 g, 63%); mp 59 – 60 °C (lit.[255] 57 – 58 °C); δ_H (400 MHz, $CDCl_3$, TMS) 6.33 (s, 2H), 6.15 (s, 1H); MS (EI^+, *m/z*): $[M]^+$ found 237.9.

4-Iodotetrathiafulvalene[256] **175**

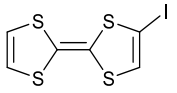

TTF (1.00 g, 4.89 mmol) was dissolved in dry Et_2O (200 mL) under Ar. After cooling the solution to –78 °C, a solution of 1.00 M LDA in THF (4.89 mL, 4.89 mmol) was added drop-wise and the resulting mixture was stirred at –78 ºC, for 1 hour, when a lemon yellow precipitate was observed. 1,2-Diiodoethane (2.07 g, 7.34 mmol), previously dissolved in dry Et_2O (5 mL) was added and the mixture maintained at –78 for 30 minutes and then allowed to warm to 0 °C and stirred for further 1 hour. The mixture was then poured into an aqueous solution of saturated $Na_2S_2O_3$ (200 mL), and stirred for 10 minutes. The organic layer was separated, washed with water (2 × 200 mL), dried over $MgSO_4$, filtered and concentrated under vacuum. The crude compound was purified by column chromatography (SiO_2, PE), affording the target compound as an orange solid (1.30 g, 80%); mp 67 – 68 °C (lit. 66 – 68 °C); δ_H (400 MHz, $CDCl_3$, TMS) 6.42 (s, 1H), 6.33 (s, 2H); MS (EI^+, *m/z*): $[M]^+$ found 329.8.

Chapter 6: Bibliography

1. P. Harrop and R. Das, *Organic Electronics Forecasts, Players & Opportunities*, 2013.
2. R. Farchioni and G. Grosso, *Organic Electronic Materials*, Springer, 2001.
3. C. K. Chiang, C. R. Fincher, Y. W. Park, A. J. Heeger, H. Shirakawa, E. J. Louis, S. C. Gau and A. G. MacDiarmid, *Phys. Rev. Lett.*, 1977, **39**, 1098-1101.
4. S. R. Forrest, *Chem. Rev.*, 1997, **97**, 1793-1896.
5. C. W. Tang, *Appl. Phys. Lett.*, 1986, **48**, 183-185.
6. H. Koezuka, A. Tsumura and T. Ando, *Synth. Met.*, 1987, **18**, 699-704.
7. C. W. Tang and S. A. VanSlyke, *Appl. Phys. Lett.*, 1987, **51**, 913-915.
8. J. H. Burroughes, D. D. C. Bradley, A. R. Brown, R. N. Marks, K. Mackay, R. H. Friend, P. L. Burns and A. B. Holmes, *Nature*, 1990, **347**, 539-541.
9. C. K. Chiang, M. A. Druy, S. C. Gau, A. J. Heeger, E. J. Louis, A. G. MacDiarmid, Y. W. Park and H. Shirakawa, *J. Am. Chem. Soc.*, 1978, **100**, 1013-1015.
10. M. Tonellato, Modellistica molecolare, http://www.pianetachimica.it/computer/Lezione_12_Argus.htm, Accessed 15/11/2015.
11. C. Kittel, *Introduction to Solid State Physics*, Wiley, 1996.
12. H. A. M. van Mullekom, J. A. J. M. Vekemans, E. E. Havinga and E. W. Meijer, *Mater. Sci. Eng., R*, 2001, **32**, 1-40.
13. J. Roncali, *Chem. Rev.*, 1997, **97**, 173-206.
14. S. Dufresne, M. Bourgeaux and W. G. Skene, *J. Mater. Chem.*, 2007, **17**, 1166-1177.
15. M. Pope and C. E. Swenberg, *Electronic Processes in Organic Crystals and Polymers*, 1999.
16. J. Frenkel, *Phys. Rev.*, 1931, **37**, 17-44.
17. J.-L. Brédas, J. E. Norton, J. Cornil and V. Coropceanu, *Acc. Chem. Res.*, 2009, **42**, 1691-1699.
18. G. H. Wannier, *Phys. Rev.*, 1937, **52**, 191-197.

19. S. Morita, A. A. Zakhidov and K. Yoshino, *Solid State Commun.*, 1992, **82**, 249-252.
20. W. D. Gill, *J. Appl. Phys.*, 1972, **43**, 5033-5040.
21. J. J. M. Halls, C. A. Walsh, N. C. Greenham, E. A. Marseglia, R. H. Friend, S. C. Moratti and A. B. Holmes, *Nature*, 1995, **376**, 498-500.
22. G. Yu, J. Gao, J. C. Hummelen, F. Wudl and A. J. Heeger, *Science*, 1995, **270**, 1789-1791.
23. N. S. Sariciftci, L. Smilowitz, A. J. Heeger and F. Wudl, *Science*, 1992, **258**, 1474-1476.
24. P. Schilinsky, C. Waldauf and C. J. Brabec, *Appl. Phys. Lett.*, 2002, **81**, 3885-3887.
25. G. Li, R. Zhu and Y. Yang, *Nat. Photon.*, 2012, **6**, 153-161.
26. J. You, L. Dou, K. Yoshimura, T. Kato, K. Ohya, T. Moriarty, K. Emery, C.-C. Chen, J. Gao, G. Li and Y. Yang, *Nat. Commun.*, 2013, **4**, 1446.
27. M. A. Green, K. Emery, Y. Hishikawa, W. Warta and E. D. Dunlop, *Prog. Photovoltaics Res. Appl.*, 2013, **21**, 827-837.
28. M. T. Greiner, L. Chai and Z.-H. Lu, ORGANIC PHOTOVOLTAICS: Transition metal oxides increase organic solar-cell power conversion, http://www.laserfocusworld.com/articles/print/volume-48/issue-06/features/transition-metal-oxides-increase-organic-solar-cell-power-conversion.html, Accessed 13/01/2016.
29. E. Verploegen and M. Toney, Effects of Thermal Annealing On the Morphology of Polymer–Fullerene Blends for Organic Solar Cells, http://www-ssrl.slac.stanford.edu/content/science/highlight/2011-01-31/effects-thermal-annealing-morphology-polymer%E2%80%93fullerene-blends-organic, Accessed 13/01/2016.
30. D. W. Zhao, P. Liu, X. W. Sun, S. T. Tan, L. Ke and A. K. K. Kyaw, *Appl. Phys. Lett.*, 2009, **95**, 153304.
31. H. Hoppe, N. S. Sariciftci and D. Meissner, *Mol. Cryst. Liq. Cryst.*, 2002, **385**, 113-119.
32. P. M. Sommeling, H. C. Rieffe, J. A. M. van Roosmalen, A. Schönecker, J. M. Kroon, J. A. Wienke and A. Hinsch, *Sol. Energy Mater. Sol. Cells*, 2000, **62**, 399-410.

33. Solar cells and IV curves, https://nationalvetcontent.edu.au/alfresco/d/d/workspace/SpacesStore/f3d90138-e7ed-41ce-8346-4d6756d0d52a/ims/content_sections/learn_about/08_solar_page_006.htm, Accessed 13/01/2016.
34. C. J. Brabec, A. Cravino, D. Meissner, N. S. Sariciftci, T. Fromherz, M. T. Rispens, L. Sanchez and J. C. Hummelen, *Adv. Funct. Mater.*, 2001, **11**, 374-380.
35. J. Liu, Y. J. Shi and Y. Yang, *Adv. Funct. Mater.*, 2001, **11**, 420-424.
36. H. Frohne, S. E. Shaheen, C. J. Brabec, D. C. Müller, N. S. Sariciftci and K. Meerholz, *ChemPhysChem*, 2002, **3**, 795-799.
37. A. Gadisa, M. Svensson, M. R. Andersson and O. Inganäs, *Appl. Phys. Lett.*, 2004, **84**, 1609-1611.
38. M. C. Scharber, D. Mühlbacher, M. Koppe, P. Denk, C. Waldauf, A. J. Heeger and C. J. Brabec, *Adv. Mater.*, 2006, **18**, 789-794.
39. J. G. F. Hide and H. Wang, *Synth. Met.*, 1997, **84**, 979-980.
40. J. Yoon, J.-J. Kim, T.-W. Lee and O.-O. Park, *Appl. Phys. Lett.*, 2000, **76**, 2152-2154.
41. T. M. Brown, R. H. Friend, I. S. Millard, D. J. Lacey, J. H. Burroughes and F. Cacialli, *Appl. Phys. Lett.*, 2000, **77**, 3096-3098.
42. W. L. Ma, C. Y. Yang, X. Gong, K. Lee and A. J. Heeger, *Adv. Funct. Mater.*, 2005, **15**, 1617-1622.
43. G. Li, V. Shrotriya, J. Huang, Y. Yao, T. Moriarty, K. Emery and Y. Yang, *Nat. Mater.*, 2005, **4**, 864-868.
44. J. Chen and Y. Cao, *Acc. Chem. Res.*, 2009, **42**, 1709-1718.
45. Y.-J. Cheng, S.-H. Yang and C.-S. Hsu, *Chem. Rev.*, 2009, **109**, 5868-5923.
46. X. Zhan and D. Zhu, *Polym. Chem.*, 2010, **1**, 409-419.
47. Z. He, B. Xiao, F. Liu, H. Wu, Y. Yang, S. Xiao, C. Wang, T. P. Russell and Y. Cao, *Nat. Photon.*, 2015, **9**, 174-179.
48. J. Zhou, Y. Zuo, X. Wan, G. Long, Q. Zhang, W. Ni, Y. Liu, Z. Li, G. He, C. Li, B. Kan, M. Li and Y. Chen, *J. Am. Chem. Soc.*, 2013, **135**, 8484-8487.
49. B. C. Thompson and J. M. J. Fréchet, *Angew. Chem. Int. Ed.*, 2008, **47**, 58-77.

50. Y. Liang, D. Feng, Y. Wu, S.-T. Tsai, G. Li, C. Ray and L. Yu, *J. Am. Chem. Soc.*, 2009, **131**, 7792-7799.
51. Y. Liang, Z. Xu, J. Xia, S.-T. Tsai, Y. Wu, G. Li, C. Ray and L. Yu, *Adv. Mater.*, 2010, **22**, E135-E138.
52. J. S. Kim, Y. Lee, J. H. Lee, J. H. Park, J. K. Kim and K. Cho, *Adv. Mater.*, 2010, **22**, 1355-1360.
53. H. Zhou, L. Yang, A. C. Stuart, S. C. Price, S. Liu and W. You, *Angew. Chem. Int. Ed.*, 2011, **50**, 2995-2998.
54. R. Mondal, H. A. Becerril, E. Verploegen, D. Kim, J. E. Norton, S. Ko, N. Miyaki, S. Lee, M. F. Toney, J.-L. Bredas, M. D. McGehee and Z. Bao, *J. Mater. Chem.*, 2010, **20**, 5823-5834.
55. S. Xiao, A. C. Stuart, S. Liu and W. You, *ACS Appl. Mater. Interfaces*, 2009, **1**, 1613-1621.
56. S. Xiao, A. C. Stuart, S. Liu, H. Zhou and W. You, *Adv. Funct. Mater.*, 2010, **20**, 635-643.
57. C. Müller, E. Wang, L. M. Andersson, K. Tvingstedt, Y. Zhou, M. R. Andersson and O. Inganäs, *Adv. Funct. Mater.*, 2010, **20**, 2124-2131.
58. M. Tong, S. Cho, J. T. Rogers, K. Schmidt, B. B. Y. Hsu, D. Moses, R. C. Coffin, E. J. Kramer, G. C. Bazan and A. J. Heeger, *Adv. Funct. Mater.*, 2010, **20**, 3959-3965.
59. R. C. Coffin, J. Peet, J. Rogers and G. C. Bazan, *Nat. Chem.*, 2009, **1**, 657-661.
60. Y. Kim, S. Cook, J. Kirkpatrick, J. Nelson, J. R. Durrant, D. D. C. Bradley, M. Giles, M. Heeney, R. Hamilton and I. McCulloch, *J. Phys. Chem. C*, 2007, **111**, 8137-8141.
61. J. K. Park, J. Jo, J. H. Seo, J. S. Moon, Y. D. Park, K. Lee, A. J. Heeger and G. C. Bazan, *Adv. Mater.*, 2011, **23**, 2430-2435.
62. S. R. Cowan, W. L. Leong, N. Banerji, G. Dennler and A. J. Heeger, *Adv. Funct. Mater.*, 2011, **21**, 3083-3092.
63. A. Saeki, M. Tsuji and S. Seki, *Adv. Energy Mater.*, 2011, **1**, 457-457.
64. J. Kettle, M. Horie, L. A. Majewski, B. R. Saunders, S. Tuladhar, J. Nelson and M. L. Turner, *Sol. Energy Mater. Sol. Cells*, 2011, **95**, 2186-2193.
65. E. Wang, M. Wang, L. Wang, C. Duan, J. Zhang, W. Cai, C. He, H. Wu and Y. Cao, *Macromolecules*, 2009, **42**, 4410-4415.

66. L. Yang, H. Zhou and W. You, *J. Phys. Chem. C*, 2010, **114**, 16793-16800.
67. H. Zhou, L. Yang, S. Xiao, S. Liu and W. You, *Macromolecules*, 2010, **43**, 811-820.
68. J. Huang, G. Li and Y. Yang, *Appl. Phys. Lett.*, 2005, **87**, 112105.
69. J. E. Anthony, *Chem. Mater.*, 2011, **23**, 583-590.
70. L. Ye, K. Sun, W. Jiang, S. Zhang, W. Zhao, H. Yao, Z. Wang and J. Hou, *ACS Appl. Mater. Interfaces*, 2015, **7**, 9274-9280.
71. B. Ebenhoch, N. B. A. Prasetya, V. M. Rotello, G. Cooke and I. D. W. Samuel, *J. Mater. Chem. A*, 2015, **3**, 7345-7352.
72. S. Holliday, R. S. Ashraf, C. B. Nielsen, M. Kirkus, J. A. Röhr, C.-H. Tan, E. Collado-Fregoso, A.-C. Knall, J. R. Durrant, J. Nelson and I. McCulloch, *J. Am. Chem. Soc.*, 2015, **137**, 898-904.
73. H. Shi, W. Fu, M. Shi, J. Ling and H. Chen, *J. Mater. Chem. A*, 2015, **3**, 1902-1905.
74. B. O'Regan and M. Gratzel, *Nature*, 1991, **353**, 737-740.
75. M. Tucker, Dye Sensitised Solar Cells (DSSCs), http://www.slideshare.net/MaxTucker/ncsas-ppt, Accessed 19/01/2016.
76. S. Ardo and G. J. Meyer, *Chem. Soc. Rev.*, 2009, **38**, 115-164.
77. Dye-sensitised cells, http://www.thesolarspark.co.uk/the-science/solar-power/excitonic-solar-cells/dye-sensitised-cells/, Accessed 12/10/2015.
78. M. Zhang, Y. Wang, M. Xu, W. Ma, R. Li and P. Wang, *Energy Environ. Sci.*, 2013, **6**, 2944-2949.
79. M. Liang and J. Chen, *Chem. Soc. Rev.*, 2013, **42**, 3453-3488.
80. M. Nazeeruddin, M. Graetzel, E. Baranoff, F. Kessler, J.-H. Yum, A. Yella and H. N. Tsao, ed. P. I. Appl., Ecole Polytechnique Federale de Lausanne (EPFL), Switzerland, 2012, p. 92.
81. K. Do, D. Kim, N. Cho, S. Paek, K. Song and J. Ko, *Org. Lett.*, 2012, **14**, 222-225.
82. D. P. Hagberg, J.-H. Yum, H. Lee, F. De Angelis, T. Marinado, K. M. Karlsson, R. Humphry-Baker, L. Sun, A. Hagfeldt, M. Grätzel and M. K. Nazeeruddin, *J. Am. Chem. Soc.*, 2008, **130**, 6259-6266.
83. J. Tang, J. Hua, W. Wu, J. Li, Z. Jin, Y. Long and H. Tian, *Energy Environ. Sci.*, 2010, **3**, 1736-1745.

84. Z. Ning, Q. Zhang, W. Wu, H. Pei, B. Liu and H. Tian, *J. Org. Chem.*, 2008, **73**, 3791-3797.

85. B. Liu, W. Zhu, Q. Zhang, W. Wu, M. Xu, Z. Ning, Y. Xie and H. Tian, *Chem. Commun.*, 2009, 1766-1768.

86. T. Horiuchi, H. Miura and S. Uchida, *Chem. Commun.*, 2003, 3036-3037.

87. T. Horiuchi, H. Miura, K. Sumioka and S. Uchida, *J. Am. Chem. Soc.*, 2004, **126**, 12218-12219.

88. N. Koumura, Z.-S. Wang, M. Miyashita, Y. Uemura, H. Sekiguchi, Y. Cui, A. Mori, S. Mori and K. Hara, *J. Mater. Chem.*, 2009, **19**, 4829-4836.

89. K. Hara, M. Kurashige, S. Ito, A. Shinpo, S. Suga, K. Sayama and H. Arakawa, *Chem. Commun.*, 2003, 252-253.

90. M. Xu, S. Wenger, H. Bala, D. Shi, R. Li, Y. Zhou, S. M. Zakeeruddin, M. Grätzel and P. Wang, *J. Phys. Chem. C*, 2009, **113**, 2966-2973.

91. D. P. Hagberg, T. Marinado, K. M. Karlsson, K. Nonomura, P. Qin, G. Boschloo, T. Brinck, A. Hagfeldt and L. Sun, *J. Org. Chem.*, 2007, **72**, 9550-9556.

92. R. Li, X. Lv, D. Shi, D. Zhou, Y. Cheng, G. Zhang and P. Wang, *J. Phys. Chem. C*, 2009, **113**, 7469-7479.

93. G. Zhang, H. Bala, Y. Cheng, D. Shi, X. Lv, Q. Yu and P. Wang, *Chem. Commun.*, 2009, 2198-2200.

94. G. Zhang, Y. Bai, R. Li, D. Shi, S. Wenger, S. M. Zakeeruddin, M. Gratzel and P. Wang, *Energy Environ. Sci.*, 2009, **2**, 92-95.

95. R. Li, J. Liu, N. Cai, M. Zhang and P. Wang, *J. Phys. Chem. B*, 2010, **114**, 4461-4464.

96. X. Zhu, H. Tsuji, A. Yella, A.-S. Chauvin, M. Gratzel and E. Nakamura, *Chem. Commun.*, 2013, **49**, 582-584.

97. N. Koumura, Z.-S. Wang, S. Mori, M. Miyashita, E. Suzuki and K. Hara, *J. Am. Chem. Soc.*, 2006, **128**, 14256-14257.

98. Y. Wu and W. Zhu, *Chem. Soc. Rev.*, 2013, **42**, 2039-2058.

99. S. Qu, C. Qin, A. Islam, Y. Wu, W. Zhu, J. Hua, H. Tian and L. Han, *Chem. Commun.*, 2012, **48**, 6972-6974.

100. S. Qu, W. Wu, J. Hua, C. Kong, Y. Long and H. Tian, *J. Phys. Chem. C*, 2010, **114**, 1343-1349.

101. U. Bach, D. Lupo, P. Comte, J. E. Moser, F. Weissortel, J. Salbeck, H. Spreitzer and M. Gratzel, *Nature*, 1998, **395**, 583-585.
102. L. Yang, U. B. Cappel, E. L. Unger, M. Karlsson, K. M. Karlsson, E. Gabrielsson, L. Sun, G. Boschloo, A. Hagfeldt and E. M. J. Johansson, *Phys. Chem. Chem. Phys.*, 2012, **14**, 779-789.
103. J. Krüger, R. Plass, L. Cevey, M. Piccirelli, M. Grätzel and U. Bach, *Appl. Phys. Lett.*, 2001, **79**, 2085-2087.
104. I. Kaiser, K. Ernst, C. H. Fischer, R. Könenkamp, C. Rost, I. Sieber and M. C. Lux-Steiner, *Sol. Energy Mater. Sol. Cells*, 2001, **67**, 89-96.
105. R. Plass, S. Pelet, J. Krueger, M. Grätzel and U. Bach, *J. Phys. Chem. B*, 2002, **106**, 7578-7580.
106. X. Ziang, L. Shifeng, Q. Laixiang, P. Shuping, W. Wei, Y. Yu, Y. Li, C. Zhijian, W. Shufeng, D. Honglin, Y. Minghui and G. G. Qin, *Optical Materials Express*, 2015, **5**, 29-43.
107. P. Umari, E. Mosconi and F. De Angelis, *Sci. Rep.*, 2014, **4**, 4467.
108. A. Kojima, K. Teshima, T. Miyasaka and Y. Shirai, Novel photoelectrochemical cell with mesoscopic electrodes sensitized by lead-halide compounds, in *210th Proc. ECS Meet.*, 2006, **1** (ECS).
109. A. Kojima, K. Teshima, Y. Shirai and T. Miyasaka, *J. Am. Chem. Soc.*, 2009, **131**, 6050-6051.
110. J.-H. Im, C.-R. Lee, J.-W. Lee, S.-W. Park and N.-G. Park, *Nanoscale*, 2011, **3**, 4088-4093.
111. H.-S. Kim, C.-R. Lee, J.-H. Im, K.-B. Lee, T. Moehl, A. Marchioro, S.-J. Moon, R. Humphry-Baker, J.-H. Yum, J. E. Moser, M. Grätzel and N.-G. Park, *Sci. Rep.*, 2012, **2**, 591.
112. New World Record of PSC Efficiency, http://www.dyesol.com/media/wysiwyg/Documents/2015-asx-announcements/2015-12-08-DYE0397_-_EPFL_achieves_21_efficiency.pdf?utm_source=2015-12-08-ASX-EPFL+achieves+21%25+efficiency+for+Perovskite&utm_campaign=http%3A%2F%2Fwww.dyesol.com%2Fmedia%2Fwysiwyg%2FDocuments%2F2015-asx-announcements%2F2015-06-17-DYE0381_-_Dyesol_joins_Solliance.pdf&utm_medium=email, Accessed 22/01/2016.

113. C. Wehrenfennig, G. E. Eperon, M. B. Johnston, H. J. Snaith and L. M. Herz, *Adv. Mater.*, 2014, **26**, 1584-1589.
114. Q. Lin, A. Armin, R. C. R. Nagiri, P. L. Burn and P. Meredith, *Nat. Photon.*, 2015, **9**, 106-112.
115. N. J. Jeon, J. H. Noh, Y. C. Kim, W. S. Yang, S. Ryu and S. I. Seok, *Nat. Mater.*, 2014, **13**, 897-903.
116. G. Kron, T. Egerter, J. H. Werner and U. Rau, *J. Phys. Chem. B*, 2003, **107**, 3556-3564.
117. A. D. Sheikh, A. Bera, M. A. Haque, R. B. Rakhi, S. D. Gobbo, H. N. Alshareef and T. Wu, *Sol. Energy Mater. Sol. Cells*, 2015, **137**, 6-14.
118. N. J. Jeon, J. Lee, J. H. Noh, M. K. Nazeeruddin, M. Grätzel and S. I. Seok, *J. Am. Chem. Soc.*, 2013, **135**, 19087-19090.
119. S. Lv, L. Han, J. Xiao, L. Zhu, J. Shi, H. Wei, Y. Xu, J. Dong, X. Xu, D. Li, S. Wang, Y. Luo, Q. Meng and X. Li, *Chem. Commun.*, 2014, **50**, 6931-6934.
120. S. D. Sung, M. S. Kang, I. T. Choi, H. M. Kim, H. Kim, M. Hong, H. K. Kim and W. I. Lee, *Chem. Commun.*, 2014, **50**, 14161-14163.
121. P. Gratia, A. Magomedov, T. Malinauskas, M. Daskeviciene, A. Abate, S. Ahmad, M. Grätzel, V. Getautis and M. K. Nazeeruddin, *Angew. Chem. Int. Ed.*, 2015, **54**, 11409-11413.
122. A. W. Blyth, *J. Chem. Soc., Dalton Trans.*, 1879, **35**, 530-539.
123. Y. Meah and V. Massey, *Proc. Natl. Acad. Sci. U.S.A.*, 2000, **97**, 10733-10738.
124. R. Kuhn and F. Weygand, *Ber. Dtsch. Chem. Ges.*, 1934, **67**, 2084-2085.
125. X. Yu, S. Eymur, V. Singh, B. Yang, M. Tonga, A. Bheemaraju, G. Cooke, C. Subramani, D. Venkataraman, R. J. Stanley and V. M. Rotello, *Phys. Chem. Chem. Phys.*, 2012, **14**, 6749-6754.
126. P. Hemmerich, C. Veeger and H. C. S. Wood, *Angew. Chem. Int. Ed.*, 1965, **4**, 671-687.
127. F. Muller, *Chemistry and Biochemistry of Flavoenzymes*, CRC Press, Boca Raton, 1991.
128. A. Losi, *Photochem. Photobiol.*, 2007, **83**, 1283-1300.
129. A. Sancar, *Chem. Rev.*, 2003, **103**, 2203-2238.
130. T. O. Baldwin, J. A. Christopher, F. M. Raushel, J. F. Sinclair, M. M. Ziegler, A. J. Fisher and I. Rayment, *Curr. Opin. Struct. Biol.*, 1995, **5**, 798-809.

131. P. F. Heelis, *Chem. Soc. Rev.*, 1982, **11**, 15-39.
132. S. O. Mansoorabadi, C. J. Thibodeaux and H.-w. Liu, *J. Org. Chem.*, 2007, **72**, 6329-6342.
133. A. M. Edwards, *Flavins: Photochemistry and Photobiology*, The Royal Society of Chemistry, Cambridge, 2006.
134. S. L. Murov, I. Carmichael and G. L. Hug, *Handbook of Photochemistry*, CRC Press, New York, 1993.
135. H. Schmaderer, J. Svoboda and B. König, *Activating Unreactive Substrates: The Role of Secondary Interactions*, Wiley-VCH, Weinheim, 2009.
136. S. Ghisla, W. C. Kenney, W. R. Knappe, W. McIntire and T. P. Singer, *Biochemistry*, 1980, **19**, 2537-2544.
137. B. König, M. Pelka, H. Zieg, T. Ritter, H. Bouas-Laurent, R. Bonneau and J.-P. Desvergne, *J. Am. Chem. Soc.*, 1999, **121**, 1681-1687.
138. F. Lipmann, *Nature*, 1939, **143**, 436-436.
139. A. A. Krasnovsky, *Dokl. Akad. Nauk.*, 1948, **61**, 91.
140. S. D. M. Islam, A. Penzkofer and P. Hegemann, *Chem. Phys.*, 2003, **291**, 97-114.
141. U. Megerle, M. Wenninger, R.-J. Kutta, R. Lechner, B. Konig, B. Dick and E. Riedle, *Phys. Chem. Chem. Phys.*, 2011, **13**, 8869-8880.
142. D. Meisel and P. Neta, *J. Phys. Chem.*, 1975, **79**, 2459-2461.
143. E. Amouyal, *Sol. Energy Mater. Sol. Cells*, 1995, **38**, 249-273.
144. E. C. Breinlinger, C. J. Keenan and V. M. Rotello, *J. Am. Chem. Soc.*, 1998, **120**, 8606-8609.
145. B. J. Jordan, Y. Ofir, D. Patra, S. T. Caldwell, A. Kennedy, S. Joubanian, G. Rabani, G. Cooke and V. M. Rotello, *Small*, 2008, **4**, 2074-2078.
146. A. A. Wiles, B. Fitzpatrick, N. A. McDonald, M. M. Westwater, D.-L. Long, B. Ebenhoch, V. M. Rotello, I. D. W. Samuel and G. Cooke, *RSC Adv.*, 2016, **6**, 7999-8005.
147. M. N. Belgacem and A. Gandini, in *Monomers, Polymers and Composites from Renewable Resources*, Elsevier, Amsterdam, 2008, pp. 385-400.
148. M. J. González-Tejera, E. S. de la Blanca and I. Carrillo, *Synth. Met.*, 2008, **158**, 165-189.
149. O. Gidron, Y. Diskin-Posner and M. Bendikov, *J. Am. Chem. Soc.*, 2010, **132**, 2148-2150.

150. O. Gidron and M. Bendikov, *Angew. Chem. Int. Ed.*, 2014, **53**, 2546-2555.
151. X.-H. Jin, D. Sheberla, L. J. W. Shimon and M. Bendikov, *J. Am. Chem. Soc.*, 2014, **136**, 2592-2601.
152. S. Sharma, N. Zamoshchik and M. Bendikov, *Isr. J. Chem.*, 2014, **54**, 712-722.
153. F. Ambrosio, N. Martsinovich and A. Troisi, *J. Phys. Chem. Lett.*, 2012, **3**, 1531-1535.
154. S. H. Yoo, J. M. Kum and S. O. Cho, *Nanoscale Res. Lett.*, 2011, **6**, 545-545.
155. K. Pilgram, M. Zupan and R. Skiles, *J. Heterocycl. Chem.*, 1970, **7**, 629-633.
156. M. Kosugi, K. Sasazawa, Y. Shimizu and T. Migita, *Chem. Lett.*, 1977, **6**, 301-302.
157. D. Milstein and J. K. Stille, *J. Am. Chem. Soc.*, 1978, **100**, 3636-3638.
158. J. Yuan, Z. Zhai, J. Li, J. Lu, X. Huang, Z. Xu and W. Ma, *J. Mater. Chem. A*, 2013, **1**, 12128-12136.
159. B. A. D. Neto, A. S. Lopes, M. Wüst, V. E. U. Costa, G. Ebeling and J. Dupont, *Tetrahedron Lett.*, 2005, **46**, 6843-6846.
160. D. M. Hall and E. E. Turner, *J. Chem. Soc.*, 1945, 699-702.
161. V. Kumar, K. A. Woode, R. F. Bryan and B. A. Averill, *J. Am. Chem. Soc.*, 1986, **108**, 490-496.
162. R. Kakkar, M. Bhandari and R. Gaba, *Comput. Theor. Chem.*, 2012, **986**, 14-24.
163. C. M. Cardona, W. Li, A. E. Kaifer, D. Stockdale and G. C. Bazan, *Adv. Mater.*, 2011, **23**, 2367-2371.
164. J.-L. Bredas, *Mater. Horiz.*, 2014, **1**, 17-19.
165. N. Miyaura, K. Yamada and A. Suzuki, *Tetrahedron Lett.*, 1979, **20**, 3437-3440.
166. H.-Z. Tang, M. Fujiki, Z.-B. Zhang, K. Torimitsu and M. Motonaga, *Chem. Commun.*, 2001, 2426-2427.
167. P. Ding, C.-C. Chu, Y. Zou, D. Xiao, C. Pan and C.-S. Hsu, *J. Appl. Polym. Sci.*, 2012, **123**, 99-107.
168. A. Williamson, *Philos. Mag.*, 1850, **37**, 350-356.
169. P. Ding, C.-C. Chu, B. Liu, B. Peng, Y. Zou, Y. He, K. Zhou and C.-S. Hsu, *Macromol. Chem. Phys.*, 2010, **211**, 2555-2561.

170. X. Wang, S. Chen, Y. Sun, M. Zhang, Y. Li, X. Li and H. Wang, *Polym. Chem.*, 2011, **2**, 2872-2877.
171. E. Tayama and Y. Toma, *Tetrahedron*, 2015, **71**, 554-559.
172. A. Millet and O. Baudoin, *Org. Lett.*, 2014, **16**, 3998-4000.
173. P. G. M. Wuts and T. W. Greene, in *Greene's Protective Groups in Organic Synthesis*, John Wiley & Sons, Inc., 2006, pp. 696-926.
174. J. N. Hernández, M. A. Ramírez and V. S. Martín, *J. Org. Chem.*, 2003, **68**, 743-746.
175. S. Ram and R. E. Ehrenkaufer, *Tetrahedron Lett.*, 1984, **25**, 3415-3418.
176. F. Yoneda, Y. Sakuma, M. Ichiba and K. Shinomura, *J. Am. Chem. Soc.*, 1976, **98**, 830-835.
177. W. Hu, N. Zhu, W. Tang and D. Zhao, *Org. Lett.*, 2008, **10**, 2669-2672.
178. R. M. Cresswell and H. C. S. Wood, *J. Chem. Soc.*, 1960, 4768-4775.
179. H. Ohshiro, K. Mitsui, N. Ando, Y. Ohsawa, W. Koinuma, H. Takahashi, S.-i. Kondo, T. Nabeshima and Y. Yano, *J. Am. Chem. Soc.*, 2001, **123**, 2478-2486.
180. M. J. Stadnik and H. Buchenauer, *J. Plant Dis. Protect.*, 1999, **106**, 466-475.
181. T. Balasankar, M. Gopalakrishnan and S. Nagarajan, *Eur. J. Med. Chem.*, 2005, **40**, 728-731.
182. H. M. Geetha and H. S. Shetty, *Crop Prot.*, 2002, **21**, 601-610.
183. A. Rocher, C. Dumas and J. M. Cock, *Gene*, 2005, **344**, 181-192.
184. A. Chimirri, R. Grasso, P. Monforte, A. Rao, M. Zappalà, A. M. Monforte, C. Pannecouque, M. Witvrouw, J. Balzarini and E. De Clercq, *Antiviral Chem. Chemother.*, 1999, **10**, 211-217.
185. B. Bak, L. Nygaard, E. J. Pedersen and J. Rastrup-Andersen, *J. Mol. Spectrosc.*, 1966, **19**, 283-289.
186. D. A. McGinty and W. G. Bywater, *J. Pharmacol. Exp. Ther.*, 1945, **84**, 342-357.
187. V. Luzzati, *C. R. Chim.*, 1948, **227**, 210-211.
188. A. M. Khaletskii and V. G. Pesin, *Zh. Obshch. Khim.*, 1950, **20**, 1914-1920.
189. J. Hou, M.-H. Park, S. Zhang, Y. Yao, L.-M. Chen, J.-H. Li and Y. Yang, *Macromolecules*, 2008, **41**, 6012-6018.
190. A. Dhanabalan, J. K. J. van Duren, P. A. van Hal, J. L. J. van Dongen and R. A. J. Janssen, *Adv. Funct. Mater.*, 2001, **11**, 255-262.

191. M. Zhang, Y. Gu, X. Guo, F. Liu, S. Zhang, L. Huo, T. P. Russell and J. Hou, *Adv. Mater.*, 2013, **25**, 4944-4949.
192. Y. Jeon, T.-M. Kim, J.-J. Kim and J.-I. Hong, *New J. Chem.*, 2015, **39**, 9591-9595.
193. N. Blouin, A. Michaud, D. Gendron, S. Wakim, E. Blair, R. Neagu-Plesu, M. Belletête, G. Durocher, Y. Tao and M. Leclerc, *J. Am. Chem. Soc.*, 2008, **130**, 732-742.
194. H.-C. Ting, Y.-H. Chen, L.-Y. Lin, S.-H. Chou, Y.-H. Liu, H.-W. Lin and K.-T. Wong, *ChemSusChem*, 2014, **7**, 457-465.
195. R. Qin, W. Li, C. Li, C. Du, C. Veit, H.-F. Schleiermacher, M. Andersson, Z. Bo, Z. Liu, O. Inganäs, U. Wuerfel and F. Zhang, *J. Am. Chem. Soc.*, 2009, **131**, 14612-14613.
196. C.-Y. Yu, C.-P. Chen, S.-H. Chan, G.-W. Hwang and C. Ting, *Chem. Mater.*, 2009, **21**, 3262-3269.
197. Z.-S. Huang, X.-F. Zang, T. Hua, L. Wang, H. Meier and D. Cao, *ACS Appl. Mater. Interfaces*, 2015, **7**, 20418-20429.
198. T. J. Kealy and P. L. Pauson, *Nature*, 1951, **168**, 1039-1040.
199. G. Wilkinson, M. Rosenblum, M. C. Whiting and R. B. Woodward, *J. Am. Chem. Soc.*, 1952, **74**, 2125-2126.
200. R. B. Woodward, M. Rosenblum and M. C. Whiting, *J. Am. Chem. Soc.*, 1952, **74**, 3458-3459.
201. D. J. Booth and B. W. Rockett, *J. Chem. Soc. C*, 1971, 3341-3344.
202. N. G. Connelly and W. E. Geiger, *Chem. Rev.*, 1996, **96**, 877-910.
203. A. Togni, in *Ferrocenes*, Wiley-VCH Verlag GmbH, 2007, pp. 433-469.
204. T. Hayashi, in *Ferrocenes*, Wiley-VCH Verlag GmbH, 2007, pp. 105-142.
205. M. Al-Eid, S. Lim, K.-W. Park, B. Fitzpatrick, C.-H. Han, K. Kwak, J. Hong and G. Cooke, *Dyes Pigm.*, 2014, **104**, 197-203.
206. T. S. Chao and O. E. J., in *Espacenet*, ed. E. P. Office, Atlantic Richfield Co., 1978.
207. D. R. van Staveren and N. Metzler-Nolte, *Chem. Rev.*, 2004, **104**, 5931-5986.
208. R. R. Gagne, C. A. Koval and G. C. Lisensky, *Inorg. Chem.*, 1980, **19**, 2854-2855.
209. T. Daeneke, T.-H. Kwon, A. B. Holmes, N. W. Duffy, U. Bach and L. Spiccia, *Nat. Chem.*, 2011, **3**, 211-215.

210. D. Sirbu, C. Turta, A. C. Benniston, F. Abou-Chahine, H. Lemmetyinen, N. V. Tkachenko, C. Wood and E. Gibson, *RSC Adv.*, 2014, **4**, 22733-22742.
211. D. H. Lee, M. J. Lee, H. M. Song, B. J. Song, K. D. Seo, M. Pastore, C. Anselmi, S. Fantacci, F. De Angelis, M. K. Nazeeruddin, M. Gräetzel and H. K. Kim, *Dyes Pigm.*, 2011, **91**, 192-198.
212. M. Karikomi, C. Kitamura, S. Tanaka and Y. Yamashita, *J. Am. Chem. Soc.*, 1995, **117**, 6791-6792.
213. L.-L. Chua, J. Zaumseil, J.-F. Chang, E. C. W. Ou, P. K. H. Ho, H. Sirringhaus and R. H. Friend, *Nature*, 2005, **434**, 194-199.
214. R. Misra, P. Gautam, T. Jadhav and S. M. Mobin, *J. Org. Chem.*, 2013, **78**, 4940-4948.
215. K. Sonogashira, Y. Tohda and N. Hagihara, *Tetrahedron Lett.*, 1975, **16**, 4467-4470.
216. C. Glaser, *Liebigs Ann. Chem.*, 1870, **154**, 137-171.
217. E. Knoevenagel, *Ber. Dtsch. Chem. Ges.*, 1898, **31**, 2596-2619.
218. M. Cariello, S. Ahn, K.-W. Park, S.-K. Chang, J. Hong and G. Cooke, *RSC Adv.*, 2016, **6**, 9132-9138.
219. T. Xu, R. Lu, X. Liu, X. Zheng, X. Qiu and Y. Zhao, *Org. Lett.*, 2007, **9**, 797-800.
220. Z. Y. Hu, F. Q. Guo, B. Guo and H. Liang, *Appl. Mech. Mater.*, 2012, **170-173**, 2851-2854.
221. F. Ullmann, *Liebigs Ann. Chem.*, 1904, **332**, 38-81.
222. I. Goldberg, *Ber. Dtsch. Chem. Ges.*, 1906, **39**, 1691-1692.
223. E. J. Corey and P. L. Fuchs, *Tetrahedron Lett.*, 1972, **13**, 3769-3772.
224. J. Kim, S. H. Park, S. Cho, Y. Jin, J. Kim, I. Kim, J. S. Lee, J. H. Kim, H. Y. Woo, K. Lee and H. Suh, *Polymer*, 2010, **51**, 390-396.
225. J.-J. Kim, H. Choi, J.-W. Lee, M.-S. Kang, K. Song, S. O. Kang and J. Ko, *J. Mater. Chem.*, 2008, **18**, 5223-5229.
226. A. Vilsmeier and A. Haack, *Ber. Dtsch. Chem. Ges.*, 1927, **60**, 119-122.
227. A. P. Zoombelt, M. Fonrodona, M. M. Wienk, A. B. Sieval, J. C. Hummelen and R. A. J. Janssen, *Org. Lett.*, 2009, **11**, 903-906.
228. X. X. Sun, X. X. Zhuang and Y. L. Ren, *Adv. Mater. Res.*, 2012, **482-484**, 1221-1224.

229. L. L. G. Justino, M. Luísa Ramos, P. E. Abreu, A. Charas, J. Morgado, U. Scherf, B. F. Minaev, H. Ågren and H. D. Burrows, *J. Phys. Chem. C*, 2013, **117**, 17969-17982.
230. J. Chappell, D. G. Lidzey, P. C. Jukes, A. M. Higgins, R. L. Thompson, S. O'Connor, I. Grizzi, R. Fletcher, J. O'Brien, M. Geoghegan and R. A. L. Jones, *Nat. Mater.*, 2003, **2**, 616-621.
231. A. Foertig, J. Kniepert, M. Gluecker, T. Brenner, V. Dyakonov, D. Neher and C. Deibel, *Adv. Funct. Mater.*, 2014, **24**, 1306-1311.
232. F. Wudl, G. M. Smith and E. J. Hufnagel, *J. Chem. Soc. D*, 1970, 1453-1454.
233. T. E. Phillips, T. J. Kistenmacher, J. P. Ferraris and D. O. Cowan, *J. Chem. Soc., Chem. Commun*, 1973, 471-472.
234. E. M. Engler and V. V. Patel, *J. Am. Chem. Soc.*, 1974, **96**, 7376-7378.
235. P. Frere and P. J. Skabara, *Chem. Soc. Rev.*, 2005, **34**, 69-98.
236. F. Wudl, D. Wobschall and E. J. Hufnagel, *J. Am. Chem. Soc.*, 1972, **94**, 670-672.
237. K. Takahashi, T. Ise, T. Mori, H. Mori and S. Tanaka, *Chem. Lett.*, 1996, **25**, 1001-1002.
238. T. Ise, T. Mori and K. Takahashi, *Chem. Lett.*, 1997, **26**, 1013-1014.
239. J. Langer, I. Díez-Pérez, F. Sanz and J. Fraxedas, *Europhys. Lett.*, 2006, **74**, 110.
240. M. Mas-Torrent, M. Durkut, P. Hadley, X. Ribas and C. Rovira, *J. Am. Chem. Soc.*, 2004, **126**, 984-985.
241. C. Winder, H. Neugebauer, N. S. Sariciftci, F. Giacalone, J. L. Segura and N. Martin, *Photophysics and photovoltaic devices of a pi-extended tetrathiafulvalene-fullerene dyad*, Electrochemical Society, Pennington, N.J., 2005.
242. S. Arumugam, D. Cortizo-Lacalle, S. Rossbauer, S. Hunter, A. L. Kanibolotsky, A. R. Inigo, P. A. Lane, T. D. Anthopoulos and P. J. Skabara, *ACS Appl. Mater. Interfaces*, 2015, **7**, 27999-28005.
243. Z. Yu, H. Tian, E. Gabrielsson, G. Boschloo, M. Gorlov, L. Sun and L. Kloo, *RSC Adv.*, 2012, **2**, 1083-1087.
244. K. L. McCall, A. Morandeira, J. Durrant, L. J. Yellowlees and N. Robertson, *J. Chem. Soc., Dalton Trans.*, 2010, **39**, 4138-4145.

245. A. Amacher, C. Yi, J. Yang, M. P. Bircher, Y. Fu, M. Cascella, M. Gratzel, S. Decurtins and S.-X. Liu, *Chem. Commun.*, 2014, **50**, 6540-6542.
246. C. Teng, X. Yang, C. Yang, H. Tian, S. Li, X. Wang, A. Hagfeldt and L. Sun, *J. Phys. Chem. C*, 2010, **114**, 11305-11313.
247. J. M. Lovell, R. L. Beddoes and J. A. Joule, *Tetrahedron*, 1996, **52**, 4745-4756.
248. D. C. Green, *J. Chem. Soc., Chem. Commun*, 1977, 161-162.
249. E. C. Constable, S. Graber, B. A. Hermann, C. E. Housecroft, M. S. Malarek and L. J. Scherer, *Eur. J. Org. Chem.*, 2008, **2008**, 2644-2651.
250. C. Shao, M. Grüne, M. Stolte and F. Würthner, *Chem. Eur. J.*, 2012, **18**, 13665-13677.
251. A. B. Tamayo, M. Tantiwiwat, B. Walker and T.-Q. Nguyen, *J. Phys. Chem. C*, 2008, **112**, 15543-15552.
252. B. Zhao, K. Sun, F. Xue and J. Ouyang, *Org. Electron.*, 2012, **13**, 2516-2524.
253. J. Nakayama, N. Toyoda and M. Hoshino, *Heterocycles*, 1986, **24**, 1145-1150.
254. M. Schnurch, M. Spina, A. F. Khan, M. D. Mihovilovic and P. Stanetty, *Chem. Soc. Rev.*, 2007, **36**, 1046-1057.
255. G. Cooke and M. Bryce, *Synthesis*, 1991, **4**, 263-265.
256. J. Riedl, P. Horáková, P. Šebest, R. Pohl, L. Havran, M. Fojta and M. Hocek, *Eur. J. Org. Chem.*, 2009, **2009**, 3519-3525.
257. O. S. Herrera, J. D. Nieto, A. C. Olleta and S. I. Lane, *J. Phys. Org. Chem.*, 2011, **24**, 398-406.
258. J. D. Nguyen, E. M. D'Amato, J. M. R. Narayanam and C. R. J. Stephenson, *Nat. Chem.*, 2012, **4**, 854-859.
259. S. Naik, G. Bhattacharjya, B. Talukdar and Bhisma K. Patel, *Eur. J. Org. Chem.*, 2004, **2004**, 1254-1260.
260. D. Gerzenstein de Mittelman, *An. Asoc. Quim. Argent.*, 1944 **32**, 84-88.
261. L. T. Higham, K. Konno, J. L. Scott, C. R. Strauss and T. Yamaguchi, *Green Chem.*, 2007, **9**, 80-84.
262. M. S. Gruzdev, U. V. Chervonova, E. A. Venediktov, E. P. Rozhkova, A. M. Kolker, E. A. Mazaev, N. A. Dudina and N. E. Domracheva, *Russ. J. Gen. Chem.*, 2015, **85**, 1431-1439.

263. J. Nakazaki, M. M. Matsushita, A. Izuoka and T. Sugawara, *Tetrahedron Lett.*, 1999, **40**, 5027-5030.